AD-A103 898 EMMANUEL COLL BOSTON MASS PHYSICS RESEARCH DIV F/G 3/2
ANALYZE AND STUDY IONOSPHERIC SCINTILLATION AND TOTAL ELECTRON --ETC(U)
MAR 81 S BASU, S BASU, D HENDRICKSON F19628-78-C-0005
UNCLASSIFIED AFGL-TR-81-0087 NL

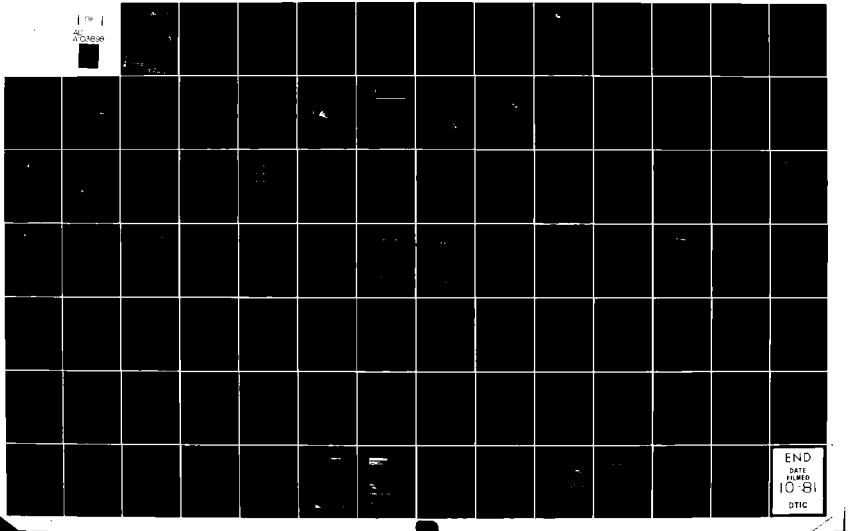

END
DATE FILMED
10-81
DTIC

(18) (19) AFGL-TR-81-0087

LEVEL II

(12)

AD A103898

(6) ANALYZE AND STUDY IONOSPHERIC SCINTILLATION AND TOTAL ELECTRON CONTENT VARIABILITY (IONOSPHERIC STUDIES AND TEC VARIATIONS).

(10) Santimay/Basu
Sunanda/Basu
David/Hendrickson
Eileen/MacKenzie
M.P. Hagan

The Trustees of Emmanuel College
400 The Fenway
Boston, Massachusetts 02115

DTIC
ELECTE
SEP 8 1981
S D

(9) Final Report
1 March 1978 — 28 February 1981

(15) F19628-78-C-0005

(11) March 1981

(12) 96

(16) 2029,
I25AAXH

Approved for public release; distribution unlimited

FILE COPY

AIR FORCE GEOPHYSICS LABORATORY
AIR FORCE SYSTEMS COMMAND
UNITED STATES AIR FORCE
HANSCOM AFB, MASSACHUSETTS 01731

MIL-STD-847A
31 January 1973

Unclassified
SECURITY CLASSIFICATION OF THIS PAGE (When Data Entered)

REPORT DOCUMENTATION PAGE	READ INSTRUCTIONS BEFORE COMPLETING FORM
1. REPORT NUMBER: AFGL-TR-81-0087	2. GOVT ACCESSION NO.: AD-A103 898	3. RECIPIENT'S CATALOG NUMBER
4. TITLE (and Subtitle): Analyze and Study Ionospheric Scintillation and Total Electron Content Variability (Ionospheric Studies and TEC Variations)	5. TYPE OF REPORT & PERIOD COVERED: Final, 01 Mar 78 - 28 Feb 81; 6. PERFORMING ORG. REPORT NUMBER
7. AUTHOR(s): Santimay Basu, Sunanda Basu, David Hendrickson, Eileen MacKenzie, M.P. Hagan	8. CONTRACT OR GRANT NUMBER(s): F19628-78-C-0005
9. PERFORMING ORGANIZATION NAME AND ADDRESS: Emmanuel College, Physics Research Division, 400 The Fenway, Boston, MA 02115	10. PROGRAM ELEMENT, PROJECT, TASK AREA & WORK UNIT NUMBERS
11. CONTROLLING OFFICE NAME AND ADDRESS: Air Force Geophysics Laboratory, Hanscom AFB, MA 01731, Contract Monitor: Herbert E. Whitney/PHP	12. REPORT DATE: 04 March 1981; 13. NUMBER OF PAGES: 96
14. MONITORING AGENCY NAME & ADDRESS (if different from Controlling Office)	15. SECURITY CLASS. (of this report): Unclassified; 15a. DECLASSIFICATION DOWNGRADING SCHEDULE

16. DISTRIBUTION STATEMENT (of this Report)

Approved for Public Release; Distribution Unlimited

17. DISTRIBUTION STATEMENT (of the abstract entered in Block 20, if different from Report)

18. SUPPLEMENTARY NOTES

This work was partially sponsored by the Defense Nuclear Agency, Subtask I25AAXHX, Space Division, Project 2029, and the National Aeronautics and Space Administration. TECH, OTHER

19. KEY WORDS (Continue on reverse side if necessary and identify by block number)

See other side

20. ABSTRACT (Continue on reverse side if necessary and identify by block number)

See other side

DD FORM 1 JAN 73 1473 EDITION OF 1 NOV 65 IS OBSOLETE

Unclassified
SECURITY CLASSIFICATION OF THIS PAGE (When Data Entered)

4/2

406576

Unclassified
SECURITY CLASSIFICATION OF THIS PAGE(When Data Entered)

19. *VHF amplitude scintillation*
Phase scintillation
F-region irregularities
Equatorial irregularities
Satellite in-situ
Radar backscatter
High-latitude irregularities
Scintillation modelling
Magnetic activity
Ionospheric heating
Underdense heating
Overdense heating
Solar Power Satellite (SPS)
Generation mechanisms
Plasma instability
Total Electron Content (TEC)
Faraday rotation
Time delay

20. *Ionospheric scintillation analyses have been conducted on several fronts, and are discussed here in the light of: (1) recent observations, current theories, and coordinated studies of equatorial scintillations; (2) morphology and analytical formulas at high latitudes; (3) measurements associated with ionospheric heating. F-region irregularities are viewed from the concepts of localized origin of patches, in-situ spectral measurements, and coexistence of km- and m-scale irregularities. The dynamics of equatorial patch formation, motion, and decay are also discussed. Generation of irregularities during underdense heating was observed for the first time. Total electron content data have been utilized to derive the statistics of the variability of ionospheric time delay in the Mediterranean region for the current solar maximum period. The implications of the results on modern satellite ranging systems are discussed.*

14/5A

Unclassified
SECURITY CLASSIFICATION OF THIS PAGE(When Data Entered)

TABLE OF CONTENTS

	Page
SUMMARY	1
The localized origin of equatorial F region irregularity patches	2
Comparison between in-situ spectral measurements of F-region irregularities and backscatter observations at 3m wavelength	8
On the coexistence of kilometer- and meter-scale irregularities in the nighttime equatorial F region	12
A review of recent observations of equatorial scintillations and their relationship to current theories of F region irregularity generation	20
The dynamics of equatorial irregularity patch formation, motion, and decay	35
Coordinated study of equatorial scintillation and in-situ and radar observations of nighttime F region irregularities	46
The morphology of high-latitude VHF scintillation near 70°W	58
High-latitude analytical formulas for scintillation levels	70
Preliminary results of scintillation measurements associated with ionosphere heating and possible implications for the solar power satellite	83
Variability of ionospheric time delay in the Mediterranean region	87

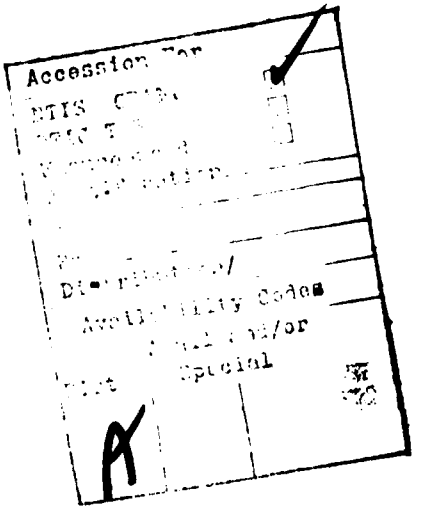

SUMMARY

Ionospheric scintillation and total electron content variability analyses have been conducted on several fronts.

Coordinated phase and amplitude scintillation and multitechnique irregularity measurements have been performed in the equatorial region. The multitechnique measurements include radar backscatter, rocket and satellite in-situ, airglow, and ionosonde. These studies have provided much insight into the transionospheric radio wave propagation problems associated with irregularities in the nighttime equatorial F region. The relationship between plasma depletions, 3-m irregularity structures, and bursts of scintillation activity (patches) leads to the association of different phenomena sensitive to different scale-lengths of the irregularities. The information on the varying behavior of these scale-sizes are discussed in the context of current theories of plasma instability. The coordinated measurements have been integrated to study the time development, motion, and decay of the irregularity structures.

A large data base of 137 MHz observations at three sites along the 70°W meridian has made it possible to develop a morphology of scintillations as a function of time of day, season, and magnetic activity. These were then formulated into empirical analytical models for each station, subject to varying irregularity configurations.

Scintillation measurements conducted during ionospheric heating by high power high frequency radio waves are used to explore artificial irregularities generated in the overdense and underdense cases of heating. A portion of these results are applicable to the proposed Solar Power Satellite (SPS).

Faraday rotation measurements of VHF radio waves from the SIRIO satellite have been used to determine the statistics of variability of ionospheric time delay in the Mediterranean region for the current solar maximum period (solar maximum 1978-79). The implications of these results on modern satellite ranging systems are discussed.

The Localized Origin of Equatorial *F* Region Irregularity Patches

JULES AARONS AND JÜRGEN BUCHAU

Air Force Geophysics Laboratory, Hanscom Air Force Base, Massachusetts 01731

SANTIMAY BASU[1]

Emmanuel College, Boston, Massachusetts 02115

J. P. MCCLURE

University of Texas at Dallas, Richardson, Texas 74080

An intensive study of nighttime irregularities of electron density in the equatorial ionosphere was performed in October 1976 by making 50-MHz radar backscatter measurements at Jicamarca, Peru, and scintillation measurements of 249-MHz transmissions from Les 9 at two ground stations (Ancon and Huancayo, both in Peru) as well as by aircraft flying in the vicinity of the stations. The 137-MHz scintillations from the orbiting Wideband satellite were also recorded at Huancayo. The results of such measurements made on October 16–17, 1976, are discussed in this report. We find that on this particular night a large-scale irregularity patch evolved first in the west, as was detected by the radar at Jicamarca, and drifted eastward to cause successive onsets of scintillation activity on propagation paths from Ancon and Huancayo. The observations indicate the east-west dimension of the large-scale structure to be 400 km drifting eastward at a speed of approximately 100 m/s, having a lifetime of several hours, and containing a hierarchy of irregularity scale sizes in the range of kilometers to meters causing both scintillations at 249 MHz and radar backscatter at 50 MHz.

INTRODUCTION

Theoretical studies, computer modeling, and experimental observations through radar backscatter and rocket and satellite in situ measurements have provided a greater insight into the formation of those equatorial irregularities which lead to deep scintillation of UHF and microwave transmissions through the ionosphere (see review by *Basu and Kelley* [1977] and references therein). The picture that emerges from these studies points to large-scale irregularity structures, tilted usually to the west, having an east-west dimension of up to several hundred kilometers, extending to altitudes as high as 1000 km, and containing a hierarchy of irregularity scale sizes in the range of several tens of kilometers to a few meters. Such irregularities of ionization are thought to result from the generation of large-scale plasma depletions in the bottomside ionosphere which rise rapidly upward against gravity, like 'bubbles' or 'plumes,' into the topside ionosphere.

Scintillation activity in a transionospheric VHF/UHF communication link results when the electron density deviation ΔN of irregularities with a scale size of about 1 km is sufficiently large. It is well known that at night in the equatorial *F* region, strong irregularities of electron density with different scale sizes exist, and these irregularities are most commonly observed to have a monotonic power law spectrum [*McClure and Hanson*, 1973; *Dyson et al.*, 1974]. By considering the above irregularity power spectrum, *Basu and Basu* [1976] demonstrated that the in situ ΔN measurements are compatible with the simultaneous ground-based scintillation observations at 6 GHz. In view of the above studies, one can assume the coexistence of irregularities in the scale size range of several tens of kilometers to several meters, although the in situ observations referenced above indicate that in certain (exceptional) cases, irregularities may have most of their spectral power either above or below a scale size of the order of 1 km. In general then, microwave fadings are likely to be associated with the plume structure seen on 50-MHz backscatter as was predicted by *Woodman and La Hoz* [1976]. Under those backscatter conditions when the plumes do not extend far into the topside ionosphere but still the product of thickness and ΔN is large, microwave fadings may also result. Most of the theoretical studies deal with the generation and motion of the small-scale structures within a large-scale bubble or patch [*Woodman and La Hoz*, 1976; *McClure et al.*, 1977]. In this report it will be shown that the generation of a large-scale bubble can be very localized and that a bubble can maintain its integrity for several hours during its eastward motion.

OBSERVATIONS

Ground Measurements

A series of 50-MHz radar backscatter observations from the Jicamarca Observatory of the Instituto Geofísico del Perú was made over a period of 2 weeks in conjunction with a large-scale ground and airborne campaign to study scintillations. On the ground, observations were made of the synchronous satellite Les 9 beacon, transmitting at 249 MHz, from two different sites, Ancon and Huancayo, both in Peru, and also of the orbiting Wideband satellite transmissions at 137 MHz from Huancayo. Figure 1 shows the geometry and geography of the observations. The 400-km subionospheric intersections of the propagation paths from Ancon and Huancayo to Les 9 and the subionospheric tracks of the Wideband satellite transit are shown. The Jicamarca vertical intersection is farthest west, while the two oblique paths to Les 9 are to the east of Jicamarca. If the time of sunset determines the timing of appearance of irregularities, then the Huancayo path should observe scintillations first, followed by Ancon, and finally, Jicamarca would record backscatter from irregularities.

Figure 2 shows the results of simultaneous radar and scintillation measurements made on October 16–17, 1976. The top

[1] On leave from the University of Calcutta, Calcutta, India.

Copyright © 1978 by the American Geophysical Union.

Paper number 7A0956.
0148-0227/78/047A-0956$03.00

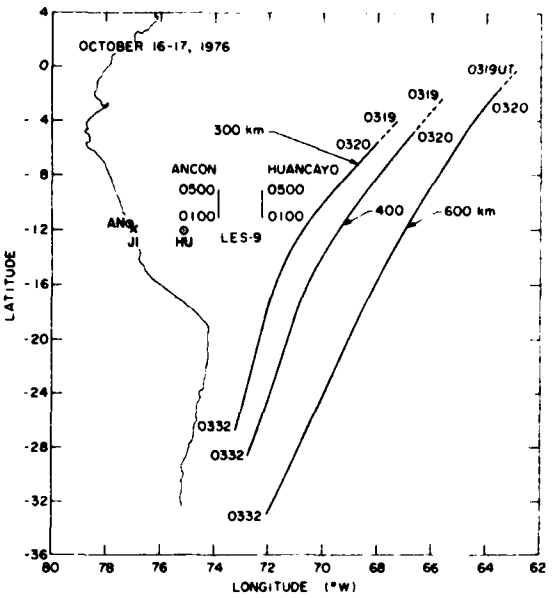

Fig. 1. Geometry of radar backscatter and scintillation measurements on October 16–17, 1976. The ground locations of Jicamarca (JI), Ancon (AN), and Huancayo (HU) are indicated. The subionospheric locations (400 km) of Les 9 observations from Ancon and Huancayo between 0100 and 0500 UT are shown. The subionospheric tracks of the Wideband satellite between 0319 and 0332 UT corresponding to 300, 400, and 600 km are also shown. The western coastline of South America is indicated for reference purposes.

panel shows the range-time-intensity plot of 50-MHz backscatter obtained at Jicamarca. Since the original digital power maps [*Woodman and La Hoz*, 1976] are difficult to reproduce, we have redrawn these and displayed the echo intensity at only three logarithmic power levels relative to the approximate maximum incoherent scatter level. The next two panels illustrate the time variation of scintillation index *SI* (in decibels) recorded at Ancon and Huancayo on propagation paths to Les 9. Comparing the three panels, we find that the initial appearance of backscatter in the Jicamarca radar is followed by the onset of scintillations at Ancon and finally at Huancayo; clearly, a localized irregularity patch was generated over Jicamarca or to the west of it and has moved eastward. This is of course based on the usually justifiable assumption that the kilometer-size irregularities causing scintillations coexist with 3-m irregularities giving rise to 50-MHz backscatter. Using the geometry of Figure 1 and the timing of the onset of irregularities, we measure an average eastward drift speed of the irregularity structure as 100 m/s. The cross-correlation analysis of scintillation data acquired at Ancon by use of antennas separated by 366 m in the east-west direction on October 16–17, 1976, also provides an average eastward drift speed of 116 m/s. This is in agreement with the previously reported values of *Woodman* [1972]. When the duration of the scintillation event is combined with the observed drift speed, the patch dimension in the east-west direction is found to be about 400 km. The correspondence between the radar map of Jicamarca and the scintillation measurements at Huancayo with a delay of 90 min indicates that the irregularity structure retained its integrity between the two stations for at least 1½ hours. The total of 3 hours between the first appearance of a plume at Jicamarca and the end of scintillation at Huancayo indicates that the total lifetime of the irregularity patch may be at least 3 hours.

On October 16–17, 1976, scintillations of the 137-MHz transmissions from the orbiting Wideband satellite were recorded at Huancayo between 0320 and 0332 UT. In Figure 1 the subionospheric tracks of the satellite transit corresponding to three ionospheric heights, 300, 400, and 600 km, are shown. The portion of the track marked by the solid line indicates the presence of scintillation, while the dotted line indicates the absence of any scintillation. Considering the 400-km track, we find that scintillations were extant between 66°W and 72°W. If we assume that the irregularity structure front (eastern edge) causing the onset of Les 9 scintillations at Huancayo had reached the 66°W location at 0320 UT, a drift speed of 160 m/s for the irregularity patch is obtained. This speed is considerably higher than that derived previously for the patch during its passage from Ancon and Huancayo. From Figure 1 we find that in view of the low elevation angle of the transit the subionospheric tracks for the three altitudes are considerably displaced. This poses problems in locating the irregularity structure and deriving the drift speed. For example, if we consider the 300-km track, a drift speed of 110 m/s, more in accord with the previously derived drift speed, may be obtained. The latitudinal extent of the track exhibiting scintillations is found to be about 20°. Owing to the low elevation angle of the satellite, there exists the possibility that the satellite will encounter discrete irregularity patches, and hence it is difficult to arrive at a definite conclusion regarding the latitudinal extent of a single patch.

Airborne Measurements

Two aircraft were used to observe scintillations from Les 9, one from the Air Force Avionics Laboratory (AFAL) and the other from the Air Force Geophysics Laboratory (AFGL). The subionospheric flight paths of the AFAL and AFGL aircraft are shown in Figure 3*a*. The heavy-lined portions of the track signify the presence of scintillations in excess of 12 dB, the moderately heavy lines indicate 6- to 8-dB scintillations, and the thin lines represent the absence of any scintillations. In Figure 3*b* we show the time variation of scintillation as recorded by the AFGL aircraft. The aircraft flew on parallel paths such that the initial portion of either subionospheric track was inclined at about 10° to the east of the magnetic meridian, while the later portion of the track was approximately in the magnetic east-west direction. From Figure 3*b* as well as the flight path map it may be noted that the AFGL aircraft encountered two scintillation events, the initial event being in excess of 12 dB and the later event having a level of about 8 dB. The subionospheric flight map of the AFAL aircraft shows that it also encountered one strong and one weak irregularity patch. The propagation path from the AFAL aircraft to Les 9 seems to have entered the eastern edge of a strong irregularity patch at 0210 UT and to have emerged from it at 0306 UT. Strong scintillations as high as 25 dB were recorded by the AFAL aircraft during some periods between 0212 and 0303 UT. The AFGL aircraft, flying to the east of the AFAL aircraft, recorded strong scintillations between 0248 and 0329 UT. If we consider that the eastern edge of the strong irregularity patch initially detected by the AFAL aircraft at 0212 UT drifted eastward to the subionospheric location of the AFGL aircraft propagation path at 0248 UT, then an eastward drift speed of 100 m/s is obtained. Further, if we assume that the irregularity patch extended southward all the way to

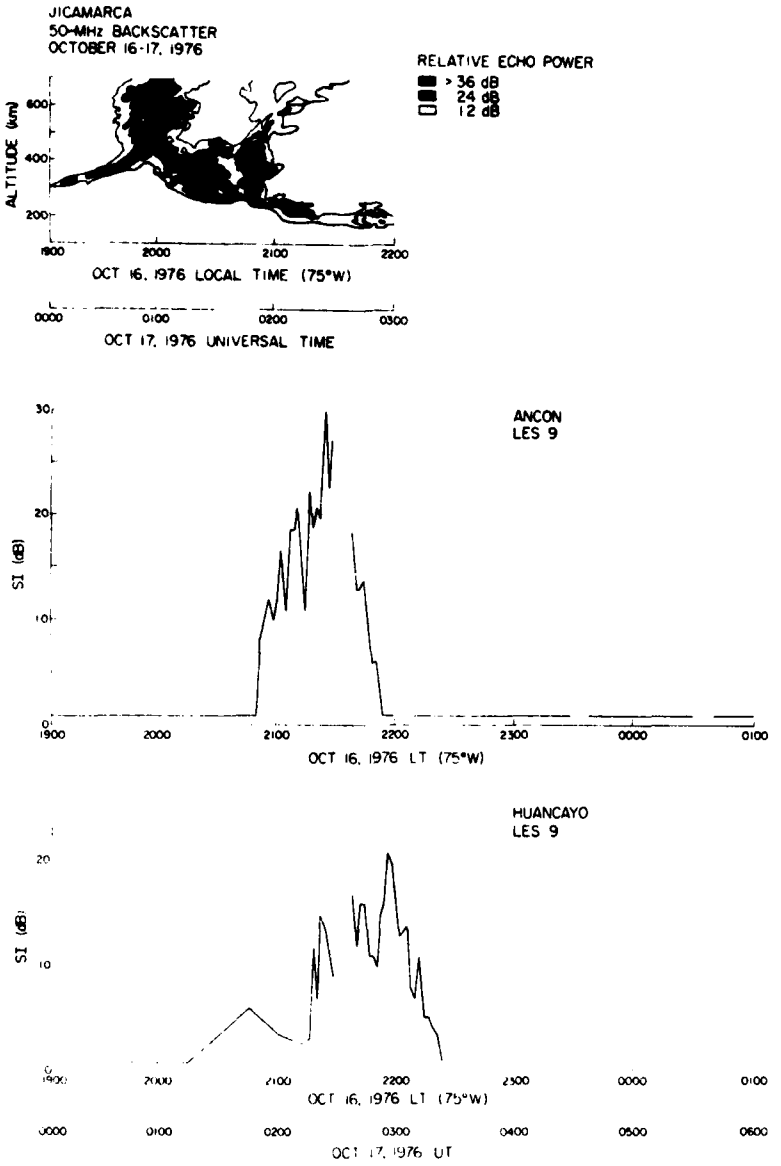

Fig. 2. Temporal variation of the 50-MHz radar backscatter observed at Jicamarca and scintillation index *SI* (in decibels) of the 249-MHz transmissions from the Les 9 satellite recorded at Ancon and Huancayo on October 16–17, 1976.

the magnetic equator, then the ends of the first scintillation event recorded by both aircraft are to be related to the passage of the western edge of the patch. Considering the duration of the scintillation event with the derived drift speed an east-west patch dimension ranging from 250 to 300 km is obtained. This is consistent with the typical data from the AE-C satellite presented by *McClure et al.* [1977]. The irregularity patch detected by the AFGL aircraft was located approximately 10° north and 4° west of Jicamarca, the position of which is indicated in the diagram. Irregularities of kilometer scale size are expected to be field aligned, and these field lines pass over the equator at altitudes of approximately 600 km. Considering the drift speed of 100 m/s these field lines should have drifted eastward to the Jicamarca meridian at about 0400 UT. The radar map obtained at Jicamarca does not, however, exhibit the presence of any 3-m irregularities at this time. It is not clear whether the absence of 3-m irregularities is related to the decay of the patch during its passage to the Jicamarca meridian or whether the irregularity power spectrum had little spectral power at the meter wavelength end. Comparison of irregularity spectral power at kilometer and meter wavelengths in the equatorial ionosphere is being actively pursued [*Woodman and Basu*, 1977].

Over the magnetic east-west portion of the flight paths, weak scintillations were recorded by both aircraft. The measurements indicate that the AFGL aircraft encountered 8-dB

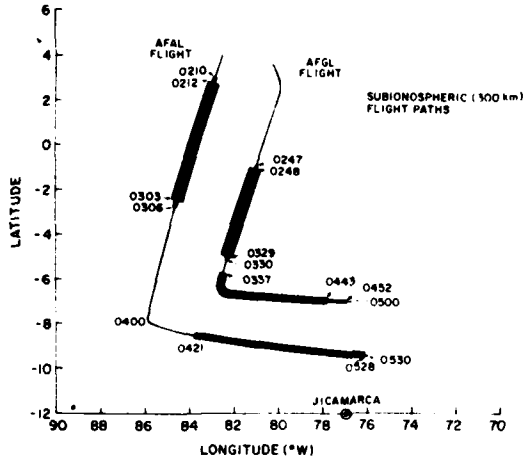

Fig. 3*a*. Scintillation measurements of the 249-MHz transmissions from the Les 9 satellite made on October 16–17, 1976, with aircraft flown by the Air Force Geophysics Laboratory (AFGL) and the Air Force Avionics Laboratory (AFAL). The subionospheric (300 km) flight paths of the two aircraft are shown.

scintillation levels whereas the AFAL aircraft encountered 6-dB levels, although the latter path was closer to the magnetic equator. Since the two aircraft did not cross the same meridian at the same time, it is difficult to separate the spatial and temporal variation and to comment on the latitude variation of the irregularity strength. During the eastward flight the AFGL and AFAL aircraft crossed the Jicamarca meridian at 0450 UT and 0520 UT, respectively, and detected about 6-dB scintillations. The Jicamarca radar did not detect any 3-m irregularity structure at this time. This is not surprising in view of the low level of scintillations observed.

The initial appearance of plumes in the early part of the night at the westernmost location of Jicamarca as observed on October 16–17, 1976, should be viewed as an exception rather than as the rule. In general, the activity on a given night starts on the eastward propagation path before it starts on the west. The illustration shown in the work of *Bandyopadhyay and Aarons* [1970] indicates that for only 20% of the time, satellite scintillations on a westward propagation path start before those on an eastward propagation path.

In order to illustrate this aspect of the problem we compare simultaneous radar backscatter and scintillation measurements made on October 17, 1973, 3 years earlier than the present set of observations. The bottom panel of Figure 4 shows that on this night, radar backscatter measurements were made at Jicamarca [*Woodman and La Hoz*, 1976] and simultaneous scintillation measurements were made at Huancayo with the 137-MHz transmissions from ATS 3 and the 254-MHz transmissions from Les 6. The subionospheric locations of ATS 3 and Les 6 corresponding to an ionospheric height of 350 km are indicated in the diagram. The top panel shows the range-time-intensity plots of 3-m irregularity structure obtained with the 50-MHz radar at Jicamarca. It may be observed that a thin irregularity structure evolved at 1925 LT, persisting until about 2000 LT, when a plume structure developed. The second panel shows the development of 137-MHz scintillation at Huancayo, the subionospheric location of ATS 3 being 1.9° to the east of Jicamarca. It may be noted that scintillations on ATS 3 developed after 2010 LT and a sharp increase from 6 to 22 dB occurred after 2030 LT. When the top two panels are compared, it is found that scintillations immediately to the east of Jicamarca occurred after the development of irregularity structure over Jicamarca. If we assume that the plume structure observed over Jicamarca drifted eastward to cause the sudden increase of scintillation on ATS 3, a drift speed of 116 m/s is obtained. If we now observe the third panel, which shows the development of 254-MHz scintillation on Les 9, the subionospheric location being far to the east with a longitude separation of 4°16′ from Jicamarca, we find that the onset of Les 6 scintillation occurred slightly earlier than the onset of ATS 3 scintillation at Huancayo. This scintillation structure (marked A in Figure 4) observed on the Les 6 propagation path cannot be associated with the drifting irregularity structure observed over Jicamarca but must have been caused by an independent irregularity structure developing to the east of the Huancayo ATS 3 ray path. In fact, the second scintillation structure observed on the Les 6 propagation path after 2100 LT (marked B in Figure 4) could be associated with the plume structure at Jicamarca and the first scintillation structure on ATS 3 if we assume an average drift speed of about 130 m/s. Comparing the set of observations made on October 16–17, 1976, discussed in detail above, with the set obtained nearly 3 years earlier, also discussed above, we conclude that on certain nights a single irregularity structure may evolve and while drifting eastward may cause scintillations to occur as long as it persists, or a series of irregularity patches may evolve and while drifting eastward may give rise to a series of scintillation structures. Thus the location of generation of the irregularities, their drift, and their lifetimes dictate the time evolution of the scintillations observed at a given ground station in the equatorial region.

Discussion

Our results indicate that intense 3-m irregularity patches detected by the radar are associated with strong scintillation

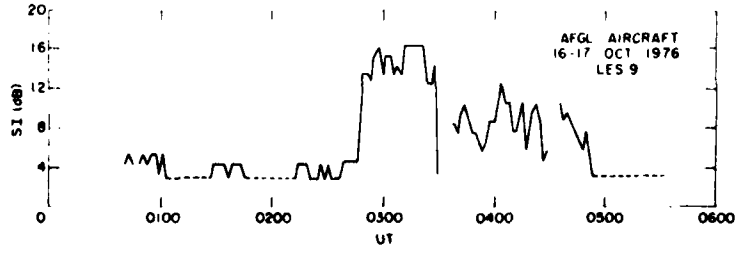

Fig. 3*b*. Same as Figure 3*a* but showing temporal variation of scintillation index *SI* (in decibels) recorded by the AFGL aircraft.

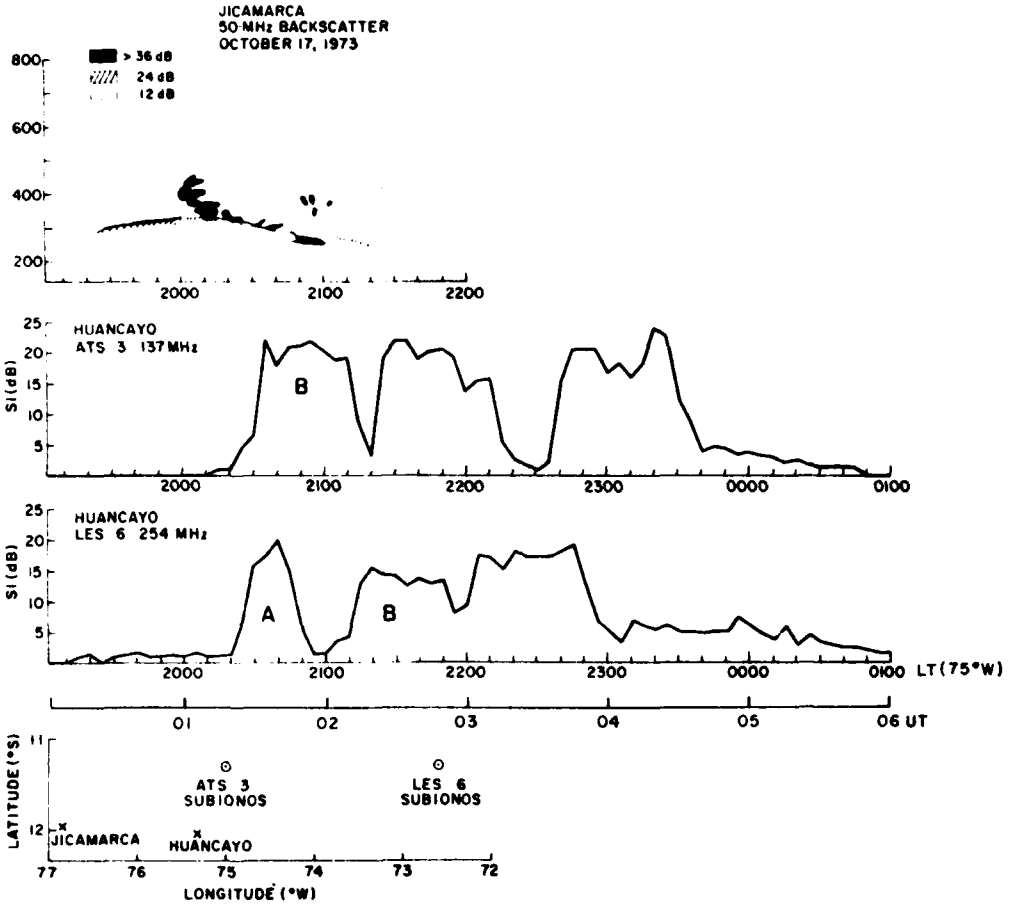

Fig. 4. Comparison of the 50-MHz radar backscatter map obtained at Jicamarca on October 17, 1973, and scintillation measurements made at Huancayo with the 137- and 254-MHz transmissions from the ATS 3 and Les 6 satellites, respectively.

events. Thus, *in general*, the kilometer-size irregularities are obtained when the 3-m irregularities are present, a finding which is of course predicted by the theory. Although they are not covered in this preliminary report, we have found cases, in particular during the postmidnight period, when patches containing kilometer-size irregularities were obtained without any associated radar event. It seems that on occasion the turbulent energy fails to cascade down to meter scale sizes. We expect to obtain more information in this regard from radar and scintillation measurements performed on a common ionospheric volume during March 1977.

We have shown that the radar backscatter and scintillation measurements are consistent with an eastward drift speed of irregularity patches at about 100 m/s. The scintillation observations as well as transequatorial propagation experiments indicate that irregularity patches can move past a fixed propagation path within a few tens of minutes to a maximum of 100 min, the latter figure being reported by *Rötger* [1976]. Combining the drift speed with the duration of the scintillation event, we obtain east-west patch dimensions of several hundred kilometers. This is consistent with the recently published in situ results [*McClure et al.*, 1977]. We have shown that the radar map corresponding to a single scintillation patch may exhibit considerable structure. The simple scintillation event observed on October 16–17, 1976, was associated with the radar event showing two plumes joined by a thick region of intense irregularities at low altitudes.

The generation of irregularity patches is indeed very localized, as was revealed by multistation scintillation measurements made with an east-west ionospheric separation as small as 175 km. The lifetime of the large-scale irregularity patches has been shown to be at least several hours.

The localized nature of irregularity formation and the dimensions of the patch indicate that very large scale global patterns of winds and tides cannot be used to determine the physical conditions necessary for the generation of the irregularities.

Acknowledgments. We thank the staff of the Instituto Geofisico del Perú for their help in recording the data and their hospitality toward the visiting scientists. In addition, the assistance of John Mullen, Herbert Whitney (Air Force Geophysics Laboratory), and Allen Johnson (Air Force Avionics Laboratory) in making the observations and reducing their data is gratefully acknowledged. This work was partially supported by National Science Foundation grants DES-71-

00555 and ATM76-17351 and by National Aeronautics and Space Administration grants NGL44-004-026 and NGL-004-13. This research was sponsored in part by Defense Nuclear Agency subtask L25 AAXHX633, entitled 'Communication Effects Data Base.'

The Editor thanks B. B. Balsley for his assistance in evaluating this report.

REFERENCES

Bandyopadhyay, P., and J. Aarons, The equatorial *F*-layer irregularity extent as observed from Huancayo, Peru, *Radio Sci.*, *5*, 931–938, 1970.

Basu, S., and S. Basu, Correlated measurements of scintillations and in-situ *F*-region irregularities from Ogo-6, *Geophys. Res. Lett.*, *3*, 681–684, 1976.

Basu, S., and M. C. Kelley, Review of equatorial scintillation phenomena in the light of recent developments in the theory and measurement of equatorial irregularities, *J. Atmos. Terr. Phys.*, *39*, in press, 1977.

Dyson, P. L., J. P. McClure, and W. B. Hanson, In situ measurements of the spectral characteristics of *F* region ionospheric irregularities, *J. Geophys. Res.*, *79*, 1497–1502, 1974.

McClure, J. P., and W. B. Hanson, A catalog of ionospheric *F* region irregularity behavior based on Ogo 6 retarding potential analyzer data, *J. Geophys. Res.*, *78*, 7431–7440, 1973.

McClure, J. P., W. B. Hanson, and J. H. Hoffman, Plasma bubbles and irregularities in the equatorial ionosphere, *J. Geophys. Res.*, *82*, 2650–2656, 1977.

Röttger, J., The macro-scale structure of equatorial spread-*F* irregularities, *J. Atmos. Terr. Phys.*, *38*, 97–101, 1976.

Woodman, R. F., East-west ionospheric drifts at the magnetic equator, *Space Res. VII*, 968–974, 1972.

Woodman, R. F., and S. Basu, Comparison between in situ spectral measurements of equatorial *F*-region irregularities and backscatter observations at 3m wavelength (abstract), *Eos Trans. AGU*, *58*, 449, 1977.

Woodman, R. F., and C. La Hoz, Radar observations of *F* region equatorial irregularities, *J. Geophys. Res.*, *81*, 5447–5466, 1976.

(Received August 11, 1977;
accepted October 10, 1977.)

COMPARISON BETWEEN IN-SITU SPECTRAL MEASUREMENTS OF F-REGION IRREGULARITIES AND BACKSCATTER OBSERVATIONS AT 3 m WAVELENGTH

R. F. Woodman
National Astronomy and Ionosphere Center,
Arecibo Observatory, Arecibo, Puerto Rico 00612

Sunanda Basu
Emmanuel College, Boston, Ma 02115

Abstract. In situ measurements of equatorial electron density irregularities in the F-region by rockets and satellites have yielded a power-law form of one-dimensional wave number spectrum of spectral index 2 in a direction transverse to the magnetic field over a scale size range of several km to several tens of m. Equatorial scintillation measurements in the VHF-UHF band which are most sensitive to irregularities of several km to several hundred m are consistent with the in situ spectral results. The backscatter measurements made at Jicamarca at 50 MHz provide an additional measurement of the spectral power at 3m wavelength. Computations are presented for the backscatter intensity expected from irregularities with power law spectrum in the transverse direction but which are infintely elongated along the magnetic field. The computed intensity is compared with actual backscatter measurements and correlated scintillation observations. It is found that in order to reconcile the backscatter measurements with the simultaneous VHF/UHF scintillation observations a gaussian type cut-off of the power-law spectrum is necessary at m wavelengths near the O^+ ion gyro-radius.

Introduction

In-situ measurements of spectral characteristics of F-region equatorial irregularities using both satellites and rockets have yielded a power law type of irregularity power spectrum between scale sizes of several km to several tens of m (*Dyson* et al., 1974; *Costa* and *Kelley*, 1976; *Morse* et al., 1977). The spectral index was usually found to be approximately two for one-dimensional measurements perpendicular to the earth's magnetic field. *Basu* and *Basu* (1976) utilized such a power spectrum in conjunction with Ogo-6 observations of large irregularity amplitudes and large outer scale sizes to explain both satured VHF and moderate GHz scintillations.

It is important to note that for scintillation measurements in the VHF/UHF band the Fresnel dimensions are of the order of a km to several hundred m. As mentioned above, this range has been covered by existing in-situ measurements. On the other hand, the maps of backscattered power obtained with the Jicamarca radar at 50 MHz by *Woodman* and *LaHoz* (1976) provide us with information regarding spectral power of irregularities at 3 m scale length. The 3 m length is outside the range of previous and existing in-situ instrumentation. Thus a comparison of scintillation and backscatter observations should, in principle, extend the domain over which spectral characteristics of irregularities can be inferred and this is the purpose of the present note. For this, we assume an irregularity model which is consistent with in-situ measurements and determine an electron density deviation using this model and observed scintillation data. We then compute the backscatter that should be observed with such a magnitude of electron density deviation and compare it with actual correlated radar observations.

Scintillation and Radar Backscatter Computations

An opportunity to make correlated observantions of scintillation and backscatter was provided during the equatorial irregularity campaign conducted byt the Air Force Geophysics Laboratory in October, 1976 (*Basu* and *Aarons*, 1977; Aarons et al., 1978). In particular, on October 29, 1976 scintillation measurements were conducted from Huancayo on the ATS-6 satellite when it was being moved from the eastern to the western hemisphere. Rather fortuitously, the ionospheric intersection point at the 350 km level was 11.3°S, 76.6°W approximately 30 m east of the Jicamarca radar location (11.95°S, 76.87°W). The simultaneous backscatter and scintillation observations are shown in Figure 1.

The backscatter map obtained using techniques similar to that of *Woodman* and *LaHoz* (1976) was kindly made available to us by Dr. J. P. McClure. The digital map obtained using 8 levels between 6 and 48 dB is rather difficult to reproduce and this the map has been redrawn to show 4 different intensity levels approximately above the incoherent scatter returns obtained from thermal fluctuations in a plasma with density on the order of 10^{12} electrons/m^3. Similar maps have been discussed in detail by *Woodman* and *LaHoz* (1976) and we shall only comment on the fact that at 2100 LT, the Jicamarca radar observed a 200 km thick irregularity layer in which the intensity of the backscatter echo varied between 30 and 42 dB above the coherent scatter level.

At the same time, the 360 MHz amplitude channel recorded a peak-to-peak fluctuation of 8 dB equivalent to the theory-based index $S_4 = 0.4$. The 137 MHz channel was observing large amplitude scintillations in excess of 20 dB. The moderate level of the 360 MHz scintillation made it possible to use weakscatter theory for the estimation of ΔN. We used equation (5) of *Costa* and *Kelley* (1976) applicable to anisotropic irregularities with power law spectrum in conjunction with the observed irregularity layer thickness of 200 km and assumed an outer scale of 20 km (Basu and Basu, 1976) to determine the value of ΔN. The magnitude of ΔN so obtained for $S_4 = 0.4$ is 6×10^{10} m^{-3}. The AFGL aircraft (used in Peru as part of the equatorial irregularity campaign) with a digital ionosonde on board was unfortunately not operating on the night of October 29, 1976. However it did observe a plasma number density of 6×10^{11} m^{-3} (f_0F2 of 7 MHz) on the following night at 2100 LT near Jicamarca (*J. Buchau*, private communication, 1977). Thus irregularities with amplitudes on the order of 10 percent were probably causing the scintillations as well as the associated backscatter.

In the Appendix, we have derived the pertinent equations for computing backscatter from irregularities which are infintely elongated along the magnetic field. It is shown that, if the one-dimensional wave number spectrum is given by

$$\phi(k_x) = \frac{\langle (\Delta N)^2 \rangle L_0}{\pi} \cdot \frac{1}{1 + k_x^2 L_0^2} \qquad (1)$$

in agreement with in-situ observations, then the three dimensional spectrum for cylindrically symmetric irregularities infiniteley enlongated along B is given by

$$\Phi(k) = \frac{\langle (\Delta N)^2 \rangle L_0^2}{2\pi} \cdot \frac{\delta(k_{\parallel})}{(1 + k_{\perp}^2 L_0^2)^{3/2}} \qquad (2)$$

where L_0 is the outer scale of irregularities with r.m.s. electron density deviation ΔN, and $k_{\parallel}$ and $k_{\perp}$ are wavenumbers parallel and perpendicular to the magnetic field B. Using equation 2 and considering the aspect sensitivity of the irregularities we obtain the following relationship for the ratio of P_{hF}, the backscattered power form irregularities at distance h, to p_{hI} the backscattered power from thermal fluctuations in the plasma at distance h.

[1]Presented at American Geophysical Union Spring Meeting, Washington, D.C., May, 1977.

Copyright 1978 by the American Geophysical Union.

Paper number 8L0620.
0094-8276/78/108L-0620$01.00

$$\frac{P_{hF}}{P_{hI}} = \frac{\langle (\Delta N)^2 \rangle}{N} \cdot \frac{8\pi^{3/2} L_o^2}{[1 + k^2 L_o^2]^{3/2} \theta k} \qquad (3)$$

As mentioned earlier, our object is to use the same value of L_o as used in the scintillation computations together with the derived value of ΔN from the scintillation measurements to obtain a numerical estimate of the ratio given in equation (3). If the same monotonic power law form of the spectrum exists up to wavelengths as short as 3 m, then it is expected that the computed value of this ratio and that observed in Figure 1 should agree. We obtain instead

$$\log \frac{P_{hF}}{P_{hI}} = 82 \text{ dB} \qquad (4)$$

where $\Delta N = 6 \times 10^{10}$ m^{-3}
$N = 6 \times 10^{11}$ m^{-3}
$L_o = 20$ km
$k = 2.09$ m^{-1}
$\theta = .0102$ radians ($\approx 0.7°$).

The last two paramenters are relevant for the Jicamarca radar.

The observed enhancement at 2100 LT was on the order of 40 dB. Thus there is a discrepancy of at least 4 orders of magnitude between the observed radar backscatter power and that given by equation 4.

Discussions

The very large discrepancy of 4 orders of magnitude between the observed radar backscatter and that computed on the basis of a monotonic power law spectrum is an interesting and unexpected result. *Farley et al.*, had stated in 1970 that as a rough guess, the irregularities were at times 10^7-10^8 times as strong as those responsible for incoherent scatter. But with improvements in experimental techniques, it seems that a figure of 10^6 is more accurate. Thus the black portions of the radar map in Figure 1 show enhancements on the order of 10^6 times the incoherent scatter returns. There is some digital saturation around this level, but the fact that this level is observed over relatively small height intervals at a time (also for instance in the maps given by *Woodman* and *LaHoz* (1976)) shows that saturation does not occur extensively. That is, most of the time the signal is even lower than 48 dB: this is the case for the signals around 2100 LT on October 29, 1976, chosen for these computations.

Our computations have been based on the power law spectrum observed by various experimenters using in-situ rocket and satellite techniques. *Fredricks* and *Coroniti* (1976) have recently pointed out that there is no unique connection between the rest frame power spectrum as a function of scale length and derived power spectrum as a function of frequency computed from the time series data taken in the moving frame such as obtained from rockets and satellites. In particular, for the anisoptropic spectrum considered here, these authors show that aliasing can be expected. Thus the real spectral index may be different from the observed index. There is also little experimental information on the actual value of the outer scale used in the scintillation computations. In addition, by using a value of 200 km for the thickness of the irregularity layer, we tacitly assumed that the km scale irregularities are distributed in the same way as the 3 m scale irregularities observed by the radar. However, all these potential sources of error cannot explain the 4 orders of magnitude discrepancy between the computed and observed backscatter power.

It is important to point out here that the 3 m scale length probed by the radar is of the same order as the O^+ ion gyro-radius (R_O) at a temperature of 700°K which is appropriate to the nighttime equatorial region under sunspot minimum conditions. Most of the recent theories specifically developed to explain equatorial spread-F (*Balsley* et al., 1972; *Haerendel*, unpublish manuscript, 1974; *Hudson* and *Kennel* 1975) have considered a perpendicular scale length regime much larger than R_O and are thus not applicable to the radar measurements. We shall put forward some qualitative arguments to explain why it is probable, from energy considerations, to expect a rapid fall-off in the spectral power of the irregularities near R_O.

The larger scale length irregularities are probably created by turbulent mixing of the background ionization in regions where there is a primary (or secondary) gradient of ionization. Small polarization fields ($E \times B/B^2$ < thermal) are sufficient to produce the turbulent mixing whereby parcels of small density are convected to regions of higher density and vice versa. Such irregularities are possible only for scale sizes larger than a gyro-radius if we want to keep polarization fields small enough and maintain the quasi-neutrality of the irregularities. In that way the ions would still gyrate in circular trajectories around a fixed or slowly drifting guiding center. As soon as we allow for larger fields, the electrostatic energic content of the irregularities becomes larger and it becomes more difficult to create the irregularities.

It is possible to associate with each magnetic field line a population of ions gyrating around it with a thermal velocity distribution of the form $\exp(-m_i v^2/2KT)$. These ions will occupy a volume in which the density is of the form $\exp(-r^2/2R_O^2)$, where r is the distance from the guiding center and R_O is the mean radius of the ionic orbit given by $(KT/m_i)^{1/2}/\omega_i$ where ω_i is the ion gyro frequency. This swarm of ions can be easily neutralized by the proper density of electrons gyrating along the neighbouring lines. It is impossible to create an elementary volume of gyrating ions with an associated Maxwellian distribution that has smaller radial extent than R_O unless one strongly distorts their circular orbits. This distortion would mean the introduction of strong small scale electric fields which we are trying to keep as low as possible (and still have irregularities) based on energy considerations. On the other hand, it is possible to synthetize any sort of large scale irregularities by the superposition of these neutralized elementary volumes of gyrating ions.

It is to be expected, then, that a drastic cut-off must exist at scale sizes comparable to the gyro radius. The above arguments suggest an autocorrelation function of the form

$$R(r) = \langle (\Delta N)^2 \rangle \exp(-r_\perp / L_o) * \exp(-r_\perp^2/2R_O^2) \qquad (5)$$

where the asterisk implies convolution. The first exponential term in equation (5), namely, $\exp(-r_\perp/L_o)$, is the experimentally determined correction function for larger scale sizes. The convolution by $\exp(-r_\perp^2/2R_O^2)$ limits the smaller scale to R_O with a gaussian type of cut-off. This leads to an equivalent wave number spectrum of the following form

$$\Phi(k) = \frac{\langle (\Delta N)^2 \rangle L_o^2}{2\pi} \cdot \frac{\delta(k_\parallel)}{(1 + k_\perp^2 L_o^2)^{3/2}} \exp(-k_\perp^2 R_O^2/2) \qquad (6)$$

which in turn gives instead of equation 3:

$$\frac{P_{hF}}{P_{hI}} = \frac{\langle (\Delta N)^2 \rangle}{N k \theta} \cdot \frac{8\pi^{3/2} L_o^2}{[1 + k_\perp^2 L_o^2]^{3/2}} \cdot \exp(-k_\perp^2 R_O^2/2) \qquad (7)$$

Now $R_O = 3.35$ m for O^+ ions at a temperature of 700°K for a magnetic field of 0.3 gauss. If we use this value of R_O in equation 7, the correction factor namely $\exp(k_\perp^2 R_O^2/2)$, is of the order of 10^{10} while an agreement with observations requires a correction of the order 10^4 or 10^5. Thus to obtain a better correspondence with experimental results the value of the radius has to be reduced by a factor of 1.5. With such an ad-hoc alteration of the value of R_O we obtain for the ratio:

$$\log \frac{P_{hF}}{P_{hI}} = 24 \text{ dB} \qquad (8)$$

which agrees quite well with the experimental observations shown in Figure 1. It is well known that a gaussian spectrum is very sensitive to the value of the scale size. Thus in equation 7, a relatively minor adjustment in the value of R_O brought agreement between computation and observation.

It is our feeling that a break in the irregularity spectrum probably exists and that ion-gyro radius plays a prominent part in determining it. It is interesting to note that a steep fall-off was found in the scattering crosssection at a perpendicular scale length of approximately 3 m in the case of multifrequency backscattering from an artificially heated ionospheric volume (*Minkoff*, 1974). In addition to its obvious impor-

tance in the determination of plasma processes which create the irregularities, the existence of a steep cut-off around a few m also has practical implications for pulse propagation within the ionosphere. For instance, if the scale length corresponding to the break-point is considered to be the effective inner scale of the power law spectrum, pulse broadening due to scattering in the 100-300 MHz band is expected to be 2 orders of magnitude less than in the case in which a monotonic power law spectrum extends all the way up to the Debye length (*Ossakow et al.*, 1978), implying that it is possible at times to have a cut-off at longer wavelengths. This does not contradict our postulate regarding a gaussian cut-off at the ion-gyro-radius. We leave open the possibility for additional factors which would prevent the formation of irregularities at the short wavelengths. In any case, from experimental as well as physical grounds we would not expect the k^{-2} power spectrum to extend beyond the ion gyro radius.

We hope that these preliminary results will provide an incentive for making multifrequency backscatter measurements at frequencies both above and below 50 MHz. We would also like to suggest the implementation of probes with 3 m resolution to determine the exact value of the break point and the actual wave number dependence at the short wavelength end of the spectrum.

Appendix

We assume an electron density one-dimensional wave number spectrum of equatorial irregularities to be of the form

$$\phi(k_x) = \frac{K}{1 + k_x^2 L_o^2} = \frac{\langle (\Delta N)^2 \rangle L_o}{\pi} \cdot \frac{1}{1 + k_x^2 L_o^2} \qquad \text{A-1}$$

in agreement with in-situ observations. In equation A-1, k_x is the wavenumber in a direction perpendicular to the magnetic field L_o is the outer scale of turbulence and K is a constant such that

$$\int_{-\infty}^{\infty} \phi(k_x)\, dk_x = \langle (\Delta N)^2 \rangle \qquad \text{A-2}$$

where $\langle (\Delta N)^2 \rangle^{1/2}$ is the rms electron density fluctuation.

For a one-dimensional wave-number spectrum of the form given in A-1, there corresponds a one-dimension correlation function

$$\rho(x) = \langle (\Delta N^2) \rangle \exp(-|x|/L_o). \qquad \text{A-3}$$

since they are a Fourier transform pair.

If we assume a rotational symmetric three-dimensional correlation function, R(r) infinitely elongated along the axis, we can write.

$$R(r) = \langle (\Delta N^2) \rangle \exp(-r_\perp / L_o). \qquad \text{A-4}$$

which, by three dimensional Fourier transformation, corresponds to a three-dimensional spectrum

$$\Phi(k) = \frac{1}{(2\pi)^3} \int d^3r\, e^{-ik \cdot r} R(r)$$

$$= \frac{\langle (\Delta N)^2 \rangle L_o^2}{2\pi} \cdot \frac{\delta(k_\parallel)}{[1 + k^2 L_o^2]^{3/2}} \cdot \qquad \text{A-5}$$

The subscripts $\parallel$ and $\perp$ above label the parallel and perpendicular magnitude of a vector component with respect to the magnetic field.

Next we derive the backscatter returns expected from irregularities with a spectrum given by A-5. For highly aspect sensitive irregularities, as the ones represented by A-5, we write

$$P = \frac{A}{(2\pi)^3} \int d\vec{x}^3 \left| I(x) \right|^2 \int d^3r\, e^{-ik(x) \cdot r} R(r) \qquad \text{(A-6)}$$

Where P is the backscatter power return and A is a constant of proportionality depending on system parameters and which includes the electron scattering cross section. We differ here with the standard text-book expression for P, in that we have written explicitly the antenna beam-pattern and radar pulse shape weighting function $F(x)^2$ in the integration over the scattering volume, and the spatial dependence of $k = k(x)$ in the typical Fourier transform term. Using the equality A-4 in A-6, we get, after integration

$$P = \frac{A \langle (\Delta N)^2 \rangle L_o^2}{2\pi [1 + k^2 L_o^2]^{2/3}} \cdot \frac{V}{\theta D} \cdot \frac{D}{k}, \qquad \text{A-7}$$

where V and θ are the effective scattering volume and beamwidth of the antenna. D is the average distance to the scattering volume.

On the other hand, the expression for the incoherent backscatter power, P_I, when the Debye length is much smaller than k^{-1} is:

$$P_I = AV \frac{N}{2(2\pi)^3} \qquad \text{A-8}$$

since under these conditions $\Phi(k) = \frac{N}{2(2\pi)^3}$ (e.g. *Salpeter* 1963).

The power ratio, P/P_I, is then given by:

$$P/P_I = \frac{8 \langle (\Delta N^2) \rangle L_o^2 \pi^2}{N [1 + k^2 L_o^2]^{3/2} \theta k} \qquad \text{A-9}$$

A more sophisticated and cumbersome approach, which takes into account the curvature of the wave front and which we will not reproduce here, gives the $\pi^{3/2}$ factor used in the text.

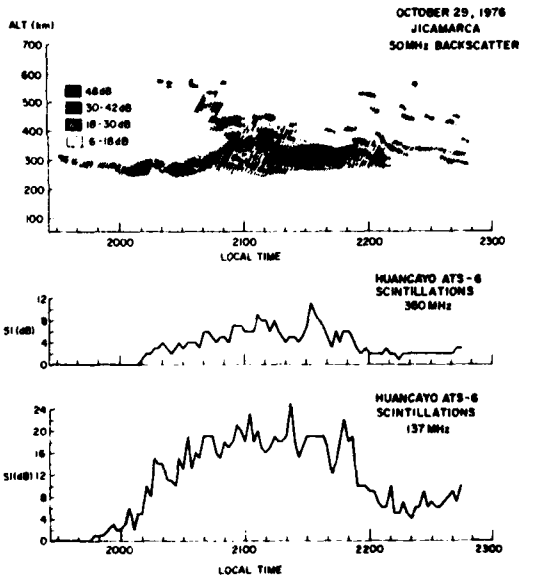

Figure 1. Correlated Backscatter and Scintillation Observations on October 29, 1976.

Acknowledgments

The AFGL equatorial irregularity campaign was conducted under the guidance of Jules Aarons. We wish to thank J.P. McClure for the backscatter map and J.P. Mullen for the Huancayo scintillation data. One of the authors (S.B.) was a NRC associate at AFGL during the course of this work. She wishes to thank the National Research Council for support and Santimay Basu for many useful discussions. The other author (R.F.W.) was a visiting scientist at the Max-Planck Institut für Aeronomie, Lindau, during the course of most of this work and would like to thank the institute for its hospitality.

References

Aarons, J., J. Buchau, S. Basu and J. P. McClure, The localized origin of equatorial F-region irregularity patches, *J. Geophys. Res.*, 83, 1659, 1978.

Balsley, B. B., G. Haerendel and R. A. Greenwald, Equatorial spread-F: Recent observations and a new interpretation, *J. Geophys. Res.*, 77, 5625, 1972.

Basu, S. and S. Basu, Correlated measurements of scintillations and in-situ F-region irregularities from Ogo-6, *Geophys. Res. Lett.*, *3*, 681, 1976.

Basu, Santimary, Sunanda Basu, J. Aarons, J. P. McClure and M. D. Cousins, On the co-existence of km- and m-scale irregularities in the nighttime equatorial F-region, *J. Geophys. Res.*, *83*, in press, 1978.

Basu, Santimay and J. Aarons, Equatorial irregularity compaigns Part I: correlated scintillation and radar backscatter measurements in October, 1976, *Report AFGL-TR-77-0264*, Air Force Geophysics. Laboratory, Hanscom AFB, Massachusetts, November 23, 1977.

Costa, E. and M. C. Kelley, Calculations of equatorial scintillations at VHF and GHz frequencies based on a new model of the disturbed equatorial ionosphere. *Geophys. Res. Lett.*, *3*, 677, 1976.

Dyson, P. L., J. P. McClure and W. B. Hanson, In-situ measurements of the spectral characteristics of F-region ionospheric irregularities, *J. Geophys. Res.*, *79*, 1495, 1974.

Fredricks, R. W. and F. V. Coroniti, Ambiguities in the deduction of rest frame fluctuation spectrums from spectrums computed in moving frames, *J. Geophys. Res.*, *81*, 5591, 1976.

Hudson, M. K. and C. F. Kennel, Linear theory of equatorial spread-F, *J. Geophys. Res.*, *80*, 4581 1975.

Minkoff, J., Radio frequency scattering from a heated ionospheric blume, 3, cross section calculations, *Radio Sci.*, *9*, 997, 1974.

Morse, F. A., B.C. Edgar, H. C. Koons, C. J. Rice, W. J. Heikkila, J. H. Hoffman, B. A. Tinsley, J. D. Winningham, A. B. Christensen, R. F. Woodman, J. Pomalaza and N. R. Teixeira, EQUION, an equatorial ionospheric irregularitu experiment, *J. Geophys. Res.*, *82*, 578, 1977.

Salpeter, E. E., Density fluctuations in a non-equilibrium plasma, *J. Geophys. Res.*, *68*, 1321, 1963.

Woodman, R. F. and C. LaHoz, Radar obsrvations of F-region equatorial irregularities, *J. Geophys. Res.*, *81*, 5447, 1976.

Yeh, K. C. and C. H. Liu, Pulse delay and pulse distortion by randon scattering in the ionosphere, paper presented at Agard Meeting, Cambridge, Ma., Oct. 3-7, 1977.

(Received May 22, 1978;
accepted June 12, 1978.)

On the Coexistence of Kilometer- and Meter-Scale Irregularities in the Nighttime Equatorial *F* Region

SANTIMAY BASU,[1] SUNANDA BASU,[1] JULES AARONS,[2] J. P. MCCLURE,[3] AND M. D. COUSINS[4]

Nighttime multifrequency scintillation and 50-MHz radar backscatter observations simultaneously performed over a nearly common ionospheric volume at the dip equator in Peru during March 1977 were used to study the relationship between the large-scale irregularities (~0.1–1 km) giving rise to scintillations and small-scale irregularities (3 m) causing 50-MHz backscatter. It is shown that during the generation phase of equatorial irregularities in the evening hours, the kilometer- and meter-scale irregularities coexist, whereas in the later phase, approximately an hour after the onset, the meter-scale irregularities decay but the large-scale ones continue to retain their high spectral intensities. Further, multistation scintillation observations from a host of geostationary satellites as well as from the Wideband satellite indicate that eastward-drifting irregularity structures detected around midnight cause significant scintillations at UHF and *L* band but generally fail to give rise to appreciable backscatter. Thus, contrary to expectations, it is possible to have even *L* band scintillations without any plume structure on backscatter maps. This indicates that at later local time a cutoff of the spectral intensity probably occurs at some scale length between 100 and 3 m. These observational results are discussed in the context of current theories of plasma instability in the equatorial ionosphere.

INTRODUCTION

The detection of spread *F*, ionospheric scintillations, and VHF radar backscatter in the nighttime equatorial ionosphere shows that irregularities with scale lengths as large as several kilometers and as small as a few meters may arise in the equatorial *F* region. In view of its importance in communications channel modeling as well as in the development of theories of irregularity generation, the problem of coexistence of irregularities with different scale lengths in a common ionospheric volume has recently engaged the attention of many workers.

As early as 1970, *Farley et al.* [1970] stated that strong irregularities observed by the Jicamarca radar were in general associated with scintillations. When the digital power mapping technique became available [*Woodman and La Hoz*, 1976], a preliminary comparison of such radar maps and scintillations during November–December 1975 made by *Basu et al.* [1977] indicated that plumelike structures on the maps were associated with intense scintillations in the VHF range at a nearby location.

Using the Atmosphere Explorer C satellite (AE-C), *McClure et al.* [1977] observed that large-scale bubbles of depleted ion concentration in the nighttime equatorial *F* region are associated with small-scale irregularities. These measurements provided the incentive for a more carefully coordinated equatorial irregularity campaign in Peru in October 1976. During this campaign, simultaneous VHF radar backscatter and ionospheric scintillation measurements were made near the magnetic equator in which the ionospheric volume explored by the radar and scintillation experiments had a minimum separation of nearly 300 km. The analysis of results obtained on one night when a single plume structure was observed by the Jicamarca radar showed that the irregularity patch in which 3-m irregularities were detected by the 50-MHz radar in the postsunset period drifted eastward and caused onsets of scintillations on two propagation paths located to the east of Jicamarca [*Aarons et al.*, 1978]. This result implied that the patch contained both 3-m and kilometer-scale irregularities which caused radar backscatter and scintillations, respectively, and the kilometer-scale irregularities persisted in a patch for at least several hours during the transit of the patch to various propagation paths involved in the scintillation experiment. Owing to the separations encountered, it was not possible to conclude whether the 3-m irregularities persisted in the patch at later periods of time when scintillations were detected.

In the course of the above campaign, scintillation measurements were made on October 29, 1976, with the ATS 6 satellite when the propagation path of the satellite to the Huancayo ground station intersected the ionospheric height at a point where the radar was performing backscatter measurements. The results of these simultaneous measurements over a common volume discussed by *Woodman and Basu* [1978] indicate that the temporal variations of 3-m and kilometer-scale irregularities were identical, establishing thereby the coexistence of irregularities with scale lengths covering nearly four decades.

A careful study of the radar maps published by *Woodman and La Hoz* [1976] and the maps acquired by us during October 1976, however, indicates that the extended 3-m irregularity structures with which strong scintillations are associated in general arise shortly after sunset. On the other hand, strong scintillation events are detected quite often even after midnight. *Basu and Aarons* [1977] concluded that during the October campaign there was a statistical preponderance of scintillation structures as compared to the extended 3-m irregularity structures. This seemed to indicate the possibility of having two types of equatorial irregularities, one type with significant spectral power at both kilometer and meter scales and the second with considerable power at kilometer-scale lengths with little or no power at 3 m.

The second equatorial campaign in March 1977 was planned to provide more definitive answers to the important problem of coexistence of kilometer and meter scales in the various phases of irregularity development and decay. The most important improvement during this campaign was the availability of scintillation and radar backscatter data pertaining to a common ionospheric volume for an extended

[1] Emmanuel College, Boston, Massachusetts 02115.
[2] Air Force Geophysics Laboratory, Hanscom Air Force Base, Bedford, Massachusetts 01731.
[3] University of Texas at Dallas, Richardson, Texas 75080.
[4] SRI International, Menlo Park, California 94025.

This paper is not subject to U.S. copyright. Published in 1978 by the American Geophysical Union.

Paper number 8A0516.

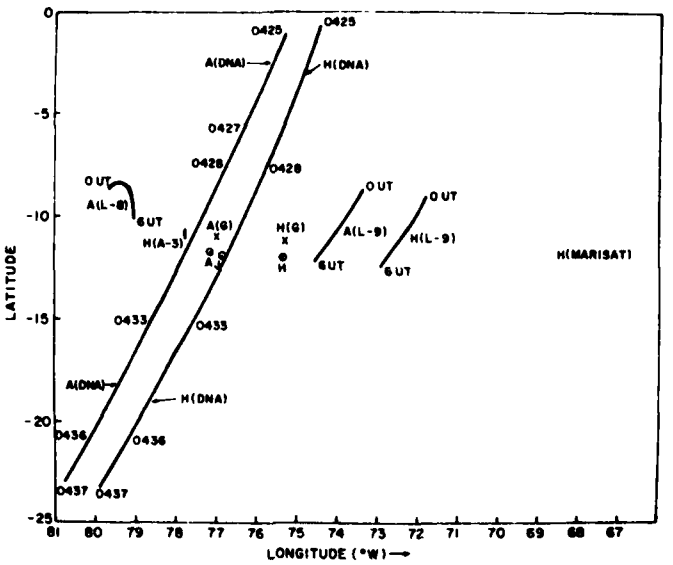

Fig. 1. Subionospheric positions (referred to an altitude of 400 km) of scintillation measurements on March 19–20, 1977. The ground stations at Ancon (A) and Huancayo (H) performing scintillation observations and Jicamarca (J) making radar backscatter observations are indicated in the diagram. The satellites LES 8, ATS 3, Goes 1, and LES 9 are abbreviated as L-8, A-3, G, and L-9, respectively.

period. We were also able to make scintillation measurements at closely spaced points both to the west and to the east of Jicamarca so that the evolution and decay of the drifting patches could be adequately monitored. With this unique data set we were able to demonstrate that it is possible to have two kinds of equatorial irregularities such as mentioned above. In this paper we discuss the results obtained on one day which seems to be fairly typical of the entire observation period. The implications of these measurements are also discussed in the context of current theories for the generation of equatorial irregularities.

OBSERVATIONS

On the night of March 19–20, 1977, 50-MHz radar backscatter observations were performed at Jicamarca (11.95°S, 76.86°W) near the magnetic equator in Peru. Radar power maps corresponding to three scattering volumes separated in the east-west direction by 6% of altitude were acquired by three antennas as discussed by *Basu et al.* [1977]. We shall present the maps obtained with the westernmost radar beam. When referred to 400-km altitude, the above location corresponds to a position which is approximately 30 km to the west of Jicamarca. Simultaneous 137-MHz scintillation measurements were made at Ancon (11.71°S, 77.15°W) with the Goes 1 satellite. The intersection of the propagation path from Ancon to Goes 1 with an ionospheric height of 400 km was located only 10 km to the east of the field line passing through the volume illuminated by the westernmost radar beam. However, the north-south (N-S) separation of the two volumes was approximately 50 km. In view of the field-aligned nature of equatorial *F* region irregularities, the relatively large N-S separation may not be of serious concern, while the much smaller east-west (E-W) separation assures that the two experiments were exploring a nearly common ionospheric volume.

Scintillation measurements were also performed with a host of geostationary satellites, LES 8, LES 9, and ATS 3, not only at Ancon but at Huancayo (11.97°S, 75.34°W) as well. The intersections of the propagation paths from these satellites to the two ground stations with an ionospheric height of 400 km are indicated in Figure 1. The subionospheric locations are specified in the diagram by the station name (A for Ancon and H for Huancayo) followed by the abbreviated name of the satellite. The ground stations at Jicamarca, Ancon, and Huancayo performing the radar and scintillation observations are shown by the dotted circles. Figure 1 also shows the subionospheric (400 km) tracks of the orbiting Wideband satellite as viewed from Ancon and Huancayo on March 19–20. The Ancon station was equipped with coherent phase-locked loop receivers and recorded both phase and amplitude scintillations at VHF (138 MHz), seven closely spaced frequencies at UHF centered at 413 MHz, and *L* band (1239 MHz) from the Wideband satellite [*Fremouw et al.*, 1978]. The station at Huancayo recorded only the amplitude scintillations of the transmissions at 138 and 413 MHz.

RESULTS

In Figure 2 we show the results of simultaneous 50-MHz radar backscatter observations at Jicamarca and 137-MHz scintillation measurements at Ancon with the Goes 1 satellite made on March 19, 1977, between 1900 and 2300 LT. The top panel shows a radar power map of 3-m irregularities indicating the temporal variation of their range and intensity. The range scale is provided by the ordinate on the left-hand side of the diagram, while the tone of the map signifies the intensity of the backscattered echoes in the range of 6–48 dB above the approximate maximum incoherent scatter level. A complete description of the digital power mapping technique has been outlined by *Woodman and La Hoz* [1976]. The bottom panel shows the temporal variation of scintillation index in decibels, *SI* (dB), scaled manually from the chart records at 2-min intervals [*Whitney et al.*, 1969].

The top panel in Figure 2 shows that the radar started to detect weak irregularities in thin layers for the first time in the evening at 1938 LT. The first plume structure developed shortly thereafter at about 1950 LT. A series of plume developments occurred up to 2040 LT, with the later plumes having a low extent in altitude. Later, the backscatter echoes arose from progressively thinner irregularity layers. Between 2110 and 2210 LT, weak patchy backscattering regions above a weak and thin layer were observed. From the bottom panel we find that the sharp onset of strong scintillations was very well matched in time with the development of strong 3-m irregularities at 1950 LT. Soon after onset, scintillation levels as high as 20 dB were encountered. It is interesting to note that although the plume structures were absent after 2040 LT and the 3-m irregularity structures were thinning out, a high level of scintillation was maintained up to 2114 LT. It is also difficult to associate the large increase of scintillation observed after 2114 LT with the weak and patchy 3-m irregularities. The first scintillation structure ended at 2230 LT when the radar map was totally free of all traces of 3-m irregularities in the F region. A study of the above event indicated that in the generation phase during the late evening hours, the kilometer- and meter-sized irregularities evolve together and coexist whereas in the later phase, approximately an hour after the onset, the meter-sized irregularities decay but the large-scale irregularities responsible for scintillations continue to retain their high spectral intensities.

Another distinctive event was recorded later during this night and is illustrated in Figure 3. From the bottom panel we see that the second scintillation event of the evening was detected at Ancon on its propagation path to the Goes 1 satellite at 2300 LT. The scintillation event was rather strong, attaining levels as high as 22 dB at 137 MHz, and decayed at about 0100 LT. A study of the top panel indicates that only very weak 3-m irregularity structures were detected between 2300 and 0000 LT and none at all between 0000 and 0100 LT. It appears that the irregularity structures detected during the late nighttime hours had little spectral power at short scale lengths, although the spectral power at large scale lengths remained high, giving rise to saturated VHF scintillations.

In order to investigate if the irregularity power spectra in the scale length range responsible for amplitude fluctuations have undergone any change, we obtained the power spectra of amplitude scintillations for both these cases, namely, strong VHF scintillations in the presence of 3-m irregularities as illustrated in Figure 4*a* and strong scintillations in the absence of 3-m irregularities shown in Figure 4*b*. The scintillation data acquired on FM analog tapes were digitized at 30 samples/s,

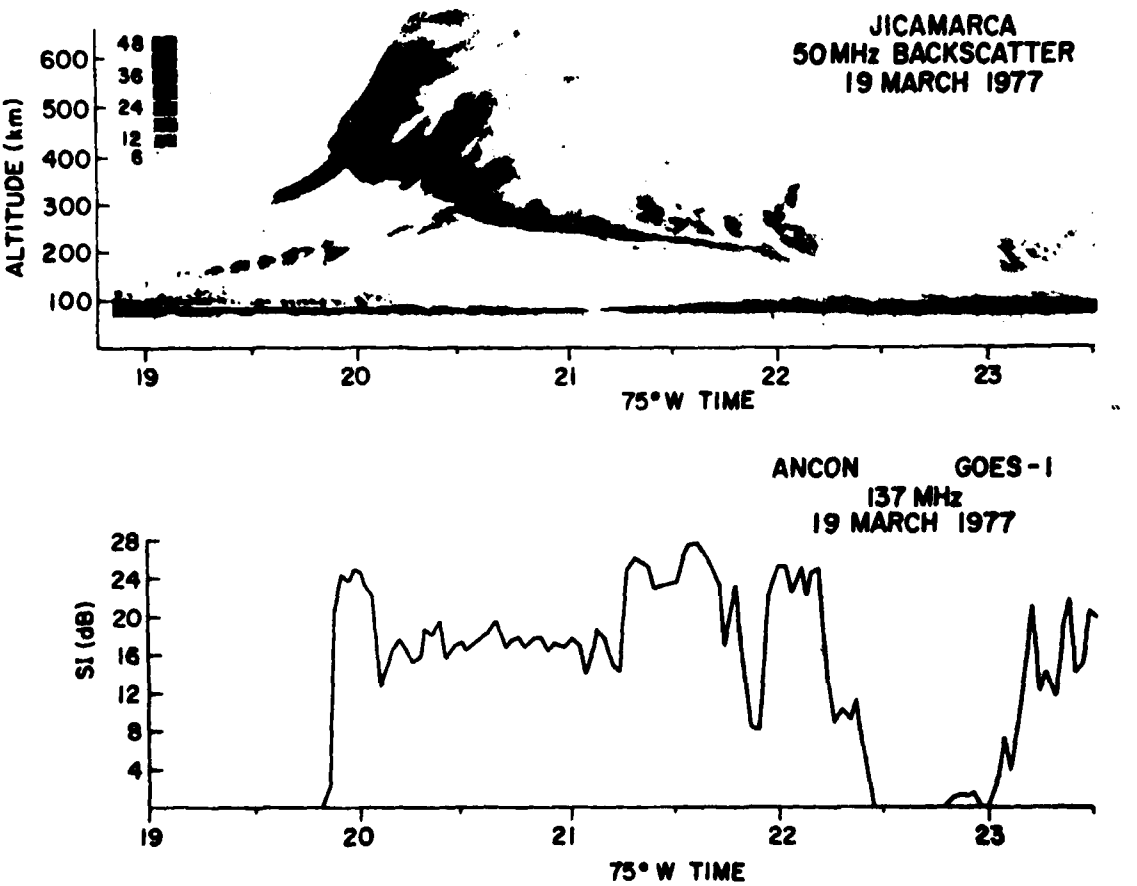

Fig. 2. Temporal variation of 50-MHz radar backscattered power obtained at Jicamarca and scintillation index *SI*, in decibels, of 137-MHz transmissions from the Goes 1 satellite recorded at Ancon on March 19, 1977, during 1900–2300 LT.

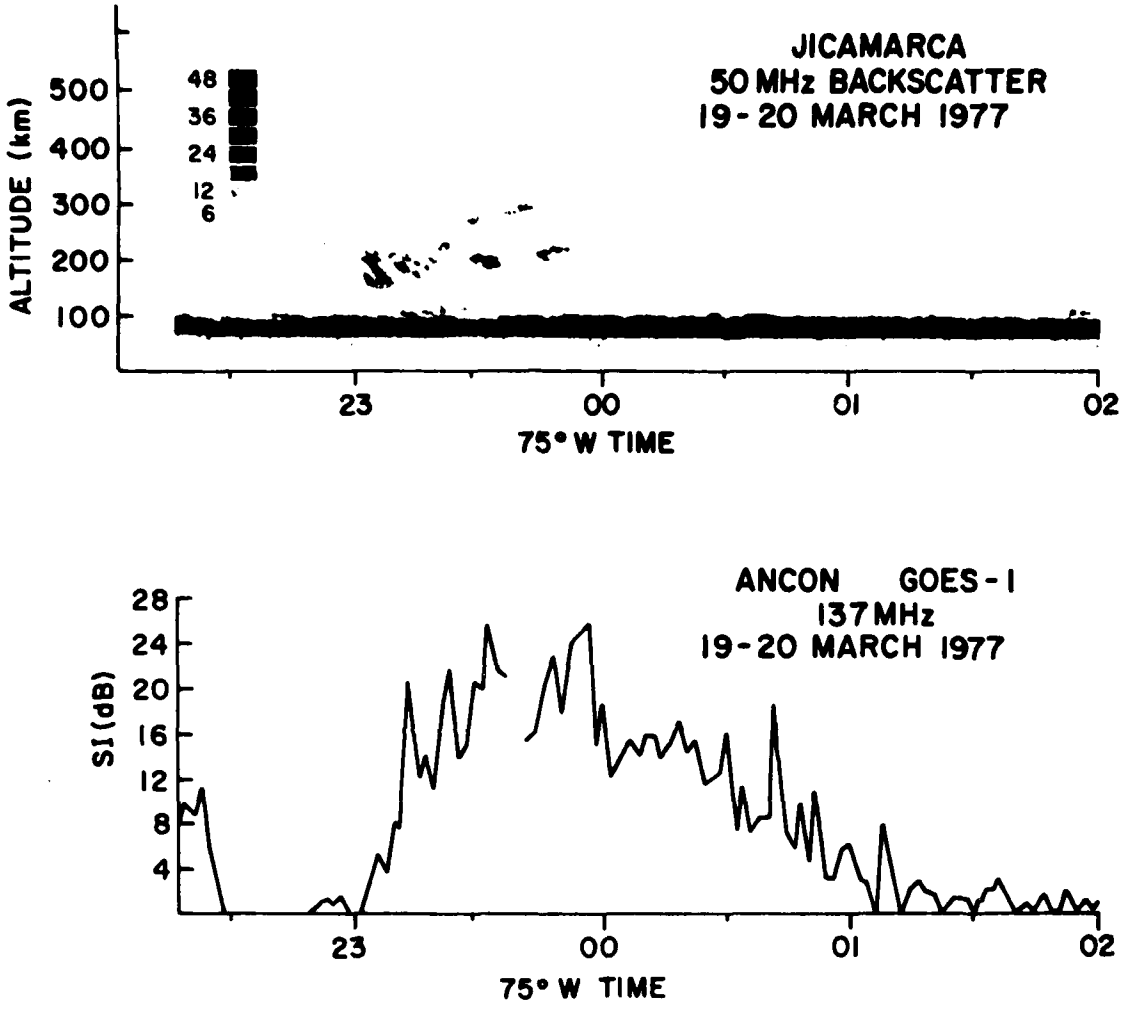

Fig. 3. Comparison of radar backscattered power and scintillation index *SI*, in decibels, as in Figure 2, on March 19–20, 1977, during 2300–0200 LT. Note that weak and patchy 3-m irregularities shown in the top panel are associated with intense scintillation activity in the bottom panel.

and the spectra for 7.5-min data samples were obtained by the use of a fast Fourier transform algorithm. The structure obtained around 3 Hz was generated by a subharmonic of the satellite spin and the multilobed satellite antenna pattern. Considering that the 95% confidence interval of power estimate is approximately 6 dB, the average high-frequency (ν) slopes of the power spectra in Figures 4*a* and 4*b* are very close to ν^{-4}. The diffraction scale length (Λ) on the ground is related to the frequency scales (ν) in Figures 4*a* and 4*b* by the drift speed (v) of the irregularities as $\Lambda = (v/\nu)$.

However, the values of the S_4 index of scintillation corresponding to Figures 4*a* and 4*b* were 0.83 and 0.73, respectively, so that both the spectra pertained to strong scatter conditions. Under such conditions, it is not possible to relate the diffraction scale lengths on the ground to irregularity scale lengths in the ionosphere in a precise manner [*Yeh et al.*, 1975]. Thus even though drift speed measurements are available from spaced receiver scintillation observations performed at the nearby ground station at Ancon [*Whitney*, 1978], it is not possible to derive the irregularity characteristics from the scintillation spectra. The similarity in the spectral forms in Figures 4*a* and 4*b* can only indicate in general terms that no drastic variation of irregularity power spectra occurred in the scale length range (~1 km to 100 m) which is responsible for VHF scintillations.

It is interesting to note that while the second scintillation event (cf. Figure 3) at VHF was being recorded at Ancon on the propagation path to the Goes 1 satellite, a transit of the Wideband satellite occurred. The subionospheric tracks of the satellite as viewed from Ancon and Huancayo have been illustrated in Figure 1 and designated as A(DNA) and H(DNA), respectively. We shall primarily discuss A(DNA) results acquired with the SRI International receiver providing both phase and amplitude scintillation data over a wide range of frequencies. Scintillations both in amplitude and in phase were recorded throughout the transit, but we shall concentrate

our attention to the interval between 0427 UT (corresponding to 75°W, time of 2327 LT) and 0428 UT, labeled on the track. Careful magnetic field line mapping indicated that at 0427.5 UT the 400-km subionospheric location of the A(DNA) intersected the field line passing over Jicamarca. In Figure 5, we illustrate the amplitude scintillation index S_4 and rms phase fluctuation ϕ_{rms} at the observing frequencies during a 20-s interval beginning 0427.5 UT. The inverse frequency (f) dependence of ϕ_{rms}, expected theoretically, is indicated by the solid line passing through the data point corresponding to 413 MHz, the UHF carrier frequency. For a three-dimensional irregularity power spectrum of power law exponent 4, the amplitude scintillation index S_4 is expected to show $f^{-1.5}$ dependence [*Rufenach*, 1974] under weak scatter conditions. This is indicated by the dotted line. The data points agree well with the theoretical curves except for the S_4 data point at VHF which obviously violates weak scatter conditions. It should be noted that even significant L band scintillation was recorded at this time while in the VHF band an S_4 index of 0.78 was obtained. *Fremouw et al.* [1978] have noted that in the L band $S_4 \geq 0.02$ may be considered significant for these Wideband measurements. It may be observed from Figure 3 that during the above scintillation event, only weak (< 12 dB) and very fragmentary signatures of the backscatter echoes could be recorded.

Woodman and Basu [1978] have recently made a quantitative comparison of 360-MHz scintillation and 50-MHz radar backscatter measurements at Jicamarca. They postulated a Gaussian type of cutoff near the ion gyroradius which is of the order of 3 m at F region heights to bring scintillation and backscatter measurement into agreement. They showed that an S_4 index of 0.4 at 360 MHz may correspond to the observed 40-dB radar backscatter from an irregularity layer of a thickness of 200 km. Similar computations made in the present case under study indicate that $S_4 = 0.18$ at 413 MHz should have been accompanied by at least 26-dB radar backscatter from a similarly extended irregularity layer, in contrast to the observed 12-dB backscatter from fragmentary patches. This result implies that the irregularity structures observed near midnight are characterized by a spectral cutoff at wavelengths longer than the ion gyroradius, probably in the vicinity of tens of meters.

In Figure 6 we illustrate the results of all scintillation measurements made on this night at the two ground stations, Ancon and Huancayo, with various geostationary satellites.

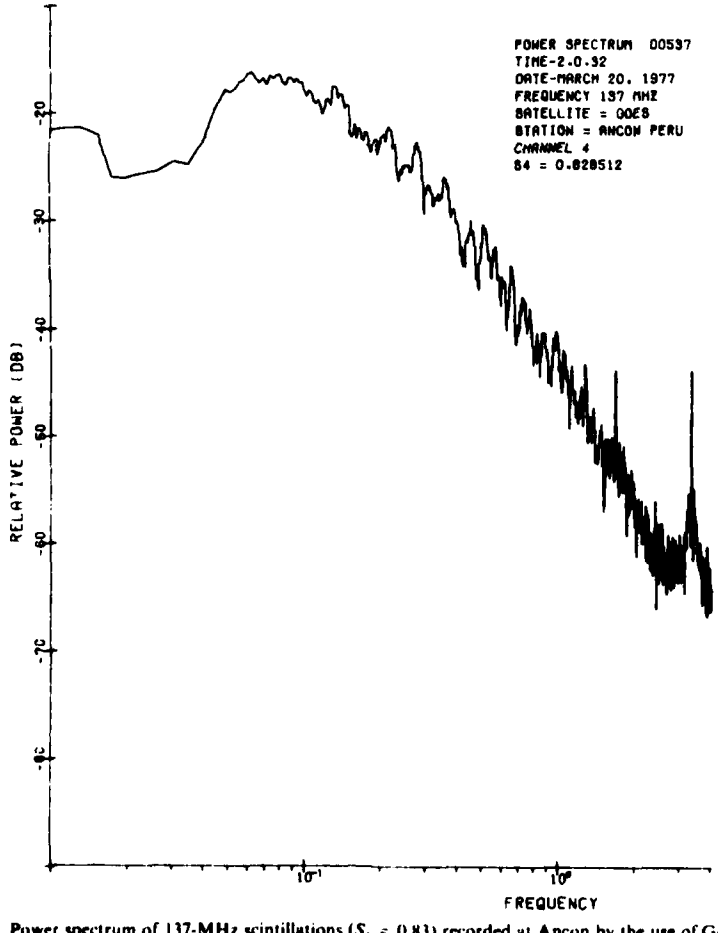

Fig. 4a. Power spectrum of 137-MHz scintillations ($S_4 = 0.83$) recorded at Ancon by the use of Goes 1 transmissions between 0200 and 0207.5 UT on March 20, 1977 (2100–2107.5 LT on March 19, 1977). The power spectrum corresponds to the period when intense 50-MHz radar backscatter was obtained.

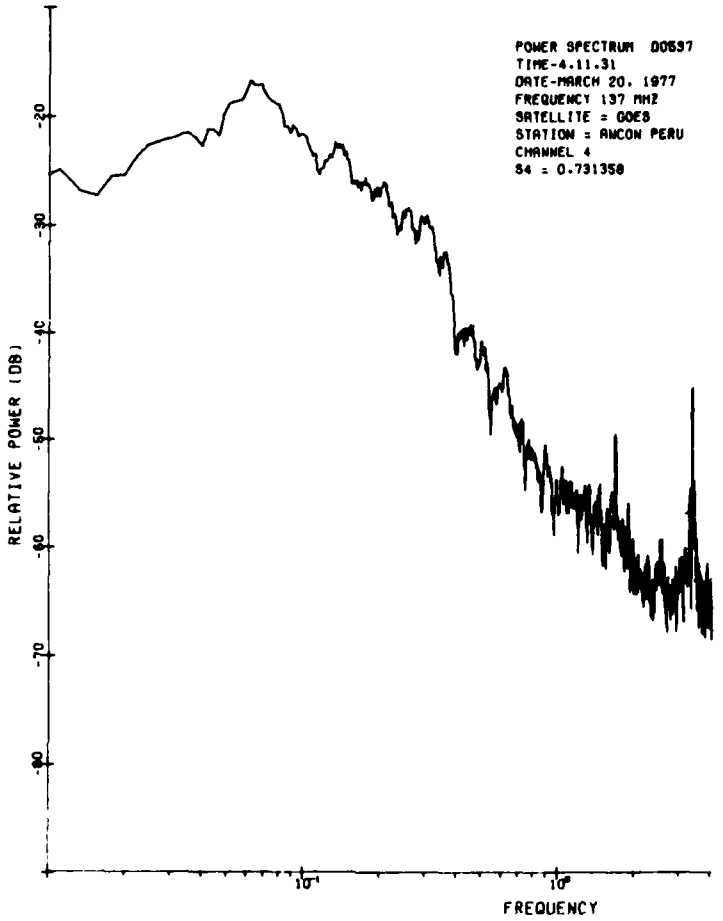

Fig. 4b. As in Figure 4a for the period 0411–0418.5 UT on March 20, 1977 (2311–2318.5 LT on March 19), when S_4 = 0.73 was recorded. The period of scintillation corresponds to weak and patchy 50-MHz radar backscattered power.

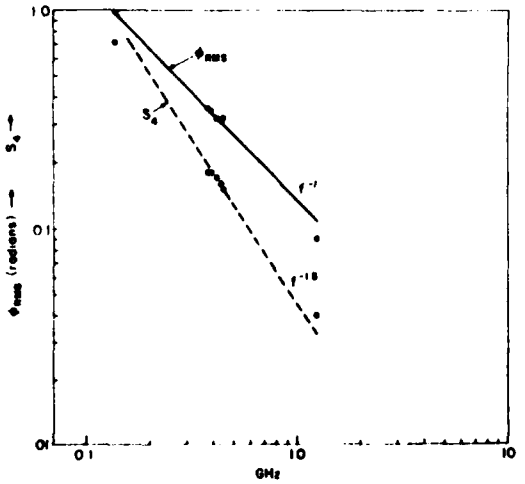

Fig. 5. Frequency dependence of rms phase ϕ_{rms} and S_4 index of Wideband satellite data recorded at Ancon on March 19, 1977, between 2327.5 and 2327.8 LT.

The panels from top to bottom in Figure 6 are arranged in the order of decreasing west longitude of the subionospheric position of scintillation measurements. From Figure 1 it may be noted that subionospheric locations of these measurements spanned a longitude interval of nearly 12° near the magnetic equator. The initial gap in the results shown in panel 1 was caused by an interruption of beacon transmission from the LES 8 satellite. The remaining panels (2–7) indicate that the onset of scintillations at different locations occurred between 0000 and 0100 UT. Considering the different longitudes of all these subionospheric locations, the onset of scintillations is found to have occurred within 4 min of 1940 LT. The local time dependence of scintillation onset on this night should not, however, be taken as a general rule, since we have observed cases when the irregularity generation has been localized in space rather than in local time [*Aarons et al.*, 1978]. In view of the consistent eastward drift speed of irregularity patches at night, the temporal variation of scintillation at an equatorial station is dictated by the localized generation, in space or time, the eastward drift of irregularity patches, and the lifetime of these drifting patches. The successive panels of Figure 6 have to be viewed in this context.

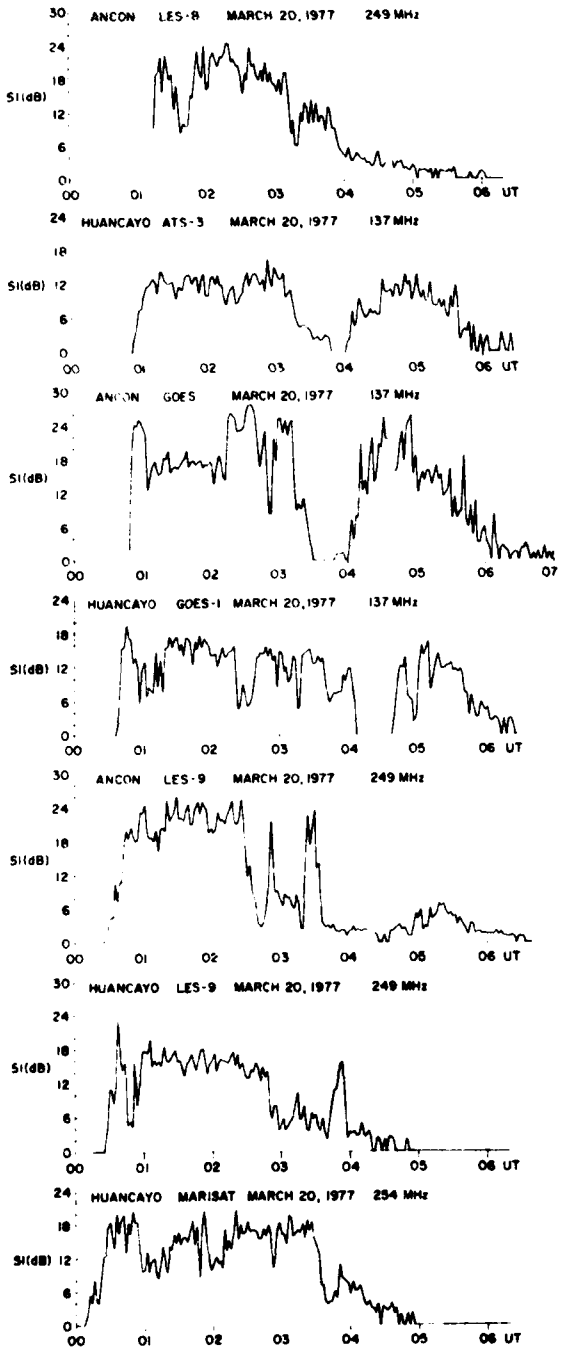

Fig. 6. Temporal variation of scintillation index *SI*, in decibels, recorded at Ancon and Huancayo on March 19–20, 1977, by the use of transmissions from various geostationary satellites. The panels are arranged in order of decreasing west longitude of ionospheric intersection points of the various ray paths as shown in Figure 1.

Discussions

We have provided evidence for the existence of at least two phases of irregularity evolution in the equatorial *F* region. In the development phase during the postsunset hours, irregularities covering the scale length range of tens of kilometers to 3 m evolve simultaneously. Near-saturated VHF-UHF scintillations are observed in this phase when strong radar backscatter is detected from an extended altitude range. The recently compiled statistics of *L* band (1.54 GHz) scintillations observed at Huancayo also indicate that the occurrence maximum of gigahertz scintillations is obtained in this development phase [*Mullen et al.*, 1978]. The evolution of such thick irregularity layers takes place within tens of minutes. The generation of irregularities covering 3–4 decades of scale lengths has been explained by invoking a hierarchy of instability mechanisms starting at the long wavelength end with the gravitational Rayleigh-Taylor instability [*Haerendel*, 1974; *Hudson and Kennel*, 1975; *Costa and Kelley*, 1978*a*, *b*]. The generation of irregularity patches extended both in altitude and in E-W direction has recently been explained by *Kelley and Ott* [1978] by adopting the theoretical analysis of a rising ionospheric bubble presented by *Ott* [1978]. Motivated by the sudden 'bite outs' of plasma density observed by in situ measurements [*Kelley et al.*, 1976; *Morse et al.*, 1977; *Hanson and Sanatani*, 1973; *McClure et al.*, 1977], *Ott* [1978] used a sharp boundary model and showed that the basic equations applicable to the rising bubble are identical with those governing the behavior of a two-dimensional fluid. Using these results, *Kelley and Ott* [1978] showed that upwelling plasma depleted regions or bubbles continually stir the medium and not only fill the wake with density irregularities in the presence of density gradients but also the regions (in the E-W direction) between the bubbles through a cascading process.

Following the development phase, the meter-scale irregularities are observed to decay, while significant kilometer-scale structures persist and continue to produce strong scintillations at VHF. *Kelley and Ott* [1978] have shown that in the late phase the dissipation scale moves to smaller k values so that the smallest-scale structures disappear first.

The irregularity structures that cause scintillations around local midnight are conspicuous by the absence of any significant spectral power at 3-m scale lengths. However, sufficient spectral power is available at long scale lengths to cause not only strong VHF/UHF scintillations but *L* band scintillations as well. It is of some interest to note that 6300-Å airglow measurements made on board the aircraft flown by the Air Force Geophysics Laboratory indicated the presence of regions with depleted ionization near Jicamarca corresponding to both the early evening and the near-midnight scintillation events (J. Buchau, private communication, 1978). Thus it is possible to detect ionization depletions and strong scintillations in the absence of extended 3-m irregularity structures or 'plumes.' A similar irregularity structure was detected on March 30, 1977, at 2314 LT (75°W time), which caused scintillation as high as 7 dB (S_4 = 0.36) at *L* band and 1 dB (S_4 = 0.07) at *S* band and yet failed to give rise to any appreciable VHF radar backscatter. It is important to note that even after considering the sharp cutoff near the ion gyroradius proposed by *Woodman and Basu* [1978] the above scintillation levels are expected to be associated with a relatively thick layer of moderately strong 3-m irregularities. Thus it seems that the irregularity structures which exist near midnight are characterized by a spectral cutoff in the vicinity of tens of meters.

The nature of the irregularity spectrum at short scale lengths needs much further study. It will be worthwhile to make observations of gigahertz scintillations in close proximity to Jicamarca to determine the relationship of irregularity scale lengths of ~100 m with the 3-m scale length during the various phases of irregularity evolution. In addition, rocket measure-

ments of the fully developed topside irregularity spectrum would be extremely useful in bridging the gap between the above scale length regimes.

Acknowledgments We wish to thank H. Whitney and J. P. Mullen for their observational efforts at Ancon and Huancayo. We acknowledge the assistance and hospitality of the personnel of the Instituto Geofisico del Perù during the campaigns. The work at the University of Texas at Dallas was supported by NSF grant ATM76-17351. This research was sponsored in part by the Defense Nuclear Agency Subtask L25AAXHX633, entitled 'Communications Data Base.'

The Editor thanks R. Woodman and M. C. Kelley for their assistance in evaluating this paper

REFERENCES

Aarons, J., J. Buchau, Santimay Basu, and J. P. McClure, The localized origin of equatorial *F* region irregularity patches, *J. Geophys. Res., 83*, 1659, 1978.

Basu, Santimay, and J. Aarons, Equatorial irregularity campaigns: Part I, Correlated scintillation and radar backscatter measurements in October, 1976, *Tech. Rep. AFGL-TR-77-0264*, Air Force Geophys. Lab., Hanscom Air Force Base, Bedford, Mass., 1977.

Basu, Sunanda, J. Aarons, J. P. McClure, C. La Hoz, A. Bushby, and R. F. Woodman, Preliminary comparisons of VHF radar maps of *F*-region irregularities with scintillations in the equatorial region, *J. Atmos. Terr. Phys., 39*, 1251, 1977.

Costa, E., and M. C. Kelley, Evidence for and development of a 2-step theory for equatorial spread *F*, *J. Geophys. Res., 83*, in press, 1978*a*.

Costa, E., and M. C. Kelley, Linear theory for collisionless drift mode waves with wavelengths near the ion gyroradius, *J. Geophys. Res., 83*, in press, 1978*b*.

Farley, D. T., B. B. Balsley, R. F. Woodman, and J. P. McClure, Equatorial spread *F*: Implications of VHF radar observations, *J. Geophys. Res., 75*, 7199, 1970.

Fremouw, E. J., R. L. Leadabrand, R. C. Livingston, M. D. Cousins, C. L. Rino, B. C. Fair, and R. A. Long, Early results from the DNA Wideband satellite experiment—Complex signal scintillation, *Radio Sci., 13*, 167, 1978.

Haerendel, G., Theory of equatorial spread-*F*, report, Max-Planck-Institut für Phys. und Astrophys., Garching, West Germany, 1974.

Hanson, W. B., and S. Sanatani, Large N_i gradients below the equatorial *F* peak, *J. Geophys. Res., 78*, 1167, 1973.

Hudson, M. K., and C. F. Kennel, Linear theory of equatorial spread *F*, *J. Geophys. Res., 80*, 4581, 1975.

Kelley, M. C., and E. Ott, On the role of two-dimensional turbulence in equatorial spread *F*, *J. Geophys. Res., 83*, in press, 1978.

Kelley, M. C., G. Haerendel, H. Kappler, A. Valenzuela, B. B. Balsley, D. A. Carter, W. L. Ecklund, C. W. Carlson, B. Hausler, and R. Torbert, Evidence for a Rayleigh-Taylor type instability and upwelling of depleted density regions during equatorial spread-*F*, *Geophys. Res. Lett., 3*, 448, 1976.

McClure, J. P., W. B. Hanson, and J. H. Hoffman, Plasma bubbles and irregularities in the equatorial ionosphere, *J. Geophys. Res., 82*, 2650, 1977.

Morse, F. A., B. C. Edgar, H. C. Koons, C. J. Rice, W. J. Heikkila, J. H. Hoffman, B. A. Tinsley, J. D. Winningham, A. B. Christensen, R. F. Woodman, J. Pomalaza, and N. R. Teixeira, Equion, an ionospheric irregularity experiment, *J. Geophys. Res., 82*, 578, 1977.

Mullen, J. P., A. Bushby, J. Lanat, and J. Pantoja, Gigahertz scintillation at the magnetic equator, in *Proceedings of the 1978 Symposium on the Effect of the Ionosphere on Space and Terrestrial Systems*, Naval Research Laboratory, Washington, D. C., 1978.

Ott, E., Theory of Rayleigh-Taylor bubbles in the equatorial ionosphere, *J. Geophys. Res., 83*, 2066, 1978.

Rufenach, C. L., Wavelength dependence of radio scintillation: Ionosphere and interplanetary irregularities, *J. Geophys. Res., 79*, 1562, 1974.

Whitney, H. E., Spaced receiver measurements of intense equatorial scintillations, in *Proceedings of 1978 Symposium on the Effect of the Ionosphere on Space and Terrestrial Systems*, Naval Research Laboratory, Washington, D. C., 1978.

Whitney, H. E., J. Aarons, and C. Mailk, A proposed index for measuring ionospheric scintillations, *Planet. Space Sci., 17*, 1069, 1969.

Woodman, R. F., and Sunanda Basu, Comparison between in-situ spectral measurements of equatorial *F*-region irregularities and backscatter observations at 3m wavelength, *Geophys. Res. Lett., 5*, in press, 1978.

Woodman, R. F., and C. La Hoz, Radar observations of *F* region equatorial irregularities, *J. Geophys. Res., 81*, 5447, 1976.

Yeh, K. C., C. H. Liu, and M. Y. Youakim, A theoretical study of the ionospheric scintillation behavior caused by multiple scattering, *Radio Sci., 10*, 97, 1975.

(Received March 2, 1978;
revised May 10, 1978;
accepted May 11, 1978.)

Radio Science, Volume 14, Number 3, pages 471-485, May-June 1979

A review of recent observations of equatorial scintillations and their relationship to current theories of *F* region irregularity generation

Sunanda Basu

Emmanuel College, Boston, Massachusetts 02115

M. C. Kelley

School of Electrical Engineering, Cornell University, Ithaca, New York 14853

(Received May 22, 1978.)

Our understanding of transionospheric radio wave propagation problems associated with irregularities in the nighttime equatorial *F* region has grown enormously in the past few years. This has been achieved by making coordinated phase and amplitude scintillations from a host of geostationary and orbiting satellites and multitechnique irregularity measurements. The variety of supporting measurements include radar backscatter, in situ irregularity observations by rockets and satellites, and airglow and ionosonde observations aboard aircraft. Because of the great volume of work in this field the scope of the present review is limited to a description of these recent coordinated observations and a discussion of the relevant theories of irregularity generation. An attempt is then made to explain some aspects of equatorial scintillations on the basis of these new theoretical developments.

1. INTRODUCTION

Four decades after the discovery of the phenomenon called 'equatorial spread *F*' [*Booker and Wells*, 1938], the general problem of nighttime equatorial *F* region irregularities continues to be a fascinating one to theoretical and experimental geophysicists. This problem is also one of serious concern to communications engineers, as it is well known that these irregularities cause amplitude scintillation which can degrade the performance of satellite communication links. More recently, it has become clear that naturally occurring phase scintillation can impair the performance of satellite systems that use synthetic aperture processing to achieve high angular resolution.

In our first review of this subject, presented at the Fifth International Symposium of Equatorial Aeronomy in August 1976 and recently published [*Basu and Kelley*, 1977], we concluded that large-scale convective upwelling of the equatorial plasma was responsible for the most intense scintillation. Evidence for this upwelling process, which carries regions of low plasma density 'bubbles' into the high-density topside region, has come from rocket experiments [*Kelley et al.*, 1976; *Morse et al.*, 1977] from radar studies [*Woodman and LaHoz*, 1976], and in a rather definitive manner from satellite measurements [*McClure et al.*, 1977]. One example of such topside 'holes' or 'bubbles' observed with the AE-C satellite is shown in Figure 1. The ion drift meter data show that the plasma inside the bubbles was moving upward and to the west in the plasma rest frame.

The connection between intense scintillations and the bubble phenomena postulated by *Basu and Kelley* [1977] was, however, based on inference rather than direct simultaneous measurement. For example, *Costa and Kelley* [1976] calculated the scintillation effects of pure bottomside equatorial spread *F*. They used the plasma density profiles shown in Figure 2 obtained by a sounding rocket and concluded that only modest scintillation would result at VHF frequencies, with negligible effect at gigahertz frequencies. On the other hand, using topside in situ irregularity data from Ogo 6 shown in Figure 3, *Basu and Basu* [1976] showed that saturated VHF scintillation and moderate gigahertz scintillation can be explained on the basis of large amplitude irregularities with large outer scales in an environment of high electron density [*McClure and Hanson*, 1973] which are distributed in thick

Copyright © 1979 by the American Geophysical Union

0048-6604/79/0506-0471$01.00

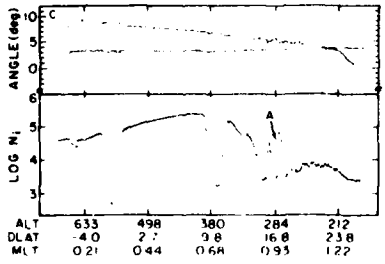

Fig. 1. Ion drift meter data from AE-C orbit 2282. The observed pitch and yaw angles are shown in the upper and lower curves of the top panel, and the total density on the bottom. Positive angles correspond to ions moving up or left with respect to the spacecraft [after *McClure et al.*, 1977].

layers [*Basu et al.*, 1977]. An alternate explanation has been offered by *Booker* [1975], who pointed out that low-level irregularities threading the plasmasphere could also create the equatorial scintillations.

Since that review, significant new information on scintillations has been obtained via dedicated experiments aimed at testing these hypotheses and relating the scintillation measurements to simultaneous multitechnique probing of equatorial irregularities. These results are summarized in the next section, which is followed by a discussion in section 3 of recent theoretical studies of equatorial irregularities and their relationship to scintillations. In the concluding section we attempt to synthesize theory and observation.

2. RECENT EQUATORIAL SCINTILLATION OBSERVATIONS

In this section we shall present two major experimental efforts undertaken by various groups to study the nature of equatorial scintillations and their relationship to other observable irregularity parameters. The first is a joint campaign conducted by the Air Force Geophysics Laboratory (AFGL), the Instituto Geophysico del Peru (IGP), the University of Texas at Dallas (UTD), and the SRI International (SRII) near the magnetic equator in Peru. The second is the DNA Wideband satellite experiment conducted by SRII at two equatorial stations, which has provided the first comprehensive measurements of phase scintillations.

2.1 *Joint equatorial irregularity campaigns in Peru.* An intensive study of nighttime electron density irregularities in the equatorial ionosphere was performed in October 1976 and March 1977 by conducting simultaneous radar and scintillation measurements near the magnetic dip equator in Peru. The 50-MHz radar observations were made at Jicamarca, and scintillation measurements were performed at the nearby ground stations of Ancon and Huancayo by receiving VHF transmissions from geostationary and orbiting satellites. In addition, the AFGL aircraft was employed to make on-board scintillation, ionosonde, and airglow measurements to provide spatial configuration of irregularity patches as well as to determine the existence of density depletions indicated by in situ measurements. Simultaneous in situ electron den-

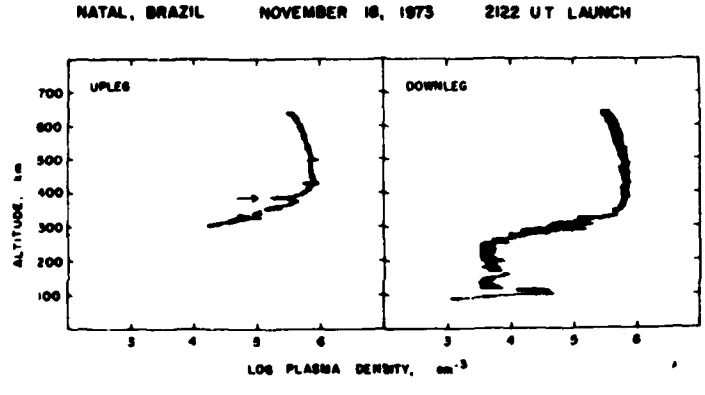

Fig. 2. Upleg and downleg plasma density profiles obtained on a sounding rocket during equatorial spread *F*. The arrow shows the locations of a deep depression in plasma density [after *Kelley et al.*, 1976].

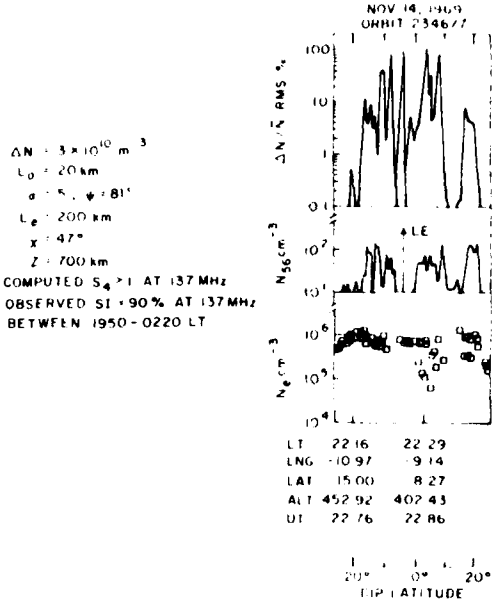

Fig. 3. Oxo 6 orbit showing equatorial electron density and rms amplitude of ionospheric irregularities in the Legon, Ghana, longitude sector during a strong VHF scintillation event. The scintillation model parameters are also indicated [after *Basu and Basu*, 1976].

sity data, similar to those shown in Figure 1, were obtained from the AE-E satellite. The multistation scintillation measurements were used to study the localized origin of large-scale irregularity patches, their drift speed, spatial extent, and lifetime in the equatorial ionosphere. The simultaneous radar and scintillation observations also provided information on the relationship between the meter- and kilometer-sized irregularities giving rise to the radar backscatter and VHF-UHF scintillations, respectively. Much new information became available as a result of this major effort, and many publications and presentations have been made based on these correlated data sets. These are summarized below with specific references.

1. There is great variability of irregularity occurrence from one night to another. On certain nights, such as on October 16–17, 1976, a single irregularity patch evolved at a particular location and then drifted eastward for a period dictated by its lifetime, as discussed by *Aarons et al.* [1978]. On some other nights, a series of irregularity patches with a large-scale quasi-periodicity was observed. A good example of such a configuration was obtained on October 19–20, as shown in Figure 4, taken from the detailed report on the October campaign done by *Basu and Aarons* [1977]. Figure 5, also taken from the report, shows the respective positions for the observations. The important point to note from the radar map is that a relatively thin layer of bottomside irregularities appeared at 1950 LT, which by 2015 developed into a plume structure extending several hundred kilometers into the topside. A second plume developed at 2140 LT. The drifting plume structures caused severe scintillations (>20 dB) at the ground stations, with periods of 4- to 6-dB scintillation caused by the bottomside structures observed in between the plumes. It is interesting to note that HF forward scatter experiments in the equatorial region had earlier obtained evidence of irregularity patches existing in quasi-periodic patterns [*Rottger*, 1976]. On yet other nights, there were no irregularities within the 900-km east-west coverage provided by the Jicamarca radar and various satellites.

2. Although the irregularity patches occur after local sunset, these are found to evolve either to the west or to the east of any specific station, signifying that local conditions and not just local time dictate the generation of irregularities [*Basu and Aarons*, 1977].

3. The large-scale irregularity patches are found to consistently drift eastward between 1900 and 2400 LT, with a speed ranging between 90 and 140 m/s. If the temporal variation of scintillation is combined with the drift speed, the east-west dimensions of the patches are found to range typically between 200 and 400 km, although some are larger [*Basu and Aarons*, 1977].

4. Another important aspect of the campaign was the determination of the relationship between the relatively large scale irregularities that cause scintillation (~1 km to 100 m) and the small-scale irregularities that cause 50-MHz backscatter (3 m). *Woodman and Basu* [1978], using the simultaneous backscatter and scintillation data obtained from a nearly common ionospheric volume, found that both these types coexisted in the developing phase of the irregularities. However, they also showed that if the commonly accepted k^{-5} power law irregularity spectrum [*Dyson et al.*, 1974] was extended to the Jicamarca backscatter wave number, a discrepancy

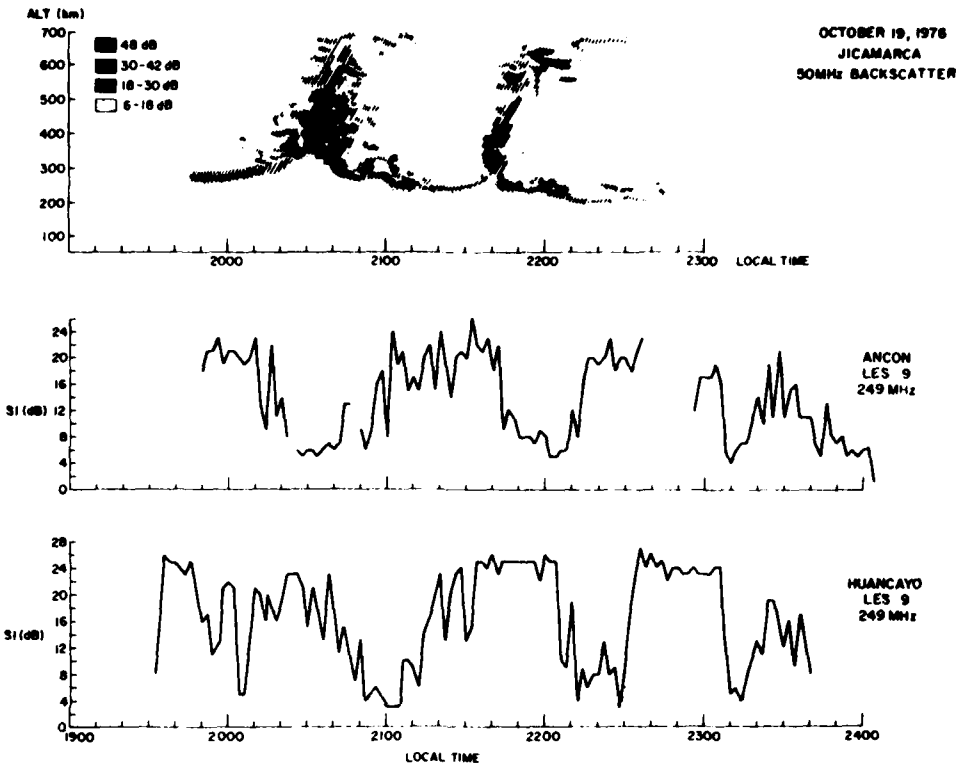

Fig. 4. Temporal variation of the 50-MHz radar backscatter observed at Jicamarca and scintillation index, SI(dB), of the 249-MHz transmissions from the Les 9 satellite recorded at Ancon and Huancayo on October 19-20, 1976 [after *Basu and Aarons*, 1977].

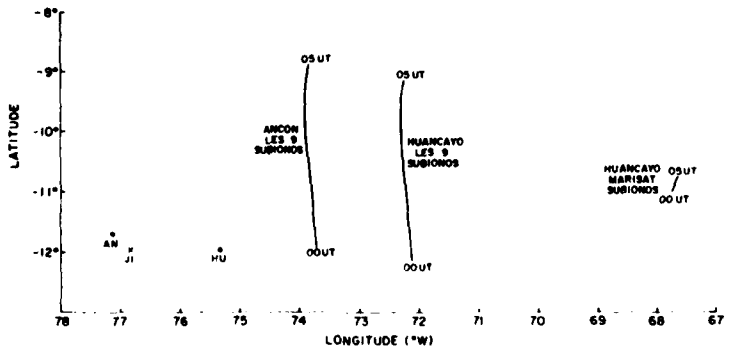

Fig. 5. The geometry of radar backscatter and scintillation measurements during the AFGL equatorial campaign in October 1976. The ground locations for various observatories and subionospheric (400 km) locations for Les 9 are shown [after *Basu and Aarons*, 1977].

of 40 dB would be found relative to the observed backscatter echo strength. To bring computations and observations into agreement, they postulated a Gaussian type of cutoff near the O^+ ion gyroradius which is on the order of 3 m in the topside ionosphere. Such a cutoff could be considered to be the 'inner scale' of turbulence. This point is discussed further in the next section. *Booker and Ferguson* [1978] have also postulated an inner scale near the ionic gyroradius to explain spread *F* signatures on equatorial ionograms in the HF band.

As a result of further co-located scintillation and radar observations during the March 1977 campaign, *Basu et al.* [1978*a*] have come to the conclusion that kilometer and meter scales coexist only during the developing phase in the early evening hours. Figure 6, obtained by combining two diagrams presented by *Basu et al.* [1978*b*], shows co-located scintillation and backscatter measurements made on March 19 20, 1977. The sharp onset of strong scintillations at 137 MHz is well correlated with the development of strong 3-m irregularities at 1950 LT. However, strong scintillations continue beyond 2040 LT, when 3-m irregularities are found to decay. By the use of multisatellite observations these authors have also established that the second scintillation structure beginning at 2300 LT was caused by a drifting irregularity patch. This structure was associated with the significant *L*-band scintillations of the Wideband satellite signal but negligible 3-m backscatter. These findings lead *Basu et al.* [1978*b*] to speculate that at later local times the cutoff scale length is probably of the order of few tens of meters.

5. The AFGL aircraft scintillation observations have helped separate the spatial and temporal behavior of irregularities, while the on-board ionosonde and optical imaging systems have found evidence of electron density depletions in the bottomside *F* region. Figure 7, using data kindly made available by J. Buchau, shows the locus of the subionospheric point as the aircraft flew between ground stations on October 19 20, 1976. The thin lines signify the absence of scintillations, while the thick lines signify their presence. The top panel shows that during 2247 UT (October 19) to 0015 UT (October 20), when the ground stations at Ancon and Huancayo did not record any scintillations, as may be observed from Figure 4, the aircraft did not detect any irregularities in the entire latitude range of 11° 13°S and longitude interval of 72°-75°W. The bottom panel shows that from 0015 UT onward the aircraft detected three irregularity patches with distinct boundaries, indicating spatially localized irregularity generation after UT midnight (i.e., 1900 LT). The imaging system provided all-sky pictures of the 6300-Å OI airglow emission, which

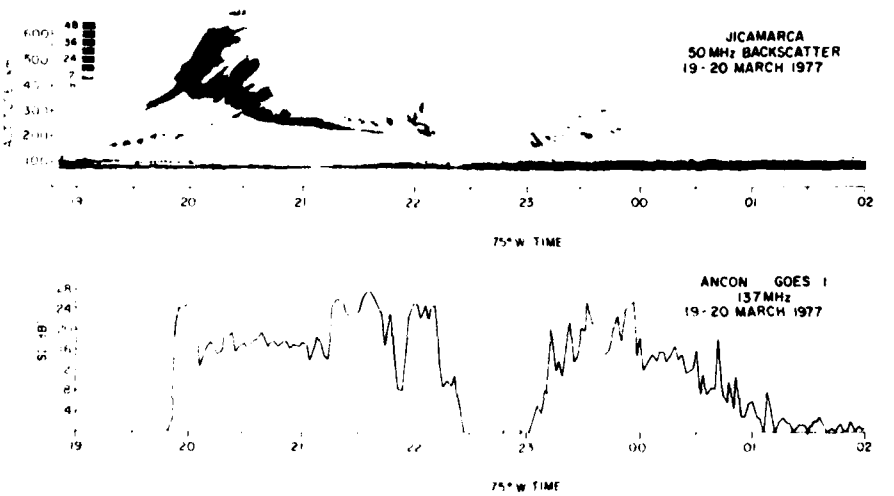

Fig. 6. Temporal variation of 50-MHz radar backscattered power obtained at Jicamarca and scintillation index, SI(dB), of 137-MHz transmissions from the Goes I satellite recorded at Ancon on March 19-20, 1977. Both sets of data refer to a nearly common ionospheric volume [after *Basu et al.*, 1978*b*]

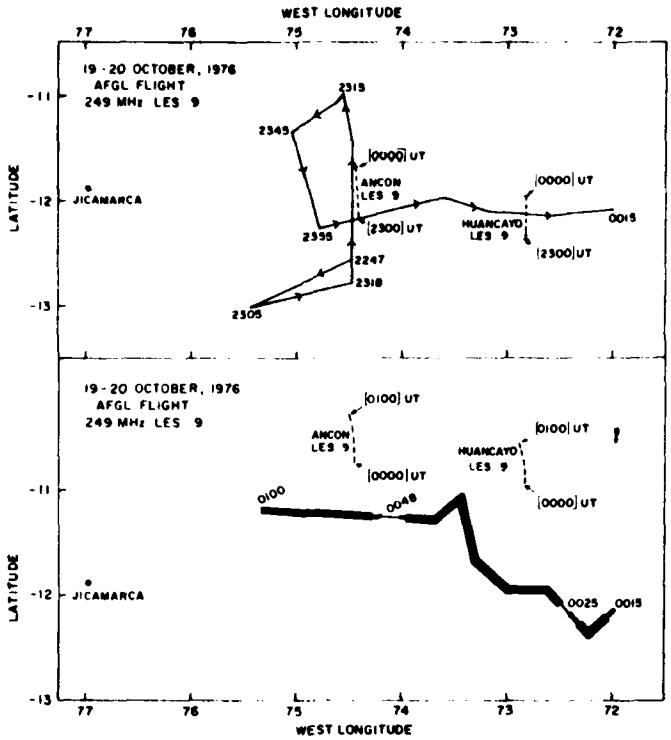

Fig. 7. Subionospheric flight path of the AFGL aircraft making 249-MHz scintillation observations with Les 9 on October 19-20, 1976. Thin and thick lines indicate the absence or presence of scintillations, respectively [after *Basu and Aarons*, 1977].

results from dissociative recombination of O_2^+ in the F region. Initial observations show the existence of north-south aligned regions of airglow depletion [*Weber et al.*, 1978]. An isolated airglow depletion band observed on March 17, 1977, is modeled in Figure 8 as a troughlike bottomside electron density depletion, which explains the observed airglow and ionosonde features. Further details regarding the association of the airglow depletion with scintillations and 3-m backscatter are provided by *Buchau et al.* [1978]. It is important to note, however, that not all airglow depletions are associated with plumes on backscatter maps [*Basu et al.*, 1978*b*].

6. The scintillation data obtained from the various ground stations (in particular, spaced receiver measurements made at Ancon) and the data obtained from the AFGL aircraft as well as the Air Force Avionics Laboratory (AFAL) aircraft have been

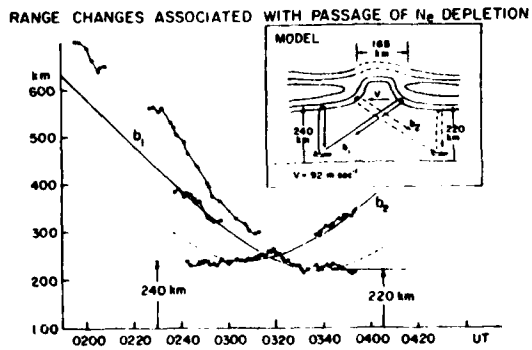

Fig. 8. Model of an eastward drifting bottomside N_e depletion based on observed ionosonde and airglow parameters. The measured ranges of oblique returns and the virtual height of overhead F region are compared with range/height changes expected from the passage of the model bottomside structure over the ionosonde [after *Weber et al.*, 1978].

used to determine whether diversity techniques can mitigate the effects of intense amplitude scintillation at 250 MHz [*Whitney et al.*, 1977]. In particular, it was found that the high degree of decorrelation over a base line of 366 m associated with rapid severe intensity fluctuations ($S_4 \sim 1$) make space diversity techniques useful [*Whitney*, 1978].

As far as radio communicators are concerned, this multitechnique study has shown that topside irregularities have an enormous effect on transionospheric propagation. These irregularities have been called 'bubbles' by those using the satellite in situ technique [*McClure et al.*, 1977] and 'plumes' by those using the radar technique [*Woodman and LaHoz*, 1976]. *Rastogi and Woodman* [1978] have shown that this radar backscatter is associated with range spread on equatorial ionograms. These campaigns have provided convincing evidence that saturated VHF and moderate gigahertz scintillations are associated with bubbles and plumes in the equatorial region. *Basu et al.* [1978*a*, *b*] have further established that the 3-m plumes are relatively short lived in comparison with the bubbles. Thus large scintillation effects on VHF-UHF channels are to be expected not only when radar plumes are observed but also when the drifting bubbles cross the ray path of a transionospheric communication channel. On the other hand, there are nights during which moderate VHF scintillation activity is noted, and these are associated with only weak bottomside radar activity [*Basu et al.*, 1977, *Basu and Aarons*, 1977]. It would thus be highly beneficial to the user community if a system could be developed to predict the occurrence of bubbles on a particular evening.

2.2. *Wideband satellite observations.* The Wideband satellite was launched into a sun synchronous, near-polar orbit on May 22, 1976, carrying a multifrequency coherent radio beacon on board. The mutually coherent signals, which range from VHF to *S* band, are being recorded by SRI at ground stations in Poker Flat, Alaska, and two equatorial stations, namely, Ancon, Peru, and Kwajalein in the Pacific sector. The equatorial station at Kwajalein was set up to determine longitudinal differences in equatorial scintillation first pointed out by *Basu et al.* [1976] on the basis of in situ irregularity data. We shall primarily discuss the equatorial data but will point out certain basic differences with auroral scintillation structure that have been reported by the SRI group. The following information has been taken from *Rino et al.* [1977] and *Fremouw et al.* [1978].

1. The most important aspect of these observations has been the realization that ionospheric radio wave propagation is dominated by large slowly varying phase scintillations. These can be large even in the absence of significant amplitude scintillations. The latter statement is particularly true for the auroral zone. Indeed, the measurement of simultaneous phase and amplitude scintillation has shown that computations of phase deviation based on the weak scatter theory using the observed amplitude scintillation would grossly underestimate the actual phase scintillation level. On the basis of these observations the SRI group has developed a multiplicative two-component model to characterize the joint first-order statistics of amplitude and phase. This model is discussed in detail by *Fremouw et al.* [1976]. Briefly, the idea is to separate two components of the total (complex) scintillating signal by filtering. Because of the power law nature of the irregularity spectrum the low-frequency cutoff had to be somewhat arbitrarily defined. Thus by using a double detrending process it was possible to separate a 'focus' component having fluctuations with periods between 2.5 and 10 s and a 'scatter' component having fluctuation periods smaller than 2.5 s. The focus component gives rise to the large slow phase fluctuations, while the scatter component causes the fast intensity fluctuations. Figure 9, taken from *Fremouw et al.* [1978], contains VHF data sets showing these two components obtained from each of the three latitudinal regions where SRI had ground stations (initially the Wideband observations were started at Stanford, the equipment being moved to Kwajalein in October 1976). It is interesting to note that for the same value of the S_4 index (a measure of the scatter component) the standard deviation of phase (a measure of the focus component) varies substantially at different locations, being the smallest at the equator. This has been found to be a consistent feature [*Fremouw*, 1977] and may be of importance for irregularity generation mechanisms, although the detrend interval and effective scan velocity of the satellite may also affect this ratio. *Whitney and Basu* [1977] have reported earlier a difference in the slope of the intensity spectrum between an equatorial and an auroral station.

For communications purposes it is important to characterize the statistics of signal fluctuations.

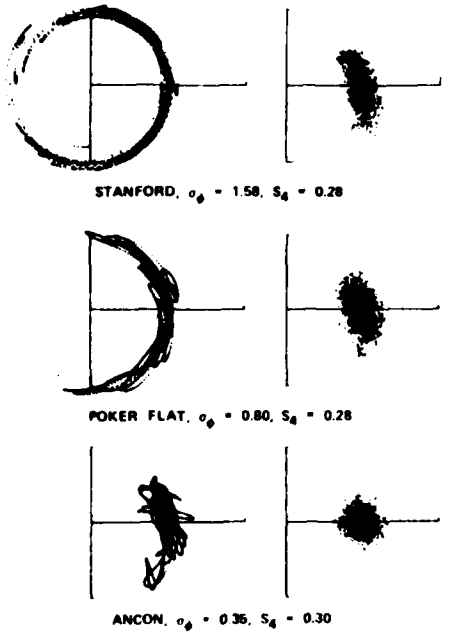

Fig. 9. Scatter diagrams on the complex plane for (left) the focus component and (right) the scatter component isolated from segments of VHF Wideband records obtained at (top) a mid-latitude, (center) an auroral, and (bottom) an equatorial station [after *Fremouw et al.*, 1978].

Hitherto, Rician statistics have been used extensively in communication theory as a model for certain noise processes [*Hatfield and Rino*, 1975]. The received signal from an ionospherically diffracted plane wave can be considered as a complex Gaussian process, $v = v_r + iv_i$. This process, v, is said to have Rician statistics when the variances of v_r and v_i are equal and their covariance is zero. It may be noted from Figure 9 that in the equatorial region the scatter component displays a very Rician characteristic, while that obtained at the mid-latitude station is highly non-Rician.

2. The SRI group has categorized scintillations qualitatively into seven groups ranging from 'extremely quiet' to 'extremely active.' It is interesting to note that equatorial stations provide the majority of cases in both these extreme situations compared with the auroral station, where a 'modestly active' behavior is most frequent. This equatorial scintillation behavior is probably caused by the great day-to-day variability in irregularity occurrence discussed in section 2.1.

3. During extremely active conditions, scintillations are found to persist in the gigahertz range. The observations of gigahertz scintillations with a low orbiting satellite proved that weak irregularities existing throughout the plasmasphere are not a necessary condition, as was suggested by *Booker* [1975].

4. The multifrequency Wideband observations have shown that the standard deviation of phase in general shows an f^{-1} behavior even under conditions of strong diffractive scatter. Occasional violation of the law has been observed in conjunction with strong scintillations in the gigahertz range. Figure 10 shows the frequency dependence of phase scintillation during two 20-s periods of a pass on December 16, 1976, which falls in the 'extremely active' category. The *L*-band point has been corrected for the *S*-band phase perturbations which were present at the beginning of the pass. In the less disturbed sample obtained at a low elevation angle in a near-magnetic meridian plane the VHF departs significantly, and even the UHF points show some scatter. At such times the slope p of the phase spectrum also flattens, with values of $p \sim -2$ being observed at VHF and UHF.

5. The frequency dependence of intensity scintillations observed during the same periods is shown in Figure 11. The fully developed or saturated nature of the intensity scintillations at VHF and the five UHF frequencies analyzed during the more disturbed period is apparent in the departure of these six data points from an $f^{-1.5}$ dependence [*Rufe-*

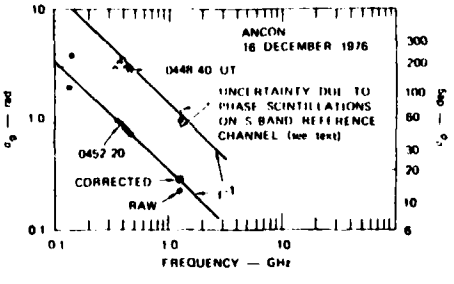

Fig. 10. Frequency dependence of phase-scintillation index during two 20-s periods of the Ancon Wideband pass on December 16, 1976, compared with an f^{-1} dependence arbitrarily passed through the 413-MHz data point [after *Fremouw et al.*, 1978].

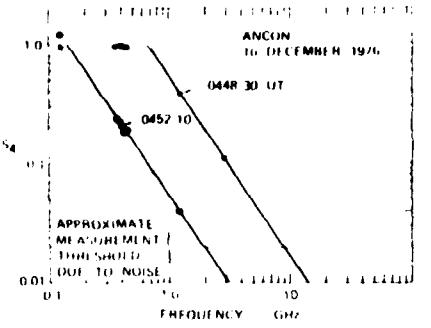

Fig. 11. Frequency dependence of intensity-scintillation index during two 20-s periods of the Ancon Wideband pass on December 16, 1976, compared with an $f^{-1.5}$ dependence [after *Fremouw et al.*, 1978].

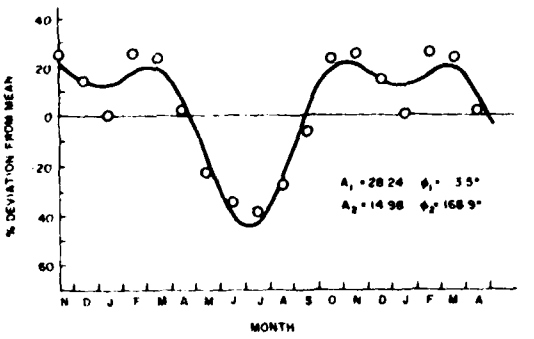

Fig. 12. Seasonal variation of 136-MHz scintillation from ATS 3 at Legon, Ghana, during the period September 1971 to December 1975. Note that the annual component (with a minimum in the June solstice) has twice the amplitude of the semiannual component [after *Koster*, 1976].

nach, 1974] that holds between *L* band and *S* band. Such a reduction in frequency dependence of intensity scintillations in the multiple-scatter regime had been discussed earlier by *Yeh et al.* [1975], *Whitney and Basu* [1977], and *Mullen et al.* [1977]. Under extremely active conditions it is possible to have intensity decorrelation across the UHF comb of frequencies. In this regard it should be noted that during the March 1977 AFGL campaign it was found that most Wideband passes, even those showing gigahertz scintillation, were not associated with 3-m radar backscatter [*Basu et al.*, 1978*b*]. This point has been discussed in section 2.1. Thus it is not yet known whether intensity decorrelation during the developing phase of equatorial irregularities will be even greater.

6. The SRI group, on the basis of their observations at Kwajalein (9°N geographic, 8°N dip) and Ancon (11°S geographic, 2°N dip), has indicated that there is a local summer maximum of equatorial scintillations. On the other hand, Ghana observations (5°N geographic, 8°S dip) over a 5-year period depict a local summer minimum [*Koster*, 1976], as shown in Figure 12. Thus the control may be longitudinal rather than seasonal, with differences being observed between the Atlantic and the Pacific sector [*Basu et al.*, 1976; *Aarons*, 1977]. The reason for such effects are as yet unclear.

7. Depletion of total electron content (TEC) has been noted at Kwajalein in conjunction with active scintillation conditions. One specific case with 30% TEC depletion has been discussed in detail [*Fremouw and Lansinger*, 1977; *Fremouw*, 1978]. *Koster* [1976] has provided extensive evidence using 42 months of simultaneous TEC and scintillation measurements at Ghana (excluding the June solstice) that scintillations in the premidnight period are associated with TEC depletions. The largest TEC depletion is noted at 2100 LT, a time that is closely associated with the development of plumes on radar maps. This agrees well with current theoretical ideas and in situ observations of the association of equatorial irregularities with density depletions. More recent data obtained at Kwajalein during August 1977 show nearly sinusoidal, long-wavelength variations in TEC measured along the Wideband trajectory at times when the Altair radar was observing backscatter at 150 MHz (M. J. Baron, R. C. Livingston, and R. T. Tsunoda, private communication, 1978). This may indicate possible gravity wave seeding of equatorial irregularities.

3. RECENT THEORETICAL RESULTS

Theoretical efforts have kept pace with the multitechnique experimental efforts described above. Numerical simulations of a Rayleigh Taylor unstable ionosphere [*Dungey*, 1956; *Haerendel*, 1974; *Hudson and Kennel*, 1975] in the collision-dominated case have been made by *Scannapieco and Ossakow* [1976]. They showed that an initial 3-km wavelength finite amplitude sinusoidal perturbation on the bottomside eventually formed a bubblelike structure which rose into the topside, such as was seen by

the experimental techniques mentioned earlier. The development time of 10^4 s determined by Scannapieco and Ossakow was considerably longer than that observed, but another simulation published recently by the same group [*Ossakow et al.*, 1978] shows much more rapid evolution. These computer simulations are strongly supported by an analytic treatment due to *Ott* [1978], who, assuming the experimental validity of the bubble concept, calculated their shape and velocity as a function of altitude and size. At low altitudes he found that the bubbles should be cylindrical (circular cross sections and uniform along B) and that they rise with the velocity

$$u = \left(\frac{n_o - n_b}{n_o + n_b}\right) g/(\nu_{in}) \tag{1}$$

where n_b is the density inside the bubble, n_o is the density outside, g is the acceleration due to gravity, and ν_{in} is the ion neutral collision frequency. At high altitudes, where ion neutral collisions can be neglected, Ott showed that the equations governing the motion are identical to the equations of two-dimensional ordinary fluids (for example, a liquid constrained between two planes with separation distance much less than the size of the planes). Considerable theoretical and experimental work has already been done on such fluids and can thus be directly applied to the present problem. The observed bubble shape is shown in Figure 13, and the velocity is given by

$$u \simeq 0.5(Rg)^{1/2} \tag{2}$$

where R is the radius of the circular 'cap' shown at the top of the diagram. (It should be noted that all statements concerning velocity fields or velocity turbulence can be replaced by discussions of electric fields or electrostatic turbulence, since $\mathbf{V} = \mathbf{E} \times \mathbf{B}/B^2$.)

From the foregoing discussion of experimental and theoretical studies we find that an outstanding feature of equatorial spread F on the topside is the presence of large-scale (~10-km scale) regions of low plasma density with very sharp gradients at the edges. The source of energy for this interchange of low- and high-density plasma is the excess gravitational potential energy which resides in the F region plasma supported against gravity by the magnetic field. The nonlinear process must be initiated, however, and several mechanisms have

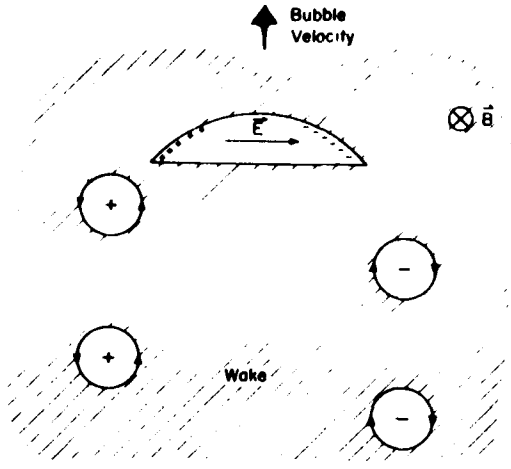

Fig. 13. Bubble shape and vortex generation mechanism [after *Kelley and Ott*, 1978]

been suggested. In the linear Rayleigh-Taylor process the zero-order upward density gradient is disrupted by the electrostatic fields in the instability. It seems clear that this process does operate on the bottomside, possibly enhanced by the $\vec{E} \times \vec{B}$ instability [*Kelley et al.*, 1979], but its role in producing topside irregularities is not proven. A strong candidate for seeding finite amplitude low-density regions near the topside is the action of atmospheric gravity waves [*Beer*, 1974; *Röttger*, 1978; *Booker*, 1978], which, if the waves have an upward group velocity, can 'spatially resonate' with plasma moving downward [*Whitehead*, 1971]. *Klostermeyer* [1978] has shown that this process indeed leads to large-amplitude long-wavelength perturbations near the F peak.

Another outstanding feature of equatorial spread F is the wide range of wavelengths exhibited by spread F irregularities. For instance, the 3-m scale length is 3–4 orders of magnitude smaller than the primary process described above. Two processes have recently been suggested which may well account both for the wide range of wavelengths and for the extended spatial extent of spread F.

Costa and Kelley [1978*a*, *b*] have considered the steep gradients in plasma density associated with bottomside irregularities (see Figure 15) and presumably also with topside bubbles and have shown that drift waves should grow rapidly on the observed

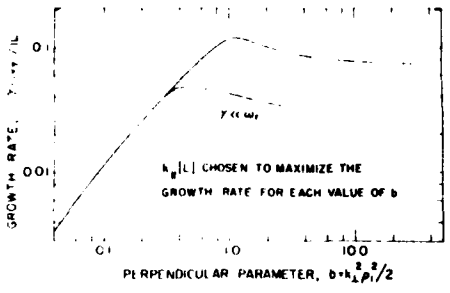

Fig. 14 Growth rate γ as function of the parameter b. The curve labeled $\gamma \ll \omega_r$ is obtained from the 'small growth rate' expression, while the unlabeled curve is obtained from the 'generalized' expressions [after *Costa and Kelley*, 1978*b*].

gradients. The normalized growth rate is plotted in Figure 14 as a function of the parameter $b = k_\perp^2 \rho_i^2/2$, where $k_\perp$ is the wave number perpendicular to **B** and ρ_i is the ion gyroradius. For reference, b at the Jicamarca backscatter wavelength is 70. The growth rate peaks at $k_\perp \rho_i = 1.5$, which corresponds to wavelengths of about 24 m. The growth rate is linearly proportional to the gradient scale length L at the bubble edge and is 1 s^{-1} for $L = 125$ m under typical ionospheric conditions. These drift waves should not only contribute to backscatter in the development phase but also play a role in the eventual merging of bubbles into the background via destruction of the steep gradient [*Burke et al.*, 1979]. *Huba et al.* [1978] have extended this concept to even smaller wavelengths.

A second and perhaps more important process from the standpoint of scintillations is the generation of a thick irregularity layer as suggested by *Kelley and Ott* [1978]. Again, use was made of Ott's findings that in the collisionless case the equations of motion are identical to those for a two-dimensional fluid. In the fluid case the upward buoyancy force is balanced by emission of vortices in the background fluid. This injects velocity turbulence into the background fluid in a wake which trails behind the bubble. In the plasma case each vortex corresponds to a line charge surrounded by a circular **E** x **B** drift of the plasma as shown in Figure 13. Since there is a background density gradient, this vortex will create density irregularities with the same scale size as the velocity turbulence.

Numerous theoretical studies of turbulence in two-dimensional fluids [*Kraichnan*, 1967; *Lilly*, 1969] have shown that velocity injected into such a fluid at some characteristic wave number k_0 will cascade to wave numbers both higher and lower than k_0. In the space domain this 'inverse cascade' to lower k implies that the velocity (and density) turbulence will spread into the largest volume available in the system. Evidence for this dual cascade in two-dimensional turbulence has been found in the earth's atmosphere [*Kao and Wendell*, 1970] and magnetosphere [*Kelley and Kintner*, 1978].

Kelley and Ott [1978] suggest that the vortices emitted by upwelling bubbles not only form a wake but tend to fill the between-bubble regions (i.e., in an east-west direction) with velocity and density irregularities via this cascade to lower k values. Cascade to higher k also occurs, the ultimate spectral cutoff occurring at some large wave number where ion viscosity plays a role. This dissipation is most effective near the ion gyroradius, and hence it seems likely that the 3-m scale (Jicamarca backscatter) lies in the dissipative subrange. Such a 'cutoff' in the amplitude of irregularities at short wavelengths was postulated by *Woodman and Basu* [1978], as was discussed earlier.

In the intermediate range of wave numbers $L_s^{-1} < k < L_d^{-1}$, where L_s is the stirring length (bubble size) and L_d is the dissipation scale, *Kelley and Ott* [1978] predicted a k^{-1} spectrum for velocity or electric field fluctuations and a k^{-1} power spectrum for density irregularities. This seems in contradiction to numerous reports of a one-dimensional k^{-2} density spectrum associated with equatorial spread F. However, *Costa and Kelley* [1978*a*] have shown that, at least in the case of bottomside nonlinear structures, the k^{-2} spectrum is due to the steep edges in density encountered. Several examples of the steep edges are clear in the data presented in the top panel of Figure 15, obtained during the passage of a sounding rocket through bottomside spread F. The relative density ($\delta n/n$) is plotted for an 8-s interval (~16 km along the trajectory).

As an illustration of the steep edge effect, *Costa and Kelley* [1978*a*] performed a Fourier transform of the data, shown in the top panel of Figure 15, randomized the phase in each Fourier component, and reassembled the data in the time domain. Two such random phase runs were made and are plotted in the lower two panels. The upper plot displays considerably more ordering into large structures with steep edges than the lower two. One property

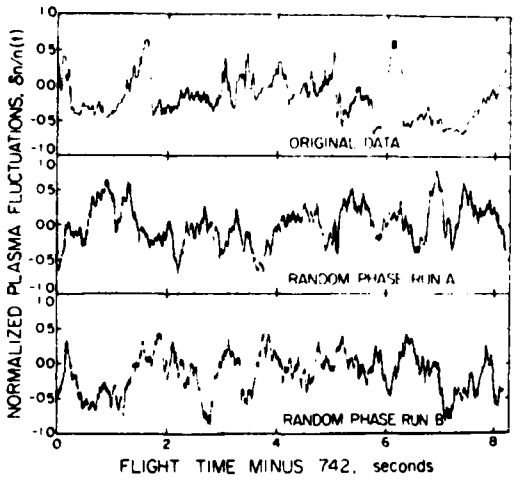

Fig. 15. The upper plot is a detrended data stream obtained on the bottomside of the F peak during equatorial spread F. The lower two plots are reconstructed time domain samples using the same data but with the addition of a random phase in the FFT (fast Fourier transform) before construction [after *Costa and Kelley*, 1978*a*].

which characterizes the Fourier transform of steep edges is a correlation between Fourier components. This correlation was destroyed in the randomization process, which results in the 'turbulencelike' data shown in the lower two panels. Note that the power spectrum of all three sets of data is identical and varies as f^{-2} over most of the spectrum.

R. F. Woodman (private communication, 1976) first suggested a phase coherence test as a way of distinguishing between the dominance of steep structure or turbulence in equatorial spread F. More recently, *Chaturvedi and Ossakow* [1977] have considered the nonlinear development of bottomside spread F. They conclude that steepened structures should evolve in time and that, in fact, a k^{-2} spectrum would result owing to the steep edges. They also suggested a phase coherence test to distinguish between such a process and a turbulencelike mechanism proposed earlier by *Chaturvedi and Kaw* [1976]. The results of *Costa and Kelley* [1978*a*] described above seem to agree with the sharp edge hypothesis.

4 SUMMARY

The following picture evolves from the discussion above. Bottomside spread F occurs in a widespread region (at least ±10° latitude) centered near the magnetic equator in the postsunset hours. This causes moderate VHF scintillation. Nonlinear evolution of this process and/or the spatial resonance of atmospheric gravity waves results in low-density regions rising into the topside, leaving behind a trail of counter-rotating vortices which mix the background density gradient and create irregularities in density. Since whole flux tubes partake in this upwelling, a two-dimensional bubble originating anywhere in this latitude range will have effects in the topside. The bubbles may also be 'wedges' extending upward from the F peak [*McClure et al.*, 1978]. In this case the plumes may not be due to a wake effect at all but to a continuous generation of irregularities at the edges. The density gradients in the bubbles or wedges also dissipate and create short-wavelength irregularities, possibly via the 'universal' drift wave instability [*Costa and Kelley*, 1978*a*, *b*; *Burke et al.*, 1979] or other gradient-driven instabilities [*Huba et al.*, 1978].

Radio waves incident upon the equatorial ionosphere under these conditions are thus subject to at least four different types of scintillating environment. (1) Just after sunset during the development phase, the bottomside irregularities cause modest amplitude scintillation effects due to the low absolute fluctuations in electron density. It is not known whether large phase fluctuations accompany such weak amplitude scintillations, as the Wideband satellite does not have equatorial crossings at this time. (2) In the fully developed stage, bubbles are continually emitted into the topside over a wide range of latitudes. These bubbles may continually stir the medium at wavelengths comparable with the bubble dimensions (~10 km). In this event, two-dimensional dual cascade spreads the velocity and density irregularities to larger and smaller k values. The cascade to smaller k, combined with the vertical wake formation, tends to fill a large volume with density irregularities. Alternatively, the bubbles may be wedges, the steep edges of which break down via a hierarchy of instabilities [*Haerendel*, 1974; *Costa and Kelley*, 1978*a*]. Incident radio waves thus are subject to sharp discontinuities in electron density in the bubbles as well as very thick (in altitude) regions of power law type density irregularities. Very intense amplitude scintillations have been observed during such times, as was discussed in section 2, and it is expected that large phase fluctuations will also be present. (3) In the decay phase (later local time) the velocity turbulence

injected by the bubbles, as well as the bubble gradients themselves, decay via dissipation at large k. In this phase the dissipation scale moves to smaller k values [*Kelley and Ott*, 1978], so the smallest-scale structures disappear first. Thus significant kilometer-scale structures will still exist in the medium and strongly affect scintillation even though backscatter measurements become less intense. (4) Finally, the irregularities observed near midnight are found to have negligible spectral power at meter scale lengths but still retain significant power at longer scale lengths, which may cause strong scintillations. Using multisatellite scintillation observations, *Basu et al.* [1978*b*] have shown that these irregularities are eastward drifting structures which seem to be characterized by a spectral cutoff in the vicinity of tens of meters.

It has to be pointed out that two-dimensional models of irregularity bubbles do not explain why density depletions are observed to rise more frequently than enhancements fall [*Hudson*, 1978]. G. Haerendel (private communication, 1977) has noted that density enhancements may be tied to the E region, whereas density depletions are free to interchange and drift up. Also, recombination tends to destroy falling enhancements as they move into regions of higher neutral density, while upwelling molecular ions in bubbles have a higher recombination coefficient than the surrounding O^+ [*Szuszczewicz*, 1978]. Finally, *McClure et al.* [1977] have suggested that density enhancements may spread out over a broader east-west extent than depletions, thereby producing a smaller relative enchancement. More extensive experiments are required during which both velocity and density irregularities are measured simultaneously as a function of k to solve the three-dimensional problem. Electric field measurements of the velocity fields are easier to perform on technical grounds and are equivalent, since $\mathbf{V} = \mathbf{E} \times \mathbf{B}/B^2$.

From the scintillation point of view it would be highly desirable to have a geostationary satellite with the capabilities of the present Wideband one to monitor the focus and scatter components during the developing phase of irregularities. Such measurements in conjunction with the Jicamarca radar observations would provide valuable information on spectral characteristics of equatorial irregularities. The finding of *Costa and Kelley* [1978*a*] and *Chaturvedi and Ossakow* [1977] regarding steepened bottomside structures and the associated k^{-3} spectrum is an important one. It is thus quite crucial to determine whether steepened structures also dominate topside irregularity behavior in the developing phase. This may have far-reaching implications in scintillation modeling.

Acknowledgments. Numerous people have contributed to the development of the ideas expounded in this paper, and it is hoped that the reference list adequately recognizes their contribution. We also thank the various authors who made their diagrams available to us for reproduction. We wish to thank Santimay Basu for many helpful comments and a careful reading of the manuscript. The equatorial irregularity campaigns in Peru were conducted under the guidance of J. Aarons, to whom Sunanda Basu is indebted for many constructive suggestions. Most of the work was done while she was a NRC Associate at AFGL. M. C. Kelley acknowledges helpful discussions with E. Costa and D. T. Farley. The work at Cornell University was sponsored by ONR under N00014-75-C-0780.

REFERENCES

Aarons, J. (1977), Equatorial scintillations: A review, *IEEE Trans. Antennas Propagat.*, *AP-25*, 729–736.

Aarons, J., J. Buchau, S. Basu, and J. P. McClure (1978), The localized origin of equatorial F region irregularity patches, *J. Geophys. Res.*, *83*, 1659–1664.

Basu, S., and J. Aarons (1977), Equatorial irregularity campaigns, I, Correlated scintillation and radar backscatter measurements in October 1976, *Tech. Rep. AFGL-TR-0264*, Air Force Geophy. Lab., Hanscom Air Force Base, Mass.

Basu, S., and S. Basu (1976), Correlated measurements of scintillations and in situ F-region irregularities from Ogo 6, *Geophys. Res. Lett.*, *3*, 681–684.

Basu, S., and M. C. Kelley (1977), Review of equatorial scintillation phenomena in the light of recent developments in the theory and measurement of equatorial irregularities, *J. Atmos. Terr. Phys.*, *39*, 1229–1242.

Basu, S., S. Basu, and B. K. Khan (1976), Model of equatorial scintillations from in situ measurements, *Radio Sci.*, *11*, 821–832.

Basu, S., J. Aarons, J. P. McClure, C. LaHoz, A. Bushby, and R. F. Woodman (1977), Preliminary comparisons of VHF radar maps of F-region irregularities with scintillations in the equatorial region, *J. Atmos. Terr. Phys.*, *39*, 1251–1262.

Basu, S., H. Whitney, J. Aarons, and J. P. McClure (1978*a*), Large and small scale properties of nighttime equatorial irregularities from scintillations and radar backscatter measurements, in *Proceedings of Symposium on the Effect of the Ionosphere on Space and Terrestrial Systems*, edited by J. M. Goodman, U.S. Government Printing Office, Washington, D.C.

Basu, S., S. Basu, J. Aarons, J. P. McClure, and M. D. Cousins (1978*b*), On the coexistence of kilometer- and meter-scale irregularities in the nighttime equatorial F region, *J. Geophys. Res.*, *83*, 4219–4226.

Beer, T. (1974), On the dynamics of equatorial spread-F, *Aust. J. Phys.*, *27*, 391–400.

Booker, H. G. (1975), The role of the magnetosphere in satellite and radiostar scintillation, *J. Atmos. Terr. Phys.*, *37*, 1089–1098.

Booker, H. G. (1978), The role of acoustic gravity waves in the generation of spread-*F* and ionospheric scintillation, paper presented at URSI General Assembly, Helsinki, Aug. 1-8.

Booker, H. G., and J. A. Ferguson (1978), A theoretical model for equatorial ionospheric spread-*F* echoes in the HF and VHF bands, *J. Atmos. Terr. Phys.*, *40*, 803-830.

Booker, H. G., and H. W. Wells (1938), Scattering of radio waves by the *F*-region of the ionosphere, *Terr. Magn. Atmos. Elect.*, *43*, 249-256.

Buchau, J., E. J. Weber, and J. P. McClure (1978), Radio and optical diagnostics applied to an isolated equatorial scintillation event, in *Proceedings of Symposium on the Effect of the Ionosphere on Space and Terrestrial Systems*, edited by J. M. Goodman, U.S. Government Printing Office, Washington, D.C.

Burke, W. J., D. E. Donatelli, R. C. Sagalyn, and M. C. Kelley (1979), Observations of low density regions at high altitudes in the topside equatorial ionosphere and their interpretation in terms of equatorial spread *F*, *Planet. Space Sci.*, *27*, in press.

Chaturvedi, P. K., and P. K. Kaw (1976), An interpretation for the power spectrum of spread *F* irregularities, *J. Geophys. Res.*, *81*, 3257-3260.

Chaturvedi, P. K., and S. L. Ossakow (1977), Nonlinear theory of the collisional Rayleigh-Taylor instability in equatorial spread-*F*, *Geophys. Res. Lett.*, *4*, 558-560.

Costa, E., and M. C. Kelley (1976), Calculations of equatorial scintillations at VHF and gigahertz frequencies based on a new model of the disturbed equatorial ionosphere, *Geophys. Res. Lett.*, *3*, 677-680.

Costa, E., and M. C. Kelley (1978*a*), On the role of steepened structures and drift waves in equatorial spread *F*, *J. Geophys. Res.*, *83*, 4359-4364.

Costa, E., and M. C. Kelley (1978*b*), Linear theory for collisionless drift wave instability with wavelengths near the ion gyroradius, *J. Geophys. Res.*, *83*, 4365-4368.

Dungey, J. W. (1956), Convective diffusion in the equatorial *F*-region, *J. Atmos. Terr. Phys.*, *9*, 304-310.

Dyson, P. L., J. P. McClure, and W. B. Hanson (1974), In situ measurements of the spectral characteristics of ionospheric irregularities, *J. Geophys. Res.*, *79*, 1497-1502.

Fremouw, E. J. (1977), Examination of data from the Wideband satellite experiment, *Rep. PD-NW-77-118-R01*, Phys. Dyn., Inc., Seattle, Wash.

Fremouw, E. J. (1978), Analysis of Wideband satellite data, *Rep. PD-NW-77-130-R01*, Phys. Dyn., Inc., Seattle, Wash.

Fremouw, E. J., C. L. Rino, and R. C. Livingston (1976), A two-component model for scintillation, in *Proceedings of COSPAR Symposium on the Geophysical Use of Satellite Beacon Observations*, edited by M. Mendillo, Boston University, Boston, Mass.

Fremouw, E. J., and J. M. Lansinger (1977), Examination of data from the Wideband satellite experiment, *Rep. PD-NW-118-R02*, Phys. Dyn., Inc., Seattle, Wash.

Fremouw, E. J., R. L. Leadabrand, R. C. Livingston, M. D. Cousins, C. L. Rino, B. C. Fair, and R. A. Long (1978), Early results from the DNA Wideband satellite experiment-complex signal scintillation, *Radio Sci.*, *13*, 167-188.

Haerendel, G. (1974), Theory of equatorial spread-*F*, report, Max-Planck-Institut fur Phys. und Astrophys., Garching, West Germany.

Hatfield, V. E., and C. L. Rino (1975), Non-Rician statistics and their implications for modeling effects of scintillation on communication channels, in *Proceedings of Symposium on the Effect of the Ionosphere on Space Systems and Communications*, edited by J. M. Goodman, U.S. Government Printing Office, Washington, D.C.

Huba, J. D., P. K. Chaturvedi, and S. L. Ossakow (1978), High frequency drift waves with wavelengths below the ion gyroradius in equatorial spread-*F*, *Geophys. Res. Lett.*, *5*, 695-698.

Hudson, M. K. (1978), Spread-*F* bubbles: Nonlinear Rayleigh-Taylor mode in two dimensions, *J. Geophys. Res.*, *83*, 3189-3194.

Hudson, M. K., and C. F. Kennel (1975), Linear theory of equatorial spread-*F*, *J. Geophys. Res.*, *80*, 4581-4590.

Kao, S. K., and L. L. Wendell (1970), The kinetic energy of the large scale atmosphere motion in wave number frequency space, *J. Atmos. Sci.*, *27*, 359-375.

Kelley, M. C., and P. M. Kintner (1978), Evidence for two dimensional inertial turbulence in a cosmic scale low β plasma, *Astrophys. J.*, *220*, 339-345.

Kelley, M. C., and E. Ott (1978), Two-dimensional turbulence in equatorial spread *F*, *J. Geophys. Res.*, *83*, 4369-4372.

Kelley, M. C., G. Haerendel, H. Kappler, A. Valenzuela, B. B. Balsley, D. A. Carter, W. L. Ecklund, C. W. Carlson, B. Hausler, and R. Torbert (1976), Evidence for a Rayleigh-Taylor type instability and upwelling of depleted density regions during equatorial spread-*F*, *Geophys. Res. Lett.*, *3*, 448-451.

Kelley, M. C., K. D. Baker, and J. C. Ulwick (1979), Late time barium cloud striations and their possible relationship to equatorial spread *F*, *J. Geophys. Res.*, *84*, in press.

Klostermeyer, J. (1978), Nonlinear investigation of the spatial resonance effect in the nighttime equatorial *F* region, *J. Geophys. Res.*, *83*, 3753-3760.

Koster, J. R. (1976), Study of the equatorial ionosphere, *Rep. AFGL-TR-77-0165*, Univ. of Ghana, Legon, Ghana.

Kraichnan, R. H. (1967), Inertial ranges in two-dimensional turbulence, *Phys. Fluids*, *10*, 1417-1423.

Lilly, D. K. (1969), Numerical simulation of two-dimensional turbulence, *Phys. Fluids*, suppl. II, II-240-II-249.

McClure, J. P., and W. B. Hanson (1973), A catalog of ionospheric *F* region irregularity behavior based on Ogo 6 retarding potential analyzer data, *J. Geophys. Res.*, *78*, 7431-7440.

McClure, J. P., W. B. Hanson, and J. H. Hoffman (1977), Plasma bubbles and irregularities in the equatorial ionosphere, *J. Geophys. Res.*, *82*, 2650-2656.

McClure, J. P., C. A. Valladares, and W. B. Hanson (1978), Simultaneous VHF radar and in situ observations of equatorial *F*-region irregularities, paper presented at URSI General Assembly, Helsinki, Aug. 1-8.

Morse, F. A., B. C. Edgar, H. C. Koons, C. J. Rice, W. J. Heikkila, J. H. Hoffman, B. A. Tinsley, J. D. Winningham, A. B. Christensen, R. F. Woodman, J. Pomalaza, and N. R. Teixeira (1977), Equion: An equatorial ionospheric irregularity experiment, *J. Geophys. Res.*, *82*, 578-592.

Mullen, J. P., H. E. Whitney, S. Basu, A. Bushby, J. Lanat, and J. Pantoja (1977), Statistics of VHF and *L* band scintillation at Huancayo, Peru, *J. Atmos. Terr. Phys.*, *39*, 1243-1250.

Ossakow, S. L., S. T. Zalesak, B. E. McDonald, and P. K. Chaturvedi (1978), Theoretical and numerical simulation pre-

dictions of the equatorial spread *F* environment, in *Proceedings of Symposium on the Effects of the Ionosphere on Space and Terrestrial Systems*, edited by J. M. Goodman, U.S. Government Printing Office, Washington, D.C.

Ott, E. (1978), Theory of Rayleigh-Taylor bubbles in the equatorial ionosphere, *J. Geophys. Res.*, *83*, 2066–2070.

Rastogi, R. G., and R. F. Woodman (1978), VHF radio wave scattering due to range and frequency types of equatorial spread *F*, *J. Atmos. Terr. Phys.*, *40*, 485–491.

Rino, C. L., E. J. Fremouw, R. C. Livingston, M. D. Cousins, and B. C. Fair (1977), Wideband satellite observations, *Rep. DNA4399F*, SRI Int., Menlo Park, Calif.

Rottger, J. (1976), The macroscale structure of equatorial irregularities, *J. Atmos. Terr. Phys.*, *38*, 97–102.

Rottger, J. (1978), Drifting patches of equatorial spread-*F* irregularities—An experimental support for the spatial resonance mechanism in the ionosphere, *J. Atmos. Terr. Phys.*, *40*, 1103.

Rufenach, C. L. (1974), Wavelength dependence of radio scintillation—Ionosphere and interplanetary irregularities, *J. Geophys. Res.*, *79*, 1562–1566.

Scannapieco, A. J., and S. L. Ossakow (1976), Nonlinear equatorial spread-*F*, *Geophys. Res. Lett.*, *3*, 451–454.

Szuszczewicz, E. P. (1978), Ionospheric holes and equatorial spread *F*—Chemistry and transport, *J. Geophys. Res.*, *83*, 2665–2670.

Weber, E. J., J. Buchau, R. H. Eather, and S. B. Mende (1978), North-south aligned equatorial airglow depletions, *J. Geophys. Res.*, *83*, 712–716.

Whitehead, J. D. (1971), Ionization disturbances caused by gravity waves in the presence of an electrostatic field and background wind, *J. Geophys. Res.*, 238–241.

Whitney, H. E. (1978), Spaced receiver measurements of intense equatorial scintillations, in *Proceedings of Symposium on the Effect of the Ionosphere on Space and Terrestrial Systems*, edited by J. M. Goodman, U.S. Government Printing Office, Washington, D.C.

Whitney, H. E., and S. Basu (1977), The effect of ionospheric scintillation on VHF/UHF satellite communications, *Radio Sci.*, *12*, 123–133.

Whitney, H. E., A. Johnson, J. Buchau, J. P. Mullen, and E. J. Weber (1977), Report on Peru scintillation tests, October 1976 and March 1977, *Tech. Rep. AFGL-TR-77-0282*, Air Force Geophys. Lab., Hanscom Air Force Base, Mass.

Woodman, R. F., and S. Basu (1978), Comparison between in situ spectral measurements of equatorial *F*-region irregularities and backscatter observations at 3m wavelength, *Geophys. Res. Lett.*, *5*, 869–872.

Woodman, R. F., and C. LaHoz (1976), Radar observations of *F* region equatorial irregularities, *J. Geophys. Res.*, *81*, 5447–5466.

Yeh, K. C., C. H. Liu, and M. Y. Youakim (1975), A theoretical study of the ionospheric scintillation behavior caused by multiple scattering, *Radio Sci.*, *10*, 97–106.

The Dynamics of Equatorial Irregularity Patch Formation, Motion, and Decay

J. AARONS, J. P. MULLEN AND H. E. WHITNEY

Air Force Geophysics Laboratory, Hanscom Air Force Base, Massachusetts 01731

E. M. MACKENZIE

Emmanuel College, Boston, Massachusetts 02115

Using scintillation observations from a series of equatorial propagation paths as well as backscatter and airglow data, the development, motion, and decay of equatorial irregularity patches have been studied. Assembling the results of earlier studies in the field with our observations, we find the following: the patch has limited east-west dimensions with a minimum of 100 km. Several patches may be melded together to reach an extent of 1500 km. Its magnetic north-south dimensions are often greater than 2000 km; the most intense irregularities (as evidenced by the Jicamarca radar at the dip equator) are from 225 to 450 km in altitude, although irregularities are found as high as 1000 km. The patch initially has a westward expansion following the solar terminator, then, maintaining its integrity, moves eastward. Evidence over a limited series of experiments suggests that premidnight patches are formed within 1½ hours after ionospheric sunset in the absence of special magnetic conditions. From Ascension Island (~16°S dip latitude) the individual patches can be clearly distinguished. The decay of patches in the midnight time period was studied, pointing to a rapid decrease in scintillation intensity in this time period.

INTRODUCTION

Through theoretical considerations [*Dungey*, 1956; *Haerendel*, 1974; *Hudson and Kennel*, 1975; *Scannapieco and Ossakow*, 1976] bolstered by backscatter [*Woodman and LaHoz*, 1976] and in situ [*Kelley et al.*, 1976; *McClure et al.*, 1977] observations, it has been established that nighttime ionospheric equatorial irregularity regions emerging after sunset develop from bottomside instabilities, probably of the Rayleigh-Taylor type. The depleted density bubble rises into the region above the peak of the F_2 layer. Steep gradients on the edges of the hole [*Haerendel*, 1974; *Costa and Kelley*, 1978] help to generate smaller-scale irregularities with the high topside density causing intense scintillation effects [*Basu and Basu*, 1976; *Costa and Kelley*, 1976]. Irregularities in the wake of upwelling structures have also been discussed [*Woodman and LaHoz*, 1976; *Kelley and Ott*, 1978].

The depletions, with their vertical motion from altitudes below the peak of the F layer into regions considerably above that height, are being studied by a variety of models [*Basu and Kelley*, 1979]. Indications of patch size and velocities have been made in early work using equatorial spread F data. *Cohen and Bowles* [1961] found patches elongated at least 1 km along the lines of force. *Calvert and Cohen* [1961] measured drift velocity of the patches slowing from ~200 m/s premidnight to ~100 m/s postmidnight. In these studies, magnetic east-west extent of the patches (of thickness of the order of 50 km) could range from 150 to 300 km to possibly 1000 km. Using scintillation, airglow, and backscatter techniques, the aim of this paper is to outline recent results on characteristics of the patches during development, size and velocities of the formed patches, and the total time that the patch maintained its integrity.

We shall refer to the patch as a unit irregularity structure. The plume, described by *Woodman and LaHoz* [1976], is one form of the patch, deriving its name from the extended height range of meter-scale irregularities detected in dramatic examples provided by the Jicamarca radar. In some plumes, irregularities are observed from 200 to 800 km. However, in other patches, detectable echoes from the Jicamarca backscatter are confined to a thickness of 50–100 km. Even though the maximum radar intensity may be identical in both cases, the thin layer could hardly be termed a plume.

In an observational model summarized in Figure 1 we shall show the following characteristics:

1. A new patch forms after sunset by expanding westward in the direction of the solar terminator with velocities probably similar to that of the terminator. It comes to an abrupt halt after typically expanding to an east-west dimension of 100 to several hundred kilometers. It appears to have a minimum size of ~100 km.
2. It is composed of field-aligned elongated rod or vertical sheet irregularities. The vertical thickness of the patch is 50 to several hundred kilometers. In the mean the patch encompasses a height region from 225 to 450 km, although irregularities have been shown to exist to 1000 km.
3. Its north-south dimensions are of the order of 2000 km or greater, far larger than noted in earlier studies.
4. Once formed, the patch drifts eastward with velocities ranging from 100 to 200 m/s.
5. Its duration as measured by scintillation techniques is known to be greater than 2½ hours; individual patches have been tracked by airglow techniques up to 3 hours where they have maintained their integrity [*Weber et al.*, 1978].
6. Between patches the irregularity structure can be completely undetectable.

Several of these characteristics have been observed in other studies. For example, the field-aligned bubble model developed by *Dyson and Benson* [1978] from topside sounder data is in form similar to Figure 1 and has been found to extend large distances along the field lines. The characteristics noted above pertain to irregularity patches formed in the pre local midnight time period. Post local midnight patches may have a different formation mechanism and hence different characteristics. Airglow measurements (E. J. Weber and J. Buchau, private communication, 1978) and scintillation observations as will be outlined suggest that no new patches arise after 1–2 hours after sunset except under special magnetic conditions.

Copyright © 1980 by the American Geophysical Union

Paper number 9A1254.
0148-0227/80/009A-1254$01.00

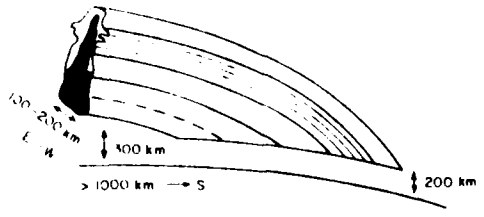

THREE DIMENSIONAL PATCH MODEL

Fig. 1. A magnetic equator cut through the general form of the equatorial patch, shown following the contours of the earth's magnetic field. North-south dimensions are typically >2000 km, while it may measure several hundred kilometers east-west and vary in vertical thickness from 50 to several hundred kilometers.

Observational Material

The data to be utilized consist of cooperative measurements made primarily with the assistance of the Instituto Geofisico del Peru. These measurements are given in Table 1.

The Formation of a New Patch

The sunset line moving westward at a velocity of ~500 m/s initiates the conditions necessary but not sufficient for a patch to form. During some evenings, irregularities develop in a systematic westward motion. In Figure 2 we have illustrated the series of scintillation starting events which took place with a westward motion on March 19–20, 1977. In the top panel a tracing of a portion of the backscatter observations at 50 MHz is shown (P. McClure, personal communication 1977). A thin layer of relatively weak 3-m irregularities forms at 1935 LST, but the plume starts to develop at 1950 LST. Greater values of ΔN and increased thickness then occur. Scintillation activity noted at Ancon on the GOES 1 beacon, the path closest to the Jicamarca magnetic meridian, increases sharply at 1950 LST.

The timing of the start of scintillation activity at each of the ionospheric paths is shown in the remaining panels. This timing coupled with the adjacent map indicates clearly a westerly development of the patch. The sequence and direction of starts are shown by arrows and a numerical order of commencements.

Using the three VHF observations in order to equalize starting time definition (Huancayo-GOES, Ancon-GOES, and Huancayo A-3), a velocity of 200–300 m/s is determined in the initial westward development. The patch has very large dimensions E-W as borne out by the continuous high level of activity at each of the stations. This relatively continuous activity through the night does not allow us to determine a subsequent eastward velocity by the gross motion of the patch.

A second illustration of a newly developed patch utilizes data from the next night, March 20–21, 1977. The Jicamarca backscatter records are shown in the top frame of Figure 3. Strongly backscattered energy was first observed at 2010 LST. In noting the scintillation activities, one can see the expansion of the irregularity patch, its finite stop in the westward direction, and finally its motion eastward across the L-9 paths from the two sites of Ancon and Huancayo.

Using the criterion of start time measured from signal scintillation greater than 6 dB, the scintillation activity was first noted at 1950 LST on the Huancayo GOES 1 intersection, developing in time on the Ancon GOES intersection, the Jicamarca backscatter (along the same magnetic meridian), and the Huancayo A-3 patch. The velocities of the developing

TABLE 1. Observational Material

Station	Experiment	Frequency, MHz	Satellite	Dates
Jicamarca	radar backscatter (UTD)	50		Oct. 1976 March 1977 March 1978
Ancon	spaced receiver scintillation	249 249	L-9	Oct. 1976 March 1977 March 1978
	scintillation	137 254	A-3 GOES 1 L-8	March 1977 March 1978
Huancayo	scintillation	249 257 1541 137	L-9 Marisat Wideband	Oct. 1976 March 1977 March 1978
	scintillation	137	A-3 GOES 1	March 1977 March 1978
AFGL Aircraft	scintillation ionosonde airglow	249	L-9	Oct. 1976 March 1977 March 1978
AFAL Aircraft	scintillation	249	L-9	Oct. 1976 March 1977
Ascension Island	scintillation	257 137 249	Marisat SIRIO L-9	March 1978

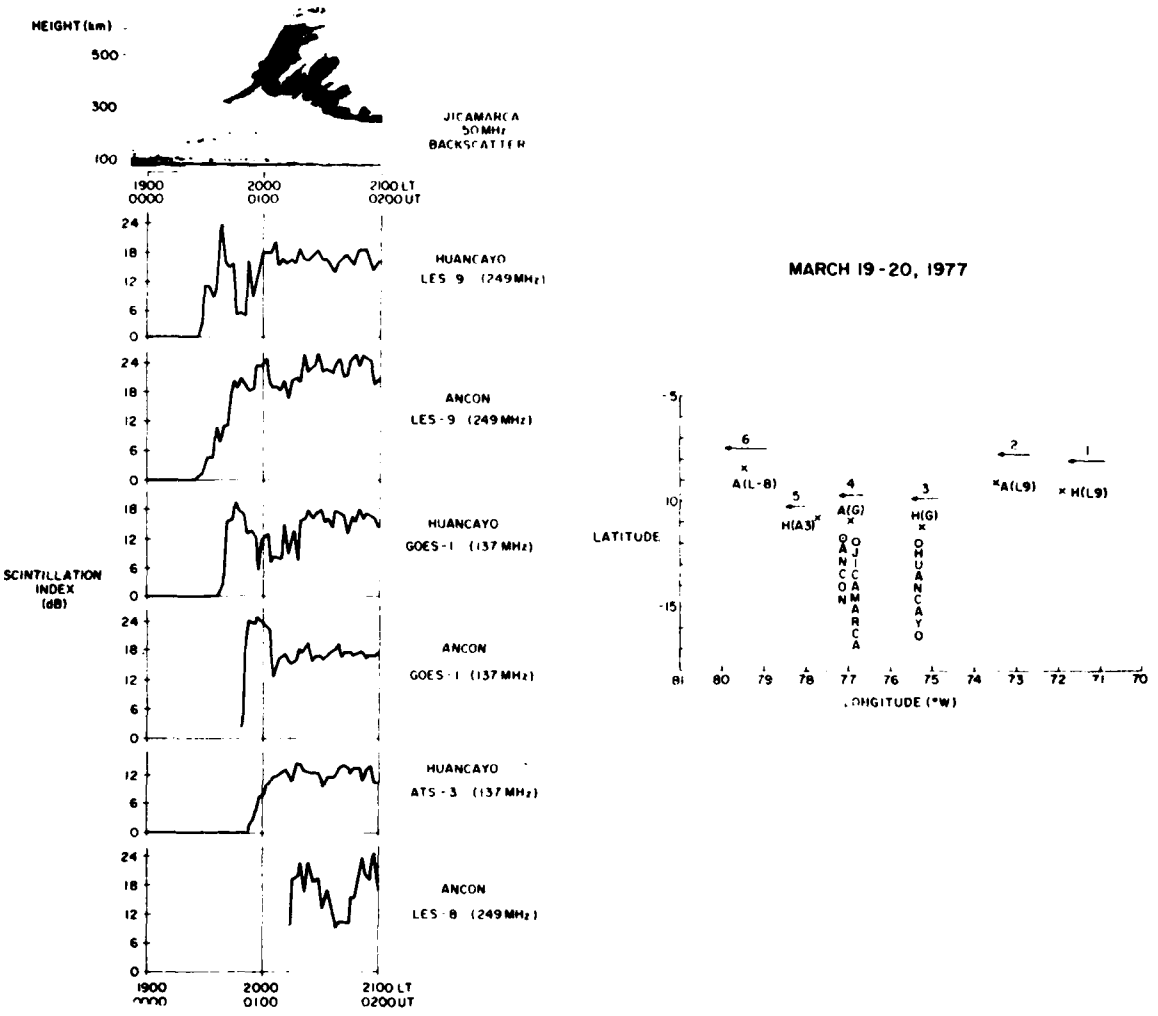

Fig. 2. Backscatter and scintillation data recorded on March 19–20, 1977, of several satellites observed from Ancon and Huancayo, Peru. The accompanying map of the 400-km subionospheric points (01 UT positions shown by x) illustrates the westward development of the patch (over a longitudinal range of ≈8°) through the use of arrows and the numerical order of commencements. The ground positions of the sites are given (i.e., ⊙) in order to picture the angle of elevation to the satellite. 'Overhead' satellites are close to the stations.

patch were of the order of 160–200 m/s westward as calculated from the times of rise at these intersections. This particular patch never extended westward far enough to reach the longitude of the Ancon intersection to L-8. However, later, another patch, originating probably west of Ancon, moved across the Ancon L-8 path and joined the irregularity activity. The minimum extent of this enlarged region was of the order of 300 km.

Once the patch was formed, its motion eastward could be followed by noting the time of passage across the paths of L-9 from Ancon and from Huancayo. Measurements of the satellite were at relatively low angles of elevation and involve an early peaking ~2020, arriving at both stations after its appearance in the west.

During all three campaigns, spaced receiver measurements of LES 9 were available from Ancon to determine drift velocity. The east-west spacings of the measurements from Ancon using the 249-MHz beacon of LES 9 were 122, 244, and 366 m. Different spacings were used on various nights. The data indicated that at the beginning of each patch, old or new, velocities were not unidirectional. On the night of March 19–20 (Figure 4), spaced receiver measurements show a low correlation and fluctuating velocity during the development period from 1930 to 2100 LST. This was perhaps due to the fact that only 366-m spacing was available, but it is also possible that the terminator motion, vertical velocities, and eastward drifts produced fluctuating velocity values (eastward and westward). After 2100 LST, the eastward velocities stabilize between 150 and 180 m/s.

In almost all cases as the patch moved to the east over the propagation path from Ancon to the LES 9 satellite, the patterns stabilized, i.e., the velocities showed consistently east-

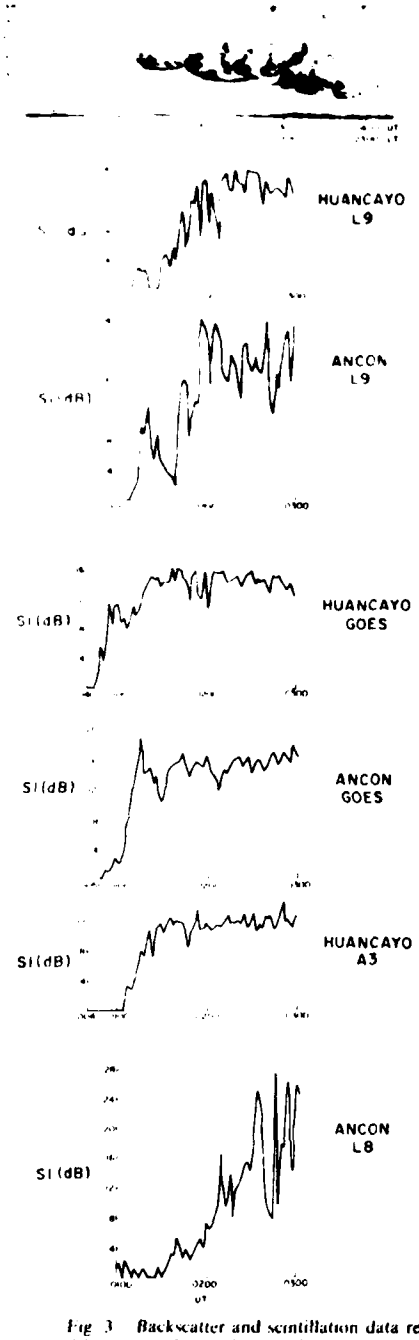

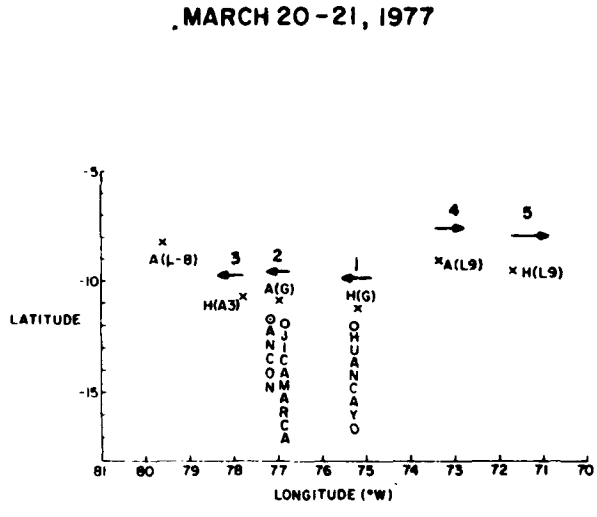

Fig. 3. Backscatter and scintillation data recorded on March 20–21, 1977, of several satellites observed from Ancon and Huancayo, Peru. Through the use of arrows and the numerical order of commencements on the accompanying map, one can see the westward development of the irregularity patch (over a longitude range 75°–78°W), the end of the westward motion, and finally the eastward motion across the L-9 paths. The ground positions of the sites and the 400-km subionospheric positions are illustrated as in Figure 2.

ward direction and exhibited high peak cross-correlation functions. On the night of March 20–21 the velocity measurements are rather stable and well correlated at a value of 150 m/s for the entire period of available spaced receiver measurements. Using this velocity and considering the scintillation duration at Ancon L-9 to be 2 hours 40 min, the patch extent would be 1440 km. By viewing the backscatter record, the patch appears to have this extent because of the large number of closely spaced plumes. This almost continuous scintillation activity makes it difficult to separate the record into individual

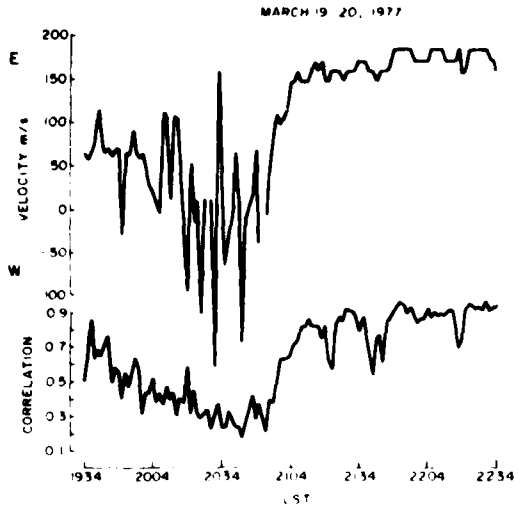

Fig. 4. Spaced receiver data showing velocity and correlation on March 19–20, 1977, exhibiting fluctuating velocities with low correlation at time of patch formation.

patches. As the patch continues eastward, some higher velocities, around 200 m/s were noted, correlating well with the velocity calculated from scintillation onset on the propagation paths.

As shown in the detailed tagging of patches in Figures 2 and 3, one can follow the path of patches as they move eastward. This was done for several sets of data including the interrelated sets from Ancon and Huancayo in the three campaigns as well as differing propagation paths as recorded simultaneously at Ascension Island. Each patch observed later than 1 hour after ionospheric sunset was observed first in the west and then in the east. After local midnight, however, due to lower velocities and to the decrease of intensity of irregularities, this test could not be used with certainty. With data similar to the cases of March 19–20 and March 20–21, we examined the hypothesis that all patches originated within 1–1½ hours of local ionospheric sunset (at 300 km ~19 hours 14 min LST in March and 19 hours 3 min LST in October); all other patches would then be old patches.

Given the limited number of days and more importantly the 'running together' of individual patches, this hypothesis held. Patches seen after 1½ hours after ionospheric sunset appeared first in the west and moved eastward.

The Decay of Patches in the Midnight Time Period

Some patches show evidence of decay observed on the propagation paths available during these campaigns. Data from the backscatter radar and the aircraft as well as ground recordings of Wideband and the synchronous satellites illustrate this for several cases.

Figure 5 illustrates the backscatter records for March 16–17, 1977. Over Jicamarca the irregularities appeared slightly before 2300 LST, maintained medium level intensity in the altitude region 300–600 km until 2330 LST, then trailed off in intensity at the higher altitudes until 0030 LST. The trailing off appears to be a decrease in intensity of the 3-m irregularities.

From Wideband data at Ancon (SRI) and at Huancayo

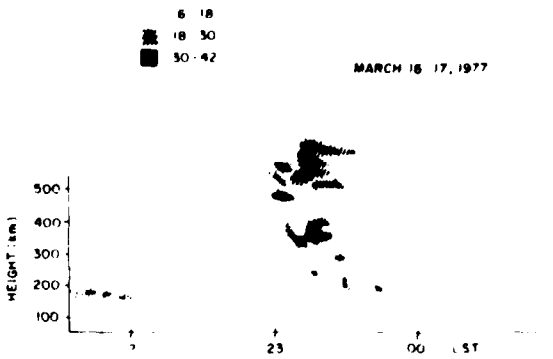

Fig. 5. Backscatter records of March 16–17, 1977. The irregularities maintain medium-level intensity from ≈2300 to 2330 LST, at heights of 300–600 km, then disappear at the lower altitudes and trail off in intensity at the higher altitudes until 0030 LST.

(AFGL-IGP) a patch could be noted nearly over Jicamarca with a sharp eastern front at 76°W at 2318 LST. In Figure 6, data from the aircraft, tracing a route from 3° north to 3° south of Jicamarca but off 3° to the west indicated scintillations as high as 12 dB across the patch in the time period from 2300 to 2325 LST. Airglow data are available which

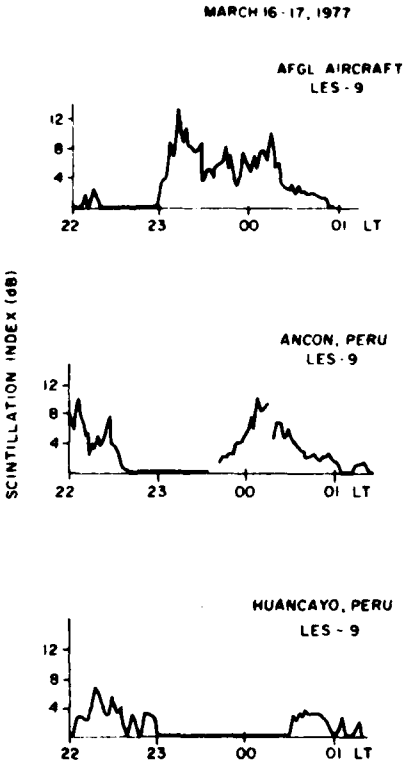

Fig. 6. Scintillation observations of the LES 9 beacon seen at Ancon and Huancayo, Peru, and by the AFGL aircraft tracing a route over Jicamarca, on the same day as the backscatter records shown in Figure 5. The eastward movement of the patch is shown with the intensity of scintillation falling off corresponding to the drop in intensity of the backscatter.

identify this patch. The activity on the path from the aircraft to the satellite decreased after 0020 until low levels were reached at 0100 LST. The Ancon path to LES 9 (also shown in Figure 6) has a maximum of 10-dB fades with a start of some activity at 2350 LST; this position is to the east of the aircraft viewing. The velocity, as determined from spaced receivers at Ancon, however, remained about 90 m/s, only the irregularity intensity decreased as the patch moved eastward. The Huancayo L-9 maximum excursions (0040–0050 LST) were of the order of 3 dB. Within 1½ hours or less, the scintillation levels decreased from 12 to 3 dB at 254 MHz. The Marisat records, far to the east, showed no scintillation activity after this time.

A second decay of a patch will be illustrated with the data from March 19–20, 1977 (earlier developments from this night were shown in Figure 2). A tracing of the contours of backscatter during the time period 2230–0130 LST is shown in Figure 7. Weak irregularities of 3-m size are present at 200-km altitudes; the large-scale irregularities are still fully developed as was shown by *Basu et al.* [1978]. Airglow observations indicate that this patch was one previously developed and not a new patch.

In Figure 7, scintillation panels are shown vertically in eastward sequence. One can note that the patch arrives sequentially later toward the east. The paths farthest to the east show low levels of activity (Ancon L-9) or no scintillation activity (Huancayo L-9).

The evidence for slowdown in velocity of this patch is from the aircraft as shown in Figure 8, where the rate of scintillation fading is shown. When the aircraft flies westward against

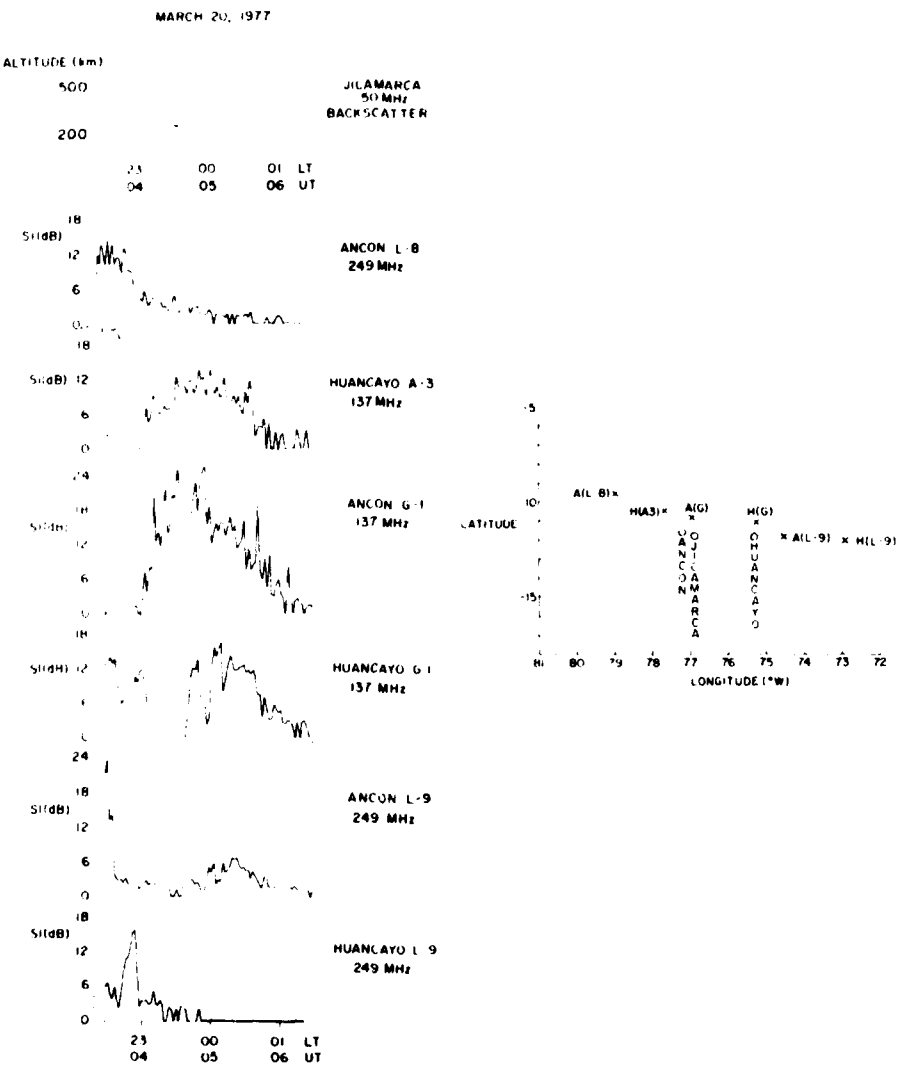

Fig. 7. Backscatter and scintillation data of several satellites observed from Huancayo and Ancon recorded on March 19–20, 1977, after 2200 LST illustrating patch decay. The accompanying map documents the eastward motion of the patch, slowing down and decaying as it travels. The ground positions of the sites and the 400-km subionospheric points are illustrated in the same manner as in Figure 2, but for 05 UT.

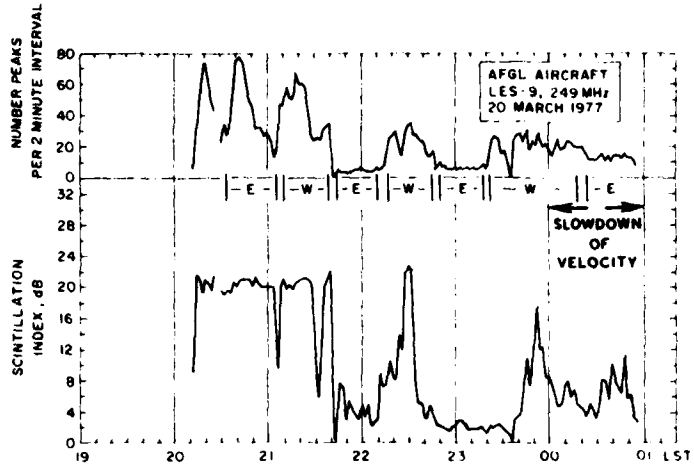

Fig. 8. Fading rates and scintillation observations made by the AFGL aircraft of the LES 9 beacon on March 19/20, 1977. These data illustrate the slowing down of the patch after 2350 LST.

irregularity motion (2120 for example), it would be expected to show a rapid rate of fading, since it moves through many irregularities. When it flies eastward along with the motion of the irregularities, it usually shows a very low rate of fading, for example, at 2200. Fading rate would be zero if the aircraft motion matched the irregularity velocity. In the case of flying eastward (0030–0050) and westward (2350–0020), when the patch was decaying, almost the same rates are shown, indicating that the velocity of the irregularities has slowed down.

The decrease in activity is also shown in this time period from 15 dB (the aircraft and Ancon L-8 levels) to less than 1 dB in somewhat over an hour later in this midnight time period. From this and other days on which there were similar

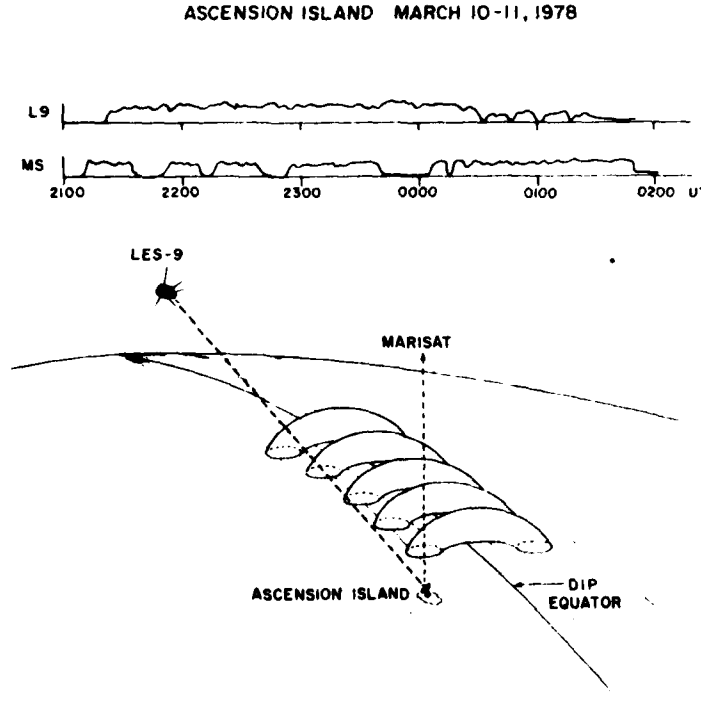

Fig. 9. Scintillation data observed from Ascension Island of the LES 9 and Marisat beacons on March 10/11, 1978. The geometry of the observation is also shown, illustrating that the obliquity of the LES 9 path wipes out the possiblity of viewing a single patch on this day. Marisat viewing is almost vertical.

TABLE 2. Distribution of Observations by Duration

Duration	Ascension Island SIRIO Patches (1978)	Ancon Goes Patches (1977)
< 30 min	33%	10%
30 min to 1 hour	33%	14%
1–2 hours	25%	41%
2–3 hours	3%	14%
>3 hours	6%	21%

occurrences it appears that the patches maintain their activity from postsunset to about midnight, then decay in time periods of the order of 1 hour.

TIME DURATION OF PATCHES

To some extent, the beginning and the end of a scintillation patch are determined by observational parameters. At microwaves, since a large ΔN and thickness are needed, only intense irregularities produce fading effects on radio waves; at VHF, weak irregularities produce small fluctuations in signals before the intense region develops or moves over the propagation path. Microwave patch durations will therefore be shorter than those noted from VHF observations. A second observational bias will be geometrical. Oblique observations to the east or to the west from equatorial positions may encompass more than one patch; therefore in these azimuths, patch duration will appear to be longer and the irregularity structure between patches more difficult to define.

The duration of scintillation is a function of the three-dimensional obliquity of the path. An example of the drawn out extent of scintillation at a low angle of elevation toward the west compared to a nearly overhead viewing is shown in Figure 9. We have plotted reduced data from Ascension Island of observations of LES 9 viewed at 300° azimuth, 20° elevation compared to those of Marisat at 80° elevation, 350° azimuth. The obliquity of the path to LES 9 effectively wipes out the opportunity to view a single patch, since for the patches depicted (data from March 10–11, 1978) the path from LES 9 encompasses three patches.

With these caveats in mind, we have chosen to compare patch E-W dimensions as noted on GOES observations at Ancon (78.6°W in 1978, 76.9°W in 1977) with the SIRIO observations from the Ascension Island (14.4° W), both at 137 MHz and both with longitudinal intersections close to their magnetic meridians, thus minimizing the effects of obliquity. These observations are distributed by duration as shown in Table 2 regardless of pre- or post-local midnight starting time of the patch.

Two thirds of the SIRIO patches are of duration less than 1 hour, while only 25% of the Ancon GOES patches lasted less than 1 hour, using the criterion of start and stop of the 6-dB level (Figure 10).

A smaller amount of data from the Ancon GOES observations in 1978 is available, taken during the same time period as the Ascension Island SIRIO data. Eight of the 10 patches observed were of duration greater than 1 hour.

It is clear that observations taken from Ascension Island showed narrower E-W dimensions than those from Peru.

The explanation is thought to lie primarily in the latitudinal distance of the intersection of the propagation path from Ascension to the satellite. The higher-altitude irregularities observed in the ionosphere above the dip equator are mapped to low altitudes when the intersection point is ~16°S dip latitude. Thus 600- to 800-km irregularities observed above the equator appear at 200–250 km on the propagation path from Ascension. The lower-altitude irregularities at the equator are probably rapidly dissipated. Thus the connecting tissue (mod-

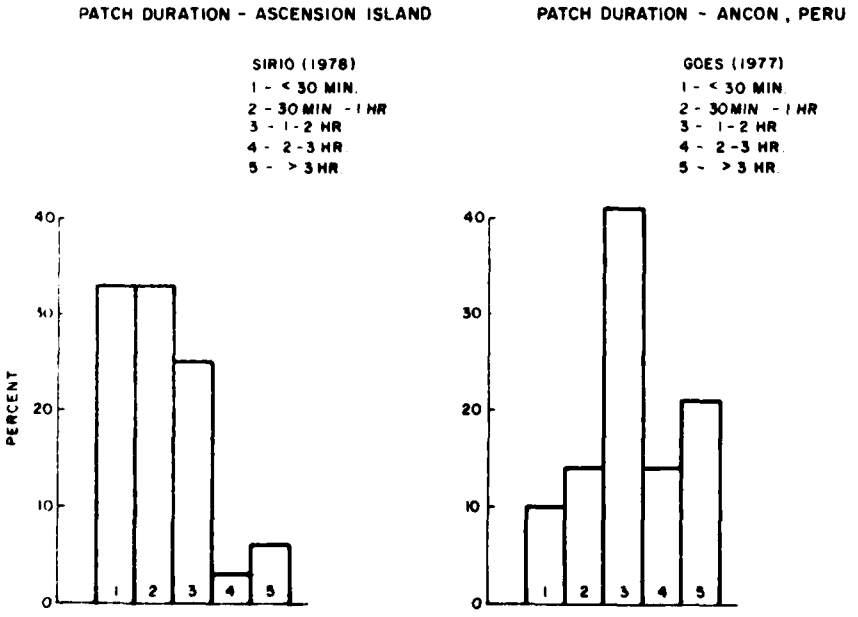

Fig. 10. Histogram comparing percent occurrence of patch duration observed in Ascension Island SIRIO (1978) scintillation data with Ancon GOES (1977) scintillation data. The Ascension Island patches are of noticeably shorter duration than those observed in the Ancon data.

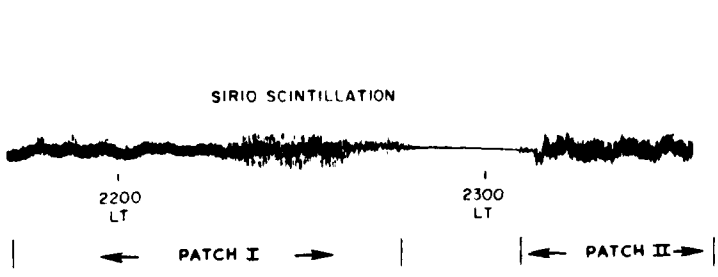

Fig. 11. Scintillation observations of the SIRIO beacon at Ascension Island on March 5, 1978. The quenching of scintillation activity (~2300) between patches is easily seen

erate irregularity levels) from one plume to another, such as seen in Figure 3, for example, disappears.

The minimum patch extent noted ~16°S dip latitude can be ascertained from this data. Using an eastward velocity of 100 m/s (obtained from airglow measurements by the AFGL aircraft (E. Weber, private communication, 1978), a minimum patch (E-W extent) of the order of 100 km is calculated for the data shown in Figure 11 on March 5, 1978. The illustration shows clearly the quenching of scintillation activity between patches at Ascension Island. Thus for ascertaining the scintillation activity encountered for a path, the latitudinal distance to the equator must be factored into the morphological picture.

Patch Altitude and Thickness

Using the backscatter observations taken at *Jicamarca* (kindly supplied to us by J. P. McClure of the University of Texas at Dallas), we developed a composite contour of height and thickness for each intense campaign period. For each night the altitudes and periods of time were used when contours were within 6 dB of the maximum backscatter return on that night. Backscatter returns have been detected at altitudes as large as 1000 km. Our data reduction techniques utilize only the stronger returns of more intense irregularities.

Figures 12*a* and 12*b* illustrate the results from 8 nights in October 1976 and 9 in March 1977. In these cases the altitude range for intense irregularities is from 225 to 450 km, predominantly in the time period before local midnight, usually 1930–2200 LST. The backscatter data for March 1978 exhibited the same temporal maximum as the March 1977 data but at slightly higher altitudes (Figures 12*c*). The 1978 data were taken during a month when the solar flux was high (~150) while in October 1976 and March 1977 the solar flux values were 75 and 77, respectively.

Discussion

In earlier papers discussing results of the backscatter measurements [*Farley et al.*, 1970; *Woodman and LaHoz*, 1976] a dilemma seemed to arise relative to the backscatter results. No distinction would be made between newly or previously developed patches. While it was known that patches were generated after sunset, a tag could not be placed on an individual patch as to its 'age.' Thus when *Farley et al.* [1970] analyzed height changes relative to the generation of patches, data for

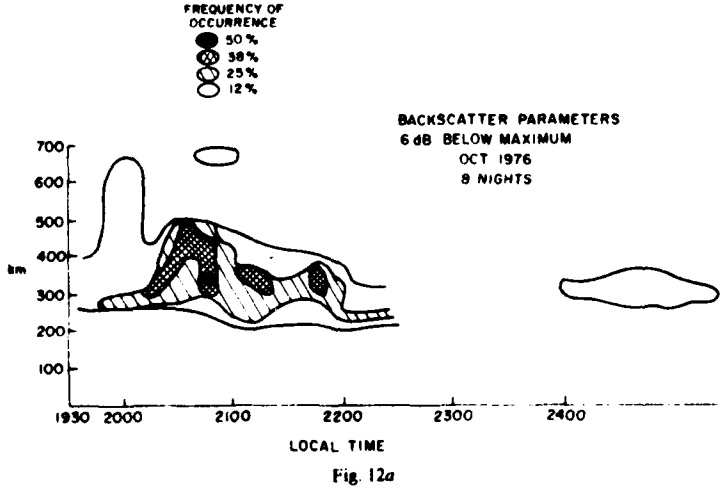

Fig. 12*a*

Fig. 12. Composite contours of height and occurrence with time of Jicamarca backscatter observations. The occurrence contours on a given night were taken to a level 6 dB down from the maximum backscatter observed on that night. (*a*) October 1976 and (*b*) March 1977 data illustrate the height range for intense irregularities as 225–450 km, at ≈1930–2200 LST. (*c*) March 1978 contours exhibit this same temporal maximum but at slightly higher altitudes.

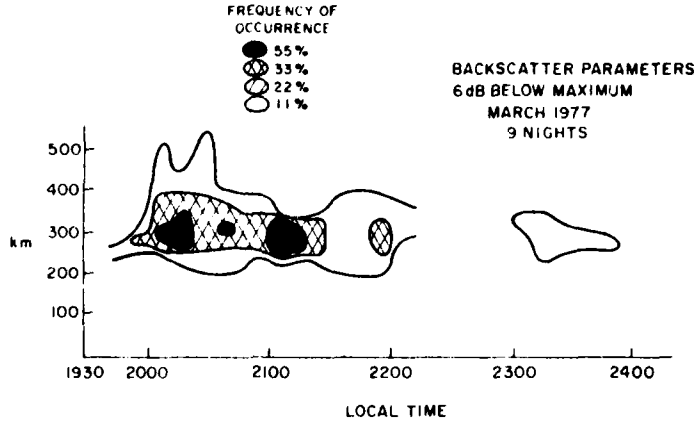

Fig. 12*b*

all patches were used in the analysis. From the data noted in this paper it is clear that even at times when the first patch was observed on any night, this could be an 'old' patch.

From scintillation observations in this limited data sample it appears that premidnight patches arise within 1–1½ hours after ionospheric sunset; the optical data acquired during the campaigns [*Weber et al.*, 1978] indicate more clearly that new patches did not develop after about 1½ hours past ionospheric sunset. Thus earlier studies on spread *F* and backscatter concerning the necessary conditions of ionospheric height and rate of vertical drift must be reevalulated, since the patch may have been formed earlier in a region far to the west of the sounder.

Although there has been considerable study of the vertical development of the irregularity patch [*Ossakow et al.*, 1979], there has been only a relatively small amount of work relative to the initiating mechanism (the necessary and sufficient conditions to develop a bubble in a realistic atmosphere). One proposal has been the spatial resonance effect, i.e., the phase velocity of atmospheric gravity waves matching the plasma drift velocity of equatorial irregularities [*Rottger*, 1978; *Klostermeyer*, 1978; *Koster and Beer*, 1972]. However, even with this hypothesis there has been little detailed correlation of atmospheric parameters. At one observing point, for example, Huancayo, Peru, a night having hours of intense irregularities may be followed by a night of no activity.

The confinement of a patch to a limited east-west extent should be explained. At the equator the plume is a dramatic example of the limited extent; at distances from the equator, the Ascension Island observations have shown the confinement of individual patches.

Once the patch is formed, it stays together for hours. It would be well to know why the patch remains a unit structure and why the patch continues to produce irregularities. *Farley et al.* [1970] state that at 300 km, diffusion would destroy the small 3-m irregularities in 10–20 s or less. Yet, the total structure, containing 3-m to larger irregularities, lasts considerably longer than that. Certainly the larger irregularities are produced in the patch over the order of hours as we have shown. The 3-m irregularities probably endure somewhat less [*Basu et*

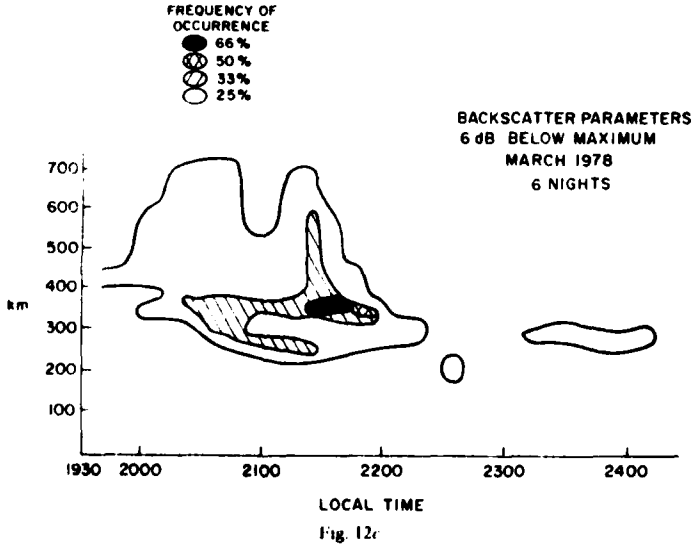

Fig. 12*c*

al., 1978]. *Kelly and Ott* [1978] have discussed density irregularities created by turbulent electrostatic fields in the wake of upwelling structures. These irregularities would expand to larger- and smaller-scale sizes of which the shortest wavelengths would dissipate more rapidly.

A detailed description is needed of the possible processes taking place along the magnetic tubes encompassed by a patch. It is not clear what occurs when the field lines from 300 to 600 km at the equator dip to altitudes of 200 km at ~8 16°S dip latitude.

The decay of patches has been outlined. The decay of the turbulent electrostatic field appears to be the mechanism responsible for the lifetime of the irregularities [*Kelley and Ott*, 1978]. The data for the midnight time period shown in Figure 8 indicates that at 250 MHz, decays of 10 dB took place in an hour. There are nights when scintillations last into the morning hours, with decreased intensity and with slow velocities. These have not been illustrated in this paper but have been observed.

CONCLUSIONS

It is now possible to observe experimentally the formation, maintenance, and decay of individual patches. The patch is the basic unit structure of the irregularities in the equatorial region. The irregularities exist along lines of force with probably the higher altitude irregularities accounting for the most distant north-south patches.

During the development phase, a westward expansion of the patch has been noted. When the patch has formed, it has a limited east-west extent. Once formed, it moves eastward. At equatorial latitudes a connecting tissue or continuing irregularity activity frequently accompanies both the backscatter and the scintillation patch. At large distances from the dip equator the individual patch stands out more dramatically.

The decay of the patch is difficult to follow, since the slowing down of the structures at times accompanies decay. Future theoretical studies should consider the patch characteristics established in this study and seek to explain the origin, maintenance, and decay of the unit patch structure.

Acknowledgments. The observational base for this study comes from many sources. In particular, the authors would like to thank the Instituto Geofisico del Peru for its part in the program, particularly the director, Alberto Giesecke, and the technical staff A. Bushby, J. Pantoja, and J. Lanat. In addition, J. P. McClure kindly supplied us with backscatter results from his operation of the Jicamarca radar. Within AFGL, assistance has been obtained from C. Malik in the Ascension Island studies. Optical data and scintillation observations from the AFGL Airborne Ionospheric Observatory were kindly supplied to J. Buchau and E. Weber. The authors wish to express their thanks to Santimay Basu and Sunanda Basu for their critiques and suggestions. This work was partially supported by the Space and Missle Systems Organization under Project 1227 and by the Defense Nuclear Agency under subtask I25AAXHX640 Communications Effects Experiments.

The Editor thanks M. C. Kelley and W. B. Hanson for their assistance in evaluating this paper.

REFERENCES

Basu, S., and S. Basu, Correlated measurements of scintillations and in situ *F* region irregularities from OGO-6, *Geophys. Res. Lett.*, *3*, 681, 1976.

Basu, S., and M. C. Kelley, A review of recent observations of equatorial scintillations and their relationship to current theories of *F* region irregularity generation, *Radio Sci.*, *14*, 471, 1979.

Basu, S., S. Basu, J. Aarons, J. P. McClure, and M. D. Cousins, On the coexistence of kilometer- and meter-scale irregularities in the nighttime equatorial *F* region, *J. Geophys. Res.*, *83*, 4219, 1978.

Calvert, W., and R. Cohen, The interpretation and synthesis of certain spread *F* configurations appearing on equatorial ionograms, *J. Geophys. Res.*, *66*, 3125, 1961.

Cohen, R., and K. L. Bowles, On the nature of equatorial spread *F*, *J. Geophys. Res.*, *66*, 1081, 1961.

Costa, E., and M. C. Kelley, Calculations of equatorial scintillations at VHF and gigahertz frequencies based on a new model of the disturbed equatorial ionosphere, *Geophys. Res. Lett.*, *3*, 677, 1976.

Costa, E., and M. C. Kelley, On the role of steepened structures and drift waves in equatorial spread *F*, *J. Geophys. Res.*, *83*, 4359, 1978.

Dungey, J. W., Convective diffusion in the equatorial *F* region, *J. Atmos. Terr. Phys.*, *9*, 304, 1956.

Dyson, P. L., and R. F. Benson, Topside sounder observations of equatorial bubbles, *Geophys. Res. Lett.*, *5*, 795, 1978.

Farley, D. T., B. B. Balsley, R. F. Woodman, and J. P. McClure, Equatorial spread *F*: Implications of VHF radar observations, *J. Geophys. Res.*, *75*, 7199, 1970.

Haerendel, G., Theory of equatorial spread *F*, report, Max Planck Inst. fur Phys. und Astrophys., Garching, W. Germany, 1974.

Hudson, M. K., and D. F. Kennel, Linear theory of equatorial spread *F*, *J. Geophys. Res.*, *80*, 4581, 1975.

Kelley, M. C., and E. Ott, Two-dimensional turbulence in equatorial spread *F*, *J. Geophys. Res.*, *83*, 4369, 1978.

Kelley, M. C., G. Haerendel, H. Kappler, A. Valenzuela, B. B. Balsley, D. A. Carter, W. L. Ecklund, C. W. Carlson, B. Hausler, and R. Torbert, Evidence for a Rayleigh-Taylor type instability and upwelling of depleted density regions during equatorial spread *F*, *Geophys. Res. Lett.*, *3*, 448, 1976.

Klostermeyer, J., Nonlinear investigation of the spatial resonance effect in the nighttime equatorial *F* region, *J. Geophys. Res.*, *83*, 3753, 1978.

Koster, J. R., and T. Beer, A new theory of equatorial spread *F*, in *Ionospheric Research Using Satellites—An Interpretation of Ionospheric Faraday Rotation Observations at the Equator*, Department of Physics, University of Ghana, Legon, Accra, Ghana, 1972.

McClure, J. P., W. B. Hanson, and J. H. Hoffman, Plasma bubbles and irregularities in the equatorial ionosphere, *J. Geophys. Res.*, *82*, 2650, 1977.

Ossakow, S. L., S. T. Zalesak, B. E. McDonald, and P. K. Chaturvedi, Nonlinear equatorial spread *F*: Dependence on altitude of the *F* peak and bottomside background electron density gradient scale length, *J. Geophys. Res.*, *84*, 17, 1979.

Rottger, J., Drifting patches of equatorial spread *F* irregularities: Experimental support for the spatial resonance mechanism in the ionosphere, *J. Atmos. Terr. Phys.*, *40*, 1103, 1978.

Scannapieco, A. J., and S. L. Ossakow, Nonlinear equatorial spread *F*, *Geophys. Res. Lett.*, *3*, 451, 1976.

Weber, E. J., J. Buchau, R. H. Eather, and S. B. Mende, North-south aligned equatorial airglow depletions, *J. Geophys. Res.*, *83*, 712, 1978.

Woodman, R. F., and C. LaHoz, Radar observations of *F* region equatorial irregularities, *J. Geophys. Res.*, *81*, 5447, 1976.

(Received April 11, 1979;
revised July 27, 1979;
accepted August 21, 1979.)

JOURNAL OF GEOPHYSICAL RESEARCH, VOL. 85, NO. A10, PAGES 5119-5130, OCTOBER 1, 1980

Coordinated Study of Equatorial Scintillation and In Situ and Radar Observations of Nighttime *F* Region Irregularities

SANTIMAY BASU,[1] J. P. MCCLURE,[2] SUNANDA BASU,[1] W. B. HANSON,[2] AND J. AARONS[3]

A coordinated set of Atmospheric Explorer E (AE-E) satellite in situ, VHF radar backscatter, and scintillation measurements performed during 1977 over a common ionospheric volume is used to study the relationship between the plasma depletions or bubbles, the extended 3-m irregularity structures known as plumes and bursts of scintillation activity or patches in the nighttime equatorial *F* region. It is shown that in the early evening hours saturated VHF and UHF scintillation and 3-dB fluctuations (propagation path in the east-west plane where the effect of anisotropy is least) at 1.54 GHz are obtained in association with strong 50 MHz radar backscatter, implying near simultaneous (~min) excitation of large scale (~km to 100 m) and 3-m irregularities. In this early developed phase of irregularities, the AE-E in situ measurements detect strong fluctuations of ion concentration with very sharp spatial gradients. The power spectra of these fluctuations in the scale length range of 10 km 100 m conform to a power law variation with one-dimensional spectral index ~1.5. The postmidnight period, on the other hand, is found to be characterized by an absence of radar backscatter and presence of only marginal GHz scintillation activity. However, strong VHF scintillations and somewhat weaker UHF activity is found to persist. The AE-E measurements indicate that during the late phase, the spatial gradients of ion concentration become shallower and the spectral intensity of the irregularities < 500 m decreases by about two orders of magnitude as compared with that recorded during the onset phase. The irregularity spectrum conforms to a quasi-gaussian description with correlation lengths of the order of a kilometer, which corresponds to the Fresnel dimensions of VHF scintillation observations. The implications of the observed spatial structures and the level of ambient concentration on the generation of 3-m irregularities and scintillation modeling are discussed.

1. INTRODUCTION

'Bubbles' and 'plumes' are new terminology currently used by geophysicists to describe the state of the irregular nighttime equatorial ionosphere that have also been identified with scintillation patches by the propagation community [*Basu and Kelley*, 1979]. Plasma bubbles signify the spatially abrupt and irregular decreases (tens of kilometers) of ion concentration as detected by satellite and rocket in situ measurements performed over the nighttime equatorial ionosphere [*Hanson and Sanatani*, 1973; *Kelley et al.*, 1976; *McClure et al.*, 1977]. The presence of large upward (~150 m/s) and smaller westward (tens of m/s) velocity in some of these bubbles has been detected, the upward component being spatially structured and the westward component being more uniform. Plumes, on the other hand, describe the tilted envelope of irregularity structures observed at irregularity wavelengths of 3 m or less in the nighttime equatorial *F* region that rise from continuous irregularity patches at lower altitudes and extend as discrete structures to the topside ionosphere at altitudes as high as 1000 km [*Woodman and LaHoz*, 1976; *Tsunoda et al.*, 1979]. Such plumelike structures that, on occasion, occur at periodic intervals were first observed by *Woodman and LaHoz* [1976] by employing the digital power mapping technique to backscattered signals obtained by the 50-MHz radar at Jicamarca.

Transionospheric communication links established near the magnetic equator indicate that during nighttime the received signal power over the VHF-GHz band exhibits considerable fluctuations, and such scintillation structures are often temporally discrete. Preliminary investigations on radar backscatter ...ps and scintillation activity near the magnetic equator ...owed that the plume structures give rise to intense scintillation activity at VHF and UHF [*Basu et al.*, 1977]. The coexistence of kilometer and meter-scale irregularities [*Basu et al.*, 1978] in the nighttime equatorial *F* region was indeed revealing from the point of view of plasma processes. It provided an impetus for performing coordinated radar and scintillation measurements near the magnetic equator that, in addition to confirming the above, yielded interesting results on the localized generation, the drift, and the decay of irregularity structures that give rise to plume structures and scintillation patches [*Basu and Aarons*, 1977; *Aarons et al.*, 1978, 1980].

It may be noted that scintillation observations in the VHF-GHz range sample the ionospheric irregularities with wavelengths ranging from about a few kilometers to 100 m, the bubble signature in the in situ measurements implies the presence of irregularities in the wavelength range of several tens of kilometers down to few tens of meters, whereas the 50-MHz radar samples the irregularities at a particular wavelength of 3 m at various ranges.

In this paper the phenomena of bubbles, plumes, and scintillation patches in the nighttime equatorial *F* region are critically examined from a coordinated set of in situ, radar, and scintillation measurements performed over a nearly common ionospheric volume. The purpose of the paper is to study the evolution and decay of the plume structures and scintillation activity over the VHF-GHz band in relation to the observed spatial structures of ion concentration within the plasma bubbles. The need for such a study has recently been emphasized in the U.S. National Report on ionospheric irregularities presented at the IUGG meeting at Australia in December, 1979 [*Ossakow*, 1979].

2. OBSERVATIONS

The coordinated set of measurements performed on March 21, 1977 (UT date) is indicated in Figure 1. At Jicamarca (ab-

[1] Emmanuel College, 400 The Fenway, Boston, Massachusetts 02115.
[2] University of Texas at Dallas, Richardson, Texas 75080.
[3] Air Force Geophysics Laboratory, Hanscom Air Force Base, Bedford, Massachusetts 01731.

Copyright © 1980 by the American Geophysical Union

Paper number 80A0853
0148-0227/80/080A-0853$01.00

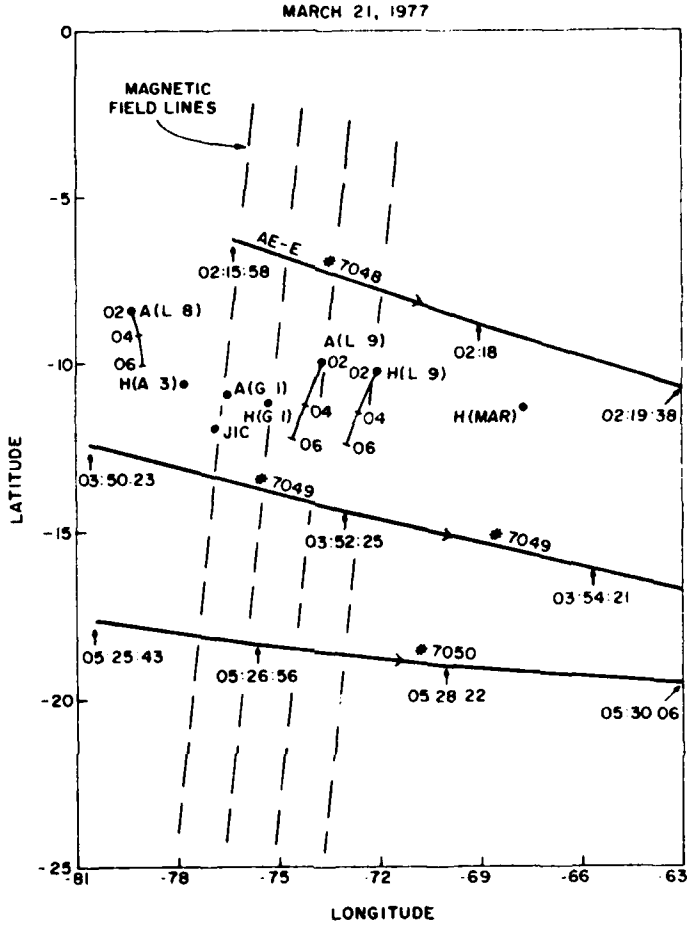

Fig. 1. Location of 50-MHz backscatter radar at Jicamarca (JIC), the subsatellite tracks of Atmospheric Explorer E (AE-E) during orbit numbers 7048, 7049, and 7050 and subionospheric positions (referred to an altitude of 400 km) of scintillation measurements performed at Ancon (A) and Huancayo (H) with various geostationary satellites on March 21, 1977, are indicated. The satellites Les 8, Les 9, ATS 3, Goes 1 and Marisat are abbreviated as L 8, L 9, A 3, G 1, and MAR, respectively. The projection of the earth's magnetic field at the ionospheric height is shown by dotted lines.

breviated as JIC in the diagram) with a magnetic dip location of 2°N, a 50-MHz radar backscatter map of echo power from 3-m irregularities at F region heights was obtained by using a modification of techniques developed by *Woodman and La-Hoz* [1976].

From the two ground stations at Ancon (A) and Huancayo (H), multifrequency scintillation observations were performed with various geostationary satellites. The satellites ATS 3 (A 3) and Goes 1 (G 1) provided transmissions at 137 MHz, Les 8 (L 8) and Les 9 (L 9) satellites provided transmissions at 249 MHz, and Marisat (MAR) provided transmissions at both 257 MHz and 1.54 GHz. The intersections of the 400-km ionospheric height with the propagation paths from different geostationary satellites to the two ground stations are indicated in the diagram by the first letter of the ground station (A or H) followed by the abbreviated name of the satellite as indicated earlier. The subionospheric positions of Les 8 and Les 9 satellites varied considerably during the period of observations owing to the finite orbital inclination of the satellites. As such, along the locus of the subionospheric positions of these satellites the universal times 0200, 0400, and 0600 are indicated. It may thus be noted that by scintillation measurements the ionospheric volumes lying within the longitude swath of 67°W to 80°W were probed at intervals of only a few degrees.

On March 21, 1977, three successive transits of Atmospheric Explorer E (AE-E) satellite occurred between 0200 UT to 0530 UT over the longitude interval under study. The subsatellite tracks of AE-E for the three successive orbits 7048, 7049, and 7050 are shown in Figure 1 with the universal times marked along the track. It should be noted that these orbits of AE-E were nearly circular with a nominal altitude of 250 km. In the present study we shall utilize the data obtained by the retarding potential analyzer (RPA) and the ion drift meter instruments on board the AE-E satellite. A complete description of the instruments and the data acquisition system can be obtained in *Hanson et al.*, [1973] and *Hanson and Heelis* [1975]. The RPA provides the total ion concentration every 4.45 ms corresponding to 35-m spatial resolution along the orbital track. The ion drift meter provides data on plasma arrival an-

Fig. 2. Temporal variation of the range and intensity of 50-MHz backscattered power obtained at Jicamarca on March 20–21, 1977.

gles (pitch and yaw) with respect to the attitude of the spacecraft. The total ion concentration is also available from this instrument every 1/16 of a second corresponding to a spatial resolution of about 500 m. Since charge neutrality can be assumed at F region heights, the electron concentration can be identified with the total ion concentration provided by the instruments. This assumption is important as both radar backscatter and scintillations are caused by the electron density fluctuations in the ionosphere.

3. Results

a. Radar Measurements

In Figure 2 we show the results of 50-MHz radar backscatter observations at Jicamarca made on March 20–21, 1977, between 1900 LT and 0140 LT. The diagram illustrates the temporal variation of range and intensity of 3-m irregularities observed on this night. The range and time scales are given by the ordinate and abscissa, respectively, while the intensity of the echo power is provided by the different shades in the range of 6–48 dB above a reference power level corresponding to one-quarter of the approximate maximum incoherent scatter level.

It may be noted that the radar commenced to detect weak 3-m irregularities from an altitude of about 300 km at 1930 LT. The layer thickness of weak irregularities increased progressively to about 25 km at 2010 LT, after which a series of intense and spectacular plume structures were observed. Some of these plumes extended all the way from the bottomside F region to 700 km, the altitude limit of the backscatter maps presented here.

Concentrating on the lowest altitude of backscatter returns shown in Figure 2 we observe a gradual rise of the minimum altitude at the commencement (1930 LT to 2010 LT), a cusp-like altitude modulation of the first plume's underside around 2050 LT and a gradual but spectacular fall between 2100 LT to 2250 LT from 350 km to 185 km. While the initial rise and final fall can be related to the typical behavior of equatorial F layer after sunset, the altitude modulation of the bottom of the 3-m echo region is rather significant. Such intrusions associated with the Rayleigh-Taylor instability [*Balsley et al.*, 1972; *Haerendel*, 1974] have been schematically represented by *Woodman and LaHoz* [1976] and recently demonstrated by computer simulations of the collisional Rayleigh-Taylor instability with initial long wavelength plasma density perturbations [*Zalesak et al.*, 1978]. It may be of interest to note that such intrusions are most marked in plumes that are detected early in the evening.

b. Scintillation Measurements

Figures 3*a* and 3*b* show the results of multifrequency scintillation measurements performed at the two ground stations. The different panels in Figure 3*a* are arranged from top to bottom in the order of decreasing west longitude of the subionospheric position (intersection of the propagation path with 400-km ionospheric height) over the interval of about 79°W to 75°W. The precise subionospheric location of propagation paths for the different panels may be obtained from Figure 1. Each panel in the diagram shows the temporal variation of scintillation index in dB [*Whitney et al.*, 1969] as scaled from the data over successive 2.5-min intervals. The different panels in Figure 3*b* are similarly arranged in the order of decreasing west longitude of the subionospheric position covering the longitude interval of 75°W to 67.5°W and indicate the temporal variation of scintillation index (dB) on respective propagation paths.

Considering the different dynamic ranges of VHF receivers, we conclude from panels 2, 3 and 4 of Figure 3*a* that VHF scintillations were saturated for more than 4 hours on all VHF links. The UHF links (panel 1 in Figure 3*a* and panels 1, 2, and 3 in Figure 3*b*) also attained saturation levels but over shorter periods of time lasting for about 2 hours. It should be noted that the dynamic ranges of VHF receivers at Huancayo were limited to about 16 dB, whereas the receivers at Ancon had wider dynamic ranges extending to about 25 dB.

In order to compare the temporal behavior of 3-m irregularity structures obtained from the radar power map (Figure 2) and the integrated strength of kilometer scale irregularities provided by scintillation measurements, we find that the observational result of the communication link between the Goes satellite and Ancon station (panel 3 of Figure 3*a*) is most suitable. The propagation path of this link was located only 10 km to the east of the radar illumination at 400-km altitude and thus the radar and scintillation measurements pertain to a nearly common ionospheric volume. In view of the spatial localization of nighttime irregularity structures in the east-west direction [*Aarons et al.*, 1978; *Basu and Aarons*, 1977], it is important that the radar and scintillation measurements probe ionospheric volumes that are separated by not more than a few tens of kilometers in the east-west direction. Comparing panel 3 of Figure 3*a* with Figure 2, we note that the onset of 137-MHz scintillations did not occur before 0050 UT (1950 LT at 75°W meridian) although the radar was detecting a weak and thin layer of 3-m irregularities at 300 km for nearly 20 min prior to this time. It is not, however, clear if the backscatter return during this time truly represents an irregularity layer or merely shows the signature of partial reflections from

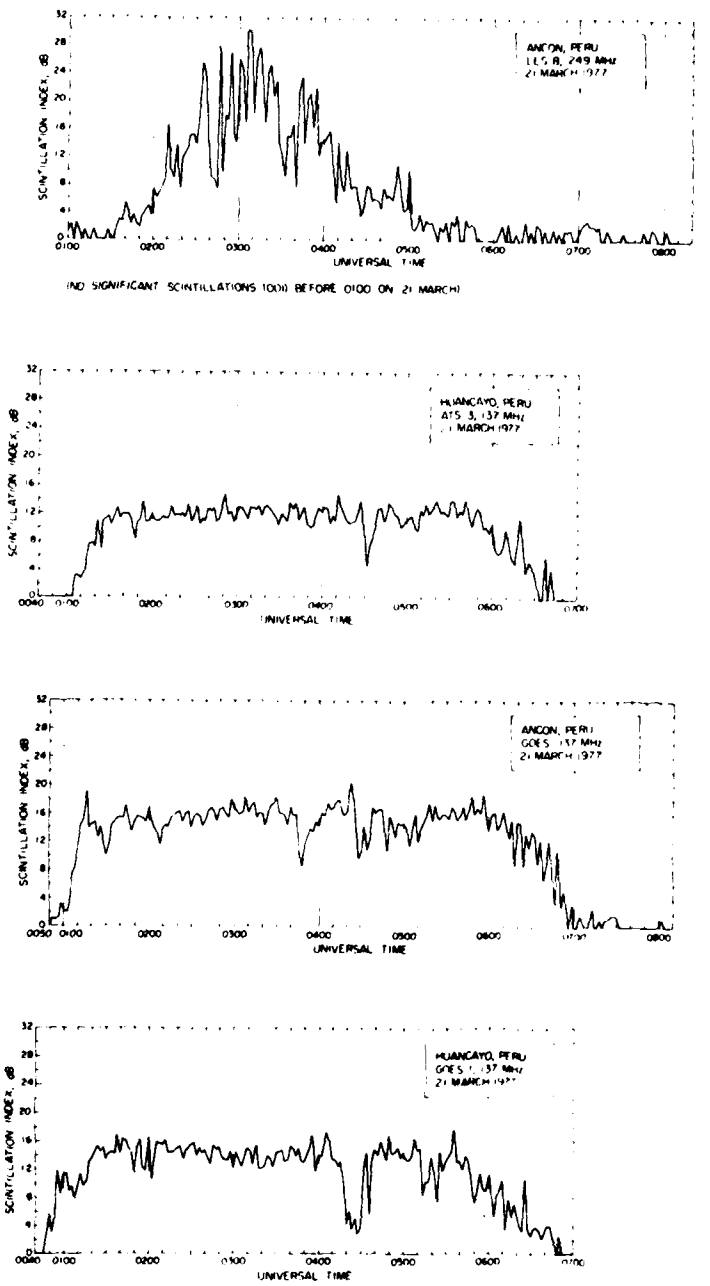

Fig. 3a

Fig. 3. (*a*) Temporal variation of scintillations recorded on different propagation paths over the subionospheric longitude interval of 79°W–75°W straddling the radar site at Jicamarca. (*b*) Same as in Figure 3*a* over the subionospheric longitude interval of 75°W–67°W.

sharp vertical gradients in electron concentration [*Balsley and Farley*, 1975]. Shortly thereafter, at 2015 LT, an explosive development of VHF scintillation to saturation occurs in conjunction with moderately strong (18–36 dB) backscatter returns from 3-m irregularities extending over an altitude interval of about 100 km. After this event, the radar map exhibits a series of spectacular plume structures until about 2250 LT, while VHF scintillations remain saturated. The radar fails to detect any conspicuous irregularities after 2300 LT except for some marginal backscatter prior to 0100 LT.

Scintillation measurements on Ancon (Goes) path indicate that scintillations persist until 0200 LT (or 0700 UT) and, in

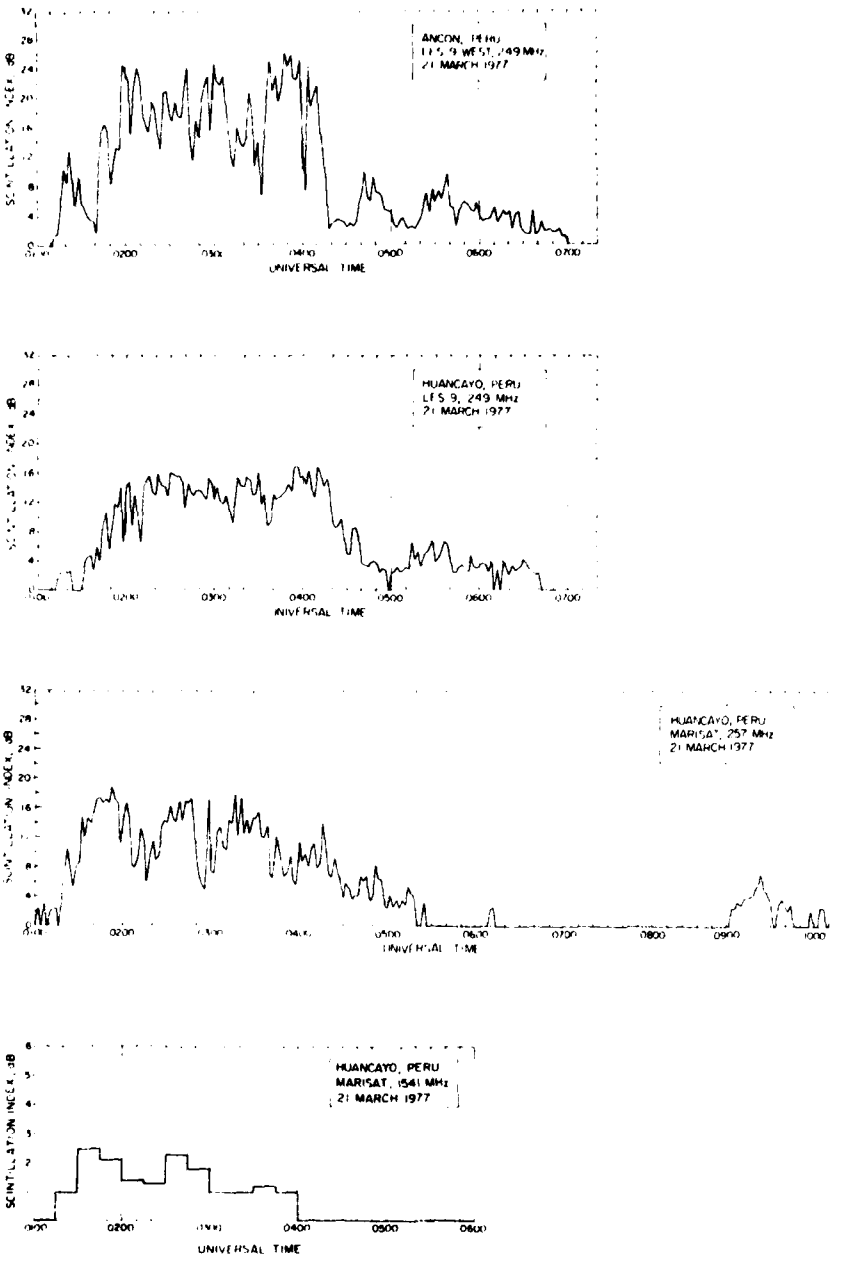

Fig. 3*b*

fact, saturated VHF scintillations are observed between 2250 LT and 0100 LT when the radar failed to detect any conspicuous backscatter events. The intercomparison confirms the earlier findings of *Basu et al.* [1978] that kilometer and meter scale irregularities coexist in the early phase of equatorial irregularity generation during nighttime, but in the late phase, even though the meter scale irregularities decay the kilometer scale irregularities persist for several hours longer.

A study of the different panels of Figures 3*a* and 3*b* indicates that the irregularity structure that caused scintillations shown in panels 2, 3, and 4 in Figure 3*a* between 0040 UT (1940 LT) and 0200 UT and also backscattered the 50-MHz signal at Jicamarca covered a longitude interval of at least 75°W to 78°W. The structure did not extend much farther to the west, as the UHF propagation link from Ancon to Les 8 (panel 1 in Figure 3*a*) failed to detect any scintillations during this period. On the other hand, the irregularity structure that caused scintillations on Ancon (L 8) propagation path between 0140 UT and 0500 UT is expected to drift eastward, intercept various propagation paths to the east and cause scintil-

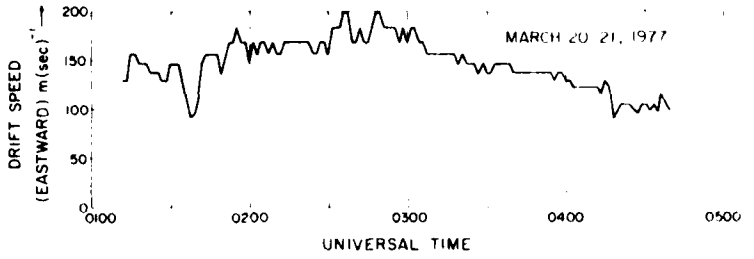

Fig. 4. East-west drift obtained on March 21, 1977, from spaced receiver (east-west baseline: 366 m) scintillation measurements at Ancon by using 249-MHz transmissions from Les 9 satellite

lations until the structure decays as determined by its lifetime. The temporal behavior of scintillations at one position is thus determined by the local generation of irregularities as well as the drifting irregularities from the west that intercept a given propagation path. We had commented earlier on the relatively shorter lifetime of 3-m scale irregularities as compared with the kilometer scales from a comparison of radar and scintillation observations. From panel 4 of Figure 3*b* we note that 1.54-GHz scintillations on this night ceased after 0400 UT, corresponding to 2330 LT at the longitude of the subionospheric position (67.5°W) although VHF and UHF scintillations at various longitudes persisted several hours longer. It is not possible to compare the features of GHz scintillation event with the radar backscatter event owing to the wide longitude separation of the ionospheric volumes probed by the two techniques. However, on a statistical basis, we note that during 1976–1977, the radar at Jicamarca did not record conspicuous 3-m irregularity structures in the postmidnight period, and the GHz communication link with Marisat over the east-west plane continued to record scintillations after the decay of meter irregularities but failed to record conspicuous (>1 dB) scintillation events during the postmidnight period.

In order to obtain information on the dynamics of ionospheric irregularities causing scintillations, drift speed measurements were made by performing spaced receiver scintillation observations. The measurement was made at Ancon by the use of 249-MHz transmissions from Les 9 and recording scintillations on two receiving systems placed on an east-west baseline of 366 m. The apparent irregularity drift in the east-west direction was determined from a cross-correlation analysis of the spaced receiver data [*Briggs and Golley*, 1968]. The present drift measurements from scintillation observations give the weighted average value and, as such, provide information on the irregularity drift around the *F* region maximum. Figure 4 shows the temporal variation of drift observed on March 21, 1977. The maximum cross-correlation coefficient for these computations exceeded 0.7 except for four data points. The local time (LT) at the subionospheric location was LT = UT − 5 h.

The irregularities are found to drift in the east-west direction just as the background plasma in the equatorial *F* region drifts during the nighttime hours [*Rishbeth*, 1971; *Woodman*, 1972]. The drift speed is found to increase from 130 m/s to values as high as 200 m/s in the early phase, and during this period, considerable fluctuations of drift speed are observed. It should be noted that because of the finite zenith angle of these observations, the apparent eastward drift will be affected by an existing vertical drift of the irregularities. Under normal conditions the vertical velocity is generally a small fraction of the horizontal drift and hence for the geometry under consideration, errors will probably not exceed 20%. However, on occasions, highly structured vertical velocities within bubbles have been measured by in situ and radar techniques [*Balsley et al.*, 1972; *Woodman and LaHoz*, 1976; *McClure et al.*, 1977]. It appears that the large fluctuations in the apparent horizontal velocity recorded in the early phase may be caused by such structures in vertical velocity.

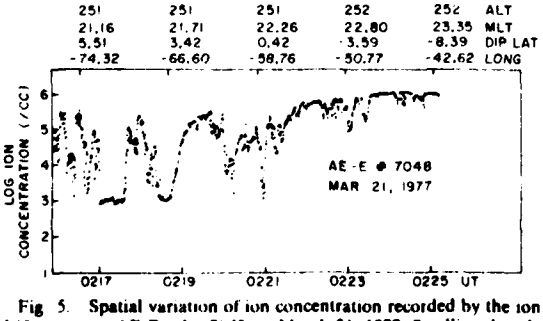

Fig. 5. Spatial variation of ion concentration recorded by the ion drift meter on AE-E orbit 7048 on March 21, 1977. Satellite altitude (ALT), magnetic local time (MLT), dip latitude (DIPLAT), and geographic longitude (LONG) are indicated in the diagram.

c. *In Situ Measurements*

We shall now discuss the in situ results obtained by the AE-E satellite over three successive orbits: 7048, 7049, and 7050. The geometry of these orbits relative to the ground stations is illustrated in Figure 1, and the nominal satellite altitude was 250 km for all these orbits.

Orbit 7048. From Figure 1 it may be noted that the satellite (orbital inclination 19.75°) was travelling from northwest to southeast and the track was somewhat to the north of the dip equator, along which various ionospheric locations were probed by radar and scintillation measurements. The ion concentration data acquired by the ion drift meter are shown in Figure 5 at 0.5-s interval. The figure provides an overall view of the large ion concentration fluctuations that existed between 21 23 MLT over the longitude interval of 70°W to 42°W. Even though the satellite was sampling at an altitude of 250 km, the relative ion concentration fluctuations recorded by it correspond to those existing at higher altitudes over the magnetic equator. This is because the plasma within the entire field tube takes part in the instability process, and the relative ion concentration fluctuations, at least at large scale lengths, can be mapped along the field lines. At the extreme left-hand edge of the orbit, at approximately 0216 UT (2116 LT), the satellite location maps up the field lines to an altitude of 390 km over Jicamarca. Owing to the orbital inclination, the satellite location further to the east near 67.5°W longitude at 0218

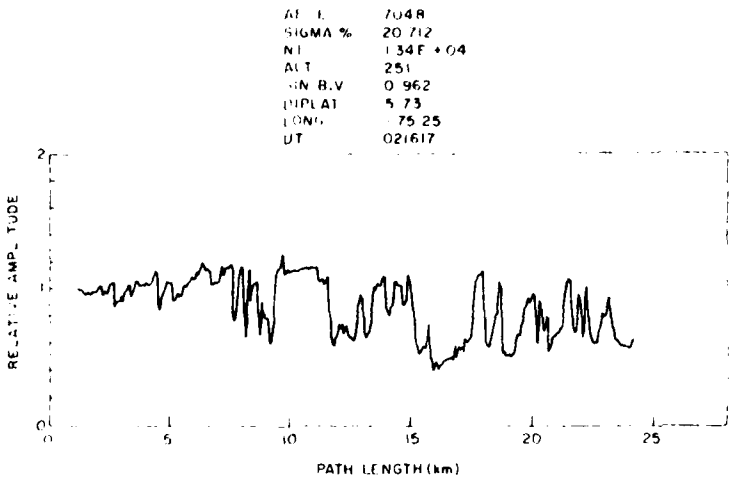

Fig. 6. A 3-s sample of high resolution RPA data of relative amplitude obtained on orbit 7048 indicating the presence of steep spatial gradients of ion concentration before the satellite entered a deep bite-out region in the early phase of irregularity generation. The satellite location maps along the earth's magnetic field lines to a 3-m plume structure over Jicamarca. The irregularity amplitude, (SIGMA), the ion concentration (NI) at the beginning of the data interval, the satellite altitude (ALT), the sine of the angle between the magnetic field (B) and the satellite velocity (V) vectors, the dip latitude (DIPLAT), geographic longitude (LONG), and the universal time (UT) are indicated in the figure

UT (2148 LT) maps to an altitude of 300 km over the subionospheric position of scintillation observations with Marisat satellite from Huancayo, H(MAR). If we examine the radar backscatter map shown in Figure 2, we find that the bottom edge of F region irregularities was not above 270 km at 2116 LT and 220 km at 2148 LT. Thus the relative ion concentration fluctuations detected by the satellite in this orbit do indeed correspond to fluctuations at F region heights above the dip equator. The scintillation observations detected intense F region irregularities near the dip equator over the longitude swath of 77°W to 67°W in agreement with the large ion concentration fluctuations present in the in situ data.

We shall now make a detailed comparison of the radar backscatter and in situ ion concentration data obtained in orbit 7048. As was mentioned earlier, the satellite location at 021558 UT maps up along magnetic field lines to an altitude of 390 km above Jicamarca where the radar measurements

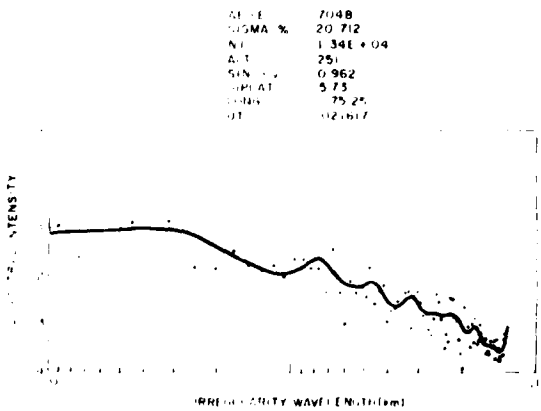

Fig. 7. Power spectrum of the linearly detrended data corresponding to the sample shown in Figure 6 obtained by the FFT (dots) and maximum entropy (solid line) techniques, respectively.

were performed. Figure 2 shows that at that time, this altitude corresponds to the beginning of the second plume structure, in situ data corresponding to which has been discussed by J. P. McClure et al. (unpublished manuscript, 1980). Here we show in Figure 6 the relative change of ion concentration obtained from the RPA in the high resolution (35 m) mode over a 3-s interval (24 km) beginning at 021617 UT when AE-E was east of Jicamarca. The relative amplitude in the diagram signifies $\Delta N/\bar{N}$, where ΔN is the change in ion concentration from the ion concentration ($\bar{N}$) at the beginning of a 3-s interval. The numbers at the top of the diagram denote the square root of the variance of $\Delta N/N$ expressed as a percentage (SIGMA%), the average ion concentration (NI), the angle between the satellite velocity (V), and magnetic field vector (B) as well as the parameters that signify the satellite altitude and location. In view of the eastward motion of the satellite and the large angle between the satellite and magnetic field, the extremely steep gradients of ion concentration portrayed in Figure 6 correspond to the gradients approximately in the magnetic east-west direction. The presence of such steep gradients is found to be a characteristic of the irregularity structures over the dip equator in the evening hours. The steep structures that we observe to the east of Jicamarca are probably associated with the first plume if the prevailing irregularity drift (Figure 4) is taken to account. A similar situation is discussed by J. P. McClure et al. (unpublished manuscript, 1980) for orbit 7049 when the satellite was much closer to the radar site.

The RPA data of total ion concentration shown in Figure 6 was linearly detrended, and the zero mean time series of positive and negative fluctuations of $\Delta N/\bar{N}$ was obtained, $\bar{N}$ being derived from the trend line. The power spectrum for this time series was then obtained from both the FFT and maximum entropy method (MEM) of spectral analyses. The FFT program was the same as the one used earlier by *Dyson et al.* [1974]. The spectra were normalized such that the integral of the fluctuation power $\int S(f)df$ over the observed frequency (f)

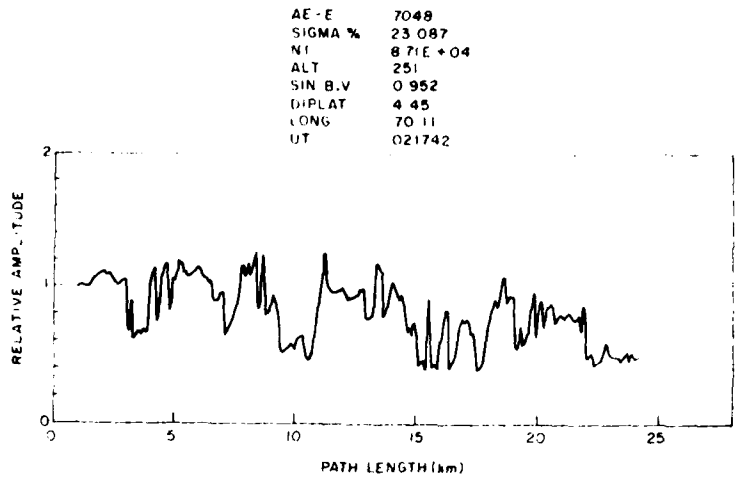

Fig. 8. Same as in Figure 6 recorded after the satellite emerged from the deep bite-out region.

range equals the variance of the original time series of $\Delta N/\bar{N}$. The frequency (f) scale was converted to irregularity wavelength (λ) by using the relation $\lambda = v_s/f$, where v_s is the satellite velocity. In view of its geophysical importance, we shall illustrate the power spectra in terms of irregularity wavelength. Figure 7 shows the power spectrum of $\Delta N/\bar{N}$ of the RPA data illustrated in Figure 6. The dots indicate the spectral estimates obtained by the FFT technique and the solid line represents the MEM spectrum. It should be kept in mind that the above spectrum obtained from in situ data is a one-dimensional power spectrum of $\Delta N/\bar{N}$. If we neglect the somewhat flat portion of the spectral intensity at large irregularity wavelengths (>5 km), then the overall spectrum can be described by a power law variation. In terms of frequency (f), the normalized spectral intensity (S) of relative ion concentration ($\Delta N/N$) fluctuations illustrated in Figure 7 can be expressed as $S = 0.025 f^{-1.7}$. Translating the frequency in terms of irregularity wavelength (λ), the spectrum may be represented as $S \propto \lambda^{1.7}$. The corresponding spectral intensity (P) of ion concentration deviation (ΔN) can be obtained by multiplying S by $(\bar{N})^2$. In general, the one-dimensional spectral intensity as provided by the in situ measurement has been expressed as $P = C_s^{(1)} f^{-n}$,

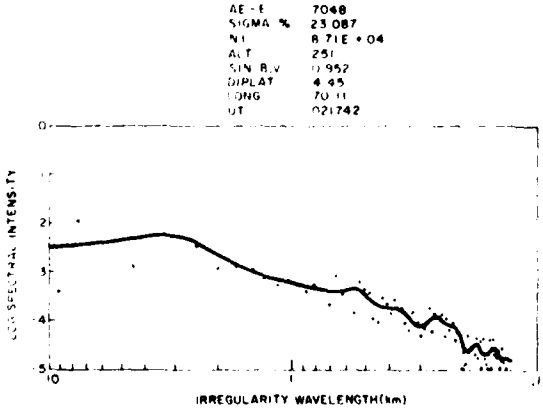

Fig. 9. Same as in Figure 7 for the sample shown in Figure 8.

where $C_s^{(1)}$ is defined as the one-dimensional strength of turbulence [*Rino*, 1979] and n is the one-dimensional spectral index. For the data sample shown in Figure 7, $\bar{N} = 1.34 \times 10^{12}$ m^{-3} and therefore $P = 4.56 \times 10^{18} f^{-1.7}$ in mks units, which gives $C_s^{(1)} = 4.56 \times 10^{18}$ mks.

For a turbulence-type distribution of irregularities, a knowledge of one-dimensional irregularity power spectrum obtained from in situ measurements and information on irregularity layer thickness as may be derived from radar backscatter observation is sufficient for an estimation of the level of scintillations in the framework of phase screen theory. The power spectrum shown in Figure 7 corresponds, however, to the data sample (Figure 6) that exhibits steep spatial gradients. The implications of such steep gradients for irregularity generation [*Chaturvedi and Ossakow*, 1977; *Costa and Kelley*, 1978] and modeling of scintillations [*Wernik et al.*, 1979] for special propagation conditions will be discussed later. From a study of the variable inclination of the plume structures in radar backscatter maps [*Woodman and LaHoz*, 1976] and structured upward drift speeds of the irregularities obtained from in situ measurements [*McClure et al.*, 1977], the sharp gradients, so evident in density fluctuations at one altitude may not, in general, be preserved in the integrated electron deviation ΔN. While we recognize the significance of steep spatial gradients of density in delineating the generation mechanism of irregularities and its importance in scintillation computations when the propagation path is aligned with the steep density structures over the entire irregularity layer thickness, we consider that, in general, the assumption of a turbulent type of integrated electron density deviation is appropriate for estimating scintillation effects. For the analytical form of power spectrum discussed in the previous paragraph, the one-dimensional strength of turbulence is $C_s^{(1)} = 4.56 \times 10^{18}$ mks and the spectral index of 1.7 may be used to obtain the three-dimensional strength of turbulence as $C_s = 1.1 \times 10^{18}$ mks [*Rino*, 1979]. The above value of C_s pertains to the satellite altitude of 250 km, and since for a constant irregularity amplitude ($\Delta N/N$) the strength of turbulence scales as the square of electron concentration, its value at 400-km altitude above the dip equator is expected to be of the order of 10^{20} mks if we assume that the local electron concentration above the dip equator is

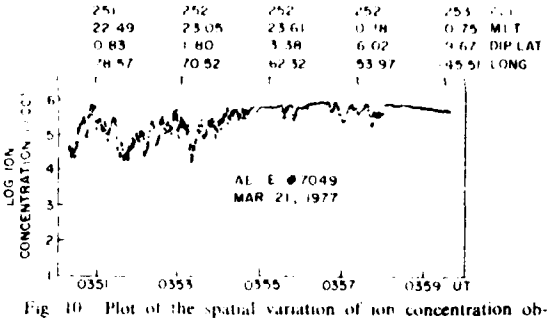

Fig. 10. Plot of the spatial variation of ion concentration obtained from the ion drift meter at 0.5-s interval on AE-E orbit 7049 over the longitude interval of interest.

10^{-1} m^{-3}. If such levels of turbulence strength ($C_s^2 = 10^{20}$) prevail over an altitude extent of 100 km as depicted by the radar power map, intensity scintillations of 2 dB are expected on *L* band frequencies for overhead propagation paths. We note that intensity scintillations on the Marisat propagation path aligned close to the magnetic east-west direction did not exceed 3-dB level at 1.54 GHz on this night.

As the satellite moves further eastward past Jicamarca, it records a deep bite-out of ion concentration below 10^9 m^{-3} at 0217 UT (Figure 5). Unfortunately, at such levels of ion concentration (<10^9 m^{-3}) the signal gets buried in noise picked up by the electrometer [*Hanson and Heelis*, 1975] precluding any study of the irregularity power spectrum within the large-scale depletion. The satellite remained within it until 021736 when the RPA failed to record ion concentrations above 10^9 m^{-3}. The east-west dimension of the bite-out region is about 240 km corresponding to the time interval of 36 s. Only 6 s later, at 021742, the satellite emerges from the bite-out region and steep spatial density structures are again recorded by the RPA as illustrated in Figure 8. The spectrum for the data sample is shown in Figure 9, and the spectral intensity of relative ion concentration (S) again conforms to a power law variation with frequency (f), and the normalized spectrum can be expressed as $S = 0.027/f^{1.5}$ or $S \propto \lambda^{1.5}$, where λ is the irregularity wavelength. Considering the average ion concentration, the strength of turbulence for the above spectrum is obtained as $C_s^2 = 2 \times 10^{20}$ mks, which is consistent with the observed GHz scintillations.

Orbit 7049. The orbit crossed the longitude interval of interest between 0350 UT and 0354 UT as indicated in Figure 1 and passed only 1.5°S of Jicamarca. The ion concentration acquired every 0.5 s by the ion drift meter is shown in Figure 10, which indicates that large scale spatial variations of ion density amounting to nearly two orders of magnitude existed in this region. As was discussed earlier, the ground to satellite links recorded saturated VHF and UHF scintillation and 1-dB gigahertz scintillation between 67°W and 79°W longitude at the time of the AE-E transit.

The high-resolution RPA data over a 3-s interval following 035114 UT (225124 LT at 75° W) and its corresponding spectrum are discussed in J. P. McClure et al. (unpublished manuscript, 1980). At that time the satellite sampled the ion concentration only 1.5°S of Jicamarca so that the satellite location maps along magnetic field lines to an altitude of 252 km over Jicamarca. It should be noted that the power spectrum of the data sample at 035124 UT shows a steeper slope ($\lambda^{2.5}$) at short wavelength end (<500 m) as compared with the spectrum registered at similar position in the earlier transit. This results in a reduction of spectral intensity at short wavelengths by approximately an order of magnitude over that obtained in the earlier orbit 7048 at 021617 identified with a plume structure near the Jicamarca meridian.

After about 3 min, the satellite sampled the ion concentration fluctuations farther to the east in the vicinity of the subionospheric location of Marisat satellite at a local time of 233428. The relative ion concentration fluctuations over a 3-s interval recorded by the RPA is indicated in Figure 11. The spatial density structures become less sharp with a consequent decrease of spectral intensity at short irregularity wavelengths. The power spectrum of this data sample is shown in Figure 12, which indicates a power law variation of $\lambda^{2.5}$ at irregularity wavelengths shorter than about 2 km accompanied by a spectral flattening at longer wavelengths. An order of magnitude

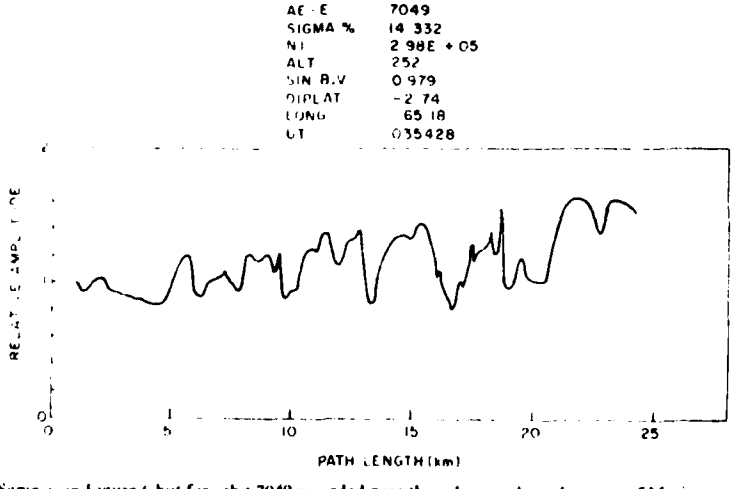

Fig. 11. Same as in Figure 6 but for orbit 7049 recorded near the subionospheric location of Marisat satellite observed from Huancayo when 1-dB scintillation at 1.54 GHz was recorded. Erosion of sharp gradients of ion concentration may be noted.

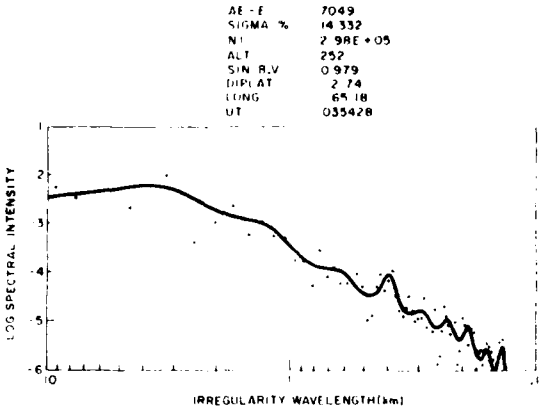

Fig. 12. Same as in Figure 7 for the sample shown in Figure 11.

reduction in spectral intensity at small irregularity wavelengths may be noted during this period as compared with that obtained 3 min earlier and discussed in the previous paragraph. At similar local time the radar failed to detect any 3-m irregularity over Jicamarca, and the 1.54-GHz link was recording only 1 dB fluctuations.

Orbit 7050. This orbit was located as far south of Jicamarca as the first orbit 7048 was to the north. The orbit spanned the longitude interval of interest near midnight when no scintillations were observed at 1.54 GHz and only marginal UHF but quite strong VHF scintillations were recorded. Figure 13 shows the ion concentration plot at 0.5-s interval obtained from the ion drift meter. A wide bite-out region with some large scale fluctuations of ion concentration is noted although the fluctuations are observed to be much less deep than those registered in earlier transits. The radar map does not provide any evidence of fresh 3-m irregularity generation near 052630 UT when AE-E crossed the meridian of Jicamarca.

In Figure 14 we show a data sample recorded by the RPA during orbit 7050 in the vicinity of the subionospheric location of Marisat satellite. The spatial variations of ion concentration appear much smoother than those noted in the earlier transits indicating a preferential decay of small scale irregularities. The power spectrum for this data sample (Figure 15) indicates a steep spectral index (~3.5) that is caused by the decay of irregularities with wavelengths smaller than 1 km. At VHF, scintillation effects of such irregularity power spectrum become equivalent to gaussian irregularities with correlation lengths of the order of a km and substantial VHF scintillations (~ 10 dB) are expected to persist. However, owing to the drastic reduction of spectral intensity between 1 km to 100 m in the vicinity of the Frensel dimension for GHz observations, scintillations at GHz frequencies cannot develop. This is in agreement with scintillation observations discussed in the paper.

4. Discussion

The correlative measurements based on radar backscatter, satellite in situ, and radio wave scintillation techniques indicate that in the initial flash phase of generation, the nighttime *F* region equatorial irregularities covering the wavelength range of tens of kilometers to a few meters or less are excited within a time scale of the order of minutes. In the late phase, however, the decay commences at short irregularity wavelengths and proceeds toward the longer wavelengths in such a manner that the 3-m irregularities decay hours before the kilometer wavelengths.

The sharp gradients of electron concentration detected by the satellite in situ measurements during the early phase of irregularity lifetime have important implications for irregularity generation mechanisms and modeling of scintillations. *Chaturvedi and Ossakow* [1977] have shown that the evolution of the nonlinear collisional Rayleigh-Taylor instability in the nighttime equatorial *F* region gives rise to such steepened structures providing a phase coherent irregularity power spectrum. They pointed out that a turbulent mechanism of irregularity generation will, on the other hand, provide a randomly phased power spectrum but with identical spectral index. From an analysis of rocket data of electron concentration through an equatorial bubble, the existence of such phase coherent structures has been confirmed [*Costa and Kelley*, 1978]. From AE-E data we have shown that the presence of steep spatial gradients is a feature of only the early generation phase of strong irregularities that give rise to a power law type of irregularity power spectrum with one-dimensional power spectral index of about 1.5.

Wernik et al. [1979] have demonstrated that if the electron concentration structures with steep gradients are stacked in altitude, a vertically propagating radio wave is affected quite differently from that expected for an identical turbulent type medium. In this study we have considered that in view of the structured upward drift speed of the irregularities, the total electron density deviation integrated through an irregularity layer along the propagation direction will, in general, be random, and conventional scintillation theory may still apply. Our 1.54-GHz scintillation observations, performed, of course, at a low elevation angle of 20°, exhibited random type of amplitude fluctuations. In view of the predictions of *Wernik et al.* [1979] model computations, it will be of interest to perform GHz scintillation observations near the dip equator at high elevation angles preferably tilted to the west and determine if the signal structure on the ground conforms to the predicted signature of steep irregularity structures.

In contrast to the above, the irregularities in the late phase are characterized by a progressive erosion of steep spatial gradients in the 10 km to 100-m range and a decay of the spectral intensity of irregularities that commences at meter wavelength and then proceeds toward the kilometer wavelength end. Confirming evidence has recently been provided by *Tsunoda and Towle* [1979], who report the persistence of total electron content bite-outs without associated backscatter from 1-m irregularities. In regard to VHF scintillations, the AE-E in situ data

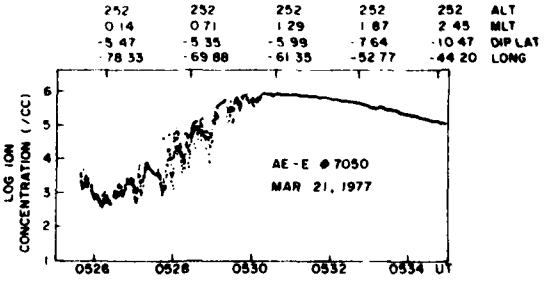

Fig. 13. Same as in Figure 10 for the AE-E orbit 7050 crossing the longitude interval of interest around local midnight.

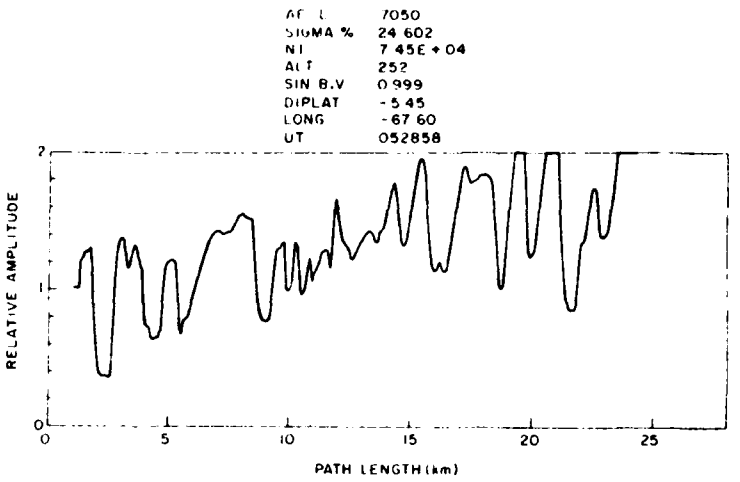

Fig. 14. Same as in Figure 6 but for orbit 7050 in the very late phase when *L* band and UHF scintillations had decayed. Absence of sharp spatial gradients in this late phase may be noted.

obtained during the very late phase are equivalent to a gaussian irregularity spectrum with correlation lengths (~1 km) of the order of the Fresnel dimension of VHF scintillation measurements. This explains the persistence of VHF scintillations in the absence of any activity in the UHF-GHz range.

The phase scintillation measurements with the orbiting Wideband satellite performed near the magnetic equator have consistently yielded a power law type of irregularity spectrum with average one-dimensional power spectral index less than 2 [*Rino*, 1979] and have not given any evidence of outer scale with detrend intervals as large as 100 s [*Rino et al.*, 1978]. In view of the fact that the Wideband satellite transits over the magnetic equator near midnight, these observations pertain to the late phase, but the derived spectrum conforms to the in situ spectrum observed in the early phase. It should, however, be pointed out that the in situ spectrum corresponds to the electron concentration fluctuation at the fixed altitude of AE-E, whereas the phase scintillations arise from the electron density deviation integrated over the irregularity layer. The relationship between the spectra obtained by these two techniques needs to be explored during the different phases of irregularity evolution and decay by the use of continuous phase scintillation measurements with geostationary satellites.

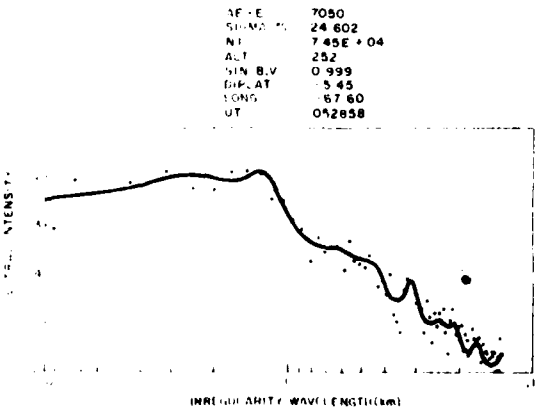

Fig. 15. Same as in Figure 7 for the sample shown in Figure 14.

The in situ measurements, of course, do not directly provide information on the small scale lengths (~m) that are explored by the backscatter radar technique. However, *Woodman and Basu* [1978], from a comparison of VHF scintillation and backscatter observations, pointed out that the predicted backscatter level at 3 m is expected to be several orders of magnitude higher if the power law power spectrum with a three-dimensional spectral index ~4 [*Dyson et al.*, 1974] of longer wavelength irregularities explored by the in situ technique is extrapolated to 3 m. Further, the recent radar observations at Kwajalein [*Towle*, 1980] indicate that the backscatter power levels at 1 m and 36 cm conform to one-dimensional spectral index of less than unity in contrast to the one-dimensional index somewhat larger than 1.5 that we observed with AE-E over the irregularity wavelength range of 0.1–1 km during the most developed phase. Thus while these observations indicate the possible existence of a cutoff and a break in slope somewhere in the range of tens of meter wavelength, we have no knowledge yet of the mechanism for the cutoff and its location in the wave number regime. It appears that high resolution rocket measurements may be helpful for a study of this range of irregularity wavelengths.

From the point of view of 3-m irregularity generation, it is significant that steep spatial gradients (scale lengths ≤100 m) and high spectral intensity of longer irregularity wavelengths (0.1–10 km) provide a signature of the presence of 3-m irregularities. Further from AE-E, it seems that 3-m irregularities are not only confined to deep bite-out regions with low (10^9 m^{-3}) electron concentration but are present in regions with concentration exceeding 10^{10} m^{-3}, where ion viscous damping becomes important enough to stabilize the collisional drift instability [*Huba and Ossakow*, 1979]. Thus the evidence obtained from the in situ technique tends to provide further weight to *Huba and Ossakow*'s [1979] suggestion that 'it may be possible for a large amplitude, long wavelength mode to nonlinearly generate the short wavelength turbulence via a parametric process.'

Acknowledgments. We thank H. E. Whitney for providing spaced receiver scintillation measurements from Ancon. The Huancayo scintillation measurements were performed by the Instituto Geofisico del

Peru. The work at Emmanuel College was partially supported by Air Force Geophysics Laboratory contract F19628-78-C-0005 and National Aeronautics and Space Administration grant NSG 5419. The work at the University of Texas at Dallas was partially supported by NASA grant 5-11407 and NSF grant ATM76-17351.

REFERENCES

Aarons, J., J. Buchau, S. Basu, and J. P. McClure, The localized origin of equatorial *F* region irregularity patches, *J. Geophys. Res., 83*, 1659, 1978.

Aarons, J., J. P. Mullen, H. E. Whitney, and E. M. MacKenzie, The dynamics of equatorial irregularity patch formation, motion, and decay, *J. Geophys. Res., 85*, 139, 1980.

Balsley, B. B., and D. T. Farley, Partial reflections: A source of weak VHF equatorial spread *F* echoes, *J. Geophys. Res., 80*, 4735, 1975.

Balsley, B. B., G. Haerendel, and R. A. Greenwald, Equatorial spread *F*: Recent observations and a new interpretation, *J. Geophys. Res., 77*, 5625, 1972.

Basu, S., and J. Aarons, Equatorial irregularity campaigns, Part I: Correlated scintillation and radar backscatter measurements in October 1976, *Tech. Rep. AFGL-TR-77-0264*, Air Force Geophys. Lab., Bedford, Mass., 1977.

Basu, S., S. Basu, J. Aarons, J. P. McClure, and M. D. Cousins, On the coexistence of kilometer- and meter-scale irregularities in the nighttime equatorial *F* region, *J. Geophys. Res., 83*, 4219, 1978.

Basu, S., and M. C. Kelley, A review of recent observations of equatorial scintillations and their relationship to current theories of *F* region irregularity generation, *Radio Sci., 14*, 471, 1979.

Basu, S., J. Aarons, J. P. McClure, C. LaHoz, A. Bushby, and R. F. Woodman, Preliminary comparisons of VHF radar maps of *F* region irregularities with scintillations in the equatorial region, *J. Atmos. Terr. Phys., 39*, 1251, 1977.

Briggs, B. H., and M. G. Golley, A test for dispersion in *F* region drifts observed by the radio star scintillation method, *J. Atmos. Terr. Phys., 30*, 963, 1968.

Chaturvedi, P. K., and S. L. Ossakow, Nonlinear theory of the collisional Rayleigh-Taylor instability in equatorial spread *F*, *Geophys. Res. Lett., 4*, 558, 1977.

Costa, E., and M. C. Kelley, On the role of steepened structures and drift waves in equatorial spread *F*, *J. Geophys. Res., 83*, 4359, 1978.

Dyson, P. L., J. P. McClure, and W. B. Hanson, In situ measurements of the spectral characteristics of ionospheric irregularities, *J. Geophys. Res., 79*, 1497, 1974.

Haerendel, G., Theory of equatorial spread *F*, report, Max-Planck-Inst. für Phys. und Astrophys., Garching, West Germany, 1974.

Hanson, W. B., and S. Sanatani, Large *N*, gradients below the equatorial *F* peak, *J. Geophys. Res., 78*, 1167, 1973.

Hanson, W. B., and R. A. Heelis, Techniques for measuring bulk gas motions from satellites, *Space Sci. Instrum., 1*, 493, 1975.

Hanson, W. B., D. R. Zuccaro, C. R. Lippincott, and S. Sanatani, The retarding potential analyzer on Atmosphere Explorer, *Radio Sci., 8*, 333, 1973.

Huba, J. D., and S. L. Ossakow, On the generation of 3-m irregularities during equatorial spread *F* by low-frequency drift waves, *J. Geophys. Res., 84*, 6697, 1979.

Kelley, M. C., G. Haerendel, H. Kappler, A. Valenzuela, B. B. Balsley, D. A. Carter, W. L. Ecklund, C. W. Carlson, B. Hausler, and R. Torbert, Evidence for a Rayleigh-Taylor type instability and upwelling of depleted density regions during equatorial spread *F*, *Geophys. Res. Lett., 3*, 448, 1976.

McClure, J. P., W. B. Hanson, and J. H. Hoffman, Plasma bubbles and irregularities in the equatorial ionosphere, *J. Geophys. Res., 82*, 2650, 1977.

Ossakow, S. L., Ionospheric irregularities, *Rev. Geophys. Space Phys., 17*, 521, 1979.

Rino, C. L., A power law phase screen model for ionospheric scintillation, 1, Weak scatter, *Radio Sci., 14*, 1135, 1979.

Rino, C. L., B. C. Fair, R. C. Livingston, and J. Owen, Continued performance of the Wideband satellite experiment, *Bimonthly Progress Rep. 4*, Stanford Res. Inst. International, Menlo Park, Calif., 1978.

Rishbeth, H., Polarization fields produced by winds in the equatorial *F* region, *Planet. Space Sci., 19*, 357, 1971.

Towle, D. M., VHF and UHF radar observations of equatorial ionospheric irregularities and background densities, *Radio Sci., 15*, 71, 1980.

Tsunoda, R. T., and D. M. Towle, On the spatial relationship of 1-meter, equatorial spread *F* irregularities and depletions in total electron content, *Geophys. Res. Lett., 6*, 873, 1979.

Tsunoda, R. T., M. J. Baron, J. Owen, and D. M. Towle, Altair: An incoherent scatter radar for equatorial spread *F* studies, *Radio Sci., 14*, 1111, 1979.

Wernik, A. W., C. H. Liu, and K. C. Yeh, Model computations of radio wave scintillation caused by equatorial ionospheric bubbles, *Radio Sci., 15*, 559, 1979.

Whitney, H. E., C. Malik, and J. Aarons, A proposed index for measuring ionospheric scintillation, *Planet Space Sci., 17*, 1069, 1969.

Woodman, R. F., East-west ionospheric drifts at the magnetic equator, *Space Res., 12*, 968, 1972.

Woodman, R. F., and C. LaHoz, Radar observations of *F* region equatorial irregularities, *J. Geophys. Res., 81*, 5447, 1976.

Woodman, R. F., and S. Basu, Comparison between in situ spectral measurements of equatorial *F* region irregularities and backscatter observations at 3-m wavelength, *Geophys. Res. Lett., 5*, 869, 1978.

Zalesak, S. T., S. L. Ossakow, B. E. McDonald, and P. K. Chaturvedi, Spatially large equatorial spread *F* bubbles (abstract), *Eos Trans. AGU, 59*, 345, 1978.

(Received March 17, 1980;
revised May 22, 1980;
accepted May 28, 1980.)

Radio Science, Volume 15, Number 1 pages 59-70, January-February 1980

The morphology of high-latitude VHF scintillation near 70°W

Sunanda Basu

Emmanuel College, Boston, Massachusetts 02115

Jules Aarons

Air Force Geophysics Laboratory, Hanscom Air Force Base, Massachusetts 01731

(Received May 29, 1979; revised August 28, 1979.)

The long-term VHF scintillation data from ATS 3 obtained at three stations situated in the North Atlantic sector at auroral and subauroral locations during the period 1968–1974 are used to determine the morphology of high-latitude scintillations near the 70°W longitude sector. The variation of the average level of scintillation at each observatory is studied as a function of time of day, season, and magnetic activity in a manner suitable for incorporation into statistical models of scintillation occurrence. The most prominent feature of the data is a seasonal dependence of scintillations with a 2:1 variation from northern summer to winter under quiet magnetic conditions. This also causes a large variation in the latitudinal gradient of scintillations from 2 dB per degree in summer to 1 dB per degree in winter for latitudes >60° invariant. The observed seasonal control of scintillations is related to the variation of the tilt angle of the earth's magnetic dipole and consequent modulation of the particle precipitation in the North Atlantic sector of the auroral oval.

INTRODUCTION

With the advent of the Early Bird synchronous satellite in 1965, stable sources of VHF transmissions became available for propagation experiments. Relatively simple antenna and receiver systems could be used to study the effects of the ionospheric medium on radio waves propagating through it. One such effect is the random fluctuation in amplitude of the radio signal caused by spatial irregularities in electron density in the ionosphere.

The study of these random fadings, known as scintillations, has been a major effort at the Air Force Geophysics Laboratory (AFGL; previously known as Air Force Cambridge Research Laboratory). This is because the subject has become of significant practical importance during recent years for application of satellite technology in communications and navigation. In particular, with a view to providing systems planning requirements for aircraft flying the North Atlantic region with satellite communications systems on board, AFGL has operated three stations at middle to high latitudes in this longitude sector for about a decade. These stations are the Sagamore Hill Radio Observatory, Massachusetts; Goose Bay, Labrador; and Narssarssuaq, Greenland; the last operated jointly with the Danish Meteorological Institute.

Data from these stations had earlier been used to determine a descriptive model of high-latitude *F* layer scintillations [*Aarons*, 1973]. The main points addressed there were the extent of the irregularity region during quiet and disturbed times as well as variation of irregularity intensity within the region as a function of latitude. Some of the same studies used by *Aarons* [1973] were also used by *Fremouw and Rino* [1973] to develop an empirical global model of scintillations. However, it was found by *Pope* [1974] that the model of *Fremouw and Rino* [1973] was somewhat inadequate in representing the equatorward edge of the nighttime scintillation boundary. The in situ measurements of *Sagalyn et al.* [1974] were also found to agree with *Aarons'* [1973] study in the boundary region.

With the steady accretion of more data at AFGL from the above mentioned stations it became obvious that in addition to the diurnal, latitudinal, and magnetic disturbance variation a predominant seasonal variation is also observed, at least, at the higher-latitude stations of Goose Bay and Narssarssuaq in the North Atlantic sector [*Basu*, 1975] along with a lesser solar flux variation. It is the object of this paper to present the observed seasonal

This paper is not subject to U.S. copyright. Published in 1980 by the American Geophysical Union

behavior and discuss causes for the same. Furthermore, during quiet times, Sagamore Hill observes the so-called plasmaspheric component of scintillations which cannot be considered to be merely an extension of the high-latitude scintillation region [*Martin and Aarons*, 1977; *Basu*, 1978].

Computer-generated plots have been developed which clearly show the existence of an increased scintillation region at mid-latitudes. These maps also allow a more meaningful estimation of the latitudinal scintillation gradients contained within the high-latitude irregularity zone. This detailed exposition of the morphological features allowed a natural extension to an empirical formulation of a limited high-latitude scintillation model to be presented in a companion paper [*Aarons et al.*, 1979].

THE DATA BASE

Observations of amplitude scintillations of the ATS 3 satellite beacon at 137 MHz form the data base. The records were reduced by the method outlined by *Whitney et al.* [1969]. Scintillation excursions in decibels for 15-min periods were used; these correspond approximately to the 1-percentile levels in the cumulative amplitude probability distribution function for the 15-min period. *Whitney* [1974] has given the approximate relationship between peak-to-peak excursion in decibels and the theory-based index S_4 which was introduced by *Briggs and Parkin* [1963]. For example, a 6-dB contour represents the S_4 level of 0.3. If one assumes a power law irregularity spectrum and realistic model parameters [*Basu*, 1978], it is possible to convert the S_4 index into an equivalent root-mean-square electron density deviation by using the weak scatter theory of *Rufenach* [1975] and *Costa and Kelley* [1976]. To meet the weak amplitude scatter condition, such a conversion to equivalent electron density deviation is only possible for scintillation contours ≤ 11 dB (i.e., $S_4 < 0.5$). Since the contours to be presented are averages of large amounts of data, obviously some violation of the weak scatter limit is involved even at this level. Further, the problem of limiting discussed by *Aarons et al.* [1979] almost certainly tends to decrease average values.

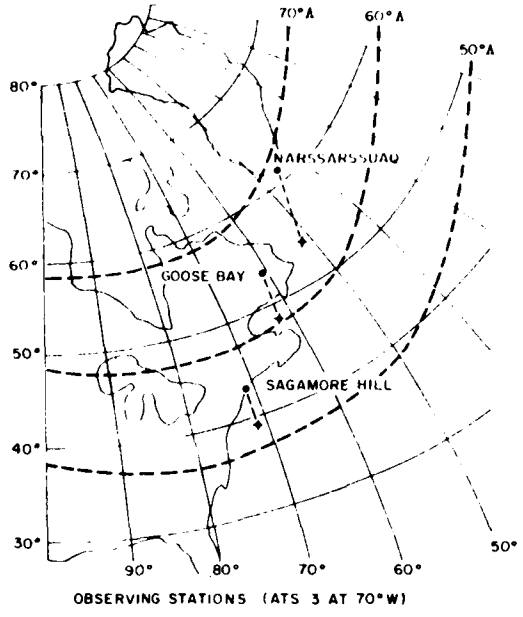

Fig. 1. The ionospheric (350-km altitude) intersections of the ray paths from ATS 3 located at 70°W to the observing sites at Sagamore Hill, Goose Bay, and Narssarssuaq.

As mentioned earlier, the three observatories are situated near the 70°W meridian. The propagation paths to the satellite from these stations are shown in Figure 1, while their geographic and invariant latitude coordinates and geometrical parameters are listed in Table 1.

NARSSARSSUAQ OBSERVATIONS

From Table 1 we find that the intersection latitude as viewed from Narssarssuaq was 63.2° invariant latitude at the 350-km height. Thus the observations pertain to the equatorward edge of the auroral oval in the midnight sector [*Feldstein and Starkov*, 1967]

TABLE 1. Position of observing stations

Station	Position	Invariant Latitude	Elevation	Azimuth	Ionospheric Z.A.	Propagation Angle
Narssarssuaq	54.2°N, 51.0°W	63.2°	18.0°	208°	64°	124°
Goose Bay	48.3°N, 61.7°W	60.3°	28.8°	191°	56°	136°
Sagamore Hill	39.3°N, 70.6°W	53.5°	40.9°	178°	46°	154°

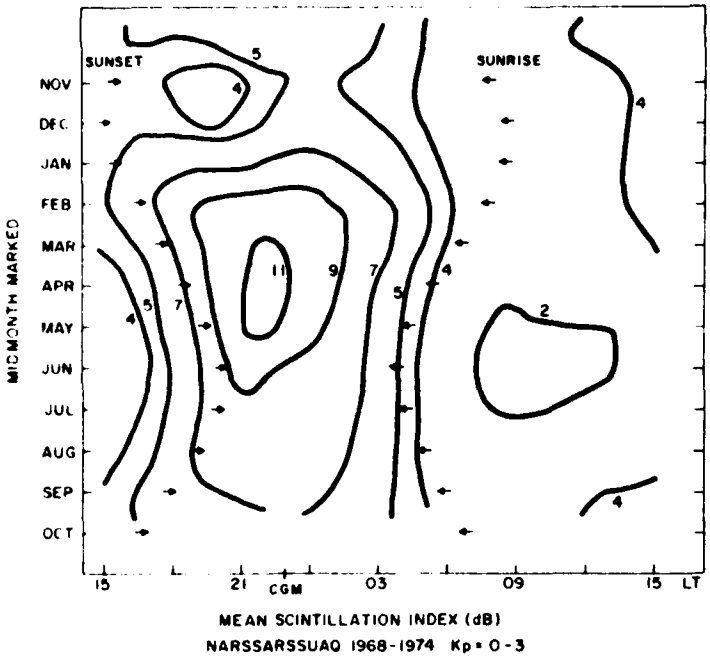

Fig. 2 Contours of monthly mean scintillation index in decibels at 137 MHz as a function of local time for quiet magnetic conditions (Kp = 0-3) obtained at Narssarssuaq with ATS 3 during 1968–1974.

for moderate magnetic activity ($Q \sim 3$), while it is 2° equatorward of the statistical oval during times of magnetic quiet ($Q \sim 1$). During disturbed times, when the oval broadens, the Narssarssuaq intersection point is within the oval in the evening-midnight sector.

In Figures 2 and 3 we show contour plots of average monthly scintillation indices as a function of local time obtained over a 6-year period for two ranges of magnetic activity. The local time variation shows a maximum just prior to corrected geomagnetic midnight (CGM) under quiet magnetic conditions and at CGM under disturbed magnetic conditions, as is to be expected at an auroral station. However, the striking and somewhat unexpected feature during quiet conditions shown in Figure 2 is the occurrence of the highest scintillation indices in the March–June period, with low levels during winter months. A peak-to-peak excursion of 11 dB is equivalent to $S_4 = 0.5$, whereas a 5-dB level represents $S_4 = 0.25$. Thus if all other scintillation model parameters remain unchanged, a 2:1 variation is expected in the rms electron density deviation

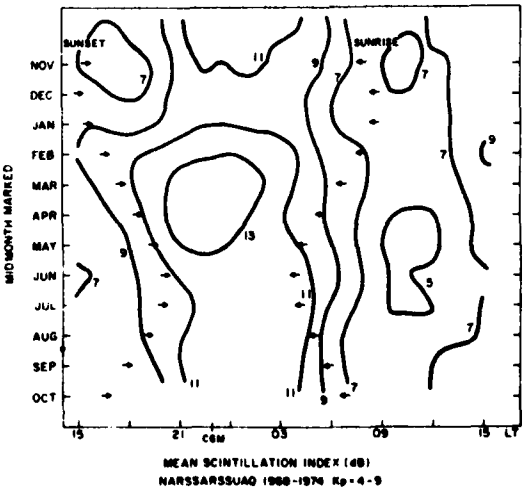

Fig. 3. Same as for Figure 2, except for disturbed magnetic conditions (Kp = 4–9).

ΔN from summer to winter. The probable causes for such a seasonal behavior of scintillations, contrary to the observed spread-F behavior in the auroral zone, were first discussed by *Basu* [1975] and will be dealt with further in a later section of the paper. The highest quiet daytime scintillations are observed in winter, and since there is a reduction in the nighttime level, the winter data are almost free of any diurnal variation.

Magnetic storms intensify the quiet time pattern, as may be observed from Figure 3. There are higher levels of daytime scintillation. However, the seasonal pattern is much less dramatic because the winter data are actually able to show the effects of the larger scintillation magnitude, whereas the summer data suffer saturation effects. It should be noted that the data for Figures 2 and 3 cover both the high-sunspot-cycle years as well as those during the declining phase. Further discussion of the effect of sunspot cycle on scintillation data is given later.

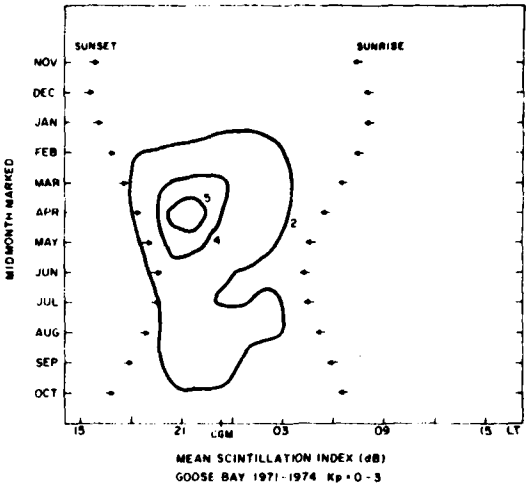

Fig. 4. Contours of monthly mean scintillation index in decibels at 137 MHz as a function of local time for quiet magnetic conditions (Kp = 0-3) obtained at Goose Bay with ATS 3 during 1971-1974.

GOOSE BAY OBSERVATIONS

The Goose Bay subionospheric position of 60°N invariant latitude moves through the electron density trough in the nighttime sector for quiet geomagnetic conditions in all seasons [*Brace and Theis*, 1974; *Ahmed et al.*, 1979]. In Figure 4, where we have shown contours in decibels of monthly average scintillation indices over a 4-year period for Kp = 0-3, we find a drastic reduction in scintillation magnitude in the February to October period as compared to that for Narssarssuaq. These findings are consistent with in situ results to be discussed later. The absence of scintillations in winter is probably due to the broad nature of the trough in this season with the consequent emphasis of those processes that inhibit scintillations within the trough.

The behavior during magnetically disturbed times is very different. Figure 5 shows larger scintillation magnitudes as well as a shift of the occurrence pattern from premidnight under quiet magnetic conditions to postmidnight under disturbed magnetic conditions. Some morning and afternoon scintillations are also observed during the February to October period. It should be noted that in contrast to Narssarssuaq data, Goose Bay data were only obtained during the waning period of the sunspot cycle.

SAGAMORE HILL OBSERVATIONS

The seasonal pattern for Sagamore Hill (at an intersection invariant latitude of 53.5°) differs from those of the higher-latitude stations. During quiet geomagnetic conditions the intersection point can be considered to be a mid-latitude station. The irregularities, in the main, are confined to the hours of darkness for both low and high magnetic activity.

For low Kp (Figure 6) for a 6-year period of observations the maximum activity occurs around midnight and shows an absence of scintillation during the summer months, with 2-dB level during the equinoctial and winter months.

For higher magnetic indices (Kp = 4-9, Figure 7) the observable scintillations extend for a longer nighttime period. Scintillation activity minimizes between March and May, with maximum activity still occurring near magnetic midnight. While during some severe magnetic storms the high-latitude irregularity structure descends to the 53° latitude [*Basu*, 1974; *Aarons*, 1976], scintillations hardly show any increase in the mean level during magnetic activity.

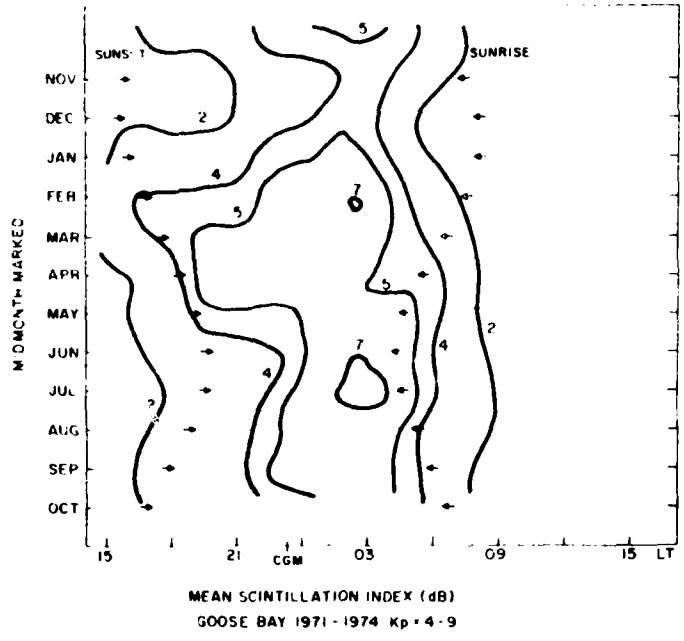

Fig. 5. Same as for Figure 4, except for disturbed magnetic conditions (Kp = 4-9).

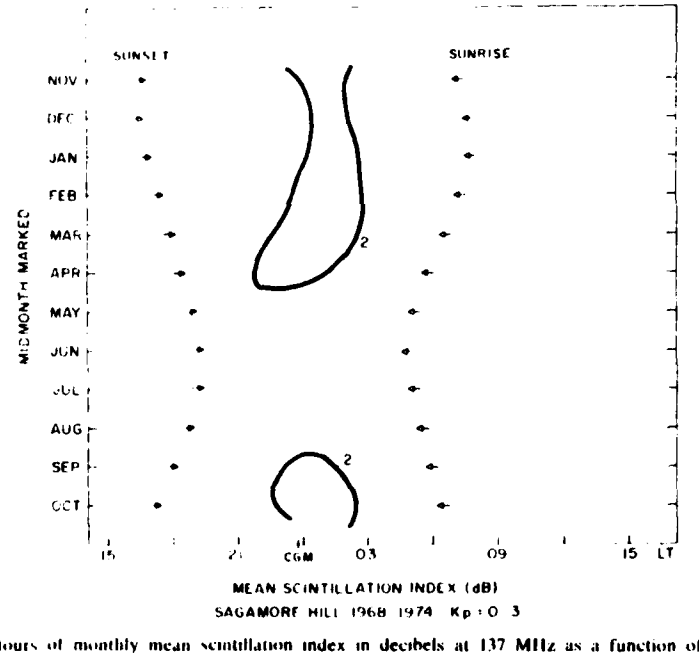

Fig. 6. Contours of monthly mean scintillation index in decibels at 137 MHz as a function of local time for quiet magnetic conditions (Kp = 0-3) obtained at Sagamore Hill with ATS 3 during 1968–1974.

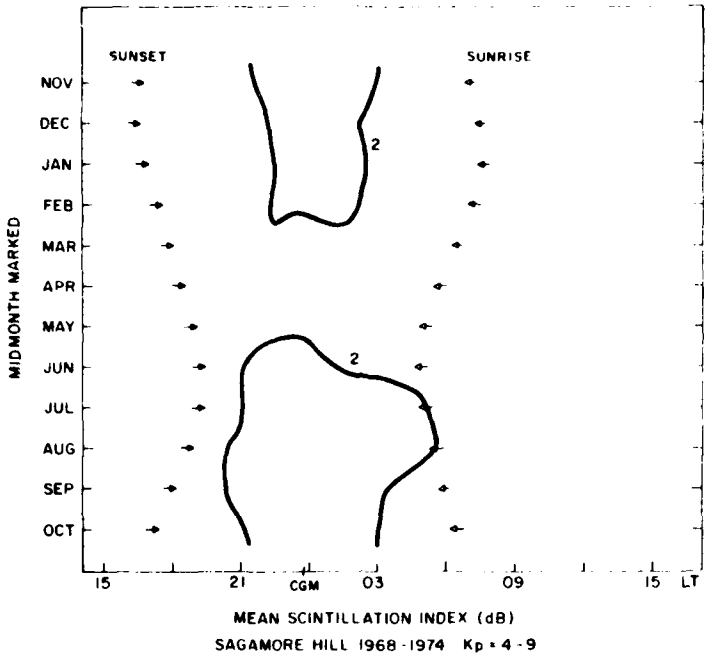

Fig. 7. Same as for Figure 6, except for disturbed magnetic conditions (Kp = 4–9).

SEASONAL PATTERNS AS DETERMINED BY THE CONTOUR PLOTS

A relatively limited data set was put together from the three observatories to determine latitudinal gradients of scintillation index and the variation of these gradients as a function of time of day, season, and magnetic activity. To minimize effects due to day-to-day variation of scintillations, only those days were chosen for which uninterrupted data were available at all three stations. Thus the data were all obtained during the lower sunspot period (1971–1974) of cycle 20. A contour program was used to link up the data obtained from these stations at the same local time. The results are shown in Figures 8–15 for four different seasons and two ranges of magnetic activity. The number of points on each diagram represents the number of hours of data from which each hourly average has been computed.

The pattern of latitudinal variation is consistent for the two sets of equinoctial data. Scintillations maximized just before local midnight in the Kp = 0–3 set as is shown in Figures 8 and 12. For the spring months, scintillations are somewhat higher than for the fall, and therefore the 3-dB contour line, for example, descends to somewhat lower latitudes during spring than it does during the fall. Also a 9-dB contour appears in the spring. The average quiet nighttime scintillation gradient at latitudes >60° is 1.5 dB per degree in the spring as compared to 1.25 dB per degree in the fall.

The more disturbed magnetic conditions bring on higher values of the scintillation index at both of the high-latitude stations without appreciable change in the latitude gradient. The relatively limited data base in both equinoctial sets peaks somewhat after midnight but has remarkably similar nighttime values at all latitudes for both seasons (Figures 9 and 13).

As is to be expected from the behavior at individual stations, the greatest difference in latitudinal gradients of scintillations occurs in the two solstices during quiet times (Figures 10 and 14). While in summer a steep positive gradient with latitude is exhibited by the two high-latitude stations during

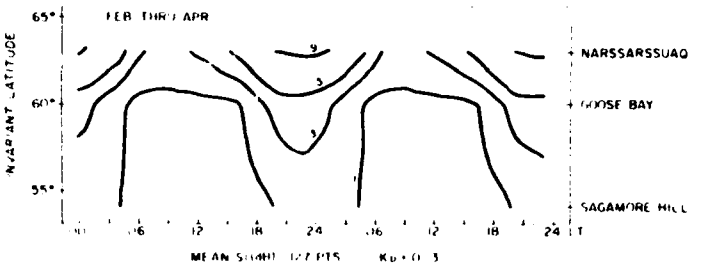

Fig. 8. Variation of mean seasonal scintillation index during the vernal equinox in decibels at 137 MHz with local time and invariant latitude derived from ~127 values for each hourly data point at the three stations under quiet magnetic conditions (Kp = 0-3).

the night, only a very weak latitude gradient is observed in winter, with virtually no diurnal variation at all. The winter nighttime gradient at latitudes greater than 60° invariant is 1 dB per degree of latitude, while in summer it is 2 dB per degree. This is a very large difference in the latitude gradient and has to be included in any realistic model of high-latitude scintillations. The other interesting aspect of Figure 14 is the appearance of a 2-dB contour at midnight near 55° invariant, with the higher-latitude 2-dB contour occurring at approximately 61°N. This points to a definite quiet time mid-latitude component of scintillations, which we shall discuss further in the next section. Although the data base is sparse, we see that the differences between these two seasons during disturbed conditions are much less severe (Figures 11 and 15).

In the data contours of the preceding sections the effects upon scintillation of diurnal, latitudinal, magnetic, and seasonal variations can be easily seen. However, it has been found that an additional parameter, solar flux, though not evident in these contours, to a lesser extent also affects scintillations.

In general, scintillation index increases with increasing solar flux, all other parameters remaining constant. A precise variation for a particular day of the year may be determined by using the model equations shown by *Aarons et al.* [1979]. For some combinations of latitudinal, magnetic, and seasonal variations this effect of increasing scintillation is mitigated and even reversed. For example, the summer data frequently suffer from saturation effects, so that any increase with solar cycle appears minimal.

To place the effect of solar flux variation in perspective, it should be noted that the percentage increase in scintillation of high over low-solar-flux years is of the order of half of the increase in scintillation when comparing disturbed magnetic conditions (Kp = 4-9) with quiet magnetic cases (Kp = 0-3).

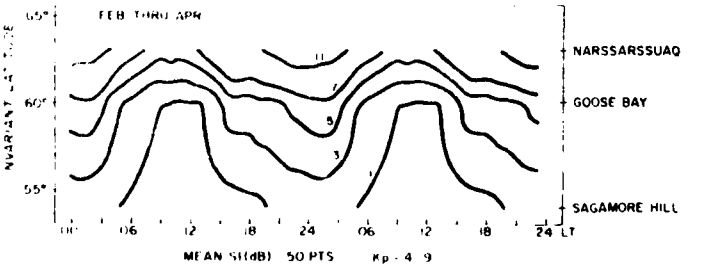

Fig. 9. Same as in Figure 8, except for ~50 values for each hourly data point under disturbed magnetic conditions (Kp = 4-9).

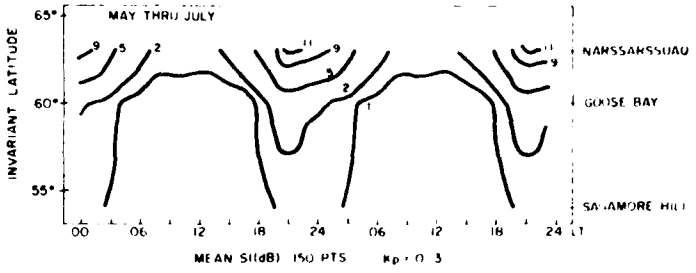

Fig. 10. Variation of mean seasonal scintillation index during the northern solstice in decibels at 137 MHz with local time and invariant latitude derived from 150 values for each hourly data point at the three stations under quiet magnetic conditions (Kp = 0-3)

DISCUSSION

The most consistent long-term result that emerges from this morphological study is the existence of a seasonal pattern of scintillations in the North Atlantic sector of the auroral oval. This is in addition to the widely known diurnal and magnetic activity variation of scintillations. Using nighttime data from Narssarssuaq only, *Basu* [1975] had established that this seasonal behavior of scintillations during quiet times, namely, a winter minimum and summer maximum, is in close agreement with the variation of the auroral electrojet index *AL* [*Davis and Sugiura*, 1966] in the same sector of the auroral oval. It was proposed by Basu, following the suggestion of *Boller and Stolov* [1970, 1974], that the varying geometry of the plasma sheet with the dipole tilt angle may cause a seasonal modulation of particle precipitation and hence of scintillations. If this hypothesis is correct, no such marked seasonal variation should be observed in the Alaskan and Scandinavian sectors of the oval. Indeed, radio star and orbiting beacon observations in those sectors had indicated no seasonal variation [*Liszka*, 1963; E. J. Fremouw, private communication, 1975]. Unfortunately, these measurements may have been contaminated by orbital considerations (in the radio star case) and by saturation of the scintillating signal because of the low frequencies used on earlier orbiting beacons. However, it is quite interesting to note that recent VHF wide band scintillation observations made at Alaska fail to show any pronounced seasonal variation (C. L. Rino, private communication, 1978).

The greater occurrence of winter daytime scintillation at Narssarssuaq can also be explained on the basis of the dipole tilt angle variation. It has been shown by *Boller and Stolov* [1970] that the maximum probability of occurrence of the Kelvin-Helmholtz instability is at 0430 UT during the June solstice and at 1630 UT during the December solstice. The June local midnight maximum of scintillations at Narssarssuaq was attributed by *Basu* [1975] to this effect. The winter maximization

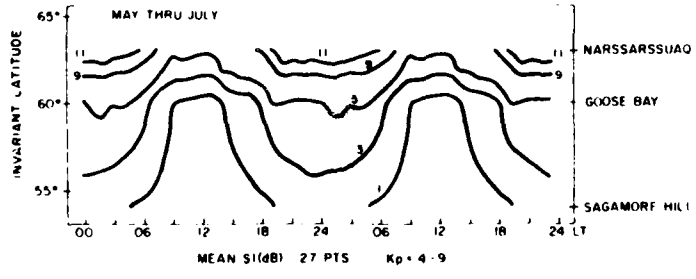

Fig. 11. Same as in Figure 10, except for ~27 values for each hourly data point under disturbed magnetic conditions (Kp = 4-9)

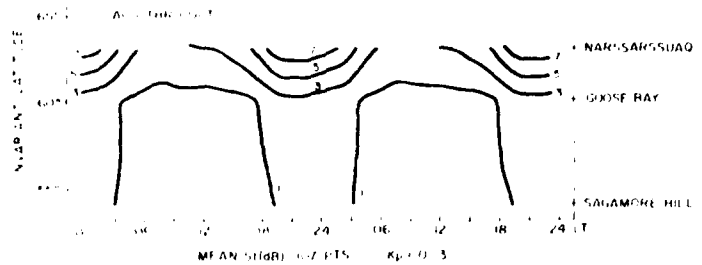

Fig. 12. Variation of mean seasonal scintillation index during the autumnal equinox in decibels at 137 MHz with local time and invariant latitude derived from 107 values for each hourly data point at the three stations under quiet magnetic conditions (Kp 0–3).

of the instability takes place at the time of local magnetic noon for Narssarssuaq. However, at midday the Narssarssuaq intersection is well equatorward of the dayside auroral oval. Hence the magnitude of the daytime winter scintillation maximum is not as large as the summer nighttime maximum but is larger than the daytime scintillation observed at any other time of the year.

In this regard, it is rather important to note the departure of the seasonal scintillation behavior from the seasonal spread-F behavior observed in the auroral region. For instance, under sunspot maximum conditions, *Tao* [1965] and *Olesen and Jepsen* [1966] both reported that maximum occurrence of spread-F behavior was observed in the winter, and *Penndorf* [1962] showed that such behavior was uniformly observed at auroral stations in all sectors of the northern hemisphere. It has recently been shown [*Wright et al.*, 1977] that $2\Delta f/f$ read from ionograms is equal to rms $\Delta N/N$ obtained from in situ measurements. Scintillations, however, are proportional to the total deviation ΔN [*Briggs and Parkin*, 1963]. Thus while scintillations and spread-F are, in general, associated, a one-to-one correlation should not be expected.

The winter minimum of scintillations at Goose Bay is probably due to its situation within the main electron density trough and the existence of a broad trough in the winter. The generally much reduced level of scintillation activity during quiet times in all other seasons is also probably due to its special location. In situ measurements of *McClure and Hanson* [1973] with Ogo 6 show that both $\Delta N/N$ and N are reduced in the trough. This led them to speculate that the physical processes that create the trough may be the same as those that inhibit irregularities. *Clark and Raitt* [1975], using in situ data from Esro 4, also discuss the existence of a distinct dip in irregularity amplitude between a narrow subauroral irregularity region and the higher-latitude irregularity zone. Thus it could be very probable that a winter minimum of nighttime

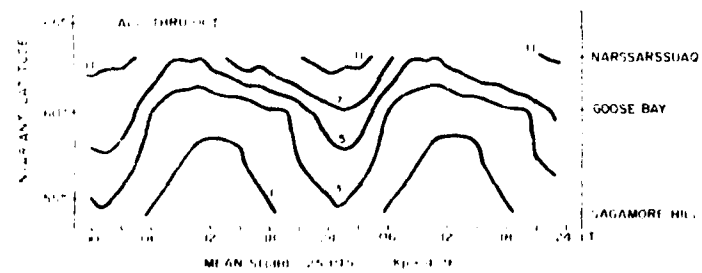

Fig. 13. Same as in Figure 12, except for 28 values for each hourly data point under disturbed magnetic conditions (Kp 4–9).

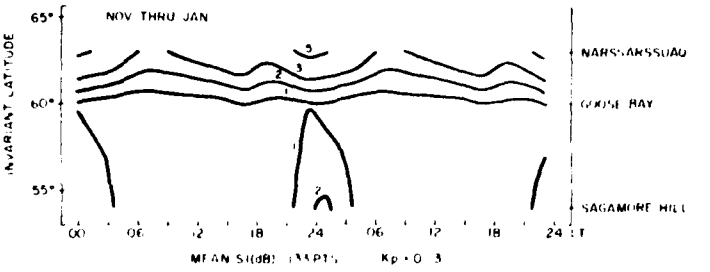

Fig. 14. Variation of mean seasonal scintillation index during the southern solstice in decibels at 137 MHz with local time and invariant latitude derived from ~133 values for each hourly data point at the three stations under quiet magnetic conditions (Kp = 0-3). Note that one 2-dB contour is at 55° invariant, whereas the other is poleward of 60° invariant.

scintillations will be observed at a position with $L \sim 4$ in any longitude sector. However, it is well known that the trough itself shows a maximum depth and width in those longitude sectors with the largest variation in dipole tilt angle [*Taylor*, 1971]. Thus the absence of scintillations in winter during quiet times at Goose Bay could be due to a superposition of both factors.

The Goose Bay data show greatly increased scintillations during disturbed times. The diurnal pattern during disturbed times also shows a consistent shift toward postmidnight hours during all seasons. During periods of sustained magnetic activity with the equatorward motion of the plasmapause, the auroral oval region moves into the vicinity of the Goose Bay intersection point. The auroral ovals [*Feldstein and Starkov*, 1967] are also greatly skewed toward early morning hours, i.e., they descend to much lower invariant latitudes in postmidnight hours as compared to the premidnight situation. This asymmetry is particularly noticeable for $Kp \geq 4$. This is in keeping with the observed shift in maximum occurrence of scintillations. There may also be such a shift in the Narssarssuaq data, but obviously, these observations are contaminated by saturation effects, and thus the shift is not quite as dramatic.

In general, of course, the effect of magnetic activity on scintillations at both stations is short-lived and highly variable. This fact can be better appreciated by considering autocorrelation coefficients of scintillation indices at Narssarssuaq and at Goose Bay under quiet and disturbed conditions. While the autocorrelation coefficients for each observation path (excluding the winter data) drop to about 0.3 at a lag of 24 hours (i.e., day 1) during quiet times, that value decreases only very slowly as the lag is extended to days 2, 3, and 4. During disturbed times, however, the autocorrelation coefficients drop sharply to 0.1 at a lag of 1 day and remain at that low level for larger lags up to day 4. This indicates that the scintillation pattern

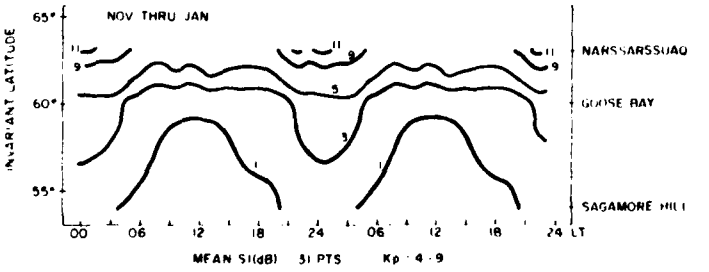

Fig. 15. Same as in Figure 14, except for ~31 values for each hourly data point for disturbed magnetic conditions (Kp = 4-9).

on the day following the magnetic storm is very different from that on the day of the storm at both stations, while the pattern on quiet days is of a long-lived nature.

Mean scintillation indices are rather low at Sagamore Hill during both quiet conditions and disturbances. In fact, the average behavior during disturbed times contrasts sharply to that observed during some large individual storms, such as those studied by *Basu* [1974], *Aarons* [1976], and *Aarons et al.* [1976]. It should be recalled that on only 8% of the days are magnetic storm effects large enough to bring the plasmapause to the vicinity of the Sagamore Hill intersection point with $L = 2.8$ [*Carpenter and Park*, 1973]. *Basu* [1974] has shown that in such cases the scintillations show a large storm time component which is ordered in universal time. It is not surprising therefore that the average local time behavior in the $Kp = 4$–9 period does not show the effects observed individually during some great magnetic storms.

The existence of a quiet time component of mid-latitude scintillations is rather clearly shown in the multistation winter plot. Even though the magnitude of this scintillation component is about 2 dB, *Basu* [1978] has pointed out that this level represents twice the intensity used to define the scintillation boundary [*Aarons et al.*, 1969]. She has shown, by analysis of in situ data from Ogo 6 and Sagamore Hill scintillation data for similar time periods, that some of these irregularities are associated with magnetically conjugate sharp density gradients and has discussed the various plasma instabilities that may create the small-scale irregularities. However, the origin of the sharp gradients themselves remains unclear. From the point of view of communications the present data base shows that mid latitude scintillation will probably not be a problem in the VHF/UHF range, and it is the auroral region that is the seat of the potential problems.

In conclusion, we wish to state that the morphology of high-latitude scintillations as observed in the North Atlantic sector with a 2:1 variation of VHF scintillation magnitude from summer to winter is quite different from that expected on the basis of even the recently modified global model proposed by *Fremouw et al.* [1977]. We feel that the empirical model presented in the companion paper [*Aarons et al.*, 1979] will be more realistic for communications channel modeling purposes, particularly in the North Atlantic sector. Much more information is necessary on the seasonal as well as the polar cap behavior before a truly global high-latitude model can be developed.

Acknowledgments. We thank E. MacKenzie for her invaluable assistance in organizing the data. The computer program for the three-station contour diagrams was developed by M. Mendillo. H. E. Whitney and J. P. Mullen were particularly helpful in the acquisition and analysis of Sagamore Hill and Goose Bay data. The Narssarssuaq data were obtained in cooperation with the Danish Meteorological Institute; in particular, we acknowledge the efforts of K. Damgaard and I. S. Mikkelsen.

REFERENCES

Aarons, J. (1973), A descriptive model of *F*-layer high latitude irregularities as shown by scintillation observations, *J. Geophys. Res.*, *78*, 7441–7450.

Aarons, J. (1976), High-latitude irregularities during the magnetic storm of October 31 to November 1, 1972, *J. Geophys. Res.*, *81*, 661–670.

Aarons, J., J. P. Mullen, and H. E. Whitney (1969), The scintillation boundary, *J. Geophys. Res.*, *74*, 884–889.

Aarons, J., S. Basu, and E. Martin (1976), The stormtime component of scintillations, in *Proceedings of Cospar Satellite Beacon Symposium*, edited by M. Mendillo, Boston University, Boston, Mass.

Aarons, J., E. MacKenzie, and K. Bhavnani (1979), High latitude analytical formulas for scintillation levels, *Radio Sci.*, *15*, this issue.

Ahmed, M., R. C. Sagalyn, P. J. L. Wildman, and W. J. Burke (1979), Topside ionospheric trough morphology: Occurrence frequency and diurnal, seasonal and altitude variations, *J. Geophys. Res.*, *84*, 489–498.

Basu, S. (1974), VHF ionospheric scintillations at $L = 2.8$ and formation of stable auroral red arcs by magnetospheric heat conduction, *J. Geophys. Res.*, *79*, 3155–3160.

Basu, S. (1975), Universal time seasonal variations of auroral zone magnetic activity and VHF scintillations, *J. Geophys. Res.*, *80*, 4725–4728.

Basu, S. (1978), Ogo-6 observations of small scale irregularity structures associated with sub-trough density gradients, *J. Geophys. Res.*, *83*, 182–190.

Boller, B. R., and H. L. Stolov (1970), Kelvin-Helmholtz instability and the semi-annual variation of geomagnetic activity, *J. Geophys. Res.*, *75*, 6073–6084.

Boller, B. R., and H. L. Stolov (1974), Investigation of the association of magnetopause instability with interplanetary sector structure, *J. Geophys. Res.*, *79*, 673.

Brace, L. H., and R. F. Theis (1974), The behavior of the plasmapause at mid-latitudes: Isis-1 Langmuir probe measurements, *J. Geophys. Res.*, *79*, 1871–1884.

Briggs, B. H., and I. A. Parkin (1963), On the variation of radio star and satellite scintillation with zenith angle, *J. Atmos. Terr. Phys.*, *25*, 339–365.

Carpenter, D. L., and C. G. Park (1973), On what ionospheric workers should know about the plasmapause-plasmasphere, *Rev. Geophys. Space Phys.*, *11*, 133–154.

Clark, D. H., and W. J. Raitt (1975), Characteristics of the high-latitude ionospheric irregularity boundary, as monitored by the total ion current probe on Esro-4, *Planet. Space Sci.*, *23*, 1643–1647.

Costa, E., and M. C. Kelley (1976), Calculations of equatorial scintillations at VHF and GHz frequencies based on a new model of the disturbed equatorial ionosphere, *Geophys. Res. Lett.*, *3*, 677–680.

Davis, T. N., and M. Sugiura (1966), Auroral electrojet activity index *AE* and its universal time variations, *J. Geophys. Res.*, *71*, 785–801.

Feldstein, Y. I., and G. V. Starkov (1967), Dynamics of auroral belt and polar geomagnetic disturbances, *Planet. Space Sci.*, *15*, 209–229.

Fremouw, E. J., and C. L. Rino (1973), An empirical model for average *F*-layer scintillation at VHF/UHF, *Radio Sci.*, *8*, 213–222.

Fremouw, E. J., C. L. Rino, A. R. Hessing, and V. E. Hatfield (1977), A transionospheric communication channel model, *Quart. Tech. Rep. 7*, SRI Int., Menlo Park, Calif.

Liszka, L. (1963), A study of ionospheric irregularities using satellite transmissions at 54 Mc/S, *Ark. Geofys.*, *4*, 227–245.

Martin, E., and J. Aarons (1977), *F*-layer scintillations and the aurora, *J. Geophys. Res.*, *82*, 2717–2722.

McClure, J. P., and W. B. Hanson (1973), A catalog of ionospheric *F* region irregularity behavior on Ogo-6 retarding potential analyzer data, *J. Geophys. Res.*, *78*, 7431–7439.

Olesen, J. K., and S. B. Jepsen (1966), Some characteristics of spread F in very high latitudes, in *Spread-F and its Effects Upon Radiowave Propagation and Communications*, edited by P. Newman, pp. 127–236, Technivision, Maidenhead, England.

Penndorf, R. (1962), Geographic distribution of spread *F* in the Arctic, *J. Geophys. Res.*, *67*, 2279–2288.

Pope, J. H. (1974), High latitude ionospheric irregularity model, *Radio Sci.*, *9*, 675–682.

Rufenach, C. L. (1975), Ionospheric scintillation by a random phase screen: Spectral approach, *Radio Sci.*, *10*, 155–165.

Sagalyn, R. C., M. Smiddy, and M. Ahmed (1974), High latitude irregularities in the top side ionosphere based on Isis-1 thermal ion probe data, *J. Geophys. Res.*, *79*, 4252–4261.

Tao, K. (1965), World-wide maps of the occurrence percentage of spread *F* in years of high and low sunspot numbers, *J. Radio Res. Lab.*, *12*, 317–357.

Taylor, H. S., Jr. (1971), Evidence of solar geomagnetic seasonal control of the topside ionosphere, *Planet. Space Sci.*, *19*, 77–93.

Whitney, H. E. (1974), Notes on the relationship of scintillation index to probability distributions and their uses for system design, *Tech. Rep. AFCRL-TR-74-0004*, Air Force Geophys. Lab., Hanscom Air Force Base, Mass.

Whitney, H. E., C. Malik, and J. Aarons (1969), A proposed index for measuring ionospheric scintillations, *Planet. Space Sci.*, *17*, 1069–1073.

Wright, J. W., J. P. McClure, and W. B. Hanson (1977), Comparisons of ionogram and Ogo-6 satellite observations of small-scale *F*-region inhomogeneities, *J. Geophys. Res.*, *82*, 548–554.

Radio Science, Volume 15, Number 1, pages 115–127, January–February 1980

High-latitude analytical formulas for scintillation levels

J. Aarons

Air Force Geophysics Laboratory, Hanscom Air Force Base, Massachusetts 01731

E. MacKenzie

Emmanuel College, Boston, Massachusetts 02115

K. Bhavnani

Logicon, Inc., Bedford, Massachusetts 01730

(Received May 29, 1979, revised August 28, 1979)

By making measurements of the scintillations of the 137-MHz beacon of ATS 3 at three sites along the 70°W meridian, it was possible to amass a data bank sufficient to obtain empirical analytical formulas of average scintillation at subauroral and auroral latitudes. The data base consisting of 15-min scintillation indices of 3 7 years of observations from Sagamore Hill, Massachusetts, Goose Bay, Labrador, and Narssarssuaq, Greenland, has been presented and discussed in a companion paper. Forcing functions for the empirical formulations are time of day, day of the year, magnetic index, and solar flux. The limitations of the data are outlined including single frequency of observations and the problem of limited excursion of scintillations. Corrections are given for geometrical effects using varying irregularity configurations.

INTRODUCTION

Over the period of 1971 to the present, a series of attempts has been made to develop an irregularity model designed to predict the irregularities responsible for scintillation of transionospheric radio signals. One model has developed from work by *Fremouw and Bates* [1971] and *Fremouw and Rino* [1973]. After a critique of the work by one of the authors of this paper [*Aarons*, 1973], *Pope* [1974] modified the high-latitude terms to show the effect of increasing magnetic activity. A further modification has been recently developed by *Fremouw et al.* [1977] in which a magnetic dependence is utilized for the high latitudes. However, seasonal variations are not considered in the high-latitude region. The aim of this paper is to introduce into the literature the seasonal, solar flux, and magnetic dependence at auroral and subauroral latitudes as well as at a mid-latitude station.

A recent attempt to expand the earlier Fremouw-Rino model using spread *F* data [*Singleton*, 1979] is considered unrealistic. The morphologies of spread *F* and of scintillation are considerably different, as has been pointed out in a companion paper (*Basu and Aarons* [1980], hereafter referred to as paper 1). At middle and equatorial latitudes, for example, it has been found [*Huang*, 1970; R. G. Rastogi, private communication, 1978] that range spread type of spread *F* is correlated with scintillation activity, while frequency spread is not. Yet the vast portion of spread *F* data used in morphology studies does not differentiate between the two types.

At high latitudes, ionosonde data frequently disappear during magnetic storms when auroral absorption is high and during polar cap events when *D* layer absorption takes place. Merely assuming that spread *F* takes place during these blackouts is inadequate, since it has been shown that the intensity of the irregularities increases considerably [*Aarons*, 1976].

In any event any model must be tested with a body of observations such as we present; the aim of the paper is to develop analytical formulas from a large data base. The levels obtained from this empirical base can then be used to realistically test more ambitious models. The data base used is a series of measurements of the scintillations of one

This paper is not subject to U.S. copyright. Published in 1980 by the American Geophysical Union.

synchronous satellite beacon, ATS 3, transmitting at 137 MHz. The analytical terms provide mean scintillation excursions as a function of time of day, month, solar flux, and magnetic index. With forecasting of solar flux and magnetic index, a user in the latitude range covered would have an indication of mean scintillation to be expected.

It should be noted that these formulations are models only in a very limited sense. The data were taken near the 70° west longitude region; therefore the validity of the formula is in all likelihood restricted, since the offset of the earth's dipole axis vis-a-vis the earth's axis of rotation would be expected to produce effects at the same invariant latitudes that differ from those at 70°W. In paper 1 the data base from which this limited modeling has been developed is presented and discussed.

There are other problems associated with the formulas, such as inadequately documented geometrical effects, the relatively limited range of excursions capable of being recorded by the equipment used, and the question of polar and auroral effects during intense magnetic storms. These problems result in limited accuracy of the developed analytical equations. However, the long-term measurements, the availability of complete diurnal coverage, and the consistency of the data reduction methods will add to the relatively sparse data base of scintillation levels available at this time.

CHARACTERIZATION OF FLUCTUATION INDEX

Scintillations in amplitude can be characterized by a depth of fading index. The most valid scintillation index, S_4, which is proportional to rms electron density deviation, is defined as the square root of the variance of received power divided by the mean value of the received power [*Briggs and Parkin*, 1963]. An alternative, less rigorous quantitative measure of scintillation index was adopted by the Joint Satellite Studies Group (JSSG) to ensure a standard method of data scaling in long-term statistical analysis. This index, known as dB_{JSSG}, is used in the current study.

The definition is

$$SI_{JSSG} = \frac{P_{max} - P_{min}}{P_{max} + P_{min}}$$

where P_{max} is the power amplitude of the third peak down from the maximum excursion of the scintillations and P_{min} is the power amplitude of the third peak up from the minimum excursion, measured in dB [*Whitney et al.*, 1969].

TABLE 1. Equivalence of various scintillation indices

S_4	dB_{JSSG}	SI_{JSSG}
0.075	1	11
0.17	3	32
0.3	6	59
0.45	10	81

The equivalence of selected values of these indices as obtained by observational comparisons is indicated in Table 1.

DATA BASE

The data were available from three stations. These stations with their transionospheric positions in the subauroral through auroral latitudes allowed a modest coverage of high-latitude scintillations.

The 15-min samples of scintillation index (dB) data for the ATS 3 satellite for the stations have been augmented into a complete data base on tape. The dates of the data used for each station are September 17, 1968, to September 1, 1974, for Narssarssuaq; January 1, 1972, to December 31, 1974, for Goose Bay; and December 1, 1969, to

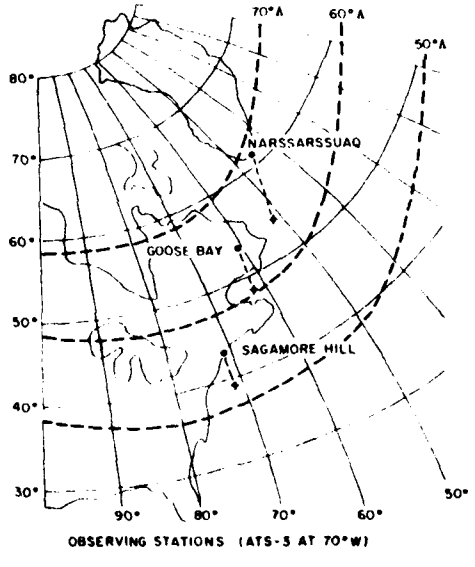

Fig. 1. The ionospheric (350-km altitude) intersections of the ray paths from ATS 3 located at 70°W to the observing sites at Sagamore Hill, Goose Bay, and Narssarssuaq.

TABLE 2 Observational coordinates

Station	Geographic Coordinates Latitude	Longitude	Invariant Latitude	Elevation Angle	Azimuth	Ionospheric Zenith Angle	Propagation Angle
Narssarssuaq	54.2°	51.0°	63.2°	18.0°	208°	64°	124°
Goose Bay	48.3°	61.7°	60.3°	28.8°	191°	56°	136°
Sagamore Hill	39.3°	70.6°	53.5°	40.9°	178°	46°	154°

November 30, 1974, for Sagamore Hill. Goose Bay data for 1974 cover mainly November and December.

The three stations are situated near the 70°W meridian, and their propagation paths to the ATS 3 satellite are shown in Figure 1. Their geographical and invariant latitude coordinates and geometrical parameters are given in Table 2. The last two columns in Table 2 provide the ionospheric zenith angles at an altitude of 350 km and the propagation angles (i.e., the angle between the ray path and the magnetic field), respectively.

FORCING FUNCTIONS

In this initial development, relatively simple equations were developed to reproduce the mean scintillation excursions at the three stations. These forcing parameters included the following.

Planetary magnetic index, Kp. It has been shown that at high latitudes (which in this case include the Narssarssuaq and Goose Bay observations and during severe magnetic storms the Sagamore Hill observations), *Kp* is a forcing function [*Aarons and Allen*, 1971].

Solar flux. Early work by *Aarons et al.* [1971] showed that sunspot activity, even when divorced from magnetic index variations, had an effect on scintillation behavior. Utilizing the 2695-MHz solar measurements at Sagamore Hill, we separated observations into three regimes of solar flux units (S_f) (1) 0–95, (2) 96–120, and (3) 121 and greater. Scintillations do not in every month increase with increasing solar flux but vary as a function of season.

Seasonal parameter. A very dramatic minimizing of diurnal effects is shown in the Narssarssuaq observations over the winter [*Basu*, 1975]. This has been accounted for in the equations.

Diurnal pattern. This includes the variation of scintillation magnitude as a function of local time under magnetically quiet and disturbed conditions as modulated by the seasonal function.

Analyses were conducted separately for each station. The data were partitioned into 12 months, 7 *Kp*, 3 solar flux (at 2.7 GHz), and 24 UT ranges. The *Kp*, S_f, and *SI* readings were averaged in each block. A compact file was thus made available for high-speed iterative modeling studies. The seven *Kp* ranges are 0–1, 1+ to 2, 2+ to 3, 3+ to 4, 4+ to 5, 5+ to 6, and 6+ and up. The three S_f ranges are 0–95, 96–120, and 121 and up. Tables of the averaged *SI* are provided for each of the stations.

Out of a maximum possible 6048 blocks ($12 \times 7 \times 3 \times 24$), the averaged files comprise the following: Narssarssuaq, 4985 blocks; Goose Bay, 4217 blocks; and Sagamore Hill, 5065 blocks. The empty blocks generally correspond to the highest two *Kp* ranges, i.e., 5+ and up, and occasionally the highest S_f range.

MODELING AT HIGH LATITUDES

A search was conducted to derive an empirical analytical formula of *SI*. Analytical forms were preferred to ensure smooth transitions as a function of the driving functions, namely, day of year, *Kp*, S_f, and universal time. These forms also permitted use of regression techniques for least squares fitting to the averaged data file. In the course of the search for improved fits, special characteristics of the data were noted which suggested elaborations of the form. Examples are the delayed peak in the diurnal *SI* variation with higher *Kp*, the seasonal effect on diurnal variation amplitude relative to the average *SI*, the seasonal effect on influence of *Kp* and S_f, and the need for higher harmonics to represent the diurnal variation.

Separate analytical formulas were developed for each station. These individual models approximate the actual data base as closely as possible, while smoothing abrupt variations to fit an analytical form.

The appendix presents the formula for each station in terms of local time. The difference between universal time and local time at the subiono-

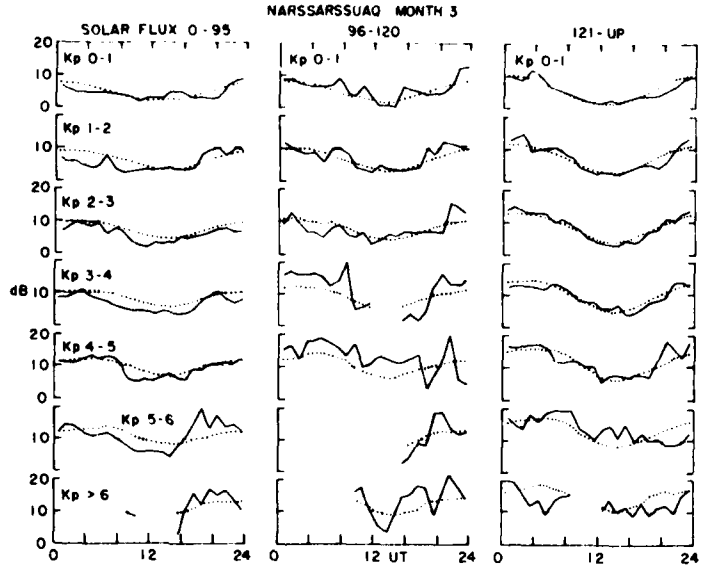

Fig. 2. Sample behavior of data (solid curve) and the best-fitting model (dashed curve) in UT at Narssarssuaq as a function of different *Kp* and solar flux groupings for the month of March.

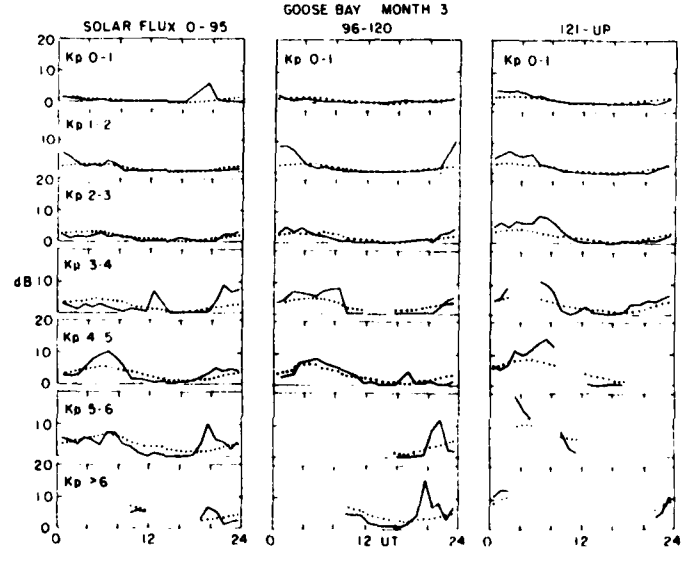

Fig. 3. Sample of behavior of data (solid curve) and the best-fitting model (dashed curve) in UT at Goose Bay as a function of different *Kp* and solar flux groupings for the month of March.

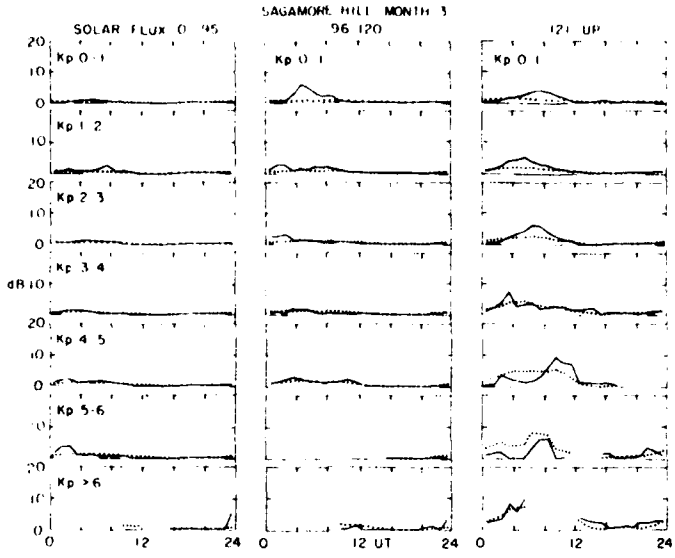

Fig. 4. Sample of behavior of data (solid curve) and the best-fitting model (dashed curve) in UT at Sagamore Hill as a function of different *Kp* and solar flux groupings for the month of March.

spheric point (350 km) was taken to be 3.4 hours at Narssarssuaq, 4.1 hours at Goose Bay, and 4.7 hours at Sagamore Hill. In the model equations the cosine arguments (in radians) that include the terms for day number (DA) and hour (HL) assume a multiplicative term of $2\pi/365$ and $2\pi/24$, respectively. Though not shown in the equation for reasons of convenience, these must be included in the calculations.

In Figures 2–4, typical comprehensive comparative plots of the averaged data (solid curve) and the model (dashed curve) are provided for each station. The model predictions used the actual averaged data, *Kp* and S_f for each hour, and are therefore absent when data are absent. These best fit models may occasionally predict small negative *SI*'s; these can be made to asymptotically approach zero by replacing a value *V* which is less than 0.5 by $e^{2(V-0.85)}$. This ensures continuity in the predictions near 0.5 and introduces minimal distortion, since only the very low scintillations are adjusted.

EQUATIONS AND DATA

To illustrate the behavior of the data and of the best fitting equations, Narssarssuaq data are shown in Figure 2 for the month of March. One can note, for example, along the left-hand side for the solar flux set of 0–95, that scintillations increase with increasing *Kp*. The dotted curve is the model equation, and the solid curve connects 1-hour means of scintillation excursions.

Along any series of boxes with identical *Kp*, one can note that the model and the data indicate that the general trend is for the scintillation excursions to increase with increasing solar flux.

The behavior of the Goose Bay data and best-fitting formula for March are shown in Figure 3. Within each particular solar grouping, scintillations increase with increasing *Kp*. For the same *Kp* grouping, the scintillation excursions increase with increasing solar flux.

Behavior of the Sagamore Hill data and model for March are shown in Figure 4. For the low solar flux group (0–95) a very slight increase in scintillations associated with increasing *Kp* is seen. The same is true of the solar flux group 96–120, while for high solar flux, the increase with *Kp* becomes more noticeable. In general, within a particular *Kp* grouping, scintillation index increases with increasing solar flux.

LIMITING

A basic problem in the data and the modeling is the problem of limiting. Since the attempt in this model was to find average excursions, the limited signal to noise ratio of the recordings resulted in excursions at 137 MHz being at their maxima 16–19 dB (depending on equipment). Thus, for example, if the 15-min indices for 2200–2215 on any month all showed excursions of 19 dB, the average would be 19 dB. As has been shown by other experiments with greater signal to noise ranges, the excursions could have been ≥26 dB. Equipment limitations would not have indicated the higher values. Thus a comparison with higher-frequency data will possibly serve only to indicate occurrence patterns and the effect of various forcing functions; frequency dependence reductions done with this model are of limited validity. In this respect it is important to note that phase scintillation measurements are generally free from the limiting problem.

AVERAGED VERSUS MEDIAN DATA

In order to test if the averaged data were skewed by problems of limiting, the mean values were compared with medians. Figure 5 illustrates this for Narssarssuaq; it can be seen that no substantial differences occur between the averaged and the median dB values. For low scintillation activity, averaged values tend to be higher than median values. Similar comparisons with roughly the same results were made with both Sagamore Hill and Goose Bay data.

DISTRIBUTION OF OCCURRENCE OF SCINTILLATION

From the engineering viewpoint, distribution of the occurrence of various levels of scintillations allows systems designers to evaluate degradation of proposed or current systems. Distribution analyses were conducted of the high-latitude data files. These data are shown partitioned into two significant scintillation blocks, ≥6 dB and ≥9 dB. The data are then divided into night (17–05 LT) and day (05–17 LT). These distributions are given in Table 3.

TABLE 3. Percentage of occurrence of scintillation (peak to peak)

	Scintillation Block	Night (17–05 LT)	Day (05–17 LT)
Narssarssuaq, Greenland, ATS 3, 137 MHz			
K = 0–3+	≥6 dB	46.3	14.5
	≥9 dB	29.4	6.2
K = 4–9	≥6 dB	78.8	47.2
	≥9 dB	61.8	31.0
Goose Bay, Labrador, ATS 3, 137 MHz			
K = 0–3+	≥6 dB	8.3	0.5
	≥9 dB	3.9	0.2
K = 4–9	≥6 dB	30.2	8.3
	≥9 dB	15.0	3.7
Sagamore Hill, Massachusetts, ATS 3, 137 MHz			
K = 0–3+	≥6 dB	5.4	0.3
	≥9 dB	2.5	0.1
K = 4–9	≥6 dB	6.9	0.7
	≥9 dB	3.6	0.3

FREQUENCY DEPENDENCE

In order to fully utilize the formulas, it is desirable to be able to extrapolate the dB values resulting from the 137-MHz data base to values for higher frequencies. This entails the use of the spectral index η, where

$$\eta = [\log (S_1 / S_2)] / [\log (f_1 / f_2)]$$

The scintillation index is in terms of S_4 [*Whitney*, 1974]. This expression is valid as long as the scintillation index is a constant power law function. Under conditions of weak scattering, a $f^{1.5}$ variation with S_4 indices is noted and is consistent with a three-dimensional irregularity power spectral index of 4 [*Rufenach*, 1974; *Whitney and Basu*, 1977].

Recent observations [*Fremouw et al.*, 1978] employing 10 frequencies between 138 MHz and 2.9 GHz, transmitted from the same satellite DNA 002, show a consistent $f^{1.5}$ behavior of S_4 for S_4 less than about 0.6. These data were taken at both equatorial latitudes (Ancon) and high latitudes (Poker Flat, Alaska). In both cases the frequency dependence becomes less steep for stronger scintillation, saturating for values of S_4 approaching unity, as expected for 'fully developed' intensity scintillation obeying a Rayleigh distribution.

GEOMETRICAL CONSIDERATIONS

It has been noted that scintillations maximize both at low angles of elevation and when the signal

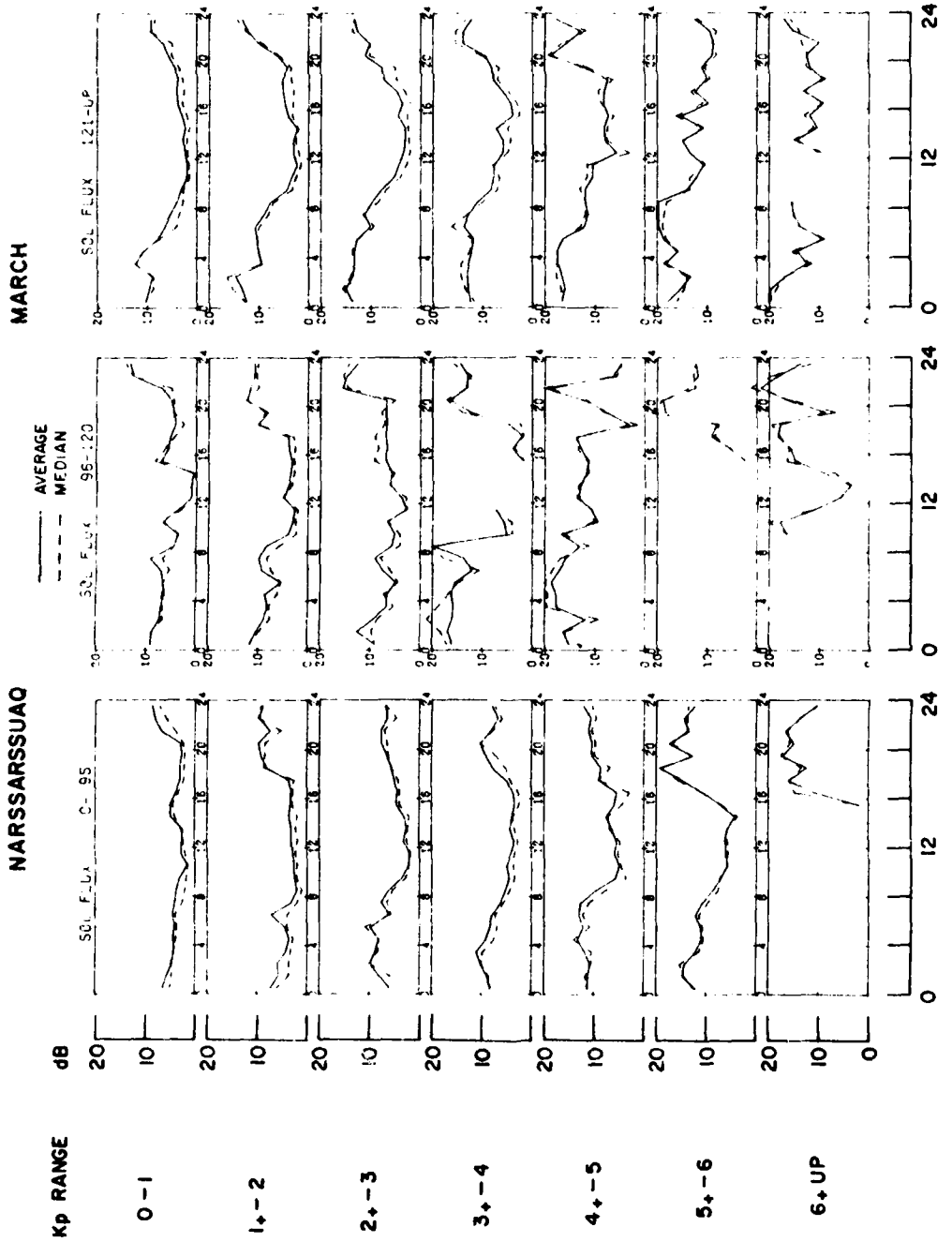

Fig. 5. Comparison of average and median values of March Narssarssuaq data.

propagation path is parallel to the lines of force of the earth's field. In order to fully examine the problem of geometry, a model would need to be developed in which the irregularity shape and elongation varied as a function of latitude, time, and geomagnetic conditions.

Martin and Aarons [1977] interpreted synchronous satellite data in the Narssarssuaq-Goose Bay area by using a Gaussian irregularity spectrum for the irregularities. They found the irregularities to be elongated along the magnetic field with a 5:2:1 configuration, where the first term is α, elongation of the irregularity along the lines of force of the magnetic field, the second term is γ, orthogonal to the elongation along the lines of force, being the magnetic east-west dimension, and the last term is orthogonal to the other two planes, i.e., magnetic north-south.

Rino et al. [1978], by observing the Wideband satellite (~1000-km altitude) in Poker Flat, Alaska, find evidence for L shell aligned, sheetlike irregularities with a lower bound to the configuration of 10:10:1.

Mikkelsen et al. [1978] have attempted to determine the theoretical scintillation index S_4 when the irregularities are described by a power law power spectrum. This utilizes the coordinates of the radio ray in the local coordinate system with set values for the elongation of the irregularities along and perpendicular to the magnetic field lines. Mikkelsen et al. assumed that the approximate dividing line between weak and strong scintillation is ~9 dB, with $SI < 9$ dB denoting the weak case. For this case the geometric variation of S_4 is given by

$$S_4 \propto [z/\cos i f(\psi, \phi)]^{1/2}$$

where

- i ionospheric zenith angle, equal to the angle between the radio ray and the irregularity layer;
- ψ propagation angle, equal to the angle between the radio ray and the magnetic field direction;
- ϕ azimuth of the radio ray in local coordinate system of z axis along the magnetic field direction and y axis in the magnetic east-west direction;

$$f(\psi, \phi) = \alpha\gamma(\gamma^2 \cos^2 \phi + \sin^2 \phi + \cos^2 \psi(\cos^2 \phi + \gamma^2 \sin^2 \phi) + \alpha^2 \sin^2 \psi)/[\gamma^2 \cos^2 \psi + \alpha^2 \sin^2 \psi(\gamma^2 \cos^2 \phi + \sin^2 \phi)]^{1/2}$$

- z reduced slant range to irregularity layer, equal to $z_1(z_2 - z_1)/z_2$, where z_1 is the slant range to irregularity layer and z_2 is the slant range to satellite;
- α elongation of the irregularities along the magnetic field lines;
- γ elongation of the irregularities in the magnetic east-west direction.

Using this irregularity formulation, *Mikkelsen et al.* [1978] found the Narssarssuaq observation of the orbiting satellite, Nimbus 4, at an altitude of 1100 km a best fit of irregularity configuration with 2.5:1.3:1.

In order to present a simplified solution to this problem, correction factors for the three high-latitude stations under the assumption of the elliptical column model of individual irregularities of 5 km along the lines of force of the earth's magnetic field, 2 km orthogonal to the lines of force (E-W), and of 1 km in the north-south meridian as determined by *Martin and Aarons* [1977] have been calculated.

For purposes of comparison, we have illustrated geometrical corrections to the data from Narssarssuaq for a 1100-km orbiting satellite assuming a Gaussian power spectrum (Figure 6) and a power law model (Figure 7). Correction factors have, in addition, been calculated for the 350-km intersection of the ATS 3 satellite using the power law model. The S_4 values derived from the formulas presented in the appendix would be reduced by 1.5 for Narssarssuaq, 1.1 for Goose Bay, and 1.2 for Sagamore Hill. We have not incorporated these correction factors in the constants, since the irregularity configuration is not agreed upon. It is possible that it changes as a function of latitude, solar and geomagnetic activity, and perhaps even local time. Factors given above are probably minimum reductions relative to overhead values.

COMPARISON OF MODEL FORMULAS WITH MILLSTONE HILL DATA

In order to validate the Narssarssuaq and Goose Bay equations using an independent set of observations at a higher frequency, a comparison was made with Millstone Hill observations of Navy Navigation Series satellites [*Wand and Evans*, 1975]. This Millstone Hill data consisted of S_4 scintillation indices, taken in the period 1971 1974 (a period of medium-high solar flux), at 400 MHz, normalized to zenith using an assumed three-dimensional power law spectrum. The data base contained >2000 tracks (~600 hours of observations). Contour plots of this data base were generated in local time over a range of 42–70°N Λ after partitioning the data into two seasons (summer and winter, defined between the equinoxes) and several different Kp levels. A

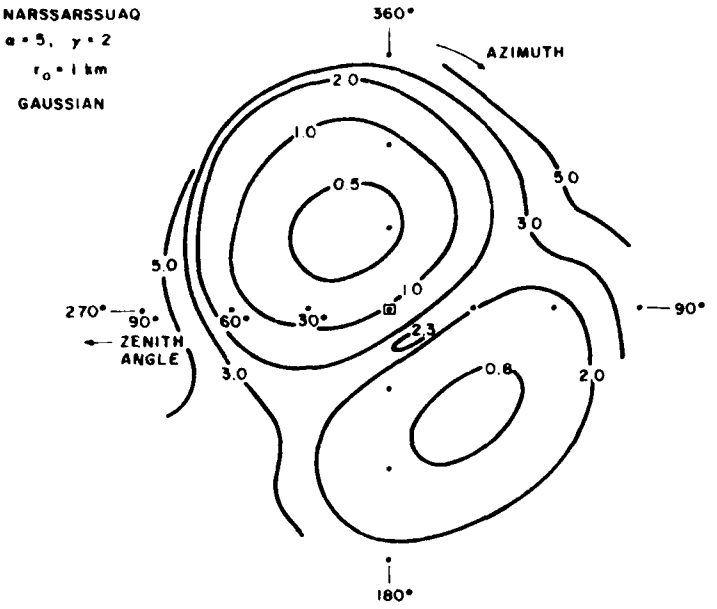

Fig. 6. Plot of correction factors for viewing a 1100-km orbiting satellite from Narssarssuaq under assumptions of elliptical column irregularity model and a Gaussian irregularity power spectrum.

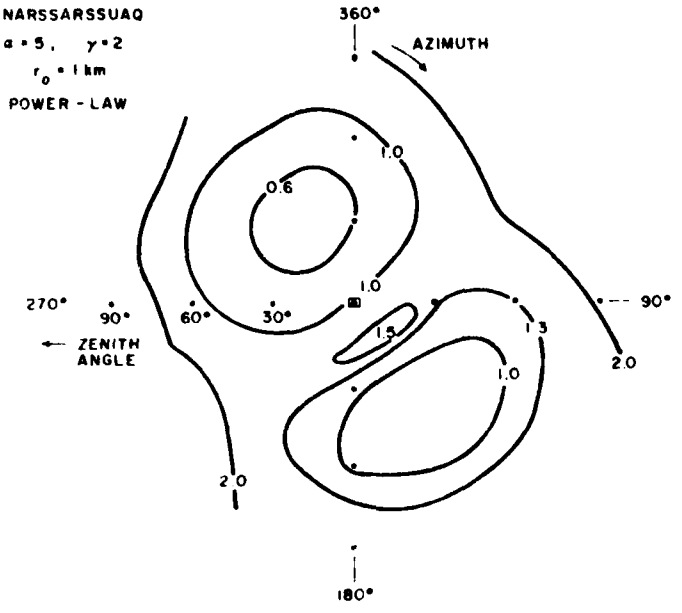

Fig. 7. Plot of correction factors for viewing a 1100-km orbiting satellite from Narssarssuaq under assumptions of elliptical column irregularity model and a power law irregularity power spectrum.

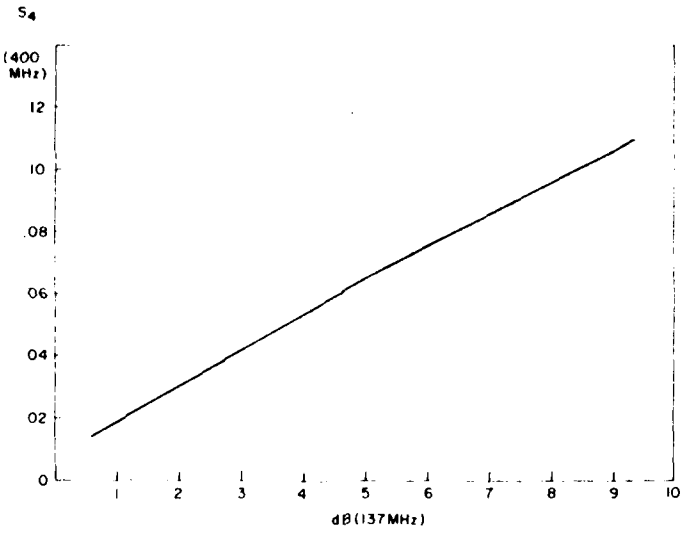

Fig. 8 Relationship between S_4 at 400 MHz and scintillation (dB) at 137 MHz.

comparison of the data was restricted to the 60–64° Λ range.

For comparison purposes, model dB values were generated for S_f = 120 (to correspond to the medium-high solar flux level of the Wand and Evans data), for each hour (local time), for each month, then averaged within the two seasons, and normalized and converted to S_4 (400 MHz) by means of Figure 8. These were then corrected to overhead zenith using correction factors determined by the method of *Mikkelsen et al.* [1978] mentioned in the previous section with irregularity form of $\alpha = 5$ (elongation along magnetic field lines) and $\gamma = 2$ (elongation of irregularity in magnetic east-west direction). These factors were approximately 1.5 for Narssarssuaq and 1.1 for Goose Bay, lower than the factors (which corrected only for elevation angle) of 2.5 and 1.8, respectively, if the corrections developed by Wand and Evans were applied to the Narssarssuaq and Goose Bay intersections. The resulting comparison of the two data sets is shown in Figures 9 and 10 for the

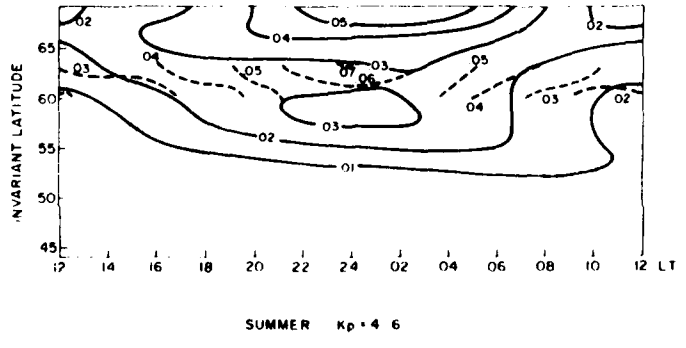

Fig. 9. Comparison of Wand and Evans 400-MHz summer data for the disturbed magnetic case (solid curves) with Narssarssuaq and Goose Bay model data (dashed curves) corrected for the ATS 3 intersection point and converted to 400 MHz.

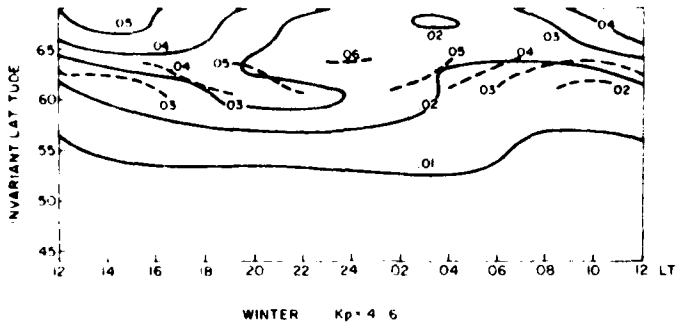

Fig. 10. Comparison of Wand and Evans 400-MHz winter data for the disturbed magnetic case (solid curves) with Narssarssuaq and Goose Bay model data (dashed curves) corrected for the ATS 3 intersection point and converted to 400 MHz.

disturbed magnetic case, $K = 4.5$. Under quiet magnetic conditions, $K = 2$, the trends are very similar, with lower S_4 values for both sets of data.

For the summer data at both $K = 2$ and $K = 4.5$ the formulas predict somewhat higher local midnight values than the Wand and Evans data show. The comparison of winter observations shows agreement within less than a factor of 2 in the region below 64°, the latitude of the Narssarssuaq intersection. The contours of Wand and Evans depict a winter maximum at ~14–16 LT at their lowest observational latitudes, i.e., in the auroral zone between 65 and 69°. Confining our comparison to latitudes below these, their winter (September–February) can be compared to the data base collected at Narssarssuaq by refering to Figure 3 of paper I the Narssarssuaq contours. In that figure for 64°, the broad maximum of activity is between 16 and 03 L.T. in September and in February and between midnight and 02 LT in December and January.

To further pursue the comparison with Wand and Evans, an independent set of measurements of scintillations of the 54-MHz beacon of the 1000-km orbiting satellite Transit IV-A (the forerunner of NNSS) were used. This data base consists of over 21,000 1-min scintillation values observed from Sagamore Hill in the period from July 1961 to April 1966 and has been divided into summer and winter observations. During these years, the average solar flux was lower than in the years of the Wand and Evans data. While the Transit measurements suffered from strong scattering at high latitudes, the form of the diurnal pattern can be easily obtained from the extensive data base.

The summer diurnal pattern in this Transit IV-A data is such that for low Kp, the lowest latitude of the $SI \geq 60\%$ contour was reached at ~21–24 LT, while under disturbed magnetic conditions, this occurs slightly later, ~21–03 LT, in agreement with the model contours. The winter diurnal pattern for both quiet and disturbed magnetic conditions shows the lowest latitudinal extent of the $SI \geq 60\%$ contour to occur ~21–24 LT.

Although the data were taken at low elevation angles to an invariant latitude of ~69°, the low frequency observed (54 MHz) and the signal recording techniques produced limiting so that the scintillation indices obtained from the Transit set could not be used quantitatively. It would appear as if the analytical formulas presented are valid to the latitude of 64° as shown by both the ATS 3 and the Transit IV-A data. The Wand and Evans observations indicate a different maximum for winter for latitudes above 64°, in no way invalidating the formulas presented.

DISCUSSION

The concept of this organization of a large data base over a limited geographic area was to provide users of scintillation data a means of predicting what changes in various forcing functions would do to the diurnal pattern of scintillation activity. Other models have been developed which attempt a wider sweep of prediction at high latitudes [*Fremouw et al.*, 1977].

However, it is the opinion of the authors of this paper that there are too many unknowns at this

time to do more than codify and simplify the data. Questions exist as to the configuration of the irregularities and to the variations of the three-dimensional structure, as to the thickness of the layer of irregularities, and as to irregularities being in the E and/or the F layer at various stages of auroral activity. The entire question of the polar ionospheric irregularities and the effect of magnetic activity on the level of scintillations in the polar cap is still open, with only a small amount of data available.

The data in this paper had limitations. While the data covered the entire day (a problem for high-inclination low-altitude satellite studies except perhaps at polar latitudes), the single-frequency data and the equipment utilized limited the precise descriptions of large excursions of signal.

The user of the formulas generated should take the following steps. The dB values calculated must first be converted into S_4 values, since geometrical corrections use S_4 values. The S_4 obtained from the formula through the conversion may be corrected by the ratio of the ATS 3 correction to the geometrical problem under consideration. It should be noted that at certain azimuths at high elevation angles (toward the north, for example) the values are lower than those overhead. At low angles of elevation, even to the north, angle of elevation effects dominate the equation, dwarfing the propagation angle corrections. The discussions relative to geophysical parameters have been given in paper 1.

Frequency dependence corrections are also done with S_4 values. They suffer from the frequency dependence being a function of strong and weak scatter. With weak scatter values, an η of 1.5 can be used, but with strong scatter the frequency dependence changes. If two frequencies are both strongly scattered, the approximate value of the frequency dependence, η, is zero, i.e., both signals are Rayleigh scattered.

APPENDIX

Analytical formulas are given below for three stations. DA is day number, $As = S_f/100$, HL is local time (hours) at subionospheric point (350 km), and S_f is solar flux at 2695 MHz in solar flux units.

Narssarssuaq

$$SI(\text{dB}) = -6.4 + 9.2(1 - 0.2FD)[1 + 0.23(1 - 0.3FD) \cdot \cos(HL + 2.0 + 0.34Kp) + 0.03\cos(2(HL - 0.6)) + 0.02\cos(3(HL + 3.0))]\,2^{[0.14Kp(1+0.12FD)+0.04(1+1.76FD)]}$$

$$FD = \cos(DA + 15.6) + 0.56\cos(2(DA - 22.4))$$

Goose Bay

$$SI(\text{dB}) = -1.3 + 1.1(1 - 0.77FD)[1 + 0.5(1 - 0.2FD) \cdot \cos(HL + 2.1 - 0.6Kp) + 0.06\cos(2(HL - 2.1)) + 0.02\cos(3(HL + 5.2))]\,2^{[0.13Kp(1+0.1FD)+0.04(1+1.2FD)]}$$

$$FD = \cos(DA + 0.5) + 0.2\cos(2(DA - 99))$$

Sagamore Hill

$$SI(\text{dB}) = 0.33 + 0.02(1 + 0.2FD)[1 + 1.2(1 - 0.01FD) \cdot \cos(HL - 0.4 - 0.15Kp) + 0.3\cos(2(HL - 0.8)) - 0.1\cos(3(HL + 6.1))]\,2^{[0.19Kp(1+0.3FD)+3.14(1-0.2FD)]}$$

$$FD = \cos(DA + 56) + 0.7\cos(2(DA - 143))$$

REFERENCES

Aarons, J. (1973), A descriptive model of F layer high-latitude irregularities as shown by scintillation observations, *J. Geophys. Res.*, *78*, 7441–7450.

Aarons, J. (1976), High-latitude irregularities during the magnetic storm of October 31 to November 1, 1972, *J. Geophys. Res.*, *81*, 661–670.

Aarons, J., and R. S. Allen (1971), Scintillation boundaries during quiet and disturbed magnetic conditions, *J. Geophys. Res.*, *76*, 170–177.

Aarons, J., H. E. Whitney, and R. S. Allen (1971), Global morphology of ionospheric scintillations, *Proc. IEEE*, *59*, 159–172.

Basu, S. (1975), Universal time seasonal variation of auroral zone magnetic activity and VHF scintillation, *J. Geophys. Res.*, *80*, 4725–4728.

Basu, S., and J. Aarons (1980), The morphology of high-latitude VHF scintillation near 70°W, *Radio Sci.*, *5*, this issue.

Briggs, B. H., and I. A. Parkin (1963), On the variation of radio star and satellite scintillation with zenith angle, *J. Atmos. Terr. Phys.*, *25*, 339–365.

Fremouw, E. J., and J. F. Bates (1971), Worldwide behavior of average VHF-UHF scintillation, *Radio Sci.*, *6*, 863–869.

Fremouw, E. J., and C. L. Rino (1973), An empirical model for average F-layer scintillation at VHF/UHF, *Radio Sci.*, *8*, 213–222.

Fremouw, E. J., C. L. Rino, A. R. Hessing, and V. E. Hatfield (1977), A transionospheric communication channel model, *Quart. Tech. Rep. 7*, SRI Int., Menlo Park, Calif.

Fremouw, E. J., R. L. Leadabrand, R. C. Livingston, M. D. Cousins, C. L. Rino, B. C. Fair, and R. A. Long (1978), Early results from the DNA Wideband satellite experiment—Complex-signal scintillation, *Radio Sci.*, *13*, 167–187.

Huang, C.-M. (1970), *F* region irregularities that cause scintillation and spread *F* at low latitude, *J. Geophys. Res.*, *75*, 4833–4841.

Martin, E., and J. Aarons (1977), *F* layer scintillation and the aurora, *J. Geophys. Res.*, *82*, 2717–2722.

Mikkelsen, I. S., J. Aarons, and E. Martin (1978), Geometrical considerations of 136 MHz amplitude scintillation in the auroral oval, *J. Atmos. Terr. Phys.*, *40*, 479–483.

Pope, J. H. (1974), High latitude ionospheric irregularity model, *Radio Sci.*, *9*, 675–682.

Rino, C. L., R. C. Livingston, and S. J. Matthews (1978), Evidence for sheet-like auroral ionospheric irregularities, *Geophys. Res. Lett.*, *5*, 1039–1042.

Rufenach, C. L. (1974), Wavelength dependence of radio scintillation: Ionosphere and interplanetary irregularities, *J. Geophys. Res.*, *79*, 1562–1566.

Singleton, D. G. (1979), An improved ionospheric irregularity model, in *Solar Terrestrial Prediction Proceedings*, NOAA, Boulder, Colo.

Wand, R. H., and J. V. Evans (1975), Morphology of ionospheric scintillation in the auroral zone, in *Effect of the Ionosphere on Space Systems and Communications*, edited by J. Goodman, *NTIS CSCL 04/1 N75-30714*, Naval Research Laboratory, Washington, D.C.

Whitney, H. E. (1974), Notes on the Relationship of Scintillation Index to Probability Distributions and Their Uses for System Design, *Tech. Rep. 74-0004*, Air Force Cambridge Res. Lab., Hanscom Air Force Base, Mass.

Whitney, H. E., and S. Basu (1977), The effect of ionospheric scintillation on VHF/UHF satellite communications, *Radio Sci.*, *12*, 123–133.

Whitney, H. E., C. Malik, and J. Aarons (1969), A proposed index for measuring ionospheric scintillation, *Planet. Space Sci.*, *17*, 1069–1073.

GEOPHYSICAL RESEARCH LETTERS, VOL. 7, NO. 8, PAGES 609-612, AUGUST 1980

PRELIMINARY RESULTS OF SCINTILLATION MEASUREMENTS ASSOCIATED WITH IONOSPHERE HEATING AND POSSIBLE IMPLICATIONS FOR THE SOLAR POWER SATELLITE

Santimay Basu and Sunanda Basu
Emmanuel College
Boston, MA 02115

Allen L. Johnson
Avionics Laboratory
Wright-Patterson AFB, OH 45433

J.A. Klobuchar
Air Force Geophysics Laboratory
Hanscom AFB, MA 01731

C.M. Rush
U.S. Department of Commerce
Institute for Telecommunication Sciences
Boulder, CO 80303

Abstract. Initial results of ground and air-borne measurements of 250 MHz scintillations associated with ionospheric heating in both the overdense (heater frequency below the critical frequency) and underdense cases (heater frequency above the critical frequency) by the high-power, high-frequency transmitter at Platteville, Colorado are discussed. The ground stations and the geostationary satellites used in the experiment were so chosen that it was possible to explore the artificial irregularities both within and outside the central heated volume. One ground station was able to view LES-8 in a field-aligned direction while, at a second ground station, spaced receiver scintillation measurements were available using FLEETSATCOM. The instrumented aircraft recorded both phase and amplitude scintillations and flew missions in the north-south and east-west directions to define the region of artificial irregularities. The preliminary results indicate a prompt excitation of artificial irregularities in the overdense case causing 2-10 dB scintillation at 244-249 MHz and a lifetime of the order of ten minutes. In the underdense case, on the other hand, the response was delayed and effects were observed to be on the order of 1-3 dB at 250 MHz, although a unique event of 10 dB scintillation was recorded along the field-aligned propagation path. The presence of such scintillations in the underdense case and their implications for the proposed Solar Power Satellite (SPS) are indicated in the paper.

Introduction

It has been established that high-power HF transmitters operating at a frequency below the maximum ionospheric plasma frequency can produce significant enhancement of the electron gas temperature near the altitude of HF reflection (Gordon et al., 1971; Utlaut and Cohen, 1971; for recent comprehensive reviews see Carlson and Duncan, 1977 and Fejer, 1979). It was also pointed out that if the power density of the incident HF radio waves is sufficiently intense (~ 10-$100\ \mu wm^{-2}$), the parametric instabilities may occur in the ionospheric plasma (Perkins et al., 1974; DuBois and Goldman, 1972). The prediction was experimentally confirmed at Arecibo (Carlson et al., 1972) and it was demonstrated that short wavelength (1cm-10m) electron waves are driven unstable by the decay instability.

The long wavelength ($\sim$1 km) field-aligned irregularities giving rise to artificial spread F (Utlaut et al., 1970; Utlaut and Violette, 1972, Wright, 1973) could not, however, be explained in terms of the above instability process. The causative mechanism for the generation of long wavelength irregularities remained obscure for quite a while and is now attributed to either a thermal self-focusing mechanism (Perkins and Valeo, 1974; Thome and Perkins, 1974) or the alternative mechanisms of stimulated Brillouin scattering (Cragin and Fejer, 1974) and stimulated diffusion scattering (Goldman, 1974). Nevertheless, this range of irregularity scale sizes having sufficient power spectral intensity can cause scintillation of radio signals received from radio stars and artificial satellites. It was demonstrated that VHF/UHF signals transmitted through the artificially heated ionospheric F region do indeed exhibit scintillations (Rufenach, 1973; Pope and Fritz, 1974; Bowhill, 1974). Radio star scintillation measurements at 26 MHz during ionospheric modification indicated the presence of either rapid and random or deep long-period ($\sim$5 mins) fluctuations. In order to avoid some of the difficulties of radio star observations, Bowhill (1974) performed scintillation measurements with both geostationary and orbiting satellites and established the field-aligned nature of the irregularities causing VHF and UHF scintillations, their transverse scale and drift speed. One feature common to all the above studies was the fact that the heater frequency was below the plasma frequency of the F region.

In this paper, we describe some preliminary results from a recent scintillation experiment performed at two ground stations in Wyoming and by an instrumented aircraft in conjunction with ionospheric heating by the high-power, high-frequency transmitter at Platteville, Colorado. The notable feature of the present experiment, in contrast to the previous ones, was the operation of the heating transmitter at a frequency not only below the critical frequency of the ionosphere (overdense heating) but above the critical frequency (underdense heating) as well. Although, fadings of signals have been reported earlier during underdense heating by obliquely reflected radio waves (Novozhilov and Savel'yev, 1978), the results presented in this paper indicate, for the first time, that underdense heating may cause intensity fluctuations of signals received from satellites. Any transionospheric propagation effects associated with underdense heating has possible implications for the proposed Solar Power Satellite (SPS) system (Basu and Basu, 1980).

Experimental Details

During the period of observations between March 7-14, 1980, the Platteville heating transmitter was put into CW, as well as, pulsed operation at frequencies varying between 5.2 and 9.9 MHz with a maximum transmitter power of 1.5 MW. Ordinary mode heating was used throughout the period of the experiment. A maximum power density of 60 μwm^{-2} at 300 km was attained at a frequency of 9.9 MHz. A full description of the transmitter and antenna systems may be obtained in Utlaut et al., (1970) and Carroll et al., (1974).

Figure 1 shows the extent of the central heated region at 300 km altitude above Platteville as limited by the half-power beam circle at 10 MHz (beam width: 11.9° at 10 MHz). The intersections of the altitude of 300 km with the ray paths from the Douglas station (42.57°N, 105.37°W) to ATS-3 and FLEETSATCOM 1 (abbreviated as FLTSAT) satellites as well as from the Carpenter station (40.87°N, 104.18°W) to LES-8 are shown.

This paper is not subject to U.S. copyright. Published in 1980 by the American Geophysical Union.

Paper number 80L0880.
0094-8276/80/0080L-0880$01.00

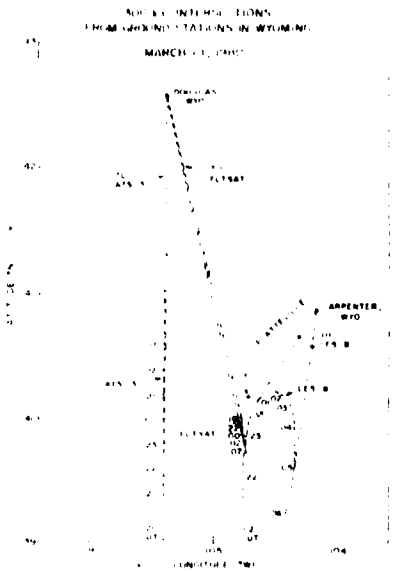

Figure 1. Geometry of observations of various geostationary satellites from Carpenter and Douglas, Wyoming in conjunction with ionospheric heating at Platteville, Colorado on March, 1980.

In view of the finite orbital inclinations of the satellites, the intersection point varied with time and, therefore, the universal time is marked alongside the foci of the subionospheric positions. It may be noted that the subionospheric position of ATS-3 satellite at its closest position was located about 40 km to the west of the heated region whereas the locus of FLTSAT was within 30 km of the southern fringe of the heated region at all universal times. Since the F-region irregularities are generally assumed to be field-aligned, and the declination of the magnetic field is only 13°, the north-south orientation of the subionospheric locus implies that the ray path to that satellite is able to intercept the irregularities generated within the beam circle at altitudes higher than 300 km. In view of the large orbital inclination of LES-8, the subionospheric position varies considerably over a diurnal cycle but it lies within the heated region between 00:02 UT and remains within 30 km of the heated volume between 23:04 UT. The advantage of the large orbital inclination lies in a high elevation angle of measurement for several hours around 0230 UT equalling the magnetic dip angle and thereby offering the unusual opportunity of field aligned scintillation measurement at a high or a low latitude station with a geostationary satellite.

At Douglas, scintillation measurements with FLTSAT satellite were performed at 244 MHz using 3 spaced receivers with magnetic E-W baseline of 1200 meters and 89.9 meters in the magnetic N-S direction, the N-S baseline being limited by terrain considerations. At the same station total electron content and amplitude scintillation measurements were made with a polarimeter using 137 MHz transmissions from ATS-3. At the Carpenter site, 249 MHz transmissions from LES-8 were received for scintillation measurements. Data were recorded on magnetic tapes at both sites and are currently being analysed to determine the irregularity drift and scintillation spectra.

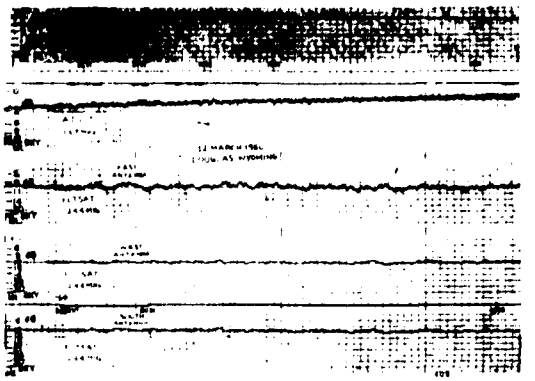

Figure 2. Amplitude scintillation data obtained at Carpenter using LES-8 as well as ATS-3 and spaced receiver FLTSATCOM data obtained at Douglas during overdense ionospheric heating on March 12, 1980. The transmitter was in CW operation with power of 1.5 MW at 9.9 MHz between 0030-0045 UT. The critical frequency was 11.9 MHz at 0050 UT.

The aircraft flew three missions on March 11-12, March 12-13, and March 13-14, 1980, and performed phase and amplitude scintillation measurements with FLTSAT and LES-8 satellites. The aircraft flew N-S and E-W legs over both ground stations at Douglas and Carpenter and was able to define the E-W and N-S extent of irregularities generated by the heater and determine the lifetime of these irregularities.

Results

The top panel of Figure 2 shows scintillation data from Carpenter and the next four data panels are from Douglas showing the amplitude recording of ATS-3 and FLTSAT signal fluctuations on the east, west and south receiving systems respectively during an overdense heating cycle on March 12, 1980. The heating transmitter was turned on at 0030 UT and turned off at 0045 UT and operated at a frequency of 9.9 MHz delivering a power of 1.5 MW. The critical frequency of the ionosphere was found to be 11.9 MHz at 0050 UT and thus this heating cycle corresponded to the overdense case.

The Carpenter data illustrated on the top panel cover the entire heating period whereas the Douglas data represented in the bottom panels cover only the initial heating period due to the higher chart speed. However, the onset of scintillations at both sites was recorded about 10 seconds after the heating transmitter was turned on and persisted for at least 9 minutes after it was turned off. The 249 MHz scintillations at the Carpenter site correspond to 5 dB peak-to-peak while at the Douglas site 2 dB scintillations at 244 MHz were recorded. No activity occurred on the ATS-3 channel. The higher level of scintillation activity at Carpenter is attributed to the near alignment of the propagation path with the magnetic field through the heated volume. Spaced receiver measurements at Douglas yield an eastward irregularity drift speed of 75 m sec^{-1} during this period. The absence of scintillation activity on the ATS-3 channel suggests that artificial irregularities did not extend 40 km to the west of the central heated volume illustrated in Figure 1. It should also be mentioned that the ATS-3 link being at 137 MHz, enhanced scintillation effects would be expected as compared

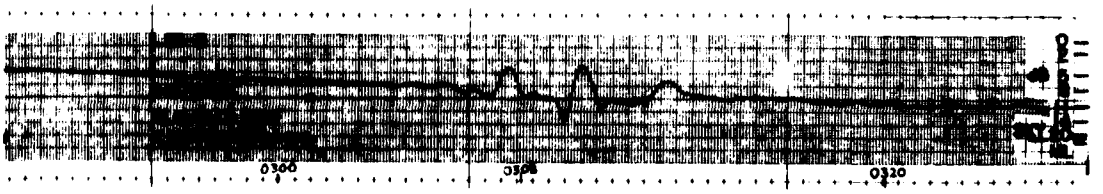

Figure 3. Amplitude scintillation data obtained at Carpenter during underdense ionospheric heating on March 12, 1980. The transmitter was in CW operation with power of 1.5 MW at 9.9 MHz between 0300-0315 UT. The critical frequencies at 0258 UT and 0312 UT were 8.1 and 7.9 MHz respectively.

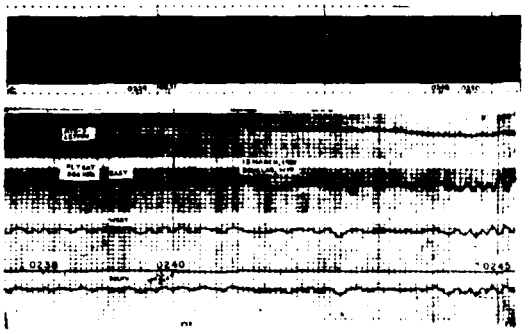

Figure 4. Same as in Figure 2 except for a marginally underdense case of heating on March 13, 1980. The transmitter was in CW operation with power of 1.5 MW at 9.9 MHz between 0230-0245 UT. The critical frequencies at 0232 UT and 0240 UT were 9.5 and 9.35 MHz respectively.

to the FLTSAT link, if irregularities with identical strength had been present at both locations.

At the end of the above heating period the transmitter remained off for more than two hours and was turned on at 0300 UT for a 15-minute cycle with an input power of 1.5 MV. It was operated at 9.9 MHz while the critical frequency was only 7.9 MHz, so that the heating was underdense. Figure 3 shows that the Carpenter station observing LES-8 in a magnetic-field-aligned direction recorded quasi-periodic scintillations with 10 dB peak-to-peak fading. The station at Douglas did not observe any corresponding effect during this underdense heating period on the FLTSAT propagation path, only 40 km to the west and south of the subionospheric position of LES-8. The quasi-periodic fadings shown in Figure 3 are reminiscent of a special type of naturally occurring scintillations caused by ionization gradients (Basu and Das Gupta, 1969; Elkins and Slack, 1969). It should be mentioned, however, that no such fadings were observed in the absence of heating during one week's continuous observations at Carpenter. Whether the underdense heating can create field-aligned density depletions (Perkins and Roble, 1978) and the resulting sharp ionization gradients can give rise to an interference pattern (Elkins and Slack, 1969) because of the special viewing geometry remains to be verified by further observations.

Figure 4 shows scintillation data obtained during a marginally underdense heating cycle between 0230-0245 UT on March 13, 1980, the heater frequency being 9.9 MHz and the critical frequency varying between 9.5 MHz and 9.35 MHz. A peak-to-peak fluctuation of 2.5 dB at Douglas and 3 dB at Carpenter was encountered during this cycle. Considerable variation of fading period ranging between 3 sec to 20 sec may be noted from the Carpenter data. The Douglas data indicate an eastward drift speed of about 12 m sec^{-1} during this heating cycle.

Figure 5 shows scintillation results obtained during another case of underdense heating performed between 0300-0315 UT on March 13, 1980. The heater frequency was 9.9 MHz and the power output was 1.5 MW. The critical frequency of the ionosphere ranged from 9.2 MHz at 0252 to 8.35 MHz at 0316 UT. During this underdense heating cycle, the Douglas site recorded 1.5 dB scintillations and the Carpenter site looking along the magnetic field lines observed scintillations of 3 dB magnitude. Both sites recorded an average fading period of about 40 sec, considerably slower as compared to the overdense cases. Considering the propagation geometry of Carpenter observations, the observed scintillations correspond to an irregularity amplitude $\Delta N/N \sim 0.3\%$ for an assumed layer thickness of 50 km and a 3-dimensional irregularity power spectrum of 4 with an outer scale of 2 km (Basu et al., 1976). A recent theory of self-focusing instability in an underdense ionosphere (Perkins and Goldman, 1980) predicts the generation of sheet-like irregularities aligned with the magnetic meridian with irregularity amplitudes ~0.5% and E-W striation size ~2 km under the conditions of the

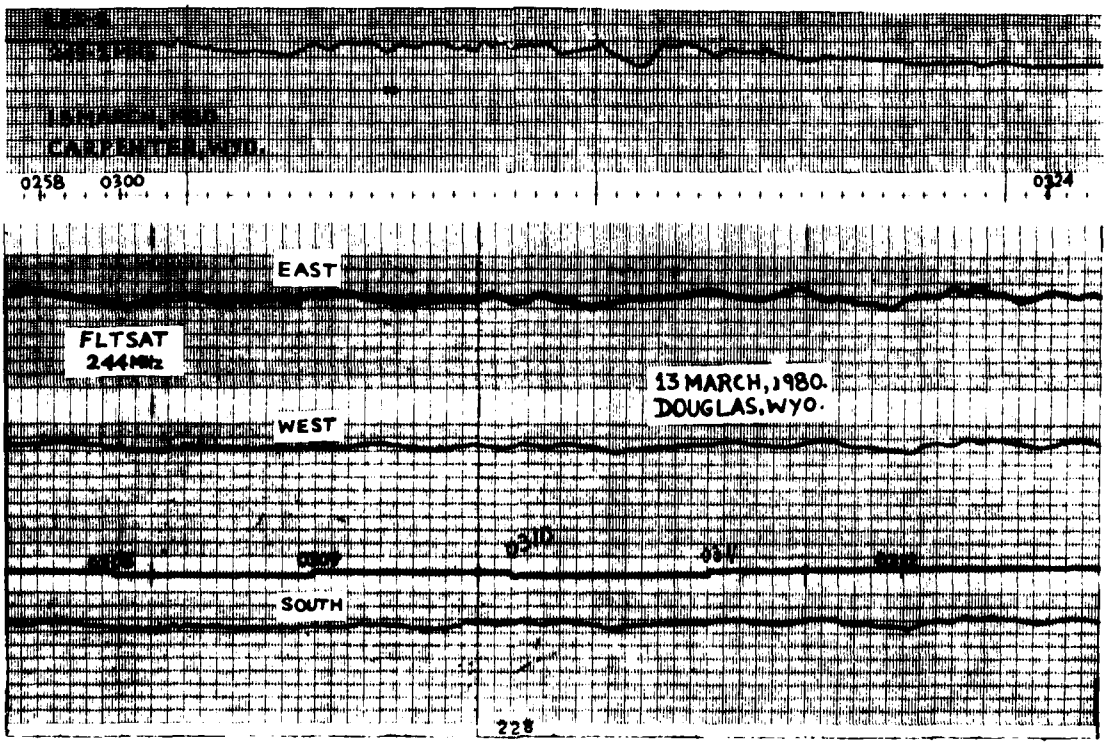

Figure 5. Same as in Figure 2 except for underdense heating on March 13, 1980. The ATS-3 data showed no effect and is not shown. The transmitter was in CW operation with power of 1.5 MW at 9.9 MHz between 0300-0315 UT. The critical frequencies at 0252 UT, 0310 UT and 0316 UT being 9.2, 8.5 and 8.35 MHz respectively.

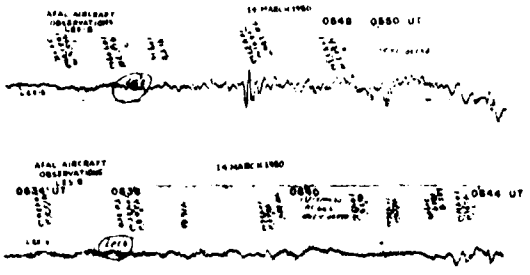

Figure 6. AFAL aircraft observations of amplitude scintillations using LFS-8 on March 14, 1980 during overdense (top panel) and underdense (bottom panel) cases of heating. For overdense case, the transmitter was in CW operation with power of 1.5 MW at 5.2 MHz between 0530-0545 UT. The critical frequency was 5.5 MHz at 0523 UT and 5.3 MHz at 0549 UT. For underdense case, the transmitter was in CW operation with power of 1.5 MW at 5.2 MHz between 0630-0645 UT. The critical frequency was 4.6 MHz at 0640 UT.

present experiment. Thus there is good agreement between the theoretical prediction and observations in regard to the irregularity amplitude.

The aircraft observations detected considerable scintillation effects on many heating cycles, as it could position itself to have the ray paths intersect the heated volume. By flying E-W and N-S legs, the aircraft measurements indicate the extent of artificial irregularities to be about 70 km E-W and 100 km N-S. In the top panel of Figure 6 we show a case of scintillation with peak-to-peak fluctuation of 7 dB and fading periods of about 10 secs during an overdense heating cycle on March 14, 1980 at 0547 UT (heater frequency = 5.2 MHz and critical frequency varying between 5.5 and 5.3 MHz). During this period, the aircraft made an E-W cut between 104°50'W and 103°56'W and 42°N latitude and then retraced its path encountering the deep fades with periods ~5 sec at 0547 UT at 42°01'N and 104°37'W. Similar fades of 2 dB magnitude were observed at both Carpenter and Douglas. In the bottom panel of Figure 6, we show the aircraft detecting 1-2 dB fades with periods ~10 sec during an underdense heating cycle between 0630-0645 UT (heater frequency = 5.2 MHz and critical frequency = 4.8 MHz) on March 14, 1980. During this period, the aircraft flew a N-S latitude leg (41°53'N to 43°01'N) maintaining a longitude of 104°31'W. During this same cycle, no effect was seen at Carpenter as the geometry was very unfavorable (cf. Figure 1) while 1 dB fluctuation with periods ~20 sec was observed at Douglas.

To summarize, we have demonstrated for the first time that HF-driven instability in the underdense ionosphere can give rise to observable scintillation effects at 250 MHz. Perkins and Goldman (1980) have recently shown that there exists a finite possibility of the generation of self-focusing instability by the microwave power beam of the SPS and have predicted irregular density fluctuations to be two orders of magnitude greater than the HF case, considered in this paper. As a consequence, the weak effects of 3 dB amplitude fluctuations corresponding to phase deviation of 10° rms at 250 MHz (Basu et al., 1976) reported here, may undoubtedly magnify even at the much higher frequency of operation envisaged for the SPS. Further, in the presence of cascading of irregularity scale sizes, propagation over a broad frequency range may be affected. In view of the present results and current instability theories, the need for further work on HF-heating effects on the underdense ionosphere cannot be overemphasized. Obviously, any realistic SPS environmental assessment will require operation of HF heaters at several higher frequencies to test the scaling law proposed by Perkins and Goldman (1980).

Acknowledgments

The authors wish to thank J. Aarons for his help in organizing the experiment and to C. Malik for help with the observations. The authors also thank the 4950th Test Wing, Wright-Patterson Air Force Base, OH for their support in the operation of the AFAL aircraft. They are grateful to the ITS personnel responsible for the operation of the Platteville Facility: J. Carroll, E. Violette, R. Espeland, R. Chavez and A. Mitz. Funding for the operation of the Platteville Facility during the experiments was provided by the Satellite Power System Project Office of the U.S. Department of Energy. The work at Emmanuel College was partially supported by NSF grant ATM-78-25264 and AFGL contract F19628-78-C-0005.

References

Basu, S., and A. Das Gupta, Scintillation of satellite signals by ionospheric irregularities with sharp boundary, J. Geophys. Res., 74, 1294, 1969.

Basu, S. and S. Basu, Proposed experimental studies for assessing ionospheric perturbations on SPS uplink pilot beam signal, Proceedings of Workshop on SPS Microwave Power Transmission and Reception, NASA Johnson Space Center, Houston, Texas, January 15-18, 1980.

Basu, S., S. Basu and B.K. Khan, Model of equatorial scintillations from in-situ measurements, Radio Sci., 11, 821, 1976.

Bowhill, S.A., Satellite transmission studies of spread-F produced by artificial heating of the ionosphere, Radio Sci., 9, 975, 1974.

Carlson, H.C., W.E. Gordon, and R.L. Showen, High frequency induced enhancements of the incoherent scatter spectrum at Arecibo, J. Geophys. Res., 77, 1242, 1972.

Carlson, H.C., and L.M. Duncan, HF excited instabilities in space plasmas, Radio Sci., 12, 1001, 1977.

Carroll, J.C., E.J. Violette and W.F. Utlaut, The Platteville high power facility, Radio Sci., 9, 889, 1974.

Cragin, B.L., and J.A. Fejer, Generation of large-scale field-aligned irregularities in ionospheric modification experiments, Radio Sci., 9, 1071, 1974.

Dubois, D.F. and M.V. Goldman, Spectrum and anomalous resistivity for the saturated parametric instability, Phys. Rev. Lett., 28, 218, 1972.

Elkins, T.J., and F.F. Slack, Observations of ionospheric disturbances using stationary satellites, J. Atmos. Terr. Phys., 31, 421, 1969.

Fejer, J.A., Ionospheric modification and parametric instabilities, Rev. Geophys. Space Phys., 17, 135, 1979.

Goldman, M.V., Field aligned instability due to stimulated scattering of intense radio waves from diffusion quasimodes, Radio Sci., 9, 1077, 1974.

Gordon, W.E., H.C. Carlson and R.L. Showen, Ionospheric heating at Arecibo: First tests, J. Geophys. Res., 76, 7808, 1971.

Novozhilov, V.I., and S.M. Savel'yev, Geomagn. Aeronomy, 18, 145, 1978.

Perkins, F.W., C. Oberman and E.J. Valeo, Parametric instabilities and ionospheric modification, J. Geophys. Res., 79, 1478, 1974.

Perkins, F.W., and E.J. Valeo, Thermal self-focusing of electromagnetic waves in plasmas, Phys. Rev. Lett., 32, 1234, 1974.

Perkins, F.W., and R.G. Roble, Ionospheric heating by radio waves: Predictions for Arecibo and the satellite power station, J. Geophys. Res., 83, 1611, 1978.

Perkins, F.W., and M.V. Goldman, Self-focusing of radio waves in an underdense ionosphere, to be published in J. Geophys. Res., 1980.

Pope, J.H., and R.B. Fritz, Observations of artificially produced scintillations using satellite transmissions, J. Geophys. Res., 79, 1074, 1974.

Rufenach, C.L., Radio scintillation of stellar signals during artificial ionospheric modification, J. Geophys. Res., 78, 5611, 1973.

Thome, G.D., and F.W. Perkins, Production of ionospheric striations by self-focusing of intense radio waves, Phys. Rev. Lett., 32, 1238, 1974.

Utlaut, W.F., E.J. Violette, and A.K. Paul, Some ionosonde observations of ionospheric modification by very high power high-frequency ground-based transmission, J. Geophys. Res., 25, 6429, 1970.

Utlaut, W.F., and Cohen, Modifying the ionosphere with intense radio waves, Science, 174, 245, 1971.

Utlaut, W.F., and E.J. Violette, Further observations of ionospheric modification by a high-powered HF transmitter, J. Geophys. Res., 77, 6804, 1972.

Wright, J.W., Kinesonde observations of ionosphere modification by intense electromagnetic fields from Platteville, Colorado, J. Geophys. Res., 78, 5622, 1973.

(Received May 5, 1980;
accepted June 18, 1980.)

Variability of ionospheric time delay in the Mediterranean region

David H. Hendrickson
EMMANUEL COLLEGE - BOSTON, MA 02115
John A. Klobuchar
AIR FORCE GEOPHYSICS LABORATORY HANSCOM AFB
BEDFORD, MA 01731

Abstract. Faraday rotation measurements of VHF radio waves from the SIRIO satellite have been used to determine statistics of variability of ionospheric time delay in the Mediterranean region for the current solar maximum period. Results show standard deviations of up to 25 percent, or up to sixteen times ten to the sixteenth power electrons per square meter column. During daytime periods the distribution of errors about the monthly average time delay is nearly Gaussian. Modern satellite ranging systems which require correction for the effects of the time delay of the earth's ionosphere need continued high accuracy ionospheric time delay data which is available from the Faraday rotation of VHF radio waves on the SIRIO satellite.

1. INTRODUCTION

Modern satellite ranging systems, navigation and satellite radars, and satellites used for precise time transfer, may require a knowledge of the time delay of the earth's ionosphere to attain the desired system accuracy. The retardation of the modulation of the radio wave imposed by the ionosphere is a function of the total number of electrons encountered by the radio wave on its passage from satellite to user on, or near, the ground. The amount of time delay caused by the ionosphere can be expressed as:

$$\Delta t = \frac{40.3\ TEC}{cf^2}$$

where
- Δt is the time delay in seconds
- TEC is the Total Electron Content in electrons/meter^2 column
- c is 3.0×10^8 meters/second
- f is the frequency of the signal in Hertz

Values of Total Electron Content (TEC) range from 10^{16} to perhaps 10^{19} el/m^2 column. Figure 1 illustrates the amount of time delay imposed by the earth's ionosphere on radio waves as a function of frequency for four values of TEC. Note that time delays of 100 microseconds can be encountered at VHF, and delays of almost a microsecond will be found at 1.6 GHz.

Since the ionosphere is a dispersive medium the amount of the time delay is an inverse function of system operating frequency, and this fact can be used to advantage in systems which require the precise correction for ionospheric time delay.

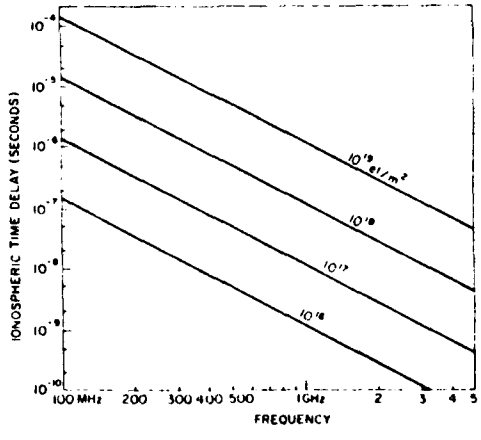

Fig. 1. Ionospheric time delay vs system operating frequency for 4 levels of TEC.

The NAVSTAR/Global Positioning System (GPS) described by [1] is an example of a two frequency satellite navigation system in which the second system operating frequency is used to automatically correct for the ionospheric first order time delay.

Other advanced satellite ranging systems may not be able to use a two frequency automatic correction method and must either use monthly average ionospheric model values of TEC or may make no correction at all for the ionospheric time delay effects. In this paper we will describe the variability of the ionospheric TEC in the Mediterranean

region for the current solar maximum period, for use by satellite systems design engineers and others who wish to know the magnitude of ionospheric time delay on their system. The current solar maximum is approximately 50% higher than an average solar maximum and is likely a worst case solar cycle for systems engineering planning purposes.

2. THE EXPERIMENTAL DATA BASE

Total Electron Content data used in this report was obtained from measurements of Faraday rotation of linearly polarized VHF telemetry radio waves transmitted from the SIRIO geostationary satellite. The SIRIO satellite was launched as an experimental advanced concept communications satellite by the Italian National Research Council. The measurements were taken at Athens, Greece, 37.97°N lat., 23.72°E long., viewing the SIRIO satellite in a direction of 30.6° elevation, 232.6° azimuth. The equivalent location in the ionosphere which is commonly used in representing trans-ionospheric propagation data was taken at a height of 420 kilometers, and was located at 34.5°N, 18.4°E. Values of measured Faraday rotation were converted to equivalent vertical TEC using the standard method described by [2].

Faraday rotation is a measure of TEC only to an approximate height of 2000 to 3000 kilometers. There is an additional small contribution to TEC due to electrons above this height, from a region called variously the plasmasphere or protonosphere. This additional contribution to TEC is estimated to be only 10 to 15 percent, at least during the daytime period when the absolute values of TEC are highest. In this report we have only used the contribution to total time delay due to the Faraday effect.

While values of Faraday polarization rotation are taken continuously from the Athens station, they are reduced to equivalent vertical TEC data only at 15 minute intervals, which is adequate for most engineering purposes. Data for five months has been compiled and monthly averages and statistical values for these months are represented here.

3. RESULTS

An immediate familiarization with the monthly variability of ionospheric time delay can be obtained by examining the plots shown in Figures 2 through 6. In these figures diurnal curves of TEC are plotted versus time for all days of each month. The scatter from day to day about a monthly mean curve can be seen easily in the figures. Note that the absolute values of TEC are highest in mid-afternoon, and are lowest in the late night hours. Note also, that the seasonal behavior shows highest values in March, with lowest values occurring in June. The data illustrated in Figures 2 through 6 are representative of all the seasons of a solar maximum year, and can be taken by systems design engineers as typical behavior of ionospheric time delay for the Mediterranean region for this solar maximum period 1978-79. Corresponding values of TEC during a solar minimum period would be approximately one-third to one-quarter as high as those illustrated here.

In Figure 7 the percentage standard deviation of individual TEC daily values from the hourly mean values for the five months is plotted. As can also be seen from the monthly TEC data overplots shown in Figures 2-6 the standard deviation of the daytime data is greatest during the month of April. Standard deviations are more important during the daytime periods as the greatest absolute values of TEC occur during those hours. The greatest percentage standard deviations occur during the early morning hours of March and April, but these values are relatively unimportant due to the very low absolute TEC values during those hours.

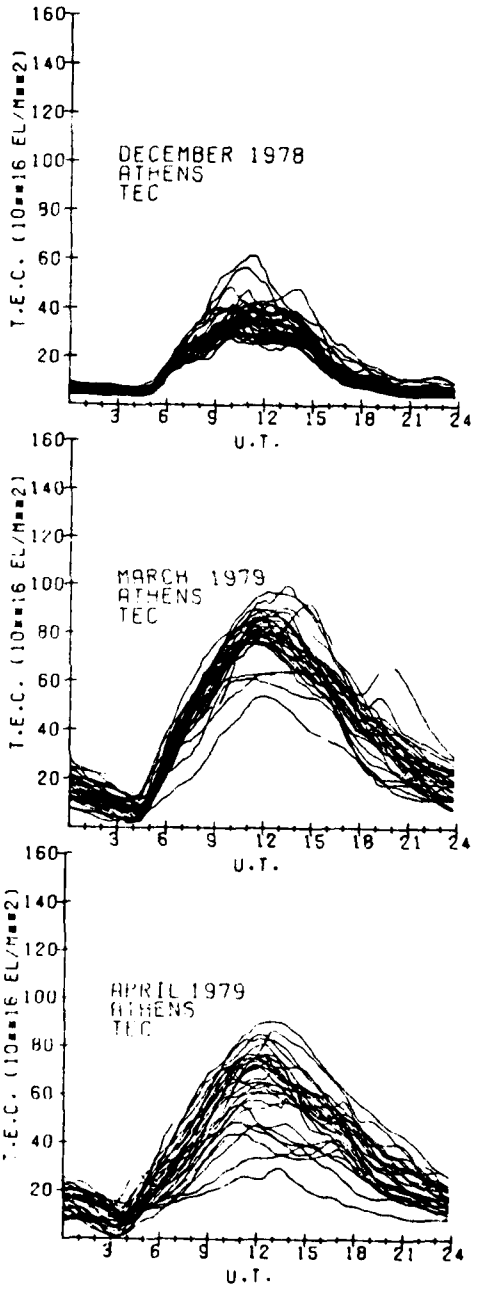

Fig. 2. Monthly overplot of TEC vs UT at Athens, Greece for December, 1978.
Fig. 3. Same as Fig. 2 for March, 1979.
Fig. 4. Same as Fig. 2 for April, 1979.

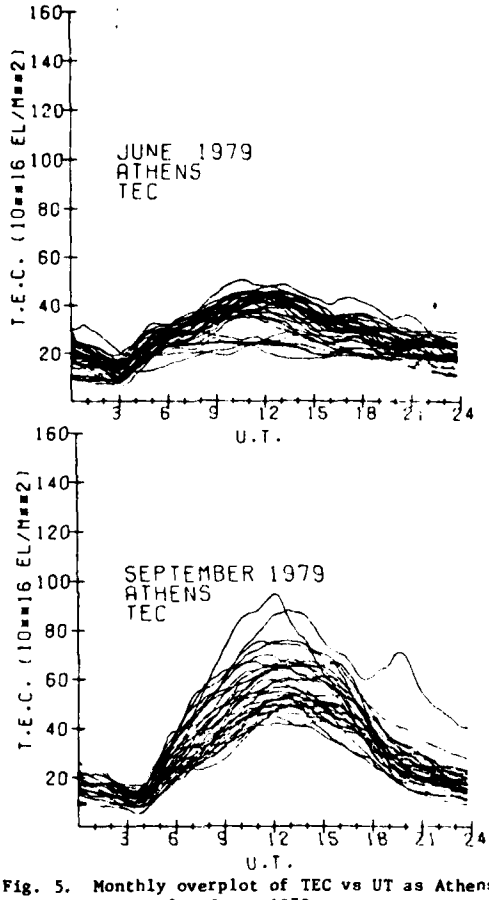

Fig. 5. Monthly overplot of TEC vs UT as Athens, Greece for June, 1979.
Fig. 6. Same as Fig. 5 for September, 1979.

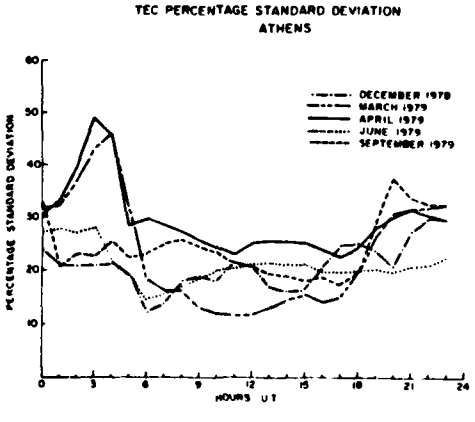

Fig. 7. Percent standard deviation of TEC vs UT for months indicated for Athens, Greece.

During the daytime hours the percent standard deviation from monthly average values is highest during the month of April 1979 and lowest during the preceding month of March 1979. In Figure 8 we have plotted the A_p daily index of planetary magnetic activity for those two months and we find that there were several periods of magnetic

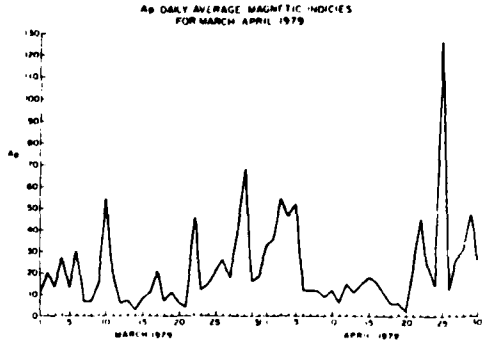

Fig. 8. Daily average magnetic Ap indices for March-April 1979.

activity during March. There was an extended period of relatively quiet magnetic conditions during the April 6 through 20 period, followed by generally very disturbed conditions from 21 April through the end of the month. The greatest changes in TEC from monthly average behavior generally occur during magnetically disturbed periods, but the difference in magnetic activity between the months of March and April was not great enough to account for the large difference in standard deviation observed in the TEC hourly daytime values for these two months. A more likely explanation for these observed differences in standard deviation is that the normal seasonal changes from winter-like to summer-like TEC diurnal behavior occur during the month of April. Those seasonal changes, along with magnetic activity, are likely responsible for the observed greater standard deviations in TEC during April.

Another important measure of the daily difference from monthly average TEC values is the distribution of the differences. The standard deviation applies to a normal, or Gaussian, distribution of differences from monthly mean values, but just how close to a Gaussian shape are these differences? In Figure 9 the distribution of the difference from mean TEC hourly values for the 1000 to 1400 UT time interval is plotted for the month of March 1979. Also plotted in the same figure is a Gaussian curve with a standard

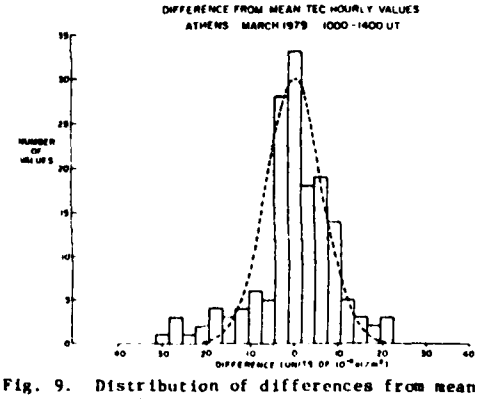

Fig. 9. Distribution of differences from mean hourly TEC values for Athens, Greece, March, 1979, 1000-1400 UT. Dashed curve is a gaussian curve of standard deviation 9.0.

Table I - Statistics of monthly TEC behavior for Athens, Greece for the indicated months.

Table I - Statistics of monthly TEC behavior for Athens, Greece for the indicated months.

TEC Station: Athens, Greece

Hourly Values of Total Electron Content vs. U.T. (units are in 10^{16} electrons/meter^2)

DECEMBER 1978

	0	1	2	3	4	5	6	7	8	9	10	11	12	13	14	15	16	17	18	19	20	21	22	23
MEAN	6.1	6.0	6.0	5.8	5.1	6.0	14.2	21.4	25.8	31.6	36.1	36.8	36.5	33.1	31.9	25.3	17.9	13.5	11.2	9.6	7.7	6.6	6.6	6.5
S.D.	1.4	1.3	1.3	1.2	1.1	1.2	1.7	2.9	4.7	6.0	6.6	7.9	7.1	5.6	5.2	4.2	3.8	3.3	2.8	2.3	1.6	1.8	2.0	1.9
25.D.	23.1	21.0	20.9	20.9	21.3	19.2	12.2	13.8	18.2	19.1	18.3	21.5	20.6	17.1	16.3	16.6	21.0	24.7	25.0	23.8	20.8	27.6	30.1	29.9
MIN	4.6	4.1	3.9	3.7	3.6	4.1	11.5	16.7	18.9	23.0	27.7	25.5	23.6	22.8	24.5	18.7	13.0	8.8	7.5	6.3	5.1	3.7	3.7	4.0
MAX	9.1	8.3	8.4	8.2	7.3	9.2	17.1	27.9	35.2	49.1	55.4	61.4	55.4	44.7	48.2	38.9	28.8	24.7	18.6	16.0	12.2	10.9	11.7	12.0
10.PCT	4.3	4.3	4.4	4.2	3.7	4.3	12.0	17.5	19.3	24.4	29.9	28.1	26.7	26.8	25.1	19.5	13.3	10.1	8.0	7.2	5.9	4.7	4.3	4.2
25.PCT	4.8	4.8	5.0	4.8	4.2	5.1	12.9	19	...	5	27.7	...	32.7	29.6	29.0	28.7	23.0	14.5	11.7	9.4	8.0	6.5	5.2	5.1	5.0
50.PCT	6.3	5.9	6.2	5.7	4.8	6.0	13.9	...	24.9	30.2	34.2	35.3	33.6	30.4	30.8	24.3	17.6	12.9	10.8	8.9	7.2	6.3	6.3	6.3
75.PCT	6.9	6.9	6.9	6.6	5.8	6.8	14.0	23.2	27.9	33.0	38.7	40.5	38.2	38.2	34.9	27.7	18.8	14.2	12.5	10.8	8.8	6.9	7.1	7.1
90.PCT	7.7	7.6	7.9	7.1	6.8	7.4	16.9	24.7	33.9	39.8	41.7	41.6	41.8	40.0	37.8	29.8	22.6	16.9	14.8	12.5	9.4	8.4	9.1	8.2
COUNT	31	31	31	31	31	31	31	31	30	31	31	30	30	30	31	31	31	31	31	31	31	31	31	31

MARCH 1979

	0	1	2	3	4	5	6	7	8	9	10	11	12	13	14	15	16	17	18	19	20	21	22	23
MEAN	17.1	14.6	12.2	9.7	7.4	13.3	28.3	40.9	51.2	62.8	71.3	77.6	79.3	77.2	72.7	66.5	59.5	50.1	41.8	37.2	32.2	26.8	22.7	19.6
S.D.	5.5	4.7	4.5	4.2	3.4	4.2	5.1	6.6	8.2	8.2	8.5	9.0	9.3	10.0	10.6	10.2	8.3	7.6	8.1	9.9	9.9	8.5	7.3	6.4
25.D.	31.7	32.4	37.1	43.1	46.0	31.3	18.3	16.2	16.1	13.1	12.0	11.6	11.8	13.0	14.6	15.4	14.0	15.2	19.5	26.6	30.9	31.7	32.0	32.6
MIN	7.7	5.7	3.0	2.7	2.1	7.2	12.3	17.8	23.6	33.8	42.1	49.3	54.1	51.0	45.1	39.2	35.8	32.5	25.9	18.5	15.3	13.0	11.6	9.7
MAX	27.9	23.3	21.8	19.5	13.7	22.9	38.5	54.2	65.8	75.6	83.3	90.7	96.1	97.1	94.5	91.0	78.5	64.5	56.6	63.5	65.5	55.8	43.9	34.6
10.PCT	10.4	8.2	5.0	3.8	2.6	8.4	22.0	34.1	38.1	51.1	60.1	60.8	63.0	63.8	60.1	54.9	51.8	39.7	27.3	21.1	17.7	17.7	13.6	11.4
25.PCT	12.3	10.9	8.7	6.8	5.8	10.1	25.6	38.0	47.8	59.2	66.9	75.8	75.3	72.4	65.7	60.7	55.0	43.1	37.5	33.4	23.8	19.8	16.2	13.4
50.PCT	17.2	13.9	12.4	9.6	7.4	12.6	28.5	42.5	53.8	64.6	71.5	78.1	80.2	78.2	73.0	65.6	58.5	49.4	42.3	38.1	32.2	27.0	23.0	19.6
75.PCT	21.2	17.9	14.9	12.1	9.2	15.5	31.5	43.8	56.0	67.9	77.8	82.8	85.6	81.3	78.9	70.1	62.5	54.9	47.3	42.9	37.3	30.3	27.4	24.2
90.PCT	23.9	19.7	17.8	14.8	11.8	19.4	32.9	47.3	57.9	69.1	79.5	86.2	88.6	88.6	87.7	79.0	73.0	59.0	50.9	45.5	39.9	35.0	28.9	26.1
COUNT	29	29	29	29	29	30	30	31	31	30	30	31	31	31	31	31	31	29	29	29	29	29	29	29

APRIL 1979

	0	1	2	3	4	5	6	7	8	9	10	11	12	13	14	15	16	17	18	19	20	21	22	23
MEAN	16.2	14.2	11.7	8.6	9.0	16.8	23.3	29.8	39.0	47.8	56.3	62.4	63.5	62.4	58.2	53.6	49.2	45.4	39.0	32.0	27.2	24.3	21.4	18.3
S.D.	4.9	4.7	4.7	4.2	4.1	4.8	6.9	8.5	10.6	12.2	13.7	14.4	16.0	16.1	14.9	13.5	11.8	10.2	9.5	9.0	8.3	7.8	6.5	5.4
25.D.	30.3	33.2	40.1	48.8	45.6	28.3	19.8	28.6	27.3	25.6	24.3	23.1	25.2	25.8	25.6	25.2	24.0	22.5	24.3	28.2	30.6	32.0	30.5	29.7
MIN	7.5	7.3	3.5	1.8	2.2	7.4	10.9	14.9	17.0	19.4	21.8	25.3	24.5	28.1	25.5	20.4	17.6	15.8	13.6	11.8	10.6	9.0	8.2	8.5
MAX	25.7	23.1	19.0	15.2	22.3	25.2	45.7	44.2	57.3	68.4	73.9	83.3	88.6	89.9	86.9	80.6	71.6	64.1	57.4	52.1	45.8	42.5	36.2	29.2
10.PCT	9.3	7.8	6.2	1.6	3.5	11.3	13.6	17.2	23.2	29.7	36.0	42.9	39.5	35.5	35.0	34.6	34.3	31.8	27.6	22.8	18.2	15.3	14.1	11.6
25.PCT	12.4	9.2	7.6	5.3	6.4	12.5	16.4	22.6	32.5	38.7	45.7	55.1	47.9	46.2	46.4	40.4	40.2	38.9	32.6	24.2	19.5	17.6	16.2	13.4
50.PCT	16.8	14.9	12.1	9.1	8.7	16.4	22.1	31.2	39.8	48.8	59.5	64.9	65.9	65.3	61.2	54.8	50.5	47.4	39.1	31.3	27.6	23.4	21.3	18.0
75.PCT	19.9	18.8	15.7	12.3	10.1	20.5	28.7	35.7	46.8	...4	65.8	72.2	74.8	73.7	65.2	60.8	56.1	51.2	44.9	38.3	31.5	28.9	26.4	22.3
90.PCT	22.1	19.7	17.5	13.5	13.9	22.2	31.7	38.6	48.6	60.2	70.5	75.0	79.8	80.4	73.5	68.7	60.8	55.0	49.0	40.9	35.2	33.4	29.1	24.3
COUNT	29	29	29	29	29	27	28	27	27	29	29	28	29	29	28	29	29	29	29	29	29	29	29	29

JUNE 1979

	0	1	2	3	4	5	6	7	8	9	10	11	12	13	14	15	16	17	18	19	20	21	22	23
MEAN	19.4	17.7	15.2	12.7	12.6	23.3	26.4	28.5	30.7	33.9	36.4	38.1	38.2	37.1	34.7	31.7	29.2	28.5	27.6	25.4	23.9	22.7	22.0	20.1
S.D.	5.3	5.9	4.1	3.6	3.8	4.4	3.8	4.5	5.2	6.3	7.4	7.8	8.1	8.0	7.3	6.7	5.7	5.6	5.5	5.2	4.7	4.7	4.7	4.6
25.D.	27.1	27.8	27.0	28.0	21.6	19.0	14.6	15.6	17.0	18.6	20.2	20.4	21.2	21.6	21.2	21.1	19.7	19.7	20.0	20.5	19.8	20.9	21.1	22.7
MIN	9.8	8.5	7.2	6.3	11.0	14.9	15.3	17.6	19.4	19.3	19.9	23.6	20.3	18.5	17.6	17.9	18.6	18.8	19.0	16.1	15.0	14.0	12.3	11.3
MAX	29.9	30.8	25.8	20.4	25.0	32.3	31.8	35.2	38.5	44.6	49.2	50.0	48.1	48.6	45.7	43.1	40.4	42.9	41.3	37.9	34.7	35.6	29.5	29.3
10.PCT	10.5	8.7	8.7	8.1	13.3	18.3	21.4	22.2	22.8	24.1	24.2	26.0	25.4	23.6	22.2	19.6	19.7	20.2	18.8	18.4	17.9	17.8	15.9	13.1
25.PCT	16.1	15.1	13.0	9.5	14.1	20.1	23.2	25.4	29.0	30.0	34.1	35.9	34.3	32.3	28.1	27.3	24.3	24.8	24.3	22.2	20.7	18.8	18.3	17.8
50.PCT	18.7	17.4	15.2	13.2	17.9	23.1	26.9	28.5	30.0	35.7	37.8	40.2	41.2	40.2	37.3	33.2	29.8	28.7	28.1	24.5	23.7	22.5	22.8	19.5
75.PCT	23.3	20.9	17.9	14.9	19.9	26.4	29.2	32.0	35.6	39.6	42.2	43.1	44.2	42.6	39.6	36.9	33.4	31.9	30.6	29.3	27.0	25.6	24.9	24.0
90.PCT	26.6	23.4	18.9	17.1	22.9	29.3	30.5	34.0	35.8	39.9	43.5	45.4	45.1	44.7	42.9	37.6	34.8	35.0	33.8	31.7	30.0	27.7	28.2	25.2
COUNT	30	30	30	30	30	30	30	30	30	30	30	30	30	30	30	30	30	30	30	30	30	30	30	30

SEPTEMBER 1979

	0	1	2	3	4	5	6	7	8	9	10	11	12	13	14	15	16	17	18	19	20	21	22	23
MEAN	17.9	15.9	14.2	12.0	11.6	20.5	28.1	34.8	40.1	46.2	52.2	56.3	59.6	58.5	56.6	53.5	49.6	43.6	36.7	29.7	25.9	22.7	20.6	18.6
S.D.	5.7	5.3	5.3	5.7	5.9	6.6	6.6	8.7	10.3	11.3	12.1	12.0	12.1	11.5	10.8	9.7	9.4	7.6	7.3	8.6	9.8	7.7	6.7	6.1
25.D.	33.6	30.7	33.0	32.6	5.5	32.6	23.2	25.0	25.7	24.5	23.5	21.3	20.9	19.4	19.1	18.7	18.9	17.5	19.9	28.9	37.7	34.0	32.7	32.5
MIN	8.5	10.9	7.6	6.2	5.5	13.5	19.6	23.7	23.9	27.6	34.7	41.1	41.8	41.2	40.5	36.7	33.2	28.8	24.7	20.1	15.9	12.7	10.9	9.4
MAX	39.8	31.6	39.2	36.8	17.1	39.6	48.8	61.0	59.8	72.9	84.9	88.0	96.7	87.3	84.8	77.2	69.9	61.9	61.1	66.1	69.1	54.0	47.6	42.5
10.PCT	10.0	10.9	9.1	8.1	7.7	12.9	19.4	27.8	32.9	37.2	41.7	46.6	44.7	44.2	42.6	39.5	33.2	26.8	21.0	17.6	15.1	12.6	12.2	12.2
25.PCT	13.9	13.7	12.7	9.8	9.6	17.6	22.9	27.1	31.3	37.1	43.0	47.2	49.5	49.4	48.6	46.3	42.9	38.7	32.8	25.0	20.9	18.6	17.0	15.6
50.PCT	17.4	15.4	14.6	12.2	12.6	19.6	27.8	33.8	38.4	45.0	50.9	54.5	56.4	56.1	53.4	50.4	48.3	40.9	35.6	28.2	23.7	20.2	19.2	17.7
75.PCT	19.4	17.3	16.9	14.7	13....	1.6	32.2	41.8	50.5	54.8	60.2	63.9	66.5	64.9	64.8	60.9	56.0	49.0	39.7	32.0	28.9	25.0	22.8	20.8
90.PCT	21.7	19.8	17.6	16.9	15.0	23.1	37.6	45.2	53.1	60.9	67.9	71.8	74.0	73.6	71.6	65.5	61.8	54.1	44.3	36.0	32.2	28.9	24.7	23.1
COUNT	30	30	29	30	30	30	30	30	30	30	30	30	30	30	30	30	30	30	30	30	30	30	30	30

deviation of 9 TEC units. It can be seen that the observed distribution is approximately Gaussian, with perhaps more actual values on the negative side than a Gaussian curve. Figure 10 shows the differences from mean TEC for the month of April 1979. In this month the actual values depart more significantly from Gaussian shape, both for large negative differences and for smaller positive differences. In general, the distribution of day-to-day differences of TEC from monthly average values is nearly Gaussian, or at least can be assumed to be, for most systems engineering study purposes.

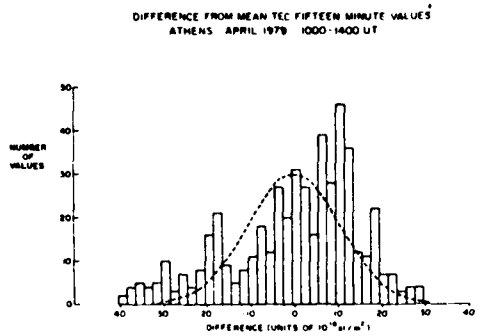

Fig. 10. Distribution of differences from mean values of TEC taken at 15 min intervals for Athens, Greece, April, 1979, 1000-1400 UT. Dashed curve is a gaussian curve of standard deviation 15.0.

In addition to the measures of monthly mean and standard deviation, either expressed in percent or in absolute value of TEC units, it is also important to know the extreme limits of the data. In Table 1 are presented the complete statistics of monthly TEC behavior for the five months typical of the various seasonal changes in the Mediterranean region during solar maximum ionospheric conditions. Presented in Table 1 are hourly values for the mean, standard deviation, percentage standard deviation, minimum and maximum values for each hour, and the upper and lower quartiles and deciles. Finally, for each hour of the statistics, the count of number of values is given.

4. CONCLUSIONS

The effects of the time delay of the earth's ionosphere may be important for precise satellite ranging systems. For the Mediterranean region for solar maximum conditions we have presented statistics for the behavior of the ionospheric TEC, which is proportional to time delay. The deviations from monthly mean conditions are approximately 15 to 25 percent during the daytime periods when absolute values of time delay are largest. The distribution of differences from monthly mean values is approximately Gaussian. The availability of linearly polarized VHF telemetry signals from the Italian SIRIO satellite has made these measurements possible, and continued transmissions from the SIRIO satellite are necessary if more data is to be gathered on the downward side of the solar cycle.

Acknowledgements. We are indebted to personnel of the United States Air Weather Service, Detachment 3, 2nd Weather Wing (MAC), for collecting the TEC data at the Athens station. We particularly appreciate the cooperation of Professor P.F. Checcacci, of the Instituto di Ricerca sulle Onde Elettromagnetiche of the Consiglio Nazionale delle Ricerche for coordinating the use of the SIRIO VHF telemetry beacon, for providing the SIRIO orbital elements, and for his interest in the scientific results of this work.

REFERENCES

[1] E.M. Lassiter and B. Parkinson: *The Status of the Development of the NAVSTAR-Global Positioning System.* "Navigation" January 1977, vol. XXV, n. 97, p. 13-26.

[2] J.E. Titheridge: *Determination of Ionospheric Electron Content from the Faraday Rotation of Geostationary Satellite Signals.* "Planet. Space Sci." 1972, vol. 20, p. 353-369.

Manuscript received on April 21, 1980.

END

DATE
FILMED
10-81

DTIC